

CR-171989

CSDL-T-950

AN ADAPTIVE NUMERIC PREDICTOR-
CORRECTOR GUIDANCE ALGORITHM FOR
ATMOSPHERIC ENTRY VEHICLES

by

Kenneth Milton Spratlin

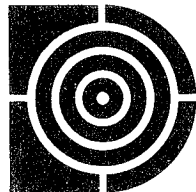
May 1987

Master of Science Thesis
Massachusetts Institute of Technology

(NASA-CR-171989) AN ADAPTIVE NUMERIC
PREDICTOR-CORRECTOR GUIDANCE ALGORITHM FOR
ATMOSPHERIC ENTRY VEHICLES M.S. Thesis -
MIT, Cambridge (Draper (Charles Stark)
Lab.) 206 p Avail: NTIS HC A10/MF A01

N87-26934

Unclassified
G3/17 0090665



The Charles Stark Draper Laboratory, Inc.

555 Technology Square
Cambridge, Massachusetts 02139



AN ADAPTIVE NUMERIC PREDICTOR-CORRECTOR
GUIDANCE ALGORITHM FOR ATMOSPHERIC
ENTRY VEHICLES

by

Kenneth Milton Spratlin •

B.A.E., Georgia Institute of Technology
(1985)

SUBMITTED IN PARTIAL FULFILLMENT
OF THE REQUIREMENTS FOR THE DEGREE OF

MASTER OF SCIENCE IN
AERONAUTICS AND ASTRONAUTICS

at the

MASSACHUSETTS INSTITUTE OF TECHNOLOGY

May 1987

©Kenneth Milton Spratlin, 1987

Signature of Author Kenneth M. Spratlin
Department of Aeronautics and Astronautics
May 8, 1987

Approved by Richard H. Battin 5/8/87
Professor Richard H. Battin
Department of Aeronautics and Astronautics
Thesis Supervisor

Approved by Timothy J. Brand 5/8/87
Timothy J. Brand
Technical Supervisor, CSDL

Accepted by _____
Professor Harold Y. Wachman
Chairman, Department Graduate Committee

AN ADAPTIVE NUMERIC PREDICTOR-CORRECTOR
GUIDANCE ALGORITHM FOR ATMOSPHERIC
ENTRY VEHICLES

by

Kenneth Milton Spratlin

Submitted to the Department of Aeronautics and Astronautics
on May 8, 1987, in partial fulfillment of the
requirements for the Degree of Master of Science in
Aeronautics and Astronautics

ABSTRACT

An adaptive numeric predictor-corrector guidance algorithm is developed for atmospheric entry vehicles which utilize lift to achieve maximum footprint capability. Applicability of the guidance design to vehicles with a wide range of performance capabilities is desired so as to reduce the need for algorithm redesign with each new vehicle. Adaptability is desired to minimize mission-specific analysis and planning. The guidance algorithm motivation and design are presented.

Performance is assessed for application of the algorithm to the NASA Entry Research Vehicle (ERV). The dispersions the guidance must be designed to handle are presented. The achievable operational footprint for expected worst-case dispersions is presented. The algorithm performs excellently for the expected dispersions and captures most of the achievable footprint.

Thesis Supervisor: Dr. Richard H. Battin

Title: Adjunct Professor of Aeronautics and Astronautics

Technical Supervisor: Timothy J. Brand

Title: Division Leader, The Charles Stark Draper Laboratory, Inc.

~~PRECEDING PAGE BLANK NOT FILMED~~

PAGE 2 INTENTIONALLY BLANK

ACKNOWLEDGEMENT

This report was prepared at The Charles Stark Draper Laboratory, Inc. in support of NASA Langley Research Center (LaRC) Task Order No. 87-43 under Contract NAS9-17560 with the NASA Lyndon B. Johnson Space Center (JSC).

Publication of this report does not constitute approval by the Draper Laboratory or the sponsoring agency of the findings or conclusions contained herein. It is published for the exchange and stimulation of ideas.

I hereby assign my copyright of this thesis to The Charles Stark Draper Laboratory, Inc., Cambridge, Massachusetts.

Kenneth M. Spratin
Kenneth M. Spratin

Permission is hereby granted by The Charles Stark Draper Laboratory, Inc. to the Massachusetts Institute of Technology to reproduce any or all of this thesis.

I wish to take this opportunity to thank some of the many people who have helped me during the preparation of this thesis and my stay at M.I.T.. I would like to express my sincere gratitude to The Charles Stark Draper Laboratory for making my graduate study possible through the Draper Fellowship. I wish to thank all of the members of the Guidance and Navigation Analysis Division for their technical assistance and willingness to share their expertise. In particular I would like to thank T. Brand, J. Higgins, and A. Engel for their patience, assistance, and support during the preparation of this thesis and work on the Aeroassist Flight Experiment. I wish to thank my thesis advisor, Dr. R.H. Battin, for his assistance and in particular for his abilities as an educator. A special thanks for his encouragement and support goes to B. Kriegsman who recently passed away. He is greatly missed. I found the opportunity to interact with the people at CSDL to be the most rewarding aspect of my studies at M.I.T..

I also wish to thank H. Stone and R. Powell of NASA/LaRC for the opportunity to work on the ERV entry guidance problem and their assistance in answering my questions.

Most importantly, I wish to thank my parents and sisters for their unending love and support over the years.

PRECEDING PAGE BLANK NOT FILMED

PAGE 1 INTENTIONALLY BLANK

TABLE OF CONTENTS

Section	Page
1.0 INTRODUCTION	21
2.0 MOTIVATION	23
2.1 Introduction	23
2.2 Dispersions	26
2.3 Reference Trajectories	28
2.4 Guidance Approach	31
3.0 GUIDANCE DESIGN	33
3.1 Introduction	33
3.2 Unit Target Vector	34
3.3 Commanded Attitude Computation	35
3.4 Corrector Algorithm	36
3.5 Predictor Algorithm	39
3.5.1 Introduction	39
3.5.2 Equations of Motion	40
3.5.3 Integration of the Equations of Motion	44
3.5.4 Termination Conditions for the Predictor	46
3.5.5 Final State Error Computation	46
3.5.6 Algorithm Coding	48

~~PRECEDING PAGE BLANK NOT FILMED~~

3.6	Estimators	48
3.7	Heat Rate Control	52
4.0	PERFORMANCE	57
4.1	Simulator	57
4.2	Open-Loop Footprint	57
4.3	Effect of Dispersions on Footprint	59
4.4	Estimator Performance	60
4.5	Closed-Loop Performance	61
4.6	Heat Rate Control Performance	63
4.7	Overcontrol	63
4.8	Algorithm Execution Time	66
5.0	FUTURE RESEARCH TOPICS AND CONCLUSIONS	69
5.1	Future Research Topics	69
5.2	Conclusions	71

Appendix	Page
Appendix A. ERV AERODYNAMICS MODEL	133
Appendix B. ALGORITHM PROGRAM LISTINGS	135
List of References	211

LIST OF ILLUSTRATIONS

Figure	Page
1. Three-View Drawing of the ERV	78
2. Atmospheric Wind Profile	79
3. Envelope of Density Profiles Derived from Shuttle Flights	80
4. STS-1 Density Profile Comparison	81
5. STS-9 Density Profile Comparison	82
6. Multiphase Bank Angle Program for L/D = 1.5	83
7. Crossrange Versus Number of Bank Steps	84
8. Comparison of Optimum Bank Angle Programs	85
9. Optimum Shuttle Angle of Attack Profile for Maximum Downrange	86
10. Optimum Shuttle Bank Angle Profile for Maximum Crossrange	87
11. Optimum Shuttle Angle of Attack Profile for Maximum Crossrange	88
12. Landing Footprint for the ERV	89
13. Altitude Histories for the Entry Missions of the ERV	90
14. Bank Angle Histories for the Entry Missions of the ERV	91
15. Angle of Attack Histories for the Entry Missions of the ERV	92
16. Heat Rate Histories for the Entry Missions of the ERV	93
17. Heat Load Histories for the Entry Missions of the ERV	94
18. Bank Angle Versus Velocity Profile	95
19. Definitions of Downrange and Crossrange Errors	96
20. Predicted Lift Coefficient Profile for the ERV	97
21. Predicted L/D Profile for the ERV	98

22.	Predicted L/D versus Angle of Attack Profile for the ERV	99
23.	ERV Open-Loop Footprint with the Control Profile	100
24.	Time Response of the Density Filter	101
25.	Time Response of the L/D Filter	102
26.	Closed-Loop Altitude History for the Maximum Downrange Case	103
27.	Closed-Loop Velocity History for the Maximum Downrange Case	104
28.	Closed-Loop Heat Rate History for the Maximum Downrange Case	105
29.	Closed-Loop Heat Load History for the Maximum Downrange Case	106
30.	Closed-Loop Downrange History for the Maximum Downrange Case	107
31.	Closed-Loop Crossrange History for the Maximum Downrange Case	108
32.	Closed-Loop Altitude History for the Maximum Crossrange Case	109
33.	Closed-Loop Velocity History for the Maximum Crossrange Case	110
34.	Closed-Loop Heat Rate History for the Maximum Crossrange Case	111
35.	Closed-Loop Heat Load History for the Maximum Crossrange Case	112
36.	Closed-Loop Downrange History for the Maximum Crossrange Case	113
37.	Closed-Loop Crossrange History for the Maximum Crossrange Case	114
38.	Closed-Loop Altitude History for the Minimum Downrange Case	115
39.	Closed-Loop Velocity History for the Minimum Downrange Case	116
40.	Closed-Loop Heat Rate History for the Minimum Downrange Case	117
41.	Closed-Loop Heat Load History for the Minimum Downrange Case	118
42.	Closed-Loop Downrange History for the Minimum Downrange Case	119
43.	Closed-Loop Crossrange History for the Minimum Downrange Case	120
44.	Angle of Attack Comparison for the Maximum Downrange Case	121
45.	Bank Angle Comparison for the Maximum Downrange Case	122
46.	Angle of Attack Comparison for the Maximum Crossrange Case	123
47.	Bank Angle Comparison for the Maximum Crossrange Case	124
48.	Angle of Attack Comparison for the Minimum Downrange Case	125

49.	Bank Angle Comparison for the Minimum Downrange Case	126
50.	Bank Angle Versus Time Comparison for Heat Rate Control	127
51.	Angle of Attack Versus Time Comparison for Heat Rate Control	128
52.	Heat Rate Versus Time Comparison for Heat Rate Control	129
53.	Bank Angle Versus Velocity Comparison for Heat Rate Control	130
54.	Angle of Attack Versus Time Comparison with Overcontrol	131
55.	Required Execution Time for the Predictor-Corrector	132

LIST OF TABLES

Table		Page
1. Characteristics of the ERV and Trajectory Entry Conditions	73	
2. Dispersions Used in Performance Study	73	
3. Dispersed Cases for Maximum Downrange Region	74	
4. Dispersed Cases for Maximum Crossrange Region	75	
5. Dispersed Cases for Minimum Downrange Region	76	
6. Maximum Downrange Region Closed-Loop Results	77	
7. Maximum Crossrange Region Closed-Loop Results	77	
8. Minimum Downrange Region Closed-Loop Results	77	

PRECEDING PAGE BLANK NOT FILMED

SYMBOLS

a	= acceleration magnitude
\vec{a}	= acceleration vector
\vec{a}_i	= inertial acceleration measured by the inertial measurement unit
\vec{A}_i	= total inertial acceleration vector
AOTV	= Aerobraking Orbital Transfer Vehicle
BTU	= British Thermal Unit
\bar{c}	= mean aerodynamic chord
$\cos(\Delta\phi)$	= cosine of incremental lift for heat rate control
C'	= proportionality factor for the linear viscosity-temperature relationship
C_d	= aerodynamic drag coefficient
C_L	= aerodynamic lift coefficient
C_s	= speed of sound
CPU	= central processing unit
CR	= crossrange
CSDL	= The Charles Stark Draper Laboratory, Inc.
det	= determinant of sensitivity matrix
DR	= downrange
DOF	= degree of freedom
ERV	= Entry Research Vehicle
f_{earth}	= flattening of oblate Earth
\vec{F}_i	= inertial force vector
g	= gravitational acceleration magnitude
\vec{g}_i	= gravitational acceleration vector

PRECEDING PAGE BLANK NOT FILMED

<i>GPS</i>	= Global Positioning System
<i>h</i>	= altitude
<i>ḣ</i>	= derivative of altitude with time
<i>ḧ</i>	= second-derivative of altitude with time
<i>h_s</i>	= scale height for exponential atmosphere model
\vec{i}	= unit vector
<i>J₂</i>	= second zonal harmonic coefficient
<i>JSC</i>	= Lyndon B. Johnson Space Center
<i>k</i>	= term in geodetic to geocentric latitude conversion
<i>K</i>	= term in heat rate control equation
\vec{K}	= velocity vector term in the integration algorithm
\vec{K}'	= acceleration vector term in the integration algorithm
<i>K_{Δt}</i>	= gain on acceleration magnitude in variable time step equation
<i>K_{L/D}</i>	= multiplicative scale factor on the nominal L/D
<i>K_{q̇}</i>	= gain on heat rate error in heat rate control equation
<i>K_{q̈}</i>	= gain on rate of change of heat rate in heat rate control equation
<i>K_{ṗ}</i>	= multiplicative scale factor on the standard density
<i>K₁</i>	= gain in first-order filter for density smoothing
<i>K₂</i>	= gain in first-order filter for L/D smoothing
<i>L/D</i>	= lift-to-drag ratio
<i>LaRC</i>	= Langley Research Center
<i>m</i>	= mass
<i>M</i>	= Mach Number
\hat{M}_i^{EF}	= inertial-to-Earth-fixed transformation matrix
<i>M₀</i>	= mean molecular weight of air at sea level
<i>n.m.</i>	= nautical mile
<i>NASA</i>	= National Aeronautics and Space Administration

<i>POST</i>	= Program to Optimize Simulated Trajectories
\bar{q}	= dynamic pressure
<i>Q</i>	= heat load
\dot{Q}	= heat rate
\ddot{Q}	= time rate of change of heat rate
<i>R</i>	= position vector magnitude
R_{equator}	= radius of oblate Earth at equator
\vec{R}_I	= inertial position vector
R_{pole}	= radius of oblate Earth at pole
<i>Re</i>	= Reynolds Number
<i>S</i>	= Sutherland's constant in viscosity equation
<i>S</i>	= aerodynamic reference area
<i>SEADS</i>	= Shuttle Entry Air Data System
t_{GMT}	= Greenwich mean time
<i>T'</i>	= reference temperature
T_M	= molecular scale temperature
T_{static}	= freestream static temperature
T_{wall}	= wall temperature
<i>TAEM</i>	= Terminal Area Energy Management
\bar{V}	= Viscous Interaction Parameter
V_I	= magnitude of inertial velocity
\vec{V}_I	= inertial velocity vector
V_R	= magnitude of Earth-relative velocity
\vec{V}_R	= Earth-relative velocity vector
<i>z</i>	= geocentric colatitude of the position vector
α	= angle of attack

β	= angle of sideslip
δ	= small incremental change
Δ	= incremental change
γ	= ratio of specific heats for air
λ	= longitude
μ	= coefficient of viscosity for air
μ	= Earth gravitational constant
$\vec{\omega}_{\text{earth}}$	= Earth's rotation vector
ω_n	= natural frequency of heat rate control response
ϕ	= bank angle
R	= universal gas constant
ρ	= atmospheric density
σ	= standard deviation
τ	= time constant of filter
ζ	= damping ratio of heat rate control response

SUBSCRIPTS

$aero$	= aerodynamic
c	= geocentric
cmd	= command
d	= desired
des	= desired
$drag$	= drag term

<i>e</i>	= error
<i>EI</i>	= entry interface
<i>f</i>	= final
<i>g</i>	= geodetic
<i>imu</i>	= inertial measurement unit
<i>inplane</i>	= projection of target unit vector into plane formed by the position vector and the relative velocity vector
<i>lat</i>	= direction perpendicular to the plane formed by the position vector and the relative velocity vector
<i>lift</i>	= lift term
<i>lim</i>	= limiting value or boundary
<i>L/D</i>	= lift-to-drag ratio
<i>max</i>	= maximum
<i>min</i>	= minimum
<i>nom</i>	= nominal
<i>perpen</i>	= direction perpendicular to the plane formed by the position vector and the relative velocity vector
<i>pole</i>	= direction of the north pole
<i>R</i>	= direction of the position vector
<i>sl</i>	= sea level
<i>std</i>	= standard value
<i>t</i>	= target aim point
<i>p</i>	= atmospheric density

SUPERSCRIPTS

<i>EF</i>	= coordinatized in Earth-fixed coordinates
<i>imu</i>	= value measured by inertial measurement unit on current cycle
imu past	= value measured by inertial measurement unit on past cycle
\wedge	= estimated or measured
,	= value from previous guidance cycle

1.0 INTRODUCTION

Routine access to space and the maintenance of a Space Station will increasingly require greater flexibility in mission planning and the requirement for lower system maintenance costs. The launch and recovery phases of space flight have historically been the most demanding phases of space flight and therefore require the most development effort and investment. Mission flexibility requires more frequent launch and deorbit opportunities. For the case of re-entry vehicles, deorbit opportunities are defined by the ranging capability of the vehicle. A high L/D vehicle increases the available deorbit opportunities increasing mission flexibility. High L/D vehicles also are of interest for over-flight missions for the purpose of reconnaissance.

Entry guidance algorithms developed to date have been highly vehicle-specific and required great development and maintenance efforts over the life of the vehicle. These algorithms were not applicable to other vehicles without extensive modification.

This study seeks to design an adaptive entry guidance algorithm that maximizes the usable footprint by making full use of the available vehicle capability. This algorithm should also be easy to maintain throughout the vehicle definition phase and operational life. Minimizing the number of mission-dependent input parameters (I-loads) is desirable. The algorithm should also be easily transported to other vehicles to minimize development cost. Transportability is accomplished by minimizing vehicle-specific features of the algorithm. Explicit heat rate control should be provided to allow full use of the entry corridor up to the heat rate limits.

This study seeks to design such an algorithm. A candidate entry guidance algorithm is defined for the NASA Entry Research Vehicle (ERV), but is easily adapted to other vehicles with minimal modification. The proposed algorithm attains almost complete coverage of the achievable footprint, while employing a simple one-phase entry algorithm with explicit heat rate control. Vehicle-specific features and I-loads are minimized, reducing algorithm development and maintenance costs.

The ERV [1] is a proposed high-performance entry vehicle designed as a test bed for future technology development in the areas of:

1. Maneuvering entry/synergetic plane change
2. Atmospheric uncertainties
3. Advanced thermal protection systems
4. Aerodynamic/aeroheating prediction
5. Adaptive guidance and navigation
6. Load-bearing thermostructures

The ERV is designed for deployment from the Space Shuttle, after which the ERV enters the atmosphere for demonstration of the synergetic plane change, over-flight, and entry missions. Figure 1 on page 78 shows a three-view drawing of the ERV and the surface areas of the aerodynamic control surfaces. Also seen is the size of the ERV in relation to the diameter of the Shuttle payload bay in which the ERV must fit.

2.0 MOTIVATION

2.1 INTRODUCTION

The goal of any entry guidance algorithm is to successfully guide the vehicle to the desired final state for the largest range of dispersions possible without violating any vehicle constraints while also maximizing the achievable footprint. It is also desirable to minimize the mission and vehicle-specific aspects of the guidance algorithm so as to minimize pre-mission analysis and planning. Transportability of the algorithm from one vehicle to another significantly reduces guidance algorithm development effort and cost.

To maximize the footprint attainable, the guidance algorithm must follow the optimal path to any particular point in the footprint. The algorithms developed to date for such vehicles as the Apollo capsule [2] and the Space Shuttle [3] have attempted to do this by fitting the optimal trajectory with phases that follow important parameters (reference profiles) over some range of conditions. These guidance algorithms were required to be computationally efficient because of the limited on-board computer resources available. Analytic expressions for the reference profiles allowed for low execution time and tailoring of the trajectory for vehicle-specific constraints. For example, trajectories for these vehicles had to be shaped to reduce and control the maximum heat rate experienced below that allowed for the available thermal protection system materials.

The Space Shuttle entry guidance system employs three major modes with seven phases:

1. Entry
 - a. Pre-entry
 - b. Temperature control
 - c. Equilibrium glide
 - d. Constant drag
 - e. Transition
2. Terminal Area Energy Management
3. Approach and Landing

Except for the pre-entry phase which is open-loop, each phase is described by an analytic expression relating the desired drag and altitude rate (the measured feedback terms used) to the desired profile. Because the algorithms are tailored for a particular vehicle and the reference profiles do not follow the optimal profile to all points in the footprint, guidance algorithms developed to date can not be easily adapted to other vehicles or provide full coverage of the theoretically achievable footprint.

The next generation of entry vehicles will not be so constrained due to advances in thermal protection system materials and computer technology. For example, flight computers are now capable of supercomputer speeds on the order of 40 million instructions per second utilizing parallel processing architecture [4]. A different approach to guidance that attempts to follow an optimal profile to maximize footprint capability is therefore possible.

The proposed approach is a predictor-corrector algorithm that numerically predicts the final state for a particular control variable history and then corrects the control variable history to satisfy the specified final state constraints. This approach, proposed previously for

various guidance problems, has most often been impractical because of the long trajectories that must be predicted and the slow computer speeds.

Such an approach has been employed for the Space Shuttle Powered Explicit Guidance (PEG) [5] used for second stage ascent and orbit insertion burns where the trajectory is short enough to be predicted with the available computer resources. The Shuttle algorithm numerically predicts the gravitational effects during the powered flight phase with a 10 step integration of the 500 second trajectory.

A predictor-corrector has also been proposed for Aerobraking Orbital Transfer Vehicles (AOTV) [6] which would utilize more advanced computers. This algorithm numerically integrates the equations of motion along a skimming trajectory through the upper atmosphere that is approximately 500 seconds long and requires about 100 integration steps.

The trajectories flown by the ERV or any high L/D entry vehicle are typically from 30 to 100 minutes long from entry interface (400K feet) to landing, so the computational demand for such an algorithm is very great early in the entry when the time to landing is long. However, because the entry is long and the vehicle has excess ranging capability for all but a small region along the edge of the footprint, the accuracy of the early predictions need not be as high as for the later predictions. Hence, large time steps can be used early in the predictor algorithm. Later, when the vehicle nears the landing site, the time remaining is short, and hence, the prediction is short. This allows the predictor-corrector to be executed more often near landing just like the current analytic algorithms. Throughout the entry, vehicles using an analytic guidance algorithm with reference profiles must closely follow the reference profile if the assumed reference profile is to guide the vehicle to the correct final state. A predictor-corrector effectively recomputes a new reference profile each time it is executed, so the guidance execution rate can be much lower than that for analytic algorithms.

2.2 DISPERSIONS

Before the guidance algorithm can be designed, the possible dispersions that may affect the trajectory must be considered. The Shuttle entry guidance system is required to reach the Terminal Area Energy Management (TAEM) interface with less than a 2.5 nautical mile position error from the target aim point. The dispersions of significance to an entry vehicle trajectory include:

1. Vehicle characteristics
 - a. Mass
 - b. Aerodynamics
 - c. Maneuver rates
2. Environment characteristics
 - a. Atmospheric density
 - b. Atmospheric winds
 - c. Atmospheric properties influencing aerodynamic flow regimes (temperature, mean free path, etc.)
3. Initial entry state vector
 - a. Velocity
 - b. Flight path angle
 - c. Heading
4. Propagation errors in navigation state vector

Of these potential dispersion sources, only the vehicle mass, aerodynamics, and the atmospheric density and winds will be significant. By the early 1990's, almost perfect navigation can be expected through use of the Global Positioning System (GPS). If the deorbit burn guidance and control systems are assumed to correctly guide to the navigated state

and there are no navigation errors, then the dispersions in the initial entry state vector are negligible.

The vehicle mass should be known accurately, so for this study, a 3σ error of $\pm 5\%$ is assumed. Experience from the Space Shuttle program shows that the vehicle aerodynamics should be known to within $\pm 5\%$ for the force coefficients on the first flight. Only the stability derivatives and control effectiveness were missed significantly [7]. Even though the force coefficients may be known to excellent accuracy, reduced control effectiveness can reduce the possible trim angle of attack range reducing the maximum L/D achievable. Therefore, for this study, a $\pm 10\%$ dispersion in the lift and drag coefficients is considered. It should be noted that the first few flights of a new vehicle are usually targeted to the middle of the footprint to maximize margin and allow for accurate determination of the vehicle characteristics before the full ranging capability of the vehicle is used. After the first few flights, the aerodynamic characteristics should be known to within a few percent, so only about a $\pm 3\%$ dispersion must be considered.

The atmospheric dispersions were obtained from two sources. Reference [8] specifies the atmospheric dispersions to which aerospace vehicles must be designed. The average of the steady state winds at four geographic locations is shown in Figure 2 on page 79. This model was incorporated into the simulator environment with a magnitude scale factor to simulate less than worst-case winds. The wind direction was selected for each run made with winds and held constant throughout the trajectory. Reference [8] specifies Reference [9] as the source for atmospheric density dispersions. However, the recent Shuttle flights have provided estimated density data of a quality never before available. Atmospheric density profiles derived from Shuttle accelerometer measurements of the normal force acceleration and the estimated normal force coefficient and relative velocity vector are presented in Reference [10]. Figure 3 on page 80, taken from that report, shows the envelope of the

derived density profiles for the first 12 Shuttle flights. Of particular interest is the range of dispersions seen: -47% to +12%. Figures 4 on page 81 and 5 on page 82 show the density profiles for the STS-1 and STS-9 Shuttle flights. High frequency density shear components and constant density biases from the standard atmosphere are seen. For this study, constant density biases of $\pm 30\%$ and the Shuttle derived density profiles from Reference [10] were used.

2.3 REFERENCE TRAJECTORIES

The size of the footprint for a particular vehicle is determined by the range in vehicle L/D and the constraints placed on the trajectory such as heat rate limits. The edges of the footprint correspond to the use of maximum or minimum L/D. Maximum downrange or crossrange, for example, requires maximum L/D, while minimum downrange requires minimum L/D.

The determination of the optimal angle of attack and bank angle control histories for maximum crossrange and downrange has been the topic of many papers [11] [12] [13]. Wagner [12] used several optimization techniques to evaluate the maximum crossrange achievable for a multiphase bank angle history flown at maximum L/D. The multiphase bank profiles considered are shown in Figure 6 on page 83. It is seen that as the number of phases increases, the multiphase profile approaches the optimal continuous profile also shown in this figure. It was determined that a three-phase bank angle profile as illustrated in Figure 6 achieved almost the same crossrange as a continuous bank profile. This is shown in Figure 7 on page 84 reproduced here from that paper. Further, as the number of phases

increases, the optimum bank angle profile approaches a continuous profile that is almost linear with velocity as shown in Figure 8 on page 85. It was also shown that flying at the maximum L/D maximizes the crossrange attained.

This result is confirmed in Reference [13] which utilized a nonlinear programming technique to optimize the Space Shuttle trajectory for the maximum downrange and maximum crossrange cases. The maximum downrange trajectory requires flying at zero bank angle and at the angle of attack corresponding to maximum L/D as shown in Figure 9 on page 86. The control histories for the maximum crossrange case are shown in Figures 10 on page 87 and 11 on page 88. Again, the optimal control history is the angle of attack corresponding to maximum L/D and an almost linear bank angle profile with velocity.

Optimized trajectories for the ERV were reported in Reference [14]. These trajectories were determined using the Program to Optimize Simulated Trajectories (POST) [15] and imposed the following constraints on the trajectories:

1. Maximum heat rate of 125 BTU/sq ft/sec
2. Maximum heat load of 150K BTU/sq ft

The achievable footprint with these constraints, reported in Reference [14], is shown here in Figure 12 on page 89. Subsequently, the heat load limit was increased to 175K BTU/sq ft resulting in the larger footprint shown in Figure 12. As will be seen, these footprints omit a large area in the minimum downrange region that is achievable within the heating constraints. Also shown is the footprint of the Space Shuttle which has a maximum hypersonic L/D of 1.2 as compared with 1.8 for the ERV.

Figure 13 on page 90 shows the altitude history for the maximum downrange, maximum crossrange, and minimum downrange cases. Figures 14 on page 91 and 15 on page 92

show the bank angle and angle of attack histories for these trajectories. Figures 16 on page 93 and 17 on page 94 show the heat rate and heat load histories for these cases.

Figure 15 shows that the constant angle of attack corresponding to maximum L/D is flown for the edge of the footprint except for the minimum downrange case. For the minimum downrange case, the angle of attack corresponding to the minimum L/D on the back side of the L/D curve (high drag coefficient) is flown early, followed by a ramp in angle of attack starting at 1500 seconds after entry interface. This ramp corresponds to the vehicle actually turning around and flying slightly back uprange, so maximum L/D is desired later to maximize the distance flown uprange. The angle of attack for the maximum downrange case is slightly greater than that for maximum L/D because this trajectory exceeds the heat load limit if flown at maximum L/D. The maximum downrange region of the footprint is therefore limited by the heat load limit set for the ERV. If the limit were relaxed, flight at maximum L/D would allow a longer downrange trajectory.

Figure 14 shows that the bank angle profile for maximum crossrange is approximately linear with time which is almost linear with velocity, which suggests that a linear bank angle profile with velocity is sufficient. The maximum downrange case has a constant bank angle of zero which is again linear with velocity. The minimum downrange case does not have a linear bank profile. As was mentioned previously, for this case, the vehicle turns around and flies back uprange.

The results of these studies suggest that use of a constant angle of attack profile and a linear bank with velocity profile will capture a large portion of the achievable footprint. As will be seen in the results, these profiles suffice to capture most of the footprint reported in Reference [14] and additionally reach a large area in the minimum downrange region out-

side the reported footprint. Only a small area of the reported footprint in the minimum downrange region is unachievable.

Also of interest are the peaks in heat rate seen in Figure 16. Because the peaks in heat rate are very short, explicit control of the heat rate should be possible in the maximum heat rate regions without significantly impacting the guidance.

2.4 GUIDANCE APPROACH

The guidance design will attempt to maximize the size of the footprint while flying a constant angle of attack profile and a linear bank angle with velocity profile. The predictor algorithm integrates the equations of motion forward in time using the assumed control profile and the necessary environment and vehicle models. The corrector then determines (using multiple predicted trajectories with various control histories) the sensitivities of the final state constraints to the control variables. The sensitivities are then used to compute the required control variable values to reach the desired final state conditions. Heat rate control is provided locally during the regions of maximum heating without significantly affecting the assumed control histories. Also, in-flight measurements are utilized to increase the accuracy of the predicted trajectories by compensating for off-nominal conditions.

Such a simple profile for the maximum downrange and crossrange cases simplifies the modeling of the control histories in the predictor. The only remaining question is how much of the footprint this profile will capture. As will be seen in Subsection "4.2 Open-Loop

"Footprint" on page 57, such a profile achieves almost complete coverage of the achievable footprint.

Also of concern is the linearity and convergence properties of the final state constraints with the control variables. As will be seen, over almost all of the footprint except near the edges, the constraints are highly linear and convergent with the control variables. Operationally, only about 75% of the achievable footprint is used to ensure guidance margin. Thus, the question of nonconvergence near the edges is avoided.

3.0 GUIDANCE DESIGN

3.1 INTRODUCTION

This section describes the implementational details of the guidance scheme described in the previous section. The equations of motion and environment and vehicle characteristics modeled in the predictor algorithm are described. The corrector algorithm to control the final state constraints with the two available control variables is derived. Also derived are the heat rate control and in-flight measurement algorithms. The heat rate control algorithm provides control of the peaks in stagnation heat rate during the early portion of entry. The in-flight measurement algorithm utilizes accelerations measured by the navigation system to more accurately model the expected environment and vehicle characteristics in the predictor algorithm. Because the predictor-corrector algorithm is computationally intensive, areas where significant execution time savings have been or can be realized are indicated. Program listings of the algorithm coded in the HAL/S computer language are presented in "Appendix B. ALGORITHM PROGRAM LISTINGS" on page 135.

As will be seen, the only inputs to the guidance system are the environment and vehicle models, the assumed control profiles, and the navigated state vector. The state vector is an input to any guidance system. The other inputs are developed for the analysis of any new vehicle. Therefore, the guidance system is highly transportable between vehicles because only the vehicle characteristics and aerodynamics model must be changed for a new vehicle.

3.2 UNIT TARGET VECTOR

The target aim point to which the vehicle is to be guided is specified by the longitude and geodetic latitude of the Terminal Area Energy Management (TAEM) interface point which occurs at 80K feet for the Shuttle. This point is selected based on the guidance algorithm employed during the TAEM guidance phase. TAEM guidance provides precise control of vehicle energy during the final stages of entry to guide to a specified runway with acceptable energy. For computational ease, the longitude and geodetic latitude are converted to a target unit vector in Earth-fixed coordinates by first computing the geocentric latitude from,

$$\phi_c = \tan^{-1}\left(\frac{\tan(\phi_g)}{k}\right) \quad (1)$$

where,

$$k = \left(\frac{R_{equator}}{R_{pole}}\right)^2 = \left(\frac{1}{1-f_{earth}}\right)^2 \quad (2)$$

The unit target vector is then computed from,

$$\vec{i}_t^{EF} = \begin{bmatrix} \cos(\phi_c) & \cos(\lambda) \\ \cos(\phi_c) & \sin(\lambda) \\ \sin(\phi_c) & 0 \end{bmatrix} \quad (3)$$

Alternatively,

$$\vec{i}_t^{EF} = \begin{bmatrix} i_x \\ i_y \\ i_z \end{bmatrix}_t^{EF} \quad (4)$$

where,

$$i_z = \sin(\phi_c) \quad (5)$$

$$i_x = \cos(\lambda) \sqrt{1 - i_z^2} \quad (6)$$

$$i_y = \text{sign}(\lambda) \sqrt{1 - i_x^2 - i_z^2} \quad (7)$$

3.3 COMMANDED ATTITUDE COMPUTATION

Because the predictor can not be executed as frequently as analytic guidance algorithms early in the entry, and because it in fact does not have to be executed as frequently, it is necessary to update the commands sent to the vehicle autopilot more frequently than the predictor-corrector execution rate. Typically, this would be done at the rate of current analytic guidance algorithms, e.g., the Space Shuttle rate of .52 hz. The commanded bank angle, ϕ_{cmd} , is computed for the linear bank with velocity profile as shown in Figure 18 on page 95 from the desired bank angle, ϕ_d , and the current navigated inertial velocity magnitude, V_I ,

$$\phi_{cmd} = \phi_d \frac{V_I - V_f}{V_E - V_f} \quad (8)$$

to yield the near-optimal linear bank with velocity profile. The desired angle of attack control history is a constant angle of attack, and therefore,

$$\alpha_{cmd} = \alpha_d \quad (9)$$

As implemented in the current design, the guidance algorithm executive is executed at 1.0 hz. The attitude commands are updated at this frequency using Eq. (8) and (9). The predictor-corrector algorithm is executed at .02 hz. during the entire entry phase, although it is practical to run it much more frequently late in the trajectory when the length of the trajectory to be predicted is short. The possible execution rate of the predictor-corrector for a typical flight computer is addressed in Subsection "4.8 Algorithm Execution Time" on page 66.

3.4 CORRECTOR ALGORITHM

The corrector algorithm is executed to update the commanded attitude control history to be flown. The guidance algorithm controls to two final state constraints, downrange error and crossrange error, using two control variables, a constant angle of attack and the intercept of the bank profile at the entry interface velocity as shown in Figure 18 on page 95 and expressed in Eq. (8).

Expanding the downrange and crossrange errors in a Taylor series expansion of the control variables and neglecting the second-order and higher terms yields,

$$\Delta DR_e = \frac{\partial DR_e}{\partial \alpha_d} \Delta \alpha_d + \frac{\partial DR_e}{\partial \phi_d} \Delta \phi_d + \dots \quad (10)$$

$$\Delta CR_e = \frac{\partial CR_e}{\partial \alpha_d} \Delta \alpha_d + \frac{\partial CR_e}{\partial \phi_d} \Delta \phi_d + \dots \quad (11)$$

To intercept the target, the change in the constraint errors must null the predicted errors, or,

$$\Delta DR_e = -DR_e \quad (12)$$

$$\Delta CR_e = -CR_e \quad (13)$$

Equations (10) through (13) provide a set of two simultaneous equations in two unknowns,

$$\begin{bmatrix} \frac{\partial DR_e}{\partial \alpha_d} & \frac{\partial DR_e}{\partial \phi_d} \\ \frac{\partial CR_e}{\partial \alpha_d} & \frac{\partial CR_e}{\partial \phi_d} \end{bmatrix} \begin{bmatrix} \Delta \alpha_d \\ \Delta \phi_d \end{bmatrix} = \begin{bmatrix} -DR_e \\ -CR_e \end{bmatrix} \quad (14)$$

which are solved for the control variable changes required,

$$\Delta \alpha_d = (\frac{\partial DR_e}{\partial \phi_d} CR_e - \frac{\partial CR_e}{\partial \phi_d} DR_e) / \det \quad (15)$$

$$\Delta \phi_d = (\frac{\partial CR_e}{\partial \alpha_d} DR_e - \frac{\partial DR_e}{\partial \alpha_d} CR_e) / \det \quad (16)$$

where \det is the determinant of the matrix in Eq. (14). The partial derivatives are approximated by finite difference equations of the form,

$$\frac{\partial DR_e}{\partial \phi_d} = \frac{DR_e(\phi_d = \phi_3) - DR_e(\phi_d = \phi_1)}{\phi_3 - \phi_1} \quad (17)$$

There are four partial derivatives that must be evaluated. They can be evaluated from three predicted trajectories with control histories selected as:

1. $\alpha_1 = \alpha'_d, \quad \phi_1 = \phi'_d$
2. $\alpha_2 = \alpha'_d + \delta\alpha_d, \quad \phi_2 = \phi'_d$
3. $\alpha_3 = \alpha'_d, \quad \phi_3 = \phi'_d + \delta\phi_d$

where the primes denote the control variables from the previous guidance solution. The new guidance commands are then,

$$\alpha_d = \alpha'_d + \Delta\alpha_d \quad (18)$$

$$\phi_d = \phi'_d + \Delta\phi_d \quad (19)$$

Protection must be provided for the case where the determinant in Eq. (15) and (16) is small or identically zero which corresponds to a loss of control authority of the control variables over the control constraints. In this case, no change is made to the control variables, and the guidance command from the previous cycle is used. As the vehicle approaches the TAEM interface altitude, the control authority decreases. Large control variable changes become necessary to null the constraint errors in the short flight time remaining. This problem can be avoided in one of two ways. First, the guidance commands can be frozen at a selected point before the termination altitude. For entry guidance, this approach is not preferred because the vehicle still has not landed. Alternatively, the target aim point can be lowered below the TAEM interface altitude point at which TAEM guidance is activated. The decreasing control authority problem is therefore reduced.

For the simulated trajectories in this report, the first approach is employed because it is desired to evaluate guidance performance by considering the dispersions in the final state at the TAEM interface altitude. Because the guidance algorithm controls only the final state and not the intermediate states, it is necessary to target for the point at which the guidance is terminated.

3.5 PREDICTOR ALGORITHM

3.5.1 *Introduction*

The predictor algorithm is a simplified three-degree-of-freedom (3-DOF) trajectory simulator complete with models for those environment and vehicle characteristics necessary to model the translational equations of motion of the vehicle. Because the predictor is computationally intensive, the algorithm must be carefully designed to minimize computation, and the coding of the algorithm in a particular computer language should make use of any language-specific features to reduce computational requirements. Also, because the corrector only utilizes the final state vector errors to correct the control variables, only the accuracy of the predicted final state vector need be considered in selecting those effects to be modeled.

The environmental effects of concern for the long trajectories flown by entry vehicles over large altitude and velocity ranges are:

1. Variation of atmospheric properties with altitude
2. Earth oblateness effect on gravity vector
3. Effect of atmospheric rotation with Earth on relative velocity vector
4. Movement of runway due to Earth rotation

The vehicle characteristics of importance are:

1. Vehicle mass
2. Aerodynamic coefficient variation with flight regime
3. Aerodynamic coefficient variation with angle of attack
4. Control history during trajectory

Dispersions to be considered are:

1. Vehicle mass variation from nominal
2. Winds
3. Atmospheric density variation from nominal atmosphere
4. Aerodynamic coefficient variation from nominal

These dispersions can be measured in-flight because they affect the sensed acceleration measured by the vehicle's inertial navigation system. The estimation of these dispersions is discussed in Subsection "3.6 Estimators" on page 48.

The predictor performs the following computations upon being called by the corrector with a desired control variable history:

1. Initialize the predictor state to the navigated state vector
2. Compute any ancillary parameters from the state vector
3. Compute the total acceleration vector from the predictor state vector and the environment and vehicle models using the control variable profiles specified by the corrector
4. Integrate the equations of motion forward in time one time step
5. Check the predictor termination conditions
 - a. Repeat steps 3 and 4 if the conditions are not met
 - b. Continue on to step 6 if the conditions are met
6. Compute and return to the corrector the final predicted state errors from the target state vector and the predicted final state vector

3.5.2 Equations of Motion

The corrector provides a time-homogeneous navigated state vector comprised of,

1. The GMT time tag of the state vector, t_{GMT}
2. The inertial position vector, \vec{R}_i
3. The inertial velocity vector, \vec{V}_i

Also provided is the control variable history to be followed for the prediction. The equations of motion to be integrated are,

$$\frac{d \vec{R}_I}{d t} = \vec{V}_I \quad (20)$$

$$\frac{d \vec{V}_I}{d t} = \vec{A}_I \quad (21)$$

The acceleration is computed from the atmosphere and vehicle models as follows,

$$\vec{A}_I = \frac{\vec{F}_I}{m} = \vec{g}_I + \vec{a}_{aero} \quad (22)$$

The gravitational acceleration, \vec{g}_I , is computed including the J_2 term as,

$$\vec{g}_I = -\frac{\mu}{|\vec{R}_I|^2} \vec{i}_g \quad (23)$$

where,

$$\vec{i}_g = \vec{i}_R + \frac{3}{2} J_2 \frac{R_{equator}^2}{|\vec{R}_I|^2} ((1 - 5 z^2) \vec{i}_R + 2 z \vec{i}_{pole}) \quad (24)$$

and,

$$z = \vec{i}_R \cdot \vec{i}_{pole} \quad (25)$$

The aerodynamic acceleration, \vec{a}_{aero} , is computed from,

$$\vec{a}_{aero} = a_{lift} \vec{i}_{lift} + a_{drag} \vec{i}_{drag} \quad (26)$$

where,

$$a_{lift} = \frac{C_L \bar{q} S}{m} \quad (27)$$

$$a_{drag} = \frac{C_D \bar{q} S}{m} \quad (28)$$

$$\bar{q} = \frac{1}{2} \rho V_R^2 \quad (29)$$

$$V_R^2 = \vec{V}_R \cdot \vec{V}_R \quad (30)$$

$$\vec{V}_R = \vec{V}_I - \vec{\omega}_{earth} \times \vec{R}_I \quad (31)$$

$$\vec{i}_{drag} = -\frac{\vec{V}_R}{|V_R|} \quad (32)$$

$$\vec{i}_{lift} = (\vec{i}_{drag} \times \vec{i}_{lat}) \cos(\phi) + \vec{i}_{lat} \sin(\phi) \quad (33)$$

$$\vec{i}_{lat} = \frac{\vec{i}_R \times \vec{i}_{drag}}{|\vec{i}_R \times \vec{i}_{drag}|} \quad (34)$$

$$\vec{i}_R = \frac{\vec{R}_I}{|R_I|} \quad (35)$$

The acceleration due to lift, a_{lift} , is more easily computed from,

$$a_{lift} = \frac{L}{D} a_{drag} \quad (36)$$

since the nominal lift-to-drag ratio, L/D, is corrected using in-flight accelerometer measurements of the actual vehicle sensed aerodynamic accelerations.

The atmospheric density, ρ , is computed by the atmosphere model using the position vector, \vec{R}_I . The 1962 U.S. Standard Atmosphere model is employed and is described in Reference [16]. If another atmosphere model is selected as being a more accurate estimate of the day-of-flight atmosphere, this model would replace the 1962 U.S. Standard Atmosphere model. An operational vehicle might employ monthly or seasonal atmospheres from such

sources as the GRAM Atmosphere [9] or even day-of-flight measurements to more accurately model the expected atmosphere in the predictions. The level of accuracy required in the atmosphere model will depend on the vehicle ranging capability and the amount of that capability to be used for a particular entry. Entries to the edges of the footprint will demand a very accurate atmosphere model.

The aerodynamic coefficients are highly vehicle dependent. To minimize computational requirements, they should be updated during the prediction as infrequently as possible. Of course, the update frequency required depends on the trajectory flown and the rate of change of the aerodynamic coefficients with flight regime change. The aerodynamic coefficient model for the ERV is presented in "Appendix A. ERV AERODYNAMICS MODEL" on page 133.

The density, ρ , from the atmosphere model and the lift-to-drag ratio, L/D, from the aerodynamic model are both corrected by in-flight measurements as covered in Subsection "3.6 Estimators" on page 48. The estimated dispersions are compensated for using the following equations,

$$\rho = K_\rho \rho_{std} \quad (37)$$

$$\frac{L}{D} = K_{\frac{L}{D}} \left(\frac{C_L}{C_D} \right)_{nom} \quad (38)$$

where the density and lift-to-drag ratio scale factors, K_ρ and $K_{\frac{L}{D}}$, are provided by the estimator and are held constant throughout the prediction being made.

The control history to be followed is the constant angle of attack, α_d , and the linear bank angle with velocity, ϕ . The latter is computed from,

$$\phi = \phi_d \frac{V_i - V_f}{V_{EI} - V_f} \quad (39)$$

where ϕ_d is the intercept of the linear bank angle profile at the entry interface velocity, V_{EI} . Because the entry interface and final velocities are not known a priori, and because small variations in them have little effect on the predicted trajectory compared with the selected control variables' values, the velocities are selected as constant values that cover all expected dispersions in the entry and final velocities. These values are,

$$V_{EI} = 26,000 \text{ ft/sec}$$

$$V_f = 1,000 \text{ ft/sec}$$

3.5.3 Integration of the Equations of Motion

The equations of motion are integrated using the 4th order Runge-Kutta algorithm with a variable time step to minimize the number of time steps required to integrate the trajectory to the final state. The 4th order Runge-Kutta algorithm requires four evaluations of the acceleration per time step, but permits a time step more than four times as large as an algorithm requiring only one acceleration evaluation per time step. The Runge-Kutta solution [17] for the differential equations of motion of the form,

$$\frac{d \vec{R}_i}{d t} = \vec{v}_i \quad (40)$$

$$\frac{d \vec{v}_i}{d t} = f(t, \vec{R}_i, \vec{v}_i) \quad (41)$$

is,

$$\vec{R}_i(t + \Delta t) = \vec{R}_i(t) + \frac{\Delta t}{6} (\vec{K}_0 + 2\vec{K}_1 + 2\vec{K}_2 + \vec{K}_3) \quad (42)$$

$$\vec{V}_i(t + \Delta t) = \vec{V}_i(t) + \frac{\Delta t}{6} (\vec{K}'_0 + 2\vec{K}'_1 + 2\vec{K}'_2 + \vec{K}'_3) \quad (43)$$

where,

$$\vec{K}_0 = \vec{V}_i \quad (44)$$

$$\vec{K}_1 = (\vec{V}_i + \frac{\vec{K}'_0}{2}) \quad (45)$$

$$\vec{K}_2 = (\vec{V}_i + \frac{\vec{K}'_1}{2}) \quad (46)$$

$$\vec{K}_3 = (\vec{V}_i + \vec{K}'_2) \quad (47)$$

$$\vec{K}'_0 = f(t, \vec{R}_i, \vec{V}_i) \quad (48)$$

$$\vec{K}'_1 = f(t + \frac{\Delta t}{2}, \vec{R}_i + \Delta t \frac{\vec{K}_0}{2}, \vec{V}_i + \Delta t \frac{\vec{K}'_0}{2}) \quad (49)$$

$$\vec{K}'_2 = f(t + \frac{\Delta t}{2}, \vec{R}_i + \Delta t \frac{\vec{K}_1}{2}, \vec{V}_i + \Delta t \frac{\vec{K}'_1}{2}) \quad (50)$$

$$\vec{K}'_3 = f(t + \Delta t, \vec{R}_i + \Delta t \vec{K}_2, \vec{V}_i + \Delta t \vec{K}'_2) \quad (51)$$

The time step is varied inversely with the total acceleration on the vehicle. This method of time step control was selected because of its simplicity. The time step control equation is of the form,

$$\Delta t = \frac{K_{\Delta t}}{|\vec{A}_i|} \quad (52)$$

and the time step is limited between a minimum and maximum value,

$$\Delta t = \text{midval}(\Delta t_{\min}, \Delta t, \Delta t_{\max}) \quad (53)$$

The optimization of the integration algorithm is important in developing a flight quality algorithm, but is beyond the scope of this study. Higher-order integration algorithms with time step control methods [17] may yield significant reductions in the required computation time.

3.5.4 Termination Conditions for the Predictor

After each integration time step, the predicted state is compared with the termination condition. The termination condition is defined by the altitude of TAEM interface (80K feet). Because the predicted state at the TAEM interface altitude may have a relatively large altitude rate and range rate, the predictor must be terminated accurately to provide an altitude-homogeneous set of predicted state errors. Also, the variable time step control may allow large integration time steps if the acceleration is low near the final state, further complicating the task of terminating accurately. Reasonable altitude homogeneity is ensured by forcing use of the minimum integration time step starting some safe altitude above the termination altitude.

3.5.5 Final State Error Computation

The final state errors are computed from the unit target vector and the predicted final state vector. Because the target is fixed to the Earth and moves a significant distance dur-

ing the long entry trajectory, the rotation of the Earth must be considered. This is done by transforming the final state vector from inertial to Earth-fixed coordinates with the rotation matrix M_i^{EF} which is computed from the predicted termination time, the known orientation of the Earth at some epoch time, and the known rotation rate of the Earth. This computation is performed in the Earth-Fixed-From-Reference subroutine of the predictor-corrector which may actually be a GN&C utility function also employed by the navigation principal function.

The downrange and crossrange errors are defined as shown in Figure 19 on page 96. The errors are computed by first computing the downrange (in-plane) and crossrange (perpendicular) directions as follows,

$$\vec{R}_i^{EF} = \hat{M}_i^{EF} \vec{R}_i^I \quad (54)$$

$$\vec{i}_R^{EF} = \frac{\vec{R}_i^{EF}}{|\vec{R}_i^{EF}|} \quad (55)$$

$$\vec{V}_R^{EF} = \hat{M}_i^{EF} \vec{V}_i^I \quad (56)$$

$$\vec{i}_{perpen}^{EF} = \frac{\vec{i}_R^{EF} \times \vec{V}_R^{EF}}{|\vec{i}_R^{EF} \times \vec{V}_R^{EF}|} \quad (57)$$

$$\vec{i}_{inplane}^{EF} = \frac{\vec{i}_t^{EF} - (\vec{i}_t^{EF} \cdot \vec{i}_{perpen}^{EF}) \vec{i}_{perpen}^{EF}}{|\vec{i}_t^{EF} - (\vec{i}_t^{EF} \cdot \vec{i}_{perpen}^{EF}) \vec{i}_{perpen}^{EF}|} \quad (58)$$

The downrange and crossrange errors are then,

$$DR_e = R_{equator} \cos^{-1}(\vec{i}_R^{EF} \times \vec{i}_{inplane}^{EF}) \operatorname{sign}((\vec{i}_R^{EF} \times \vec{i}_{inplane}^{EF}) \cdot \vec{i}_{perpen}^{EF}) \quad (59)$$

$$CR_e = R_{equator} \cos^{-1}(\vec{i}_{inplane}^{EF} \cdot \vec{i}_t^{EF}) \operatorname{sign}((\vec{i}_{inplane}^{EF} \times \vec{i}_t^{EF}) \cdot (\vec{i}_{perpen}^{EF} \times \vec{i}_{inplane}^{EF})) \quad (60)$$

These errors have the dimensions of $R_{equator}$ and are converted to nautical miles for ease of interpretation.

3.5.6 Algorithm Coding

A few comments regarding implementation of the predictor are appropriate. The computations required to update the aerodynamic coefficients are the major computational load for the predictor. It was found that it is not necessary to update the aerodynamics on each of the four acceleration evaluations of the 4th order Runge-Kutta algorithm. They are therefore only evaluated once each integration time step. The computational load could be reduced further if they are only updated when the independent variables (altitude, viscous interaction parameter, and Mach Number) change by a significant amount from the previous update. Also, although not done in this implementation, the aerodynamic coefficients should be curve-fit if possible to avoid a table lookup and interpolation implementation. It is noted in Figures 20 on page 97 and 21 on page 98 that the aerodynamic coefficients do not change very much below 300K feet until the Mach Number decreases below 2, so perhaps, two tables or curve-fits would suffice instead of the thirty tables currently used.

3.6 ESTIMATORS

The final state predicted by the predictor algorithm for a particular control history is a function of the assumed environment and vehicle characteristics. The accuracy of the predicted final state can be increased, and hence, the guidance margin increased, if in-flight

measurements are utilized to make the assumed models more accurately reflect the conditions actually experienced by the vehicle.

The accelerations modeled in the predictor are due to gravity and the aerodynamic forces. The gravity acceleration can be modeled to sufficient accuracy using standard gravity models. However, the aerodynamic accelerations are subject to significant variations due to uncertainties in the atmospheric density, atmospheric winds, vehicle aerodynamics, and vehicle mass. These uncertainties can be compensated for in the predictor by applying a multiplicative scale factor to the lift and drag accelerations modeled in the predictor that is equal to the ratio of the actual accelerations experienced to the predicted accelerations at any point in the trajectory.

The measured lift and drag accelerations are derived from the inertial measurement system sensed acceleration assuming a zero sideslip angle as follows,

$$\hat{a}_{drag} = -\vec{a}_i \cdot \frac{\vec{V}_R}{|\vec{V}_R|} \quad (61)$$

$$\hat{a}_{lift} = \sqrt{\vec{a}_i \cdot \vec{a}_i - \hat{a}_{drag}^2} \quad (62)$$

where the inertial acceleration, \vec{a}_i , is computed by back-differencing the accumulated sensed velocity counts from the inertial measurement unit,

$$\vec{a}_i = \frac{\vec{V}_i^{imu} - \vec{V}_i^{imu past}}{\Delta t_{imu}} \quad (63)$$

In the predictor, the aerodynamic accelerations are,

$$a_{drag} = \frac{C_D S}{m} \frac{1}{2} \rho V_R^2 \quad (64)$$

$$a_{lift} = \frac{L}{D} a_{drag} \quad (65)$$

Data from the Shuttle program [10] shows that the primary dispersion affecting the aerodynamic acceleration is in the atmospheric density. Further, over large altitude ranges, this dispersion can be modeled to an accuracy sufficient for the prediction process as a constant multiplicative bias. Therefore, for implementational purposes, the dispersion in the aerodynamic accelerations due to the atmospheric uncertainties will be lumped into a density scale factor as follows,

$$K_\rho = \frac{\hat{\rho}}{\rho_{std}} \quad (66)$$

where,

$$\hat{\rho} = \frac{2 \hat{a}_{drag}}{V_R^2} \left(\frac{m}{C_D S} \right)_{nom} \quad (67)$$

and the values for the nominal vehicle characteristics and the nominal atmospheric density are determined using the predictor models for the vehicle state at the time of the measurement. Because the nominal ballistic coefficient is assumed in deriving the measured density, and the measured acceleration is due to the actual ballistic coefficient, uncertainties in the ballistic coefficient will be reflected in the measured density. The equation for the drag acceleration in the predictor is then,

$$a_{drag} = \left(\frac{C_D S}{m} \right)_{nom} \frac{1}{2} V_R^2 K_\rho \rho_{std} \quad (68)$$

or substituting for K_ρ from Eq. (66) yields,

$$a_{drag} = \left(\frac{C_D S}{m} \right)_{nom} \frac{1}{2} V_R^2 \hat{\rho} \quad (69)$$

Substituting for $\hat{\rho}$ from Eq. (67) then yields,

$$a_{drag} = \hat{a}_{drag} \quad (70)$$

so the modeled drag is corrected for the dispersed drag coefficient, density, relative velocity, and vehicle mass.

In general, the measured drag acceleration is a noisy signal and will exhibit short term variations due to short lived local atmospheric dispersions [10]. Filtering of the density scale factor is therefore necessary and is implemented using a first-order filter,

$$K_p = (1 - K_1) K_p + K_1 \frac{\hat{\rho}}{\rho_{std}} \quad (71)$$

which has a time constant, τ_p , of,

$$\tau_p = -\frac{\Delta t}{\ln(1 - K_1)} \quad (72)$$

where Δt is the sample rate of the measured drag acceleration, and K_1 is the filter gain. A similar lift-to-drag ratio scale factor is derived and applied to the lift acceleration,

$$a_{lift} = K_{\frac{L}{D}} \left(\frac{L}{D} \right)_{nom} a_{drag} \quad (73)$$

where,

$$K_{\frac{L}{D}} = \frac{\left(\frac{\hat{L}}{D} \right)}{\left(\frac{L}{D} \right)_{nom}} \quad (74)$$

and,

$$\left(\frac{\hat{L}}{D}\right) = \frac{\hat{a}_{lit}}{\hat{a}_{drag}} \quad (75)$$

Again, filtering is necessary,

$$K_{\frac{L}{D}} = (1 - K_2) K_{\frac{L}{D}} + K_2 \frac{\left(\frac{\hat{L}}{D}\right)}{\left(\frac{L}{D}\right)_{nom}} \quad (76)$$

yielding a time constant, $\tau_{\frac{L}{D}}$, of,

$$\tau_{\frac{L}{D}} = -\frac{\Delta t}{\ln(1 - K_2)} \quad (77)$$

A time constant of 25 seconds was selected for both the density and L/D filters. This value filtered out the high frequency density shear components seen in the Shuttle profiles while still providing adequate response to long term disturbances.

3.7 HEAT RATE CONTROL

The primary trajectory constraint on entry vehicles is the maximum heat rate the vehicle can withstand. In general, the thermal protection system material is selected to withstand

the maximum local heat rate on any particular portion of the vehicle, and the material thickness is selected to withstand the total integrated heat load over the trajectory. Accurate pre-flight predictions of the expected heat rate during entry can significantly reduce the thermal protection system weight yielding significant performance increases for an entire mission.

Inspecting the reference trajectories in Figure 16 on page 93 shows that sharp peaks in the heat rate occur. If these peaks are accurately controlled, and this control can be accomplished using only short term departures from the predictor assumed control history, no significant departure will occur from the desired trajectory.

Heat rate control can be accomplished using either angle of attack, bank angle, or a combination of both. Of these, bank angle alone is preferred because a constant angle of attack trajectory is assumed and because angle of attack changes the vehicle drag coefficient resulting in a rapid change in energy rate and a rapid departure from the desired trajectory. Also, most entry vehicles restrict the angle of attack range during maximum heat rate regions to reduce the area on the vehicle that must be protected from the high heat rate. Although the ERV does not need to restrict the angle of attack range, and hence, the guidance does not provide for such a capability, the restriction can be handled by replacing the constant angle of attack control history by a reference angle of attack control history about which a constant angle of attack bias is applied for control.

Heat rate control is accomplished by computing the incremental bank angle required to fly along the specified heat rate boundary (assumed to be a constant heat rate for any flight regime) and then modulating bank angle according to the guidance value or the guidance value plus the incremental lift for heat rate control, whichever requires more lift up. Hence, no effort is made to pull the vehicle down into the atmosphere to follow the heat rate bound-

ary; instead, lift up is applied if the vehicle is flying "too low". The incremental lift for heat rate control is computed to provide a second-order control response as follows,

$$\cos(\Delta\phi) = \frac{K_{\ddot{Q}}}{\bar{q}} (\ddot{Q} - \dot{Q}_{des}) + \frac{K_{\dot{Q}}}{\bar{q}} (\dot{Q} - \dot{Q}_{lim}) \quad (78)$$

To fly along a constant heat rate boundary,

$$\dot{Q}_{lim} = \text{constant} \quad (79)$$

and the desired rate of change of heat rate, \ddot{Q}_{des} , is,

$$\ddot{Q}_{des} = 0 \quad (80)$$

so,

$$\cos(\Delta\phi) = \frac{K_{\ddot{Q}}}{\bar{q}} \ddot{Q} + \frac{K_{\dot{Q}}}{\bar{q}} (\dot{Q} - \dot{Q}_{lim}) \quad (81)$$

The stagnation heat rate is determined using the Engineering Correlation Formula [18] for a one foot radius reference sphere as,

$$\dot{Q} = 17700 \sqrt{\rho} \left(\frac{V_R}{10000} \right)^{3.05} \quad (82)$$

The time rate of change of heat rate, \ddot{Q} , is determined by back-differencing the heat rate between guidance cycles,

$$\ddot{Q} = \frac{\dot{Q} - \dot{Q}_{past}}{\Delta t} \quad (83)$$

The equations of motion assuming small flight path angle yield,

$$\ddot{h} = \frac{C_L \bar{q} S}{m} \cos(\phi) - g \quad (84)$$

Considering only the perturbations due to the incremental lift, $\cos(\Delta\phi)$, from Eq. (81) yields,

$$\ddot{h} - \frac{C_L S}{m} K_{\dot{Q}} \ddot{Q} + K_Q (\dot{Q} - Q_{lim}) = 0 \quad (85)$$

Proper selection of the gains $K_{\dot{Q}}$ and K_Q is accomplished by linearizing Eq. (85) in altitude and assuming that the time rate of change of V_R is small compared to the change in $\sqrt{\rho}$.

With these assumptions,

$$\dot{Q} = 17700 \left(\frac{V_R}{10000} \right)^{3.05} \frac{d\sqrt{\rho}}{dh} h \quad (86)$$

and,

$$\ddot{Q} = 17700 \left(\frac{V_R}{10000} \right)^{3.05} \frac{d\sqrt{\rho}}{dh} \frac{dh}{dt} \quad (87)$$

Therefore, the homogeneous second-order differential equation in altitude is,

$$\ddot{h} + K K_{\ddot{Q}} \dot{h} + K K_{\dot{Q}} h = 0 \quad (88)$$

where,

$$K = - \frac{C_L S}{m} 17700 \left(\frac{V_R}{10000} \right)^{3.05} \frac{d\sqrt{\rho}}{dh} \quad (89)$$

The natural frequency and damping ratio of the second-order differential equation are,

$$\omega_n = \sqrt{K K_{\dot{Q}}} \quad (90)$$

$$\zeta = \frac{K K_{\ddot{Q}}}{2 \omega_n} \quad (91)$$

or alternatively, for a desired natural frequency and damping ratio, $K_{\dot{Q}}$ and $K_{\ddot{Q}}$ are selected as,

$$K_Q = \frac{\omega_n^2}{K} \quad (92)$$

$$K_{\ddot{Q}} = \frac{2 \zeta \omega_n}{K} \quad (93)$$

The derivative in Eq. (89) can be evaluated assuming an exponential atmosphere of the form,

$$\rho = \rho_{sl} e^{-(h/h_s)} \quad (94)$$

yielding,

$$\frac{d\sqrt{\rho}}{dh} = -\frac{\sqrt{\rho_{sl}}}{2h_s} e^{-(h/2h_s)} \quad (95)$$

This logic is contained in the guidance algorithm in the Heat Rate Control subroutine. The incremental lift required for heat rate control is provided to the Attitude Command subroutine which adds it into the guidance command if it requires more lift up than the guidance command. This occurs when the incremental lift given by Eq. (81) is greater than zero,

$$\cos(\Delta\phi) > 0 \quad (96)$$

Appropriate values of the natural frequency and damping ratio were determined parametrically as,

$$\omega_n = 0.10 \frac{\text{rad}}{\text{sec}} \quad (97)$$

$$\zeta = 1.00 \quad (98)$$

4.0 PERFORMANCE

4.1 SIMULATOR

Open-loop and closed-loop entry trajectories were simulated for the Entry Research Vehicle (ERV) using a derivative of the 6-DOF Aeroassist Flight Experiment Simulator (AFES-IM) [19] developed at The Charles Stark Draper Laboratory which is coded in the HAL computer language. For this study, the aerodynamic model described in “Appendix A. ERV AERODYNAMICS MODEL” on page 133 and the wind model shown in Figure 2 on page 79 were incorporated into the AFESIM. The characteristics of the ERV [14] are listed in Table 1 on page 73. The entry conditions with which all trajectories were initialized are also listed in Table 1 on page 73. Because only the performance characteristics of the guidance were being evaluated, the simulator was operated in the 3-DOF mode.

4.2 OPEN-LOOP FOOTPRINT

Open-loop trajectories were run using the constant angle of attack and linear bank with velocity profiles to determine the portion of the footprint achievable. All trajectories were terminated at the TAEM interface altitude of 80K feet, so the footprint can be increased about 100 nautical miles in all directions due to the range flown below 80K feet.

Figure 22 on page 99 shows the lift-to-drag ratio, L/D, for the ERV at Mach 10 versus angle of attack, α . It is seen that maximum L/D is obtained at an angle of attack of 15 degrees. It is desirable to fly on the back side of the L/D curve (angle of attack greater than 15 degrees) so as to maximize the drag coefficient for a given L/D. This reduces heating by causing a quicker loss of velocity early in entry than flying at the same L/D on the front side of the L/D curve. The L/D versus angle of attack curve shows the same shape with the maximum L/D at 15 degrees for all flight regimes with only a variation in the magnitude of L/D across the angle of attack range. Therefore, angle of attack is modulated between 15 and 50 degrees for the footprint with 15 degrees corresponding to maximum L/D and 50 degrees corresponding to minimum L/D.

The open-loop footprint is shown in Figure 23 on page 100. Also shown for comparison is the reported footprint for a heat load limit of 175K BTU/sq ft (shown earlier in Figure 12 on page 89). That footprint included the range flown below 80K feet, hence the slight differences. It is seen that almost the entire reportedly achievable footprint is captured with the assumed control profile. Most importantly, all of the maximum crossrange region is reached when the range flown below 80K feet is included. Also, most of the minimum downrange region of the footprint was captured even though the control profiles used do not correspond to the optimal profiles determined using POST and shown in Figures 14 on page 91 and 15 on page 92. Additionally, the footprint reported in Reference [14] does not include the large area in the minimum downrange region that the open-loop trajectories reached. The small area not reached in the minimum downrange region by the control profiles is relatively unimportant because the downrange ranging capability of the vehicle can be adjusted by changing the deorbit time. A vehicle in low earth orbit travels at about four nautical miles per second, so downrange is easily adjusted while on-orbit.

Because the predictor-corrector guidance algorithm will follow the same control histories as used to generate the open-loop footprint for a nominal trajectory, the guidance algorithm can reach all of the open-loop footprint for nominal conditions. It is seen that the achievable footprint is bounded by the heat rate and heat load limits imposed on the ERV. At least an additional 2000 nautical miles of ranging capability in the downrange direction exists if the heat limits are relaxed.

4.3 EFFECT OF DISPERSIONS ON FOOTPRINT

The effect of dispersions on the achievable footprint was determined by repeating the open-loop trajectories with the dispersions discussed in Subsection "2.2 Dispersions" on page 26. The worst-case (3σ) dispersions are summarized in Table 2 on page 73. Table 3 on page 74 shows the dispersions in downrange and crossrange for three of the control histories in the maximum downrange region of the footprint. It is seen that only variations in the lift and drag coefficients cause significant dispersions in the final state. Also, it is seen that the effect of a +10% C_L dispersion is the same as that of a -10% C_D dispersion. This is expected because both dispersions cause the same increase in the vehicle L/D. The same occurs for a -10% C_L dispersion and a +10% C_D dispersion, both of which decrease the vehicle L/D.

The effects of the dispersions on trajectories to the maximum crossrange region of the footprint are seen in Table 4 on page 75. Again, it is seen that aerodynamic dispersions have the greatest effect. A dispersion that increases L/D increases the range, while a dispersion that decreases L/D decreases the range.

Table 5 on page 76 shows the effects of the dispersions on the minimum downrange region of the footprint. The worst-case range dispersions again occur for the aerodynamic dispersions.

4.4 ESTIMATOR PERFORMANCE

Figure 24 on page 101 shows the time response of the density filter with a 25 second time constant for the STS-9 atmosphere. This trajectory also has dispersions of +1.9% in C_D , -3.2% in mass, and a 63.8% crosswind. Therefore, the filter output does not follow the actual density dispersion also shown in the figure. When the acceleration level is below 0.07 g's, the measurements are not incorporated, so the filter is inactive before 300 seconds and from 600 to 850 seconds. As the velocity drops, the wind becomes a greater contributor to the measured density error, hence the divergence in the measured density ratio starting at 1000 seconds. Figure 25 on page 102 shows the response of the L/D filter with a 25 second time constant for a -1.9% C_L and a +1.9% C_D dispersion. Again, the winds affect the measurement by creating errors in the navigated angle of attack, so the estimated L/D ratio is slightly in error.

The use of an air data system like the Shuttle Entry Air Data System (SEADS) could significantly improve the estimation process by providing accurate estimates of the angle of attack, atmospheric density, and wind magnitude and direction. More accurate estimates will increase the guidance margin, thereby increasing the achievable footprint for dispersed trajectories.

4.5 CLOSED-LOOP PERFORMANCE

Based on the results of the open-loop trajectories with dispersions, worst-case dispersions were selected for each of three regions of the footprint: maximum downrange, maximum crossrange, and minimum downrange. Closed-loop trajectories with the predictor-corrector guidance algorithm were then run to the three regions of the footprint. The three target points selected for the closed-loop performance evaluation are shown in Figure 23 on page 100. The 3σ errors defined in Table 2 on page 73 were scaled such that the total error due to multiple error sources would still represent a 3σ dispersion so as to test the guidance system for reasonably probable dispersion cases [20]. To run all dispersions at their 3σ levels would be unrealistic.

The nominal and dispersed results for trajectories to each of the three regions are listed in Tables 6 on page 77 through 8 on page 77. Plots of selected parameters from these cases are included. Figures 26 on page 103 through 31 on page 108 present the altitude, velocity, heat rate, heat load, downrange, and crossrange time histories for the nominal maximum downrange trajectory. Figures 32 on page 109 through 37 on page 114 present the altitude, velocity, heat rate, heat load, downrange, and crossrange time histories for the nominal maximum crossrange trajectory. Figures 38 on page 115 through 43 on page 120 present the altitude, velocity, heat rate, heat load, downrange, and crossrange time histories for the nominal minimum downrange trajectory. In each of these cases, it is seen that the heat rate does not approach the heat rate limit, so no incremental bank angle is needed for heat rate control.

The control histories for the nominal maximum downrange trajectory and the dispersed case listed second in Table 6 on page 77 are presented in Figure 44 on page 121 and

Figure 45 on page 122. Figure 44 shows the angle of attack histories for the nominal and dispersed maximum downrange cases. It is seen that a two degree change in angle of attack is required early in the trajectory increasing to four degrees by the end of the trajectory. Figure 45 shows the bank angle histories for the nominal and dispersed maximum downrange cases. The bank angle required shows no change from zero degrees for this case.

The control histories for the nominal maximum crossrange trajectory and the dispersed case listed second in Table 7 on page 77 are presented in Figure 46 on page 123 and Figure 47 on page 124. Again, it is seen that a four degree change in angle of attack is required for the dispersed case. The bank angle history shows no change for the dispersed case from that of the nominal case.

The control histories for the nominal minimum downrange trajectory and the dispersed case listed second in Table 8 on page 77 are presented in Figure 48 on page 125 and Figure 49 on page 126. For this case, approximately a one degree change in angle of attack is required. No change is required in the bank angle profile.

The required change in angle of attack for each of the dispersed cases shown was primarily due to the change in the vehicle L/D as this was shown to be the primary dispersion source in Subsection "4.3 Effect of Dispersions on Footprint" on page 59. The breaking point of the guidance occurs when the vehicle does not have enough L/D range to overcome the loss in L/D due to aerodynamic dispersions. As mentioned previously, the Shuttle entry guidance algorithm was required to guide to the TAEM interface aim point to within 2.5 nautical miles of position. The results presented for the nominal and dispersed cases show that this requirement is met with the predictor-corrector guidance algorithm. Also, the trajectory plots show that the algorithm achieves this performance with very infrequent guidance

updates (.02 hz.) and with very small control variable changes from the nominal constant angle of attack and linear bank with velocity profiles. Most importantly, almost all of the achievable footprint is captured using the predictor-corrector algorithm.

4.6 HEAT RATE CONTROL PERFORMANCE

The closed-loop trajectories shown previously did not require heat rate control because the maximum heat rate experienced was significantly lower than the limit imposed on the ERV. The time responses for bank angle, angle of attack, and heat rate for the beginning of a typical trajectory with and without heat rate control are shown in Figures 50 on page 127 through 52 on page 129. The resulting bank angle versus velocity profile is shown in Figure 53 on page 130. These trajectories are for the middle of the footprint where the peak heat rate does not exceed the limit for the ERV. Therefore, for illustrative purposes, the heat rate limit was reduced to 100 BTU/sq ft/sec. Comparing the trajectories with and without heat rate control, it is seen that the heat rate control takes place over a fairly long time range, but requires a significant departure from the linear bank profile over only a very short velocity range. The impact on the trajectory is therefore small, and the predictor-corrector stays converged on almost the same control history even though the vehicle does not follow the assumed control profile during the heat rate control area.

4.7 OVERCONTROL

For those trajectories not at the edge of the footprint, excess vehicle capability exists that can be utilized to increase guidance margin for dispersions that may occur later in the trajectory. For example, a 13,800 nautical mile downrange trajectory for the ERV only requires flying at 20 degrees angle of attack instead of 15 degrees for the nominal trajectory. The ERV can modulate angle of attack between 15 degrees (maximum L/D) and 50 degrees (minimum L/D) on the back side of the L/D curve, so the modulation capability is not equally centered about the commanded angle of attack if flying at 20 degrees. By flying at 15 degrees (maximum L/D) early in the trajectory, guidance can center the remaining guidance capability equally about the aim point to cover dispersions in all directions, not just those that require less L/D to reach the target point. This approach is referred to here as overcontrol or command biasing.

Overcontrol can be implemented in several ways. First, the command can be biased from the desired command when that command is not in the center of the modulation range. As the vehicle flies a biased angle of attack, for example, the predicted final state will differ from that for the unbiased command in such a direction that the next guidance command will be moved in the direction opposite to the bias. By biasing in the proper direction, the command can be driven toward the center of the modulation range. If the guidance requires an L/D higher than that in the middle of the L/D range, flying at an even higher L/D will drive the required L/D toward the middle. Secondly, the target aim point can be moved from the nominal aim point early in the entry. For example, for a trajectory to the maximum downrange region of the footprint, the target aim point can be moved even farther downrange. Of course, at some point in the trajectory, the aim point must be moved back to the desired point.

The first approach was implemented in the predictor-corrector algorithm by biasing the angle of attack by five degrees when it was more than two degrees away from 30 degrees. The biasing was terminated at an inertial velocity of 13,500 feet per second so as to allow the guidance to fly the proper control history near the end of the trajectory to reach the target aim point.

Figure 54 on page 131 compares the angle of attack control history for a 13,760 nautical mile downrange trajectory with the dispersions used for the closed-loop trajectories shown earlier. Without overcontrol, the vehicle misses the target aim point by 19.20 nautical miles. This occurs because the wind contribution to the dispersion increases as the vehicle velocity drops, so the multiplicative scale factor on density does not properly model this dispersion. As the wind contribution increases, a higher L/D is required, and the angle of attack is driven to 15 degrees or maximum L/D. Because maximum L/D was not utilized earlier in the trajectory, the vehicle did not reach the target. Late in the trajectory, the predictor-corrector goes un converged as control authority is exhausted, causing the angle of attack to jump between 15 and 30 degrees. By this point, the target aim point was unreachable anyway due to the dispersions.

With command biasing, the commanded angle of attack early in the trajectory is that corresponding to maximum L/D or 15 degrees. It is seen that biasing drives the commanded angle of attack to 25 degrees once the biasing is terminated at a velocity of 13,500 feet per second or a time of 3,700 seconds. Later, when the wind dispersion drives the angle of attack toward 15 degrees, there is significant margin remaining, and the angle of attack is only driven to 24.5 degrees by the dispersion. With command biasing, the miss distance at TAEM interface is only 0.27 nautical miles. Therefore, guidance margin is increased by using overcontrol. More of the theoretically achievable footprint is attainable for dispersed

cases. An even larger magnitude dispersion could have been handled late in the trajectory since the angle of attack was not driven to that for maximum L/D.

Further work is needed in this area to determine the proper way to utilize overcontrol to maximize guidance margin for the expected dispersions. The probability of the various dispersions occurring and the histories of those dispersions along a trajectory must be considered. For example, if a "thick" atmosphere is encountered early in the trajectory equal to the worst-case expected dispersion, it is highly unlikely that the atmosphere will get "thicker" later in the trajectory. Therefore, it is unnecessary to preserve guidance margin in the direction needed to cover a "thicker" atmosphere beyond that already required for the expected worst-case atmosphere. Such considerations should be taken into account in the design of the overcontrol algorithm.

4.8 ALGORITHM EXECUTION TIME

An estimate of the execution time required for the predictor-corrector algorithm was made using the execution time estimate feature of the HAL compiler. The estimate is for the AP101 Shuttle flight computer. Figure 55 on page 132 shows the execution time required in seconds as a function of the time to the TAEM interface point for a maximum downrange trajectory. It is seen that early in the entry when the trajectory to be predicted is long, the predictor requires 43.7 seconds of CPU time. When only 500 seconds to the TAEM interface point remains, the required time drops to 4.5 seconds. This figure can also be interpreted as the minimum update interval for the predictor-corrector. Also, the guidance command will be computed and sent to the vehicle autopilot a period of time after the start of the guidance

cycle equal to the required execution time. It is seen that early in the entry, a significant delay occurs between the start of the guidance cycle and the computation of the guidance command. This delay was not simulated in the closed-loop trajectories, but will have a minimal effect on the guidance margin because the guidance is not trying to fly a reference trajectory like the analytic guidance algorithms. The predictor-corrector is numerically computing a trajectory that will fly directly to the target aim point. Any error that builds up between the start of the guidance cycle and the issuing of the guidance command can be nulled easily since the entry is long, and the error will shrink as the delay decreases with decreasing time to the TAEM interface point.

The Shuttle AP101 CPU is the product of early 1970's technology and is significantly slower than flight computers that might be employed in future entry vehicles. The 80C86 CPU for example is two to five times faster than the AP101 CPU, so the execution time required shown in Figure 55 on page 132 can be scaled down by a factor of two to five. Computers utilizing parallel processing architecture could predict the three required trajectories simultaneously in three CPUs, cutting the required execution time by a factor of three. If scaled by a factor of four due to the faster CPU and a factor of three due to parallel processing architecture, the maximum time required drops to 3.6 seconds, and the time with 500 seconds remaining to the TAEM interface point drops to 0.4 seconds. The predictor-corrector is therefore a viable guidance scheme for future entry vehicles.

5.0 FUTURE RESEARCH TOPICS AND CONCLUSIONS

5.1 FUTURE RESEARCH TOPICS

Several topics for further algorithm development and optimization are discussed. These are:

1. Further reductions in CPU execution time
2. Use of an air data system for in-flight measurements
3. Use of overcontrol to increase guidance margin
4. Control of more than two state constraints

Optimization of the predictor algorithm and the integration scheme can yield significant reductions in execution time beyond that already attained. Simplifying the aerodynamic model can yield a great reduction in execution time and an equally important reduction in the computer core required. The current model has 30 tables, each with 51 breakpoints over the angle of attack range. A curve fit of the aerodynamic coefficients over the angle of attack range and the flow regimes would reduce the core required to store the model data and the computations required for each lookup.

The estimator algorithm was shown to be effective in determining the dispersions from in-flight measurements. However, the estimator is unable to differentiate between density dispersions and atmospheric winds. Figure 24 on page 101 showed that the multiplicative density scale factor did not accurately model the wind contribution to the drag acceleration because the relative contribution of the wind to the dispersion increases as the vehicle

PRECEDING PAGE BLANK NOT FILMED

velocity drops late in the trajectory. An air data system could provide an independent measurement of the atmospheric winds, improving the estimation process and increasing guidance margin by increasing the accuracy of the predicted trajectories.

The concept of overcontrol was introduced and shown to be effective for at least one dispersed case. Further investigations should be made to determine how much overcontrol is optimal for the expected dispersions. It may be possible to use the sensitivities of the constraints to the control variables to determine a proper amount of command biasing for any particular dispersion at any point in the trajectory.

Only the downrange error and crossrange error at TAEM interface are controlled in the current design. The vehicle energy is not controlled which can allow significant dispersions in the ranging capability during the TAEM phase of entry. Approaches include redefining the TAEM aim point in terms of a desired energy level or utilizing a third control variable to provide control over an energy level constraint. The Space Shuttle makes use of a split rudder as a speedbrake to provide a large energy control capability. Such an approach could be utilized with the predictor-corrector by computing the sensitivity of the three constraints to the three control variables. This would require four predictions instead of the three currently needed, but the fourth prediction could be made only during the latter part of entry to clean up any dispersions in energy level that occur during the entry due to dispersions. The CPU execution time would then increase by one-third-over that currently projected when the third constraint is controlled.

5.2 CONCLUSIONS

A predictor-corrector entry guidance algorithm has been demonstrated that exhibits excellent performance and almost complete coverage of the achievable footprint. This algorithm employs a simple control variable history to achieve near-optimal guidance for the maximum downrange and maximum crossrange trajectories. Explicit heat rate control is employed without significantly impacting the achievable footprint. This is achieved because unlike previous guidance algorithms that included a long heat rate control phase with no active targeting, the proposed algorithm always actively targets to the aim point and only controls heat rate in the short high heat rate regions as required.

The algorithm has been demonstrated to handle atmospheric and aerodynamic dispersions within the capability of the vehicle. The required computer execution time is shown to be within the capability of new flight computers.

Algorithm adaptability is provided through the utilization of in-flight measurements to improve the accuracy of the predicted trajectory. Algorithm maintenance is simplified because there are no reference trajectories used, and there are a minimum of vehicle/mission-specific input parameters (I-loads). Transportability of the algorithm between different entry vehicles is provided by eliminating vehicle-specific entry phases other than the heat rate control phase which only requires the input of a heat rate limit. The guidance algorithm does require a vehicle aerodynamic model, but this is developed in the normal vehicle definition phase anyway.

In summary, an entry guidance algorithm has been developed that achieves near-optimal performance while maximizing flexibility, adaptability, and transportability. Although

more computationally intensive than analytic algorithms, execution of the predictor-corrector is within the capability of current flight computers. It is hoped that this guidance approach will significantly reduce the development and maintenance costs for new entry guidance systems.

Table 1. Characteristics of the ERV and Trajectory Entry Conditions

Mass	186.0	slugs
Reference area	177.6	sq ft
Mean Aerodynamic Chord	25.0	ft
Altitude	400,000.0	ft
Inertial Velocity	25,778.843	ft/sec
Flight Path Angle	-0.996	deg
Inclination	28.50	deg
Latitude	-28.071	deg
Longitude	-69.313	deg
Vacuum Apogee	150.0	n.m.
Vacuum Perigee	20.0	n.m.

Table 2. Dispersions Used in Performance Study

Dispersion	Symbol	Magnitude (%)	Direction (deg)
<hr/>			
Aerodynamics			
Lift Coefficient	CL^+ CL^-	+ 10% - 10%	
<hr/>			
Drag Coefficient	CD^+ CD^-	+ 10% - 10%	
<hr/>			
Vehicle Properties			
Mass	M^+ M^-	+ 5% - 5%	
<hr/>			
Atmospheric Properties			
Density	ρ^+ ρ^-	+ 30% - 30%	
<hr/>			
Tailwind	TW	99%	61.5 deg
Positive Crosswind	CW^+	99%	151.5 deg
Headwind	HW	99%	241.5 deg
Negative Crosswind	CW^-	99%	331.5 deg

Table 3. Dispersed Cases for Maximum Downrange Region

α_d (deg)	ϕ_d (deg)	Dispersion	Downrange (n.m.)	Crossrange (n.m.)
15	0	NOMINAL	14817	497
15	0	CL+	16445	456
15	0	CL-	13229	420
15	0	CD+	13242	422
15	0	CD-	16810	427
15	0	M ⁺	14890	498
15	0	M ⁻	14739	496
15	0	ρ^+	14615	494
15	0	ρ^-	15089	498
15	0	TW	14882	498
15	0	CW ⁺	14829	497
15	0	HW	14751	496
15	0	CW ⁻	14802	497
20	0	NOMINAL	13849	463
20	0	CL ⁺	15388	499
20	0	CL ⁻	12355	344
20	0	CD ⁺	12384	347
20	0	CD ⁻	15711	491
20	0	M ⁺	13909	466
20	0	M ⁻	13785	460
20	0	ρ^+	13659	453
20	0	ρ^-	14105	475
20	0	TW	13901	466
20	0	CW ⁺	13857	464
20	0	HW	13796	461
20	0	CW ⁻	13838	463
25	0	NOMINAL	12116	321
25	0	CL ⁺	13415	439
25	0	CL ⁻	10822	178
25	0	CD ⁺	10858	183
25	0	CD ⁻	13715	456
25	0	M ⁺	13161	325
25	0	M ⁻	12068	316
25	0	ρ^+	11950	305
25	0	ρ^-	12339	342
25	0	TW	12155	324
25	0	CW ⁺	12121	321
25	0	HW	12076	317
25	0	CW ⁻	12108	320

Table 4. Dispersed Cases for Maximum Crossrange Region

α_d (deg)	ϕ_d (deg)	Dispersion	Downrange (n.m.)	Crossrange (n.m.)
15	60	NOMINAL	8308	1822
15	60	CL+	9035	2149
15	60	CL-	7602	1506
15	60	CD+	7605	1531
15	60	CD-	9200	2193
15	60	M+	8342	1825
15	60	M-	8271	1819
15	60	ρ^+	8197	1823
15	60	ρ^-	8465	1820
15	60	TW	8260	1737
15	60	CW+	8473	1890
15	60	HW	8313	1866
15	60	CW-	7984	1692
20	60	NOMINAL	7791	1661
20	60	CL+	8476	1966
20	60	CL-	7125	1370
20	60	CD+	7132	1392
20	60	CD-	8622	2007
20	60	M+	7820	1664
20	60	M-	7761	1659
20	60	ρ^+	7689	1662
20	60	ρ^-	7934	1660
20	60	TW	7766	1607
20	60	CW+	7846	1686
20	60	HW	7775	1673
20	60	CW-	7580	1572
25	60	NOMINAL	6940	1344
25	60	CL+	7539	1602
25	60	CL-	6355	1100
25	60	CD+	6363	1119
25	60	CD-	7661	1635
25	60	M+	6963	1345
25	60	M-	6915	1342
25	60	ρ^+	6848	1344
25	60	ρ^-	7070	1342
25	60	TW	6933	1317
25	60	CW+	6958	1355
25	60	HW	6921	1347
25	60	CW-	6819	1290

Table 5. Dispersed Cases for Minimum Downrange Region

α_d (deg)	ϕ_d (deg)	Dispersion	Downrange (n.m.)	Crossrange (n.m.)
30	90	NOMINAL	2982	938
30	90	CL+	3014	1102
30	90	CL-	2934	778
30	90	CD+	2914	793
30	90	CD-	3045	1119
30	90	M+	2996	937
30	90	M-	2969	938
30	90	ρ^+	2914	943
30	90	ρ^-	3078	930
30	90	TW	2993	914
30	90	CW+	2992	941
30	90	HW	2996	939
30	90	CW-	2982	907
30	80	NOMINAL	3851	1041
30	80	CL+	4011	1233
30	80	CL-	3680	858
30	80	CD+	3668	875
30	80	CD-	4060	1254
30	80	M+	3865	1041
30	80	M-	3865	1041
30	80	ρ^+	3778	1046
30	80	ρ^-	3954	1034
30	80	TW	3856	1020
30	80	CW+	3841	1044
30	80	HW	3834	1042
30	80	CW-	3828	1007
30	70	NOMINAL	4932	1075
30	70	CL+	5262	1279
30	70	CL-	4602	881
30	70	CD+	4600	898
30	70	CD-	5337	1304
30	70	M+	4949	1075
30	70	M-	4915	1075
30	70	ρ^+	4854	1078
30	70	ρ^-	5043	1069
30	70	TW	4934	1057
30	70	CW+	4925	1077
30	70	HW	4914	1074
30	70	CW-	4884	1040

Table 6. Maximum Downrange Region Closed-Loop Results

Dispersions					Final State		
CL (%)	CD (%)	Mass (%)	ρ (%)	Wind (%)	ϕ_g (deg)	λ (deg)	Error (n.m.)
TARGET POINT					+ 9.800	+ 144.700	-
NOMINAL					+ 9.799	+ 144.702	0.13
- 1.9	+ 1.9	- 3.2	+ 19.1	63.8 HW	+ 9.799	+ 144.701	0.08
- 1.9	+ 1.9	- 3.2	STS 1	63.8 HW	+ 9.803	+ 144.694	0.30
- 1.9	+ 1.9	- 3.2	STS 9	63.8 HW	+ 9.802	+ 144.696	0.27
- 1.9	+ 1.9	- 3.2	STS11	63.8 HW	+ 9.801	+ 144.698	0.13

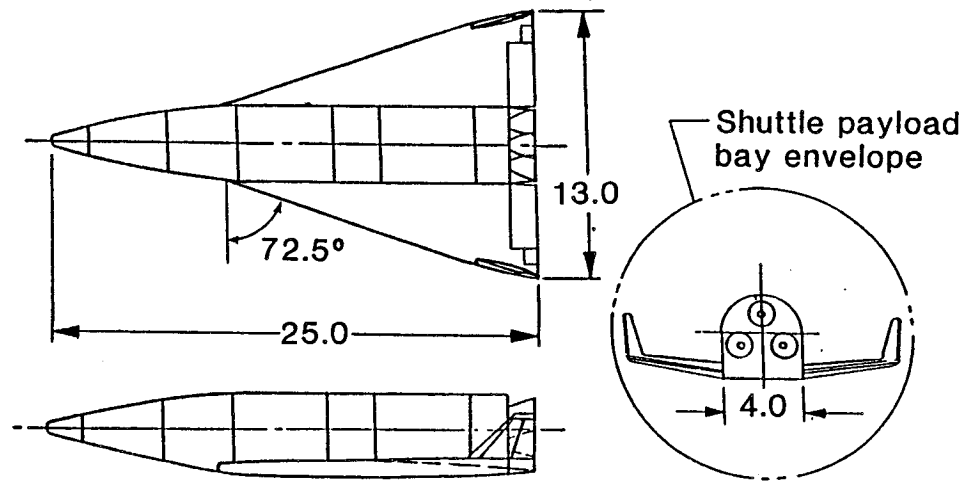
Table 7. Maximum Crossrange Region Closed-Loop Results

Dispersions					Final State		
CL (%)	CD (%)	Mass (%)	ρ (%)	Wind (%)	ϕ_g (deg)	λ (deg)	Error (n.m.)
TARGET POINT					- 2.300	+ 55.000	-
NOMINAL					- 2.301	+ 55.000	0.06
- 1.9	+ 1.9	- 3.2	+ 19.1	63.8 CW-	- 2.295	+ 54.998	0.32
- 1.9	+ 1.9	- 3.2	STS 1	63.8 CW-	- 2.304	+ 55.001	0.25
- 1.9	+ 1.9	- 3.2	STS 9	63.8 CW-	- 2.301	+ 54.990	0.60
- 1.9	+ 1.9	- 3.2	STS11	63.8 CW-	- 2.299	+ 55.000	0.06

Table 8. Minimum Downrange Region Closed-Loop Results

Dispersions					Final State		
CL (%)	CD (%)	Mass (%)	ρ (%)	Wind (%)	ϕ_g (deg)	λ (deg)	Error (n.m.)
TARGET POINT					-14.900	+ 9.800	-
NOMINAL					-14.897	+ 9.798	0.22
+ 1.9	- 1.9	+ 3.2	- 19.1	63.8 TW	-14.902	+ 9.801	0.13
+ 1.9	- 1.9	+ 3.2	STS 1	63.8 TW	-14.901	+ 9.800	0.06
+ 1.9	- 1.9	+ 3.2	STS 9	63.8 TW	-14.900	+ 9.800	0.00
+ 1.9	- 1.9	+ 3.2	STS11	63.8 TW	-14.899	+ 9.799	0.08

Theoretical wing area = 177.40 ft²
Body flap area = 7.50 ft²
Elevon area per side = 6.07 ft²
Aileron area per side = 0.88 ft²
Tip fin area per side = 4.16 ft²

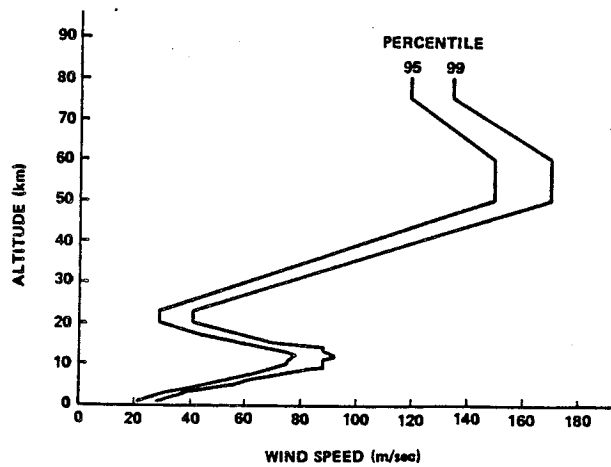


Reproduced from Reference (14)

Figure 1. Three-View Drawing of the ERV

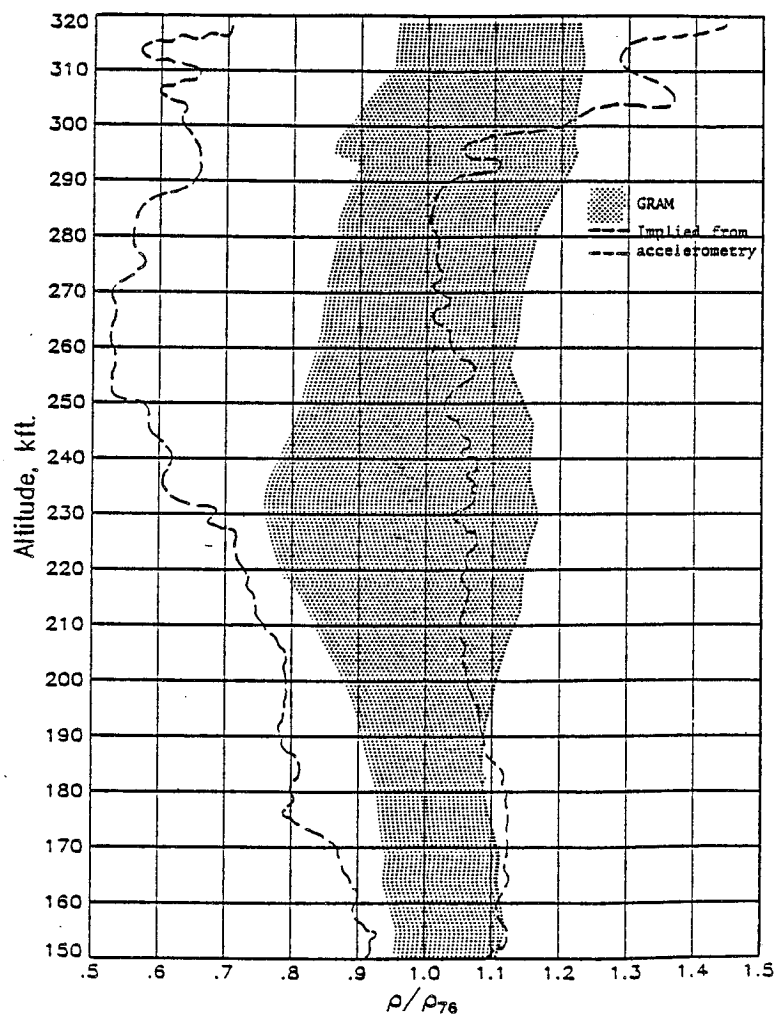
SCALAR WIND SPEED V (m/sec) STEADY-STATE ENVELOPES AS FUNCTIONS
OF ALTITUDE H (km) FOR TWO PROBABILITIES P (%) ENCOMPASSING
ALL FOUR LOCATIONS

P = 95				P = 99			
H	V	H	V	H	V	H	V
1	22	17	44	1	28	15	70
3	31	20	29	3	38	20	41
		23	29	5	56	23	41
6	54	50	150	6	60	50	170
		60	150	7	68	60	170
10	75	75	120	9	88	75	135
11	76	80	120	11	88	80	135
12	78			12	92		
13	74			13	88		
				14	88		



Reproduced from Reference (8)

Figure 2. Atmospheric Wind Profile



Reproduced from Reference (10)

Figure 3. Envelope of Density Profiles Derived from Shuttle Flights

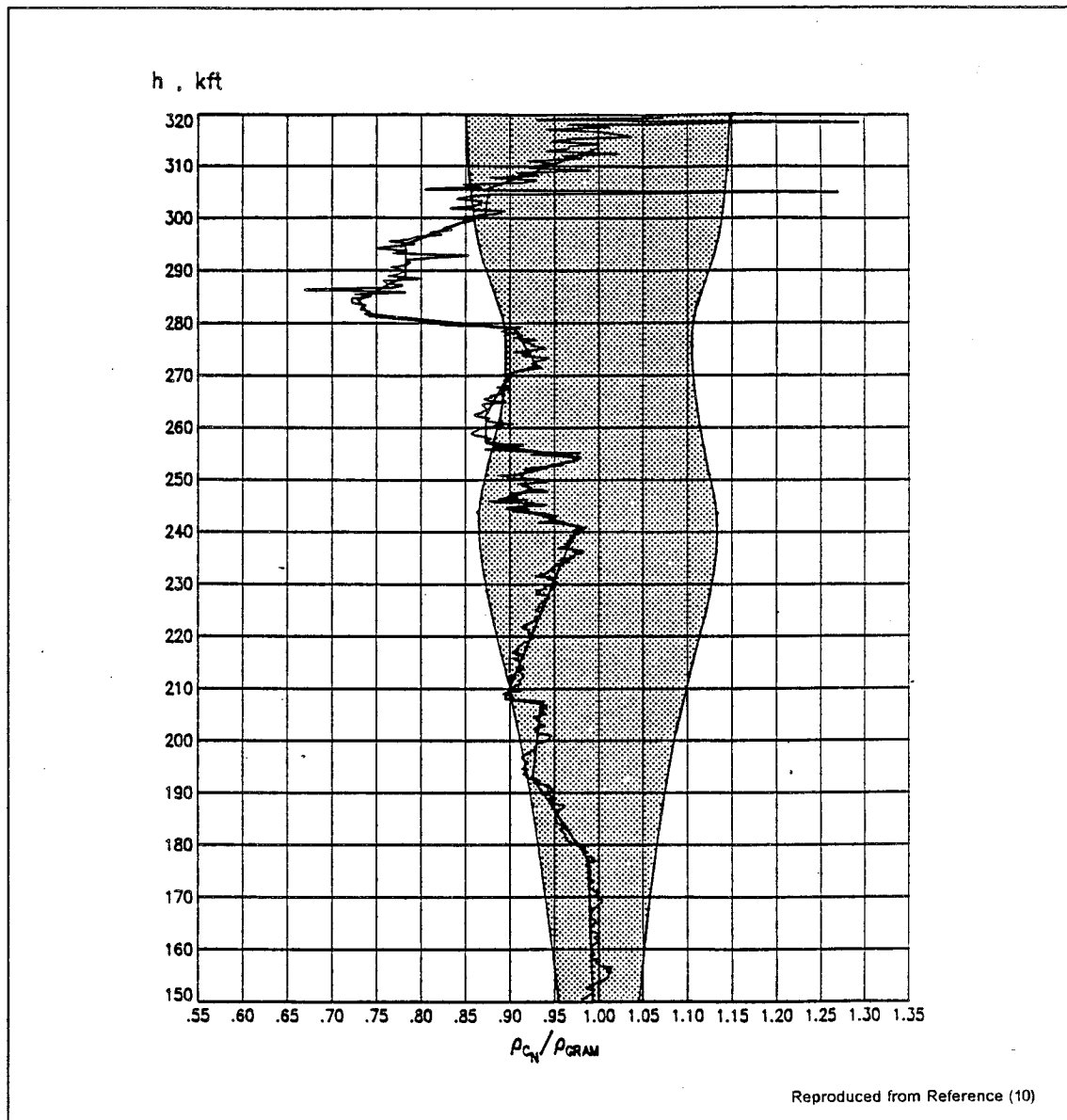


Figure 4. STS-1 Density Profile Comparison

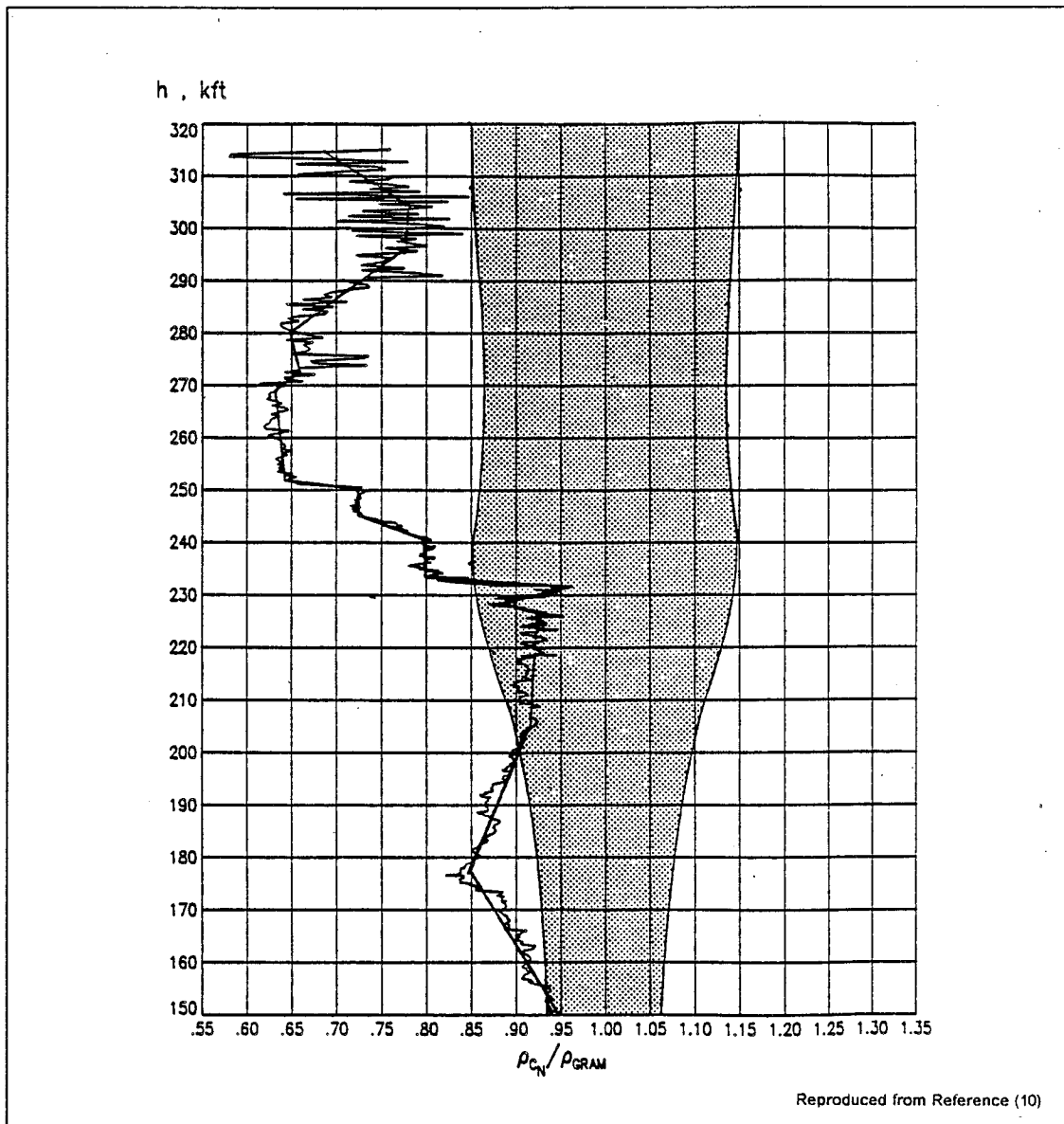
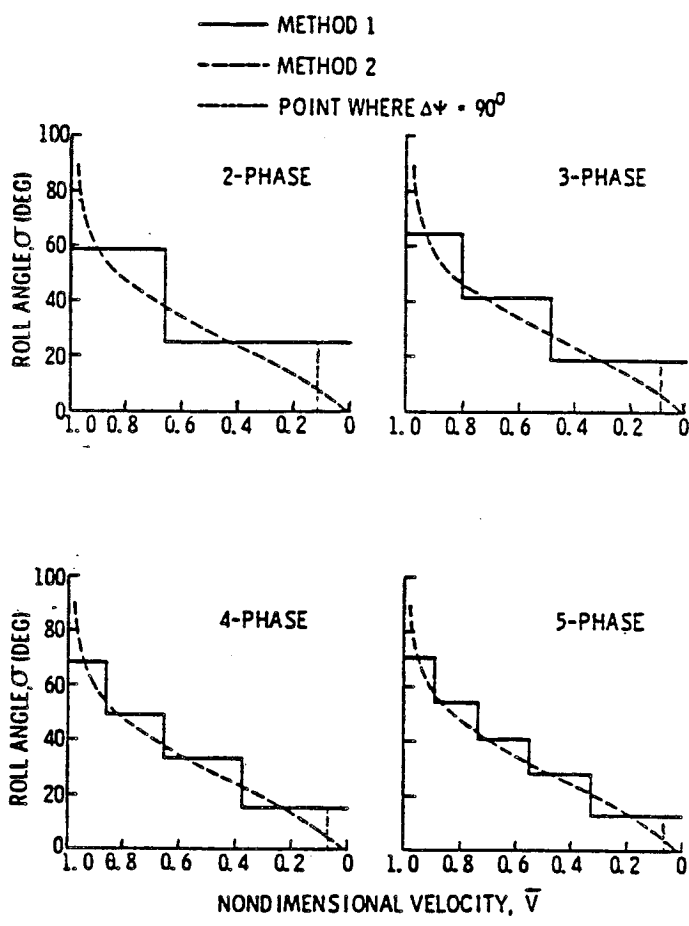


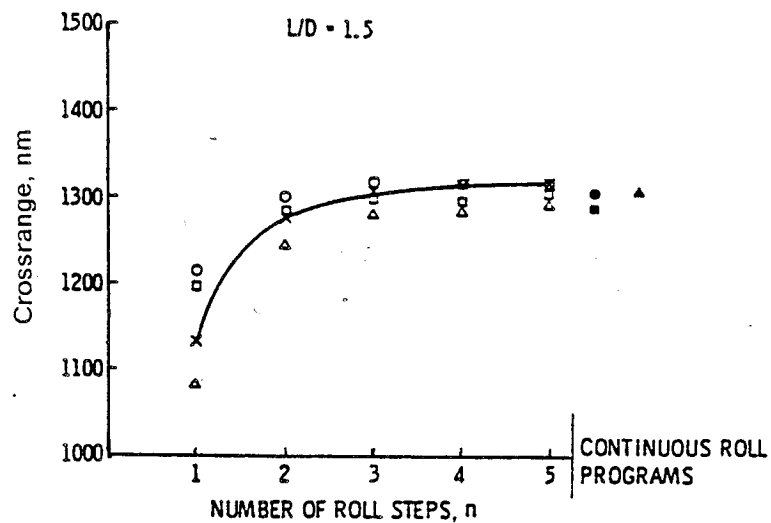
Figure 5. STS-9 Density Profile Comparison



Reproduced from Reference (12)

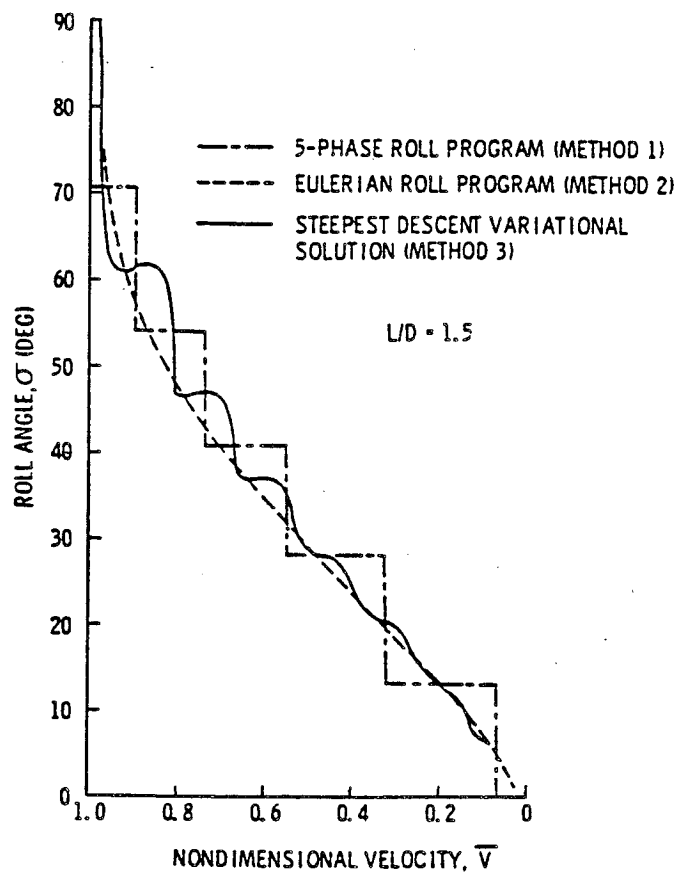
Figure 6. Multiphase Bank Angle Program for $L/D = 1.5$

- * MULTIPHASE ROLL PROGRAM (JACKSON'S EQUATIONS)
 - TO \bar{V} = 0.02 }
 - TO h = 80,000 FT }
 - △ TO ψ = 90° }
 - TO \bar{V} = 0.02 }
 - TO h = 80,000 FT }
 - ▲ TO h = 80,000 FT }
- MULTIPHASE ROLL PROGRAMS SOLVED ON
INTEGRATED TRAJECTORY PROGRAM (METHOD 1)
- EULERIAN ROLL ANGLE FROM SLYE'S
EQUATIONS SOLVED ON INTEGRATED
TRAJECTORY PROGRAM (METHOD 2)
- STEEPEST DESCENT SOLUTION (METHOD 3)



Reproduced from Reference (12)

Figure 7. Crossrange Versus Number of Bank Steps



Reproduced from Reference (12)

Figure 8. Comparison of Optimum Bank Angle Programs

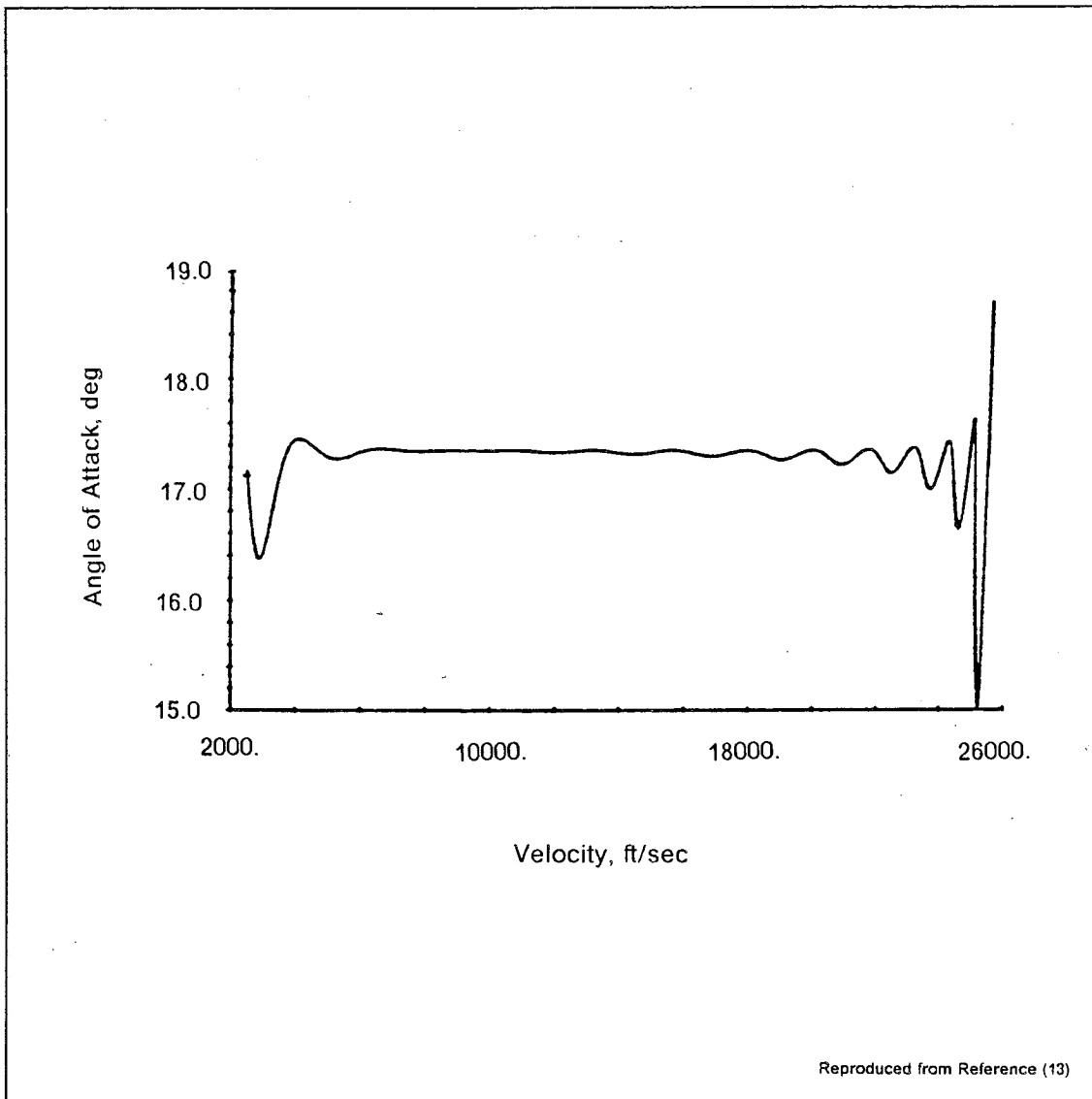


Figure 9. Optimum Shuttle Angle of Attack Profile for Maximum Downrange

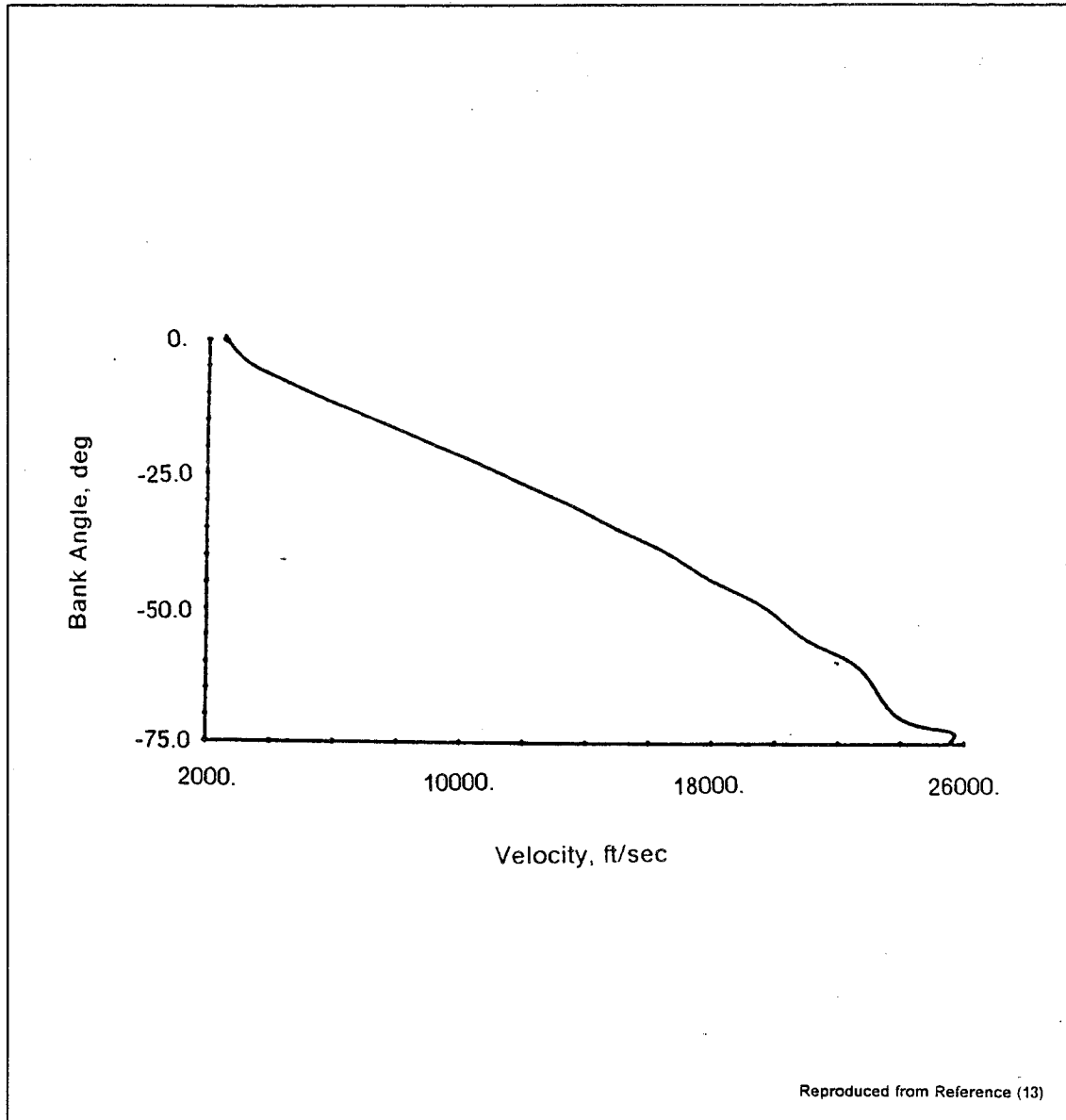


Figure 10. Optimum Shuttle Bank Angle Profile for Maximum Crossrange

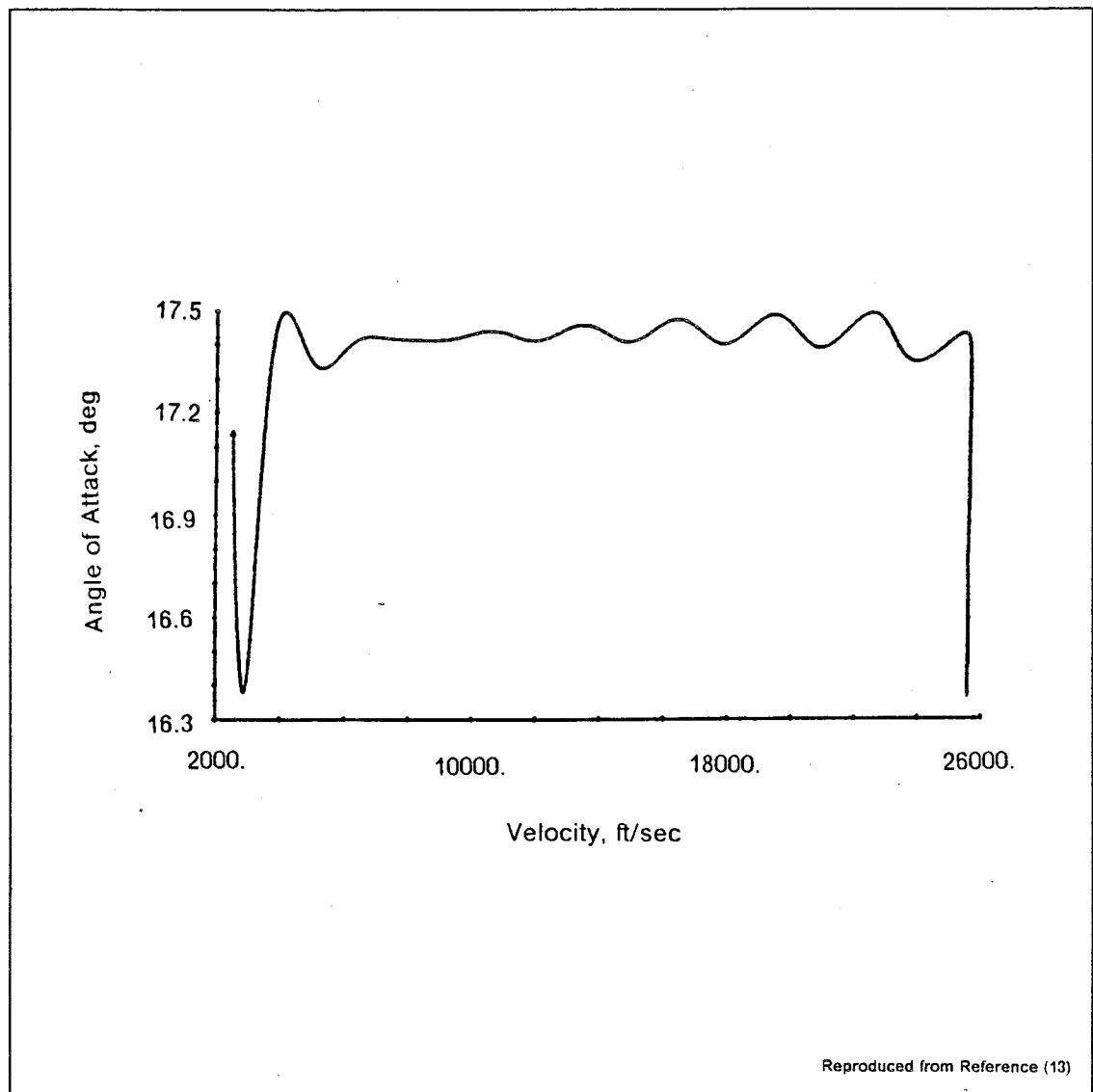
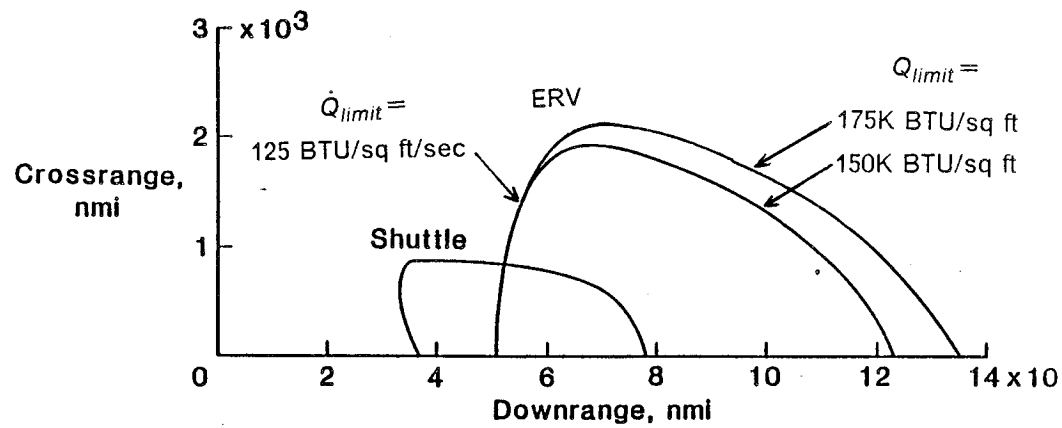
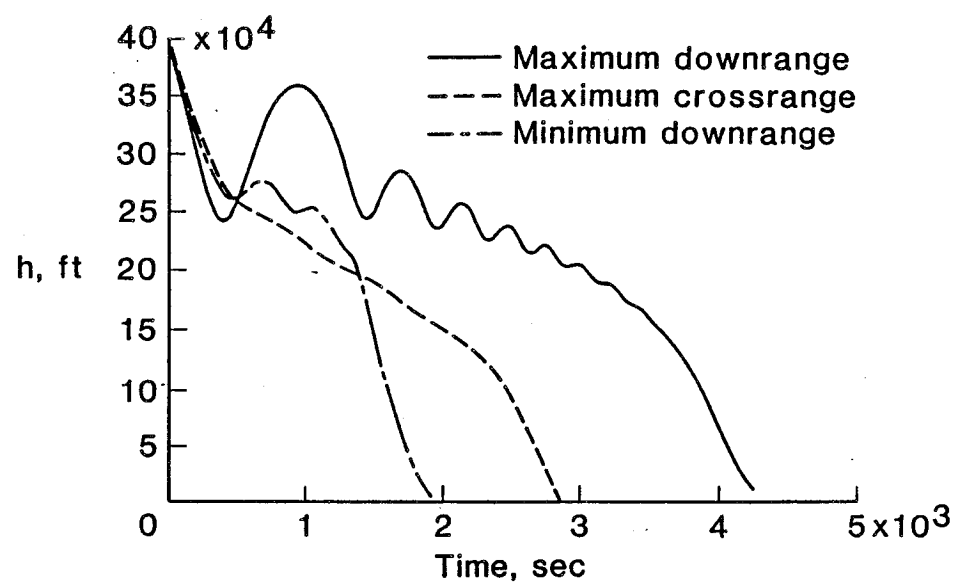


Figure 11. Optimum Shuttle Angle of Attack Profile for Maximum Crossrange



Reproduced from Reference (14)

Figure 12. Landing Footprint for the ERV



Reproduced from Reference (14)

Figure 13. Altitude Histories for the Entry Missions of the ERV

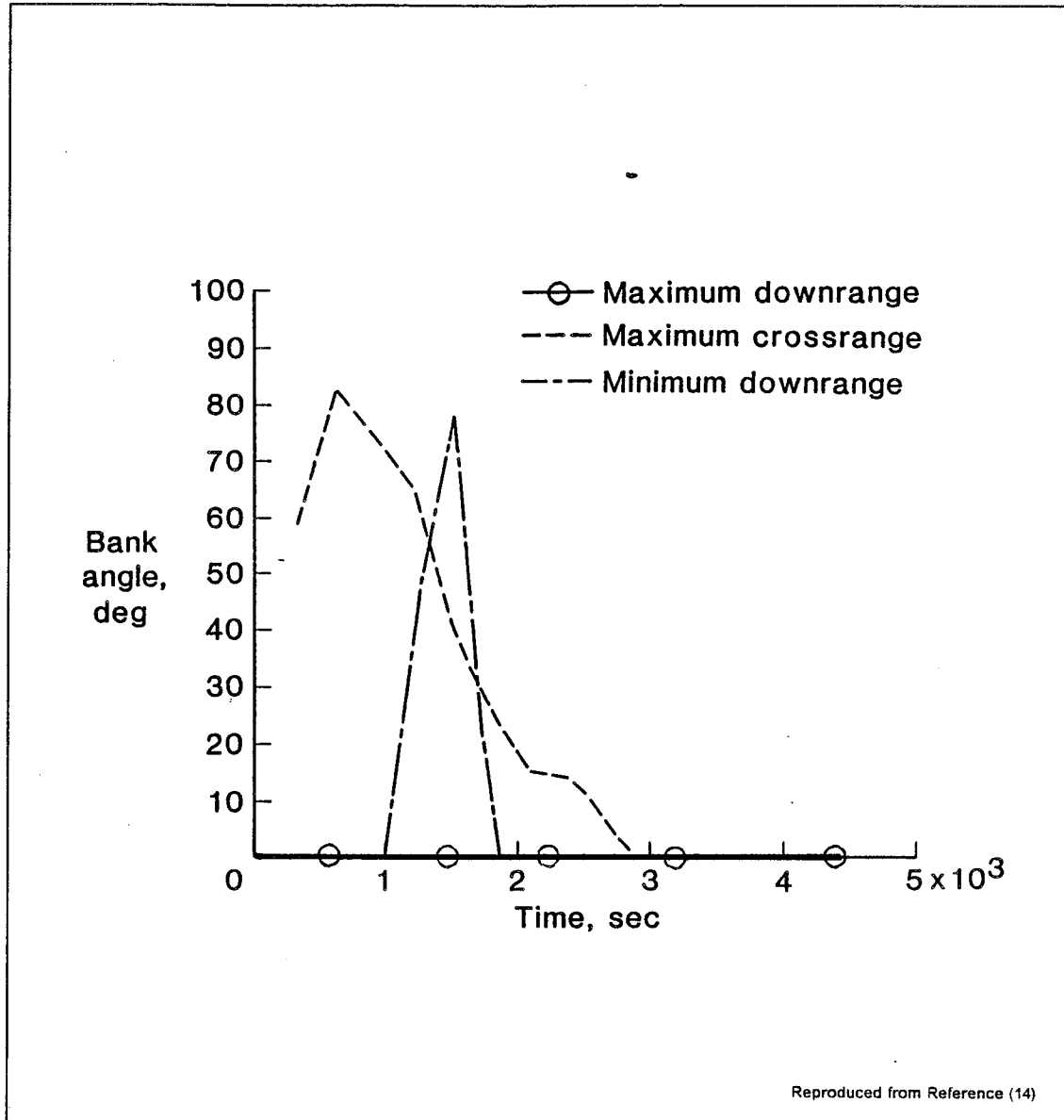


Figure 14. Bank Angle Histories for the Entry Missions of the ERV

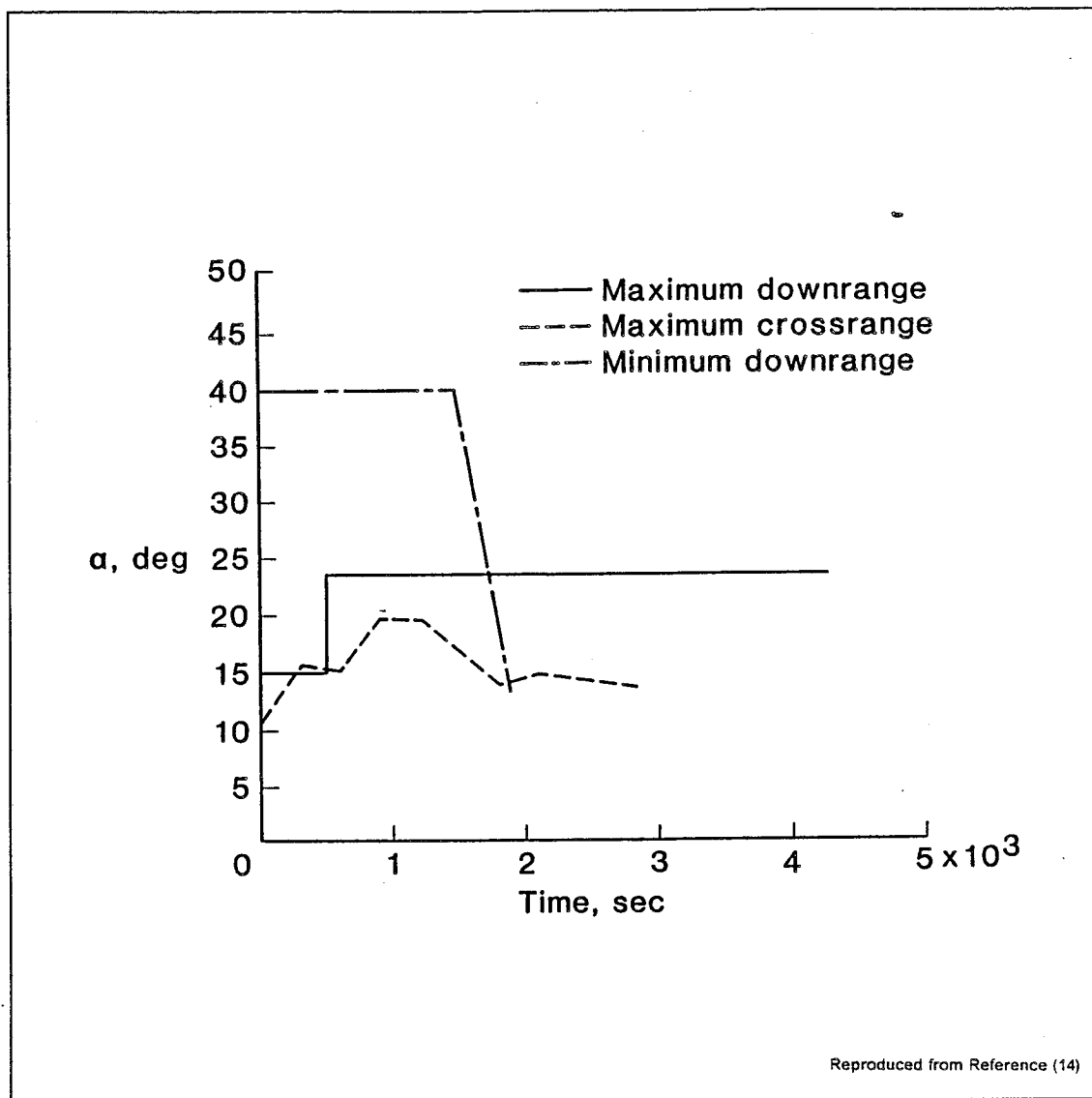


Figure 15. Angle of Attack Histories for the Entry Missions of the ERV

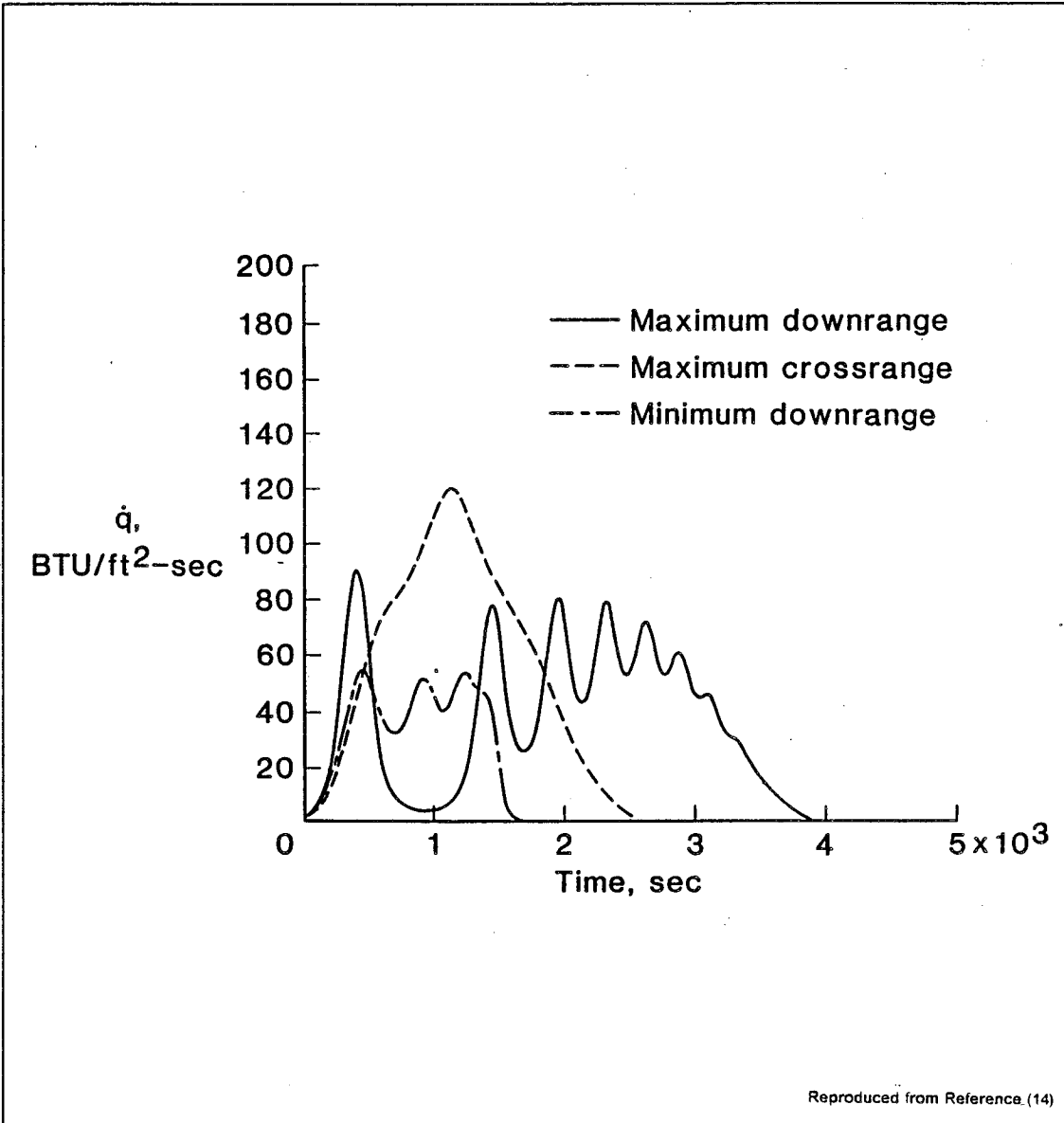
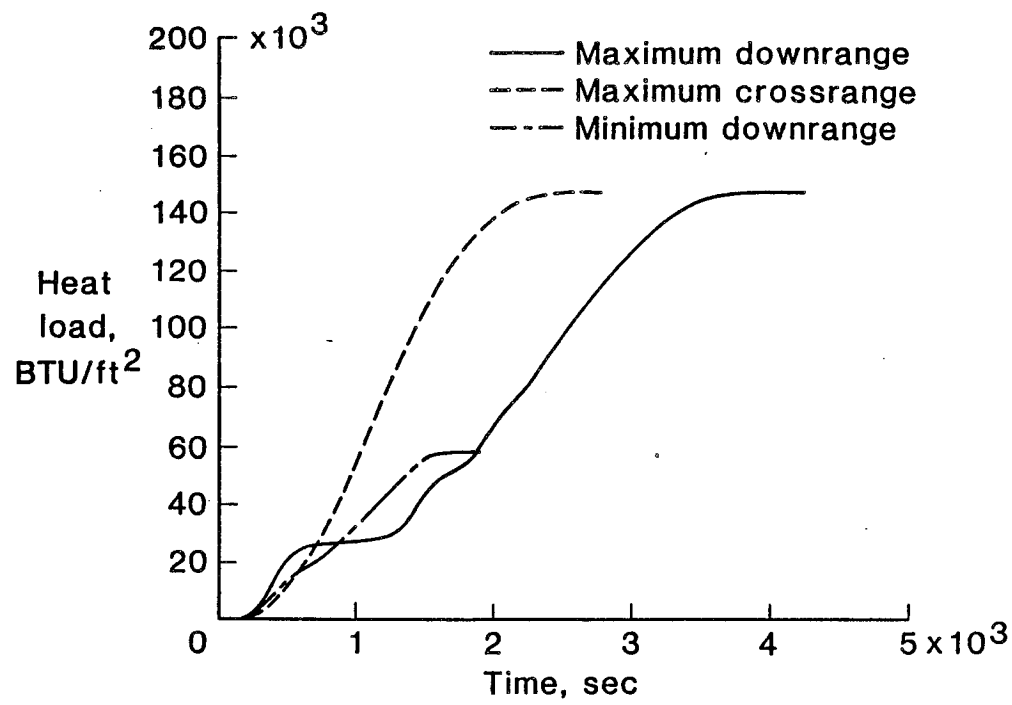


Figure 16. Heat Rate Histories for the Entry Missions of the ERV



Reproduced from Reference (14)

Figure 17. Heat Load Histories for the Entry Missions of the ERV

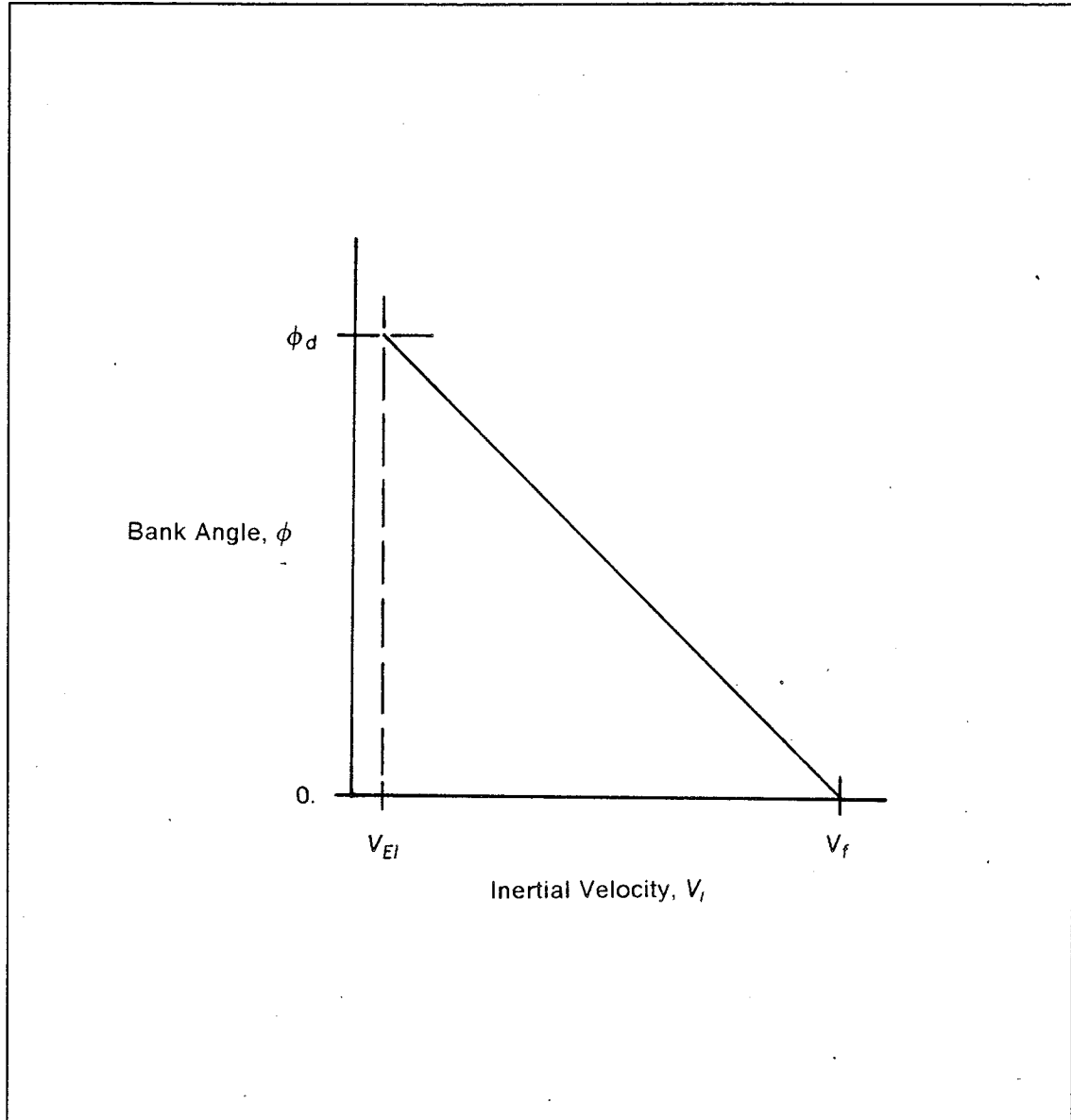


Figure 18. Bank Angle Versus Velocity Profile

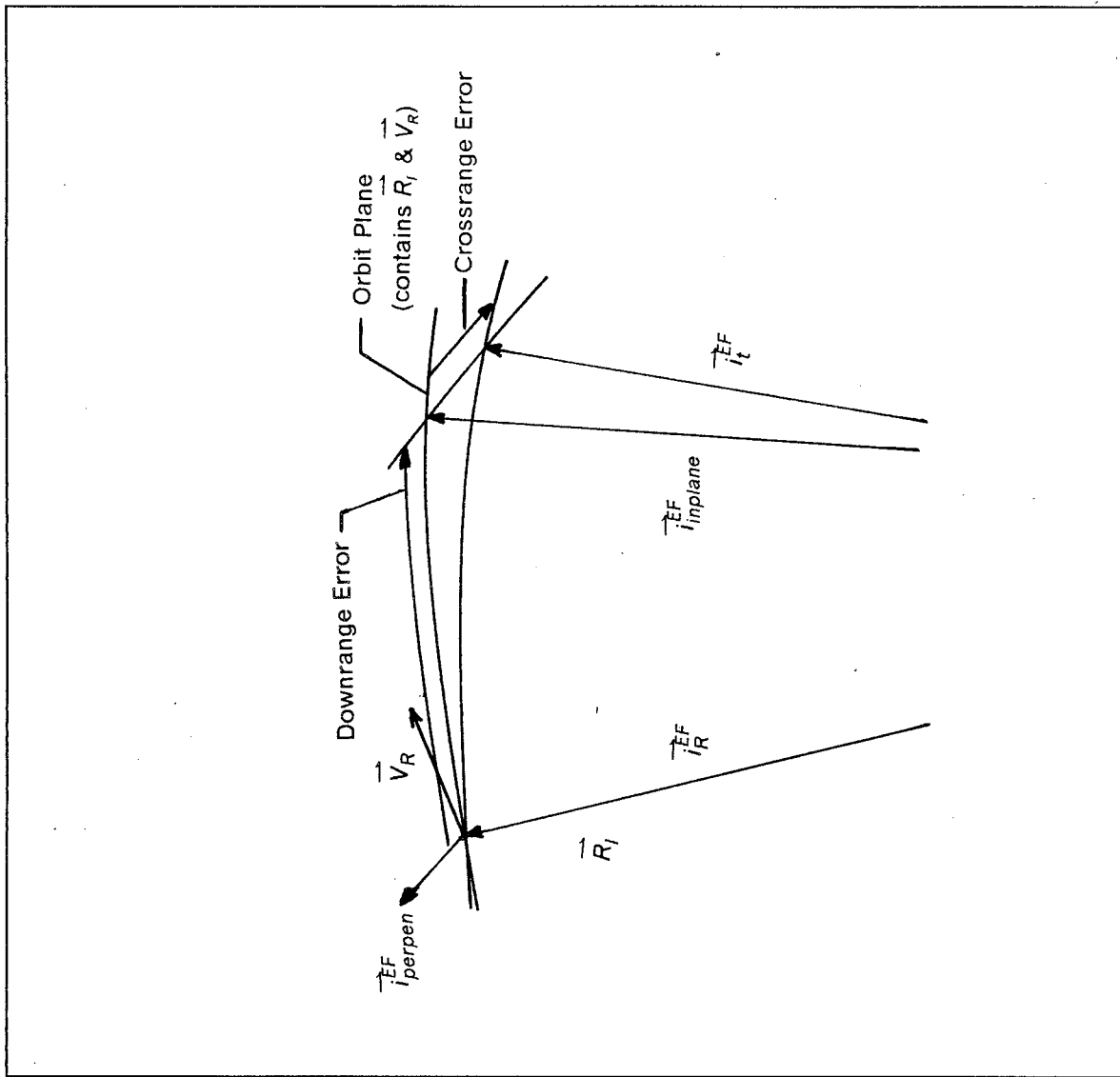
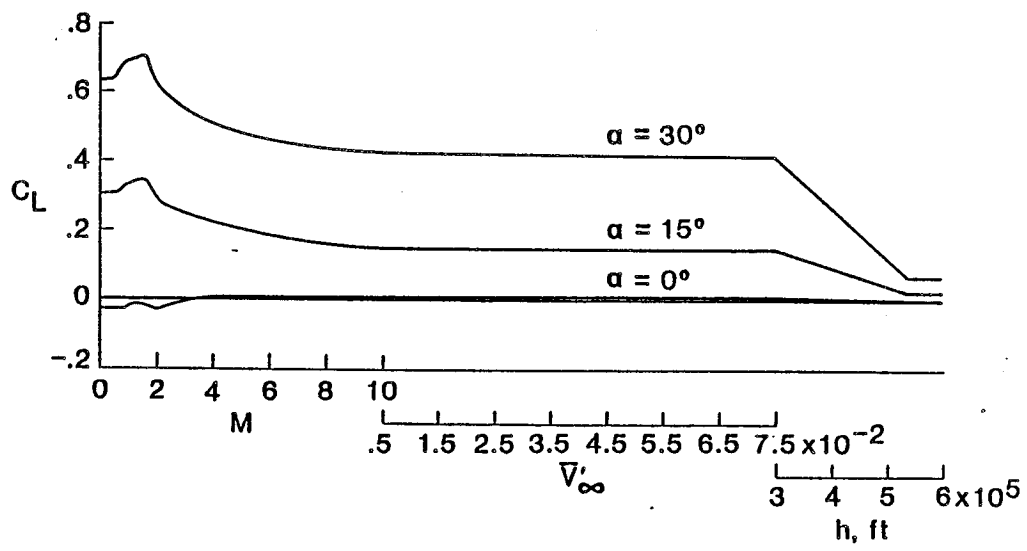
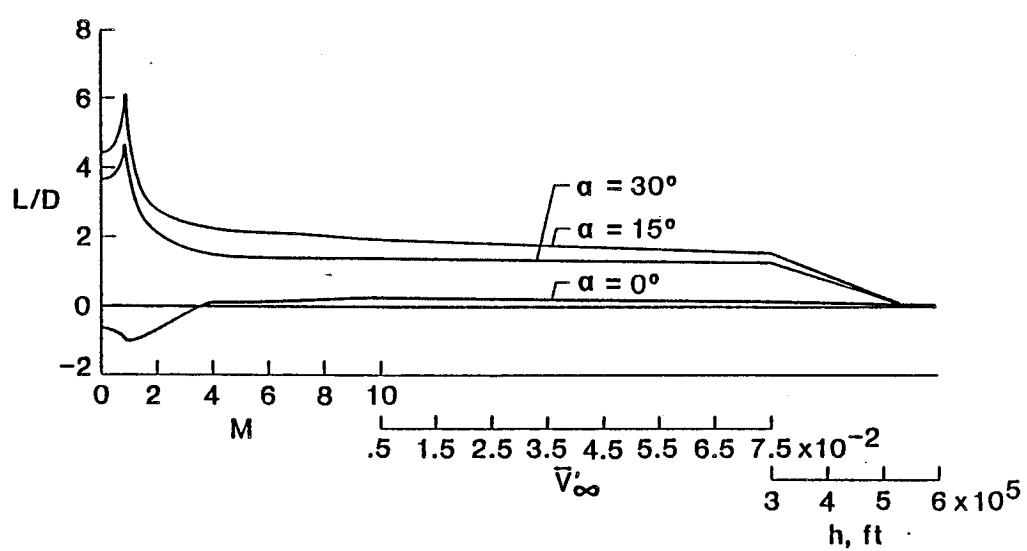


Figure 19. Definitions of Downrange and Crossrange Errors



Reproduced from Reference (14)

Figure 20. Predicted Lift Coefficient Profile for the ERV



Reproduced from Reference (14)

Figure 21. Predicted L/D Profile for the ERV

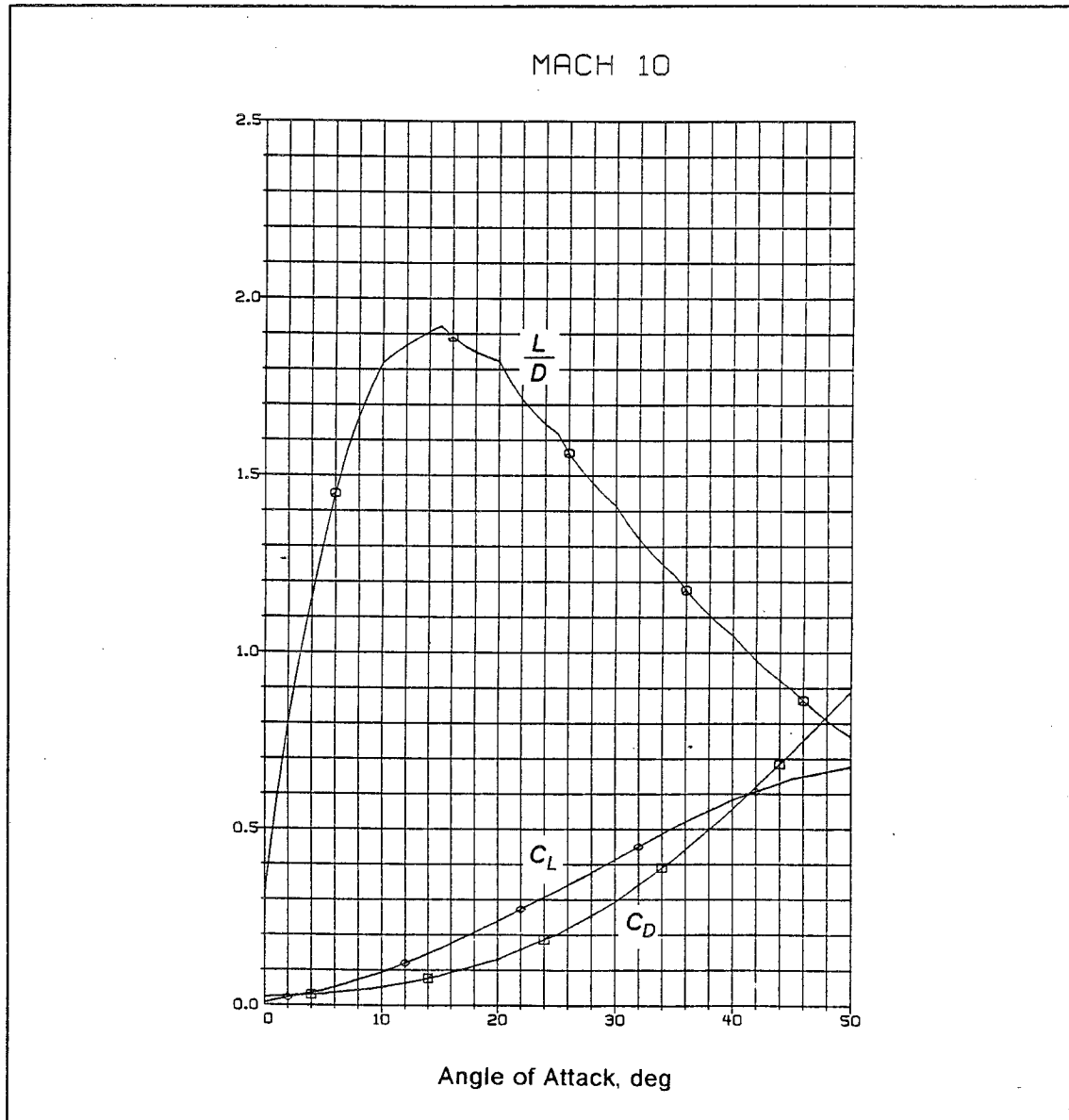


Figure 22. Predicted L/D versus Angle-of Attack Profile for the ERV

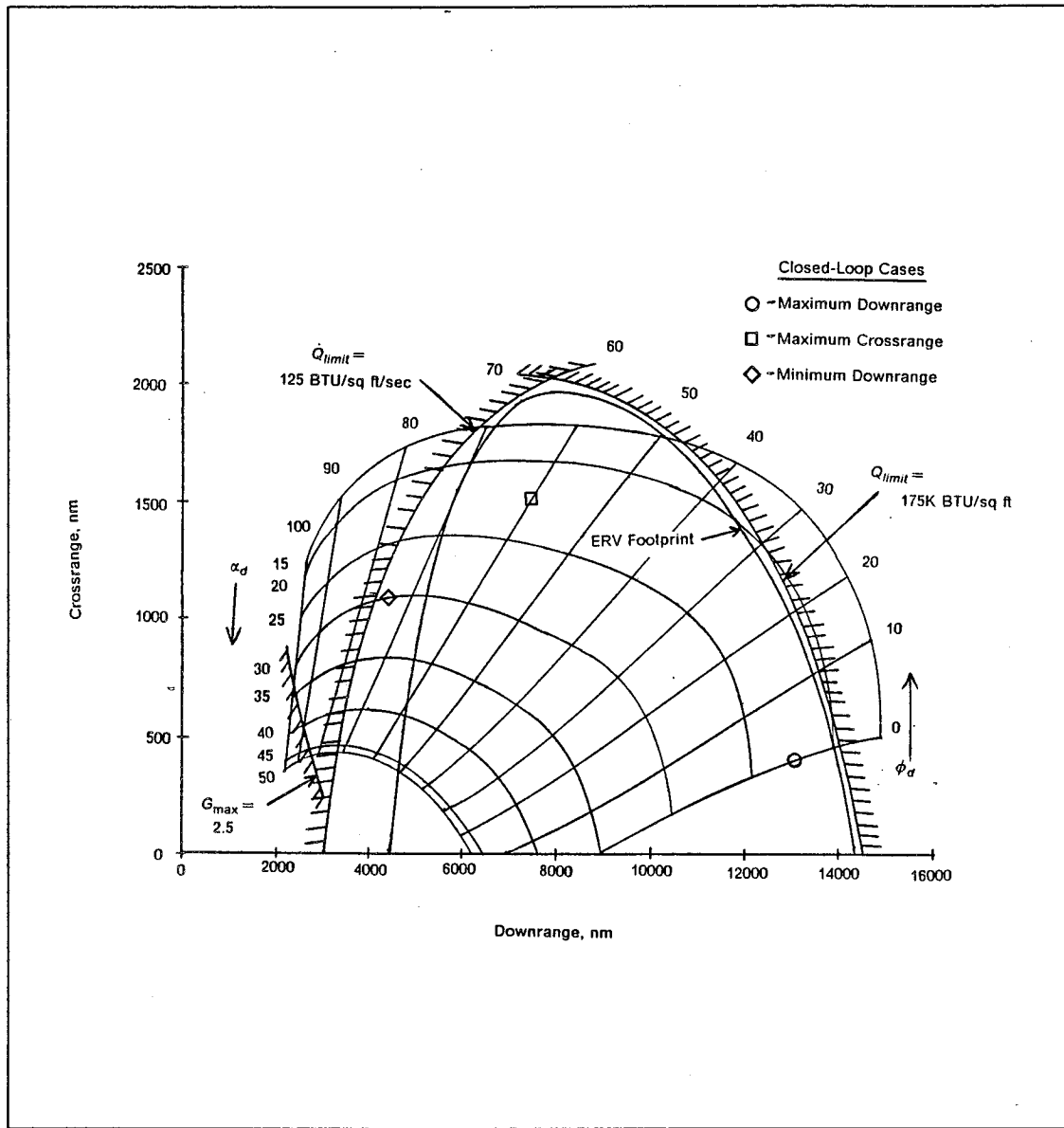


Figure 23. ERV Open-Loop Footprint with the Control Profile

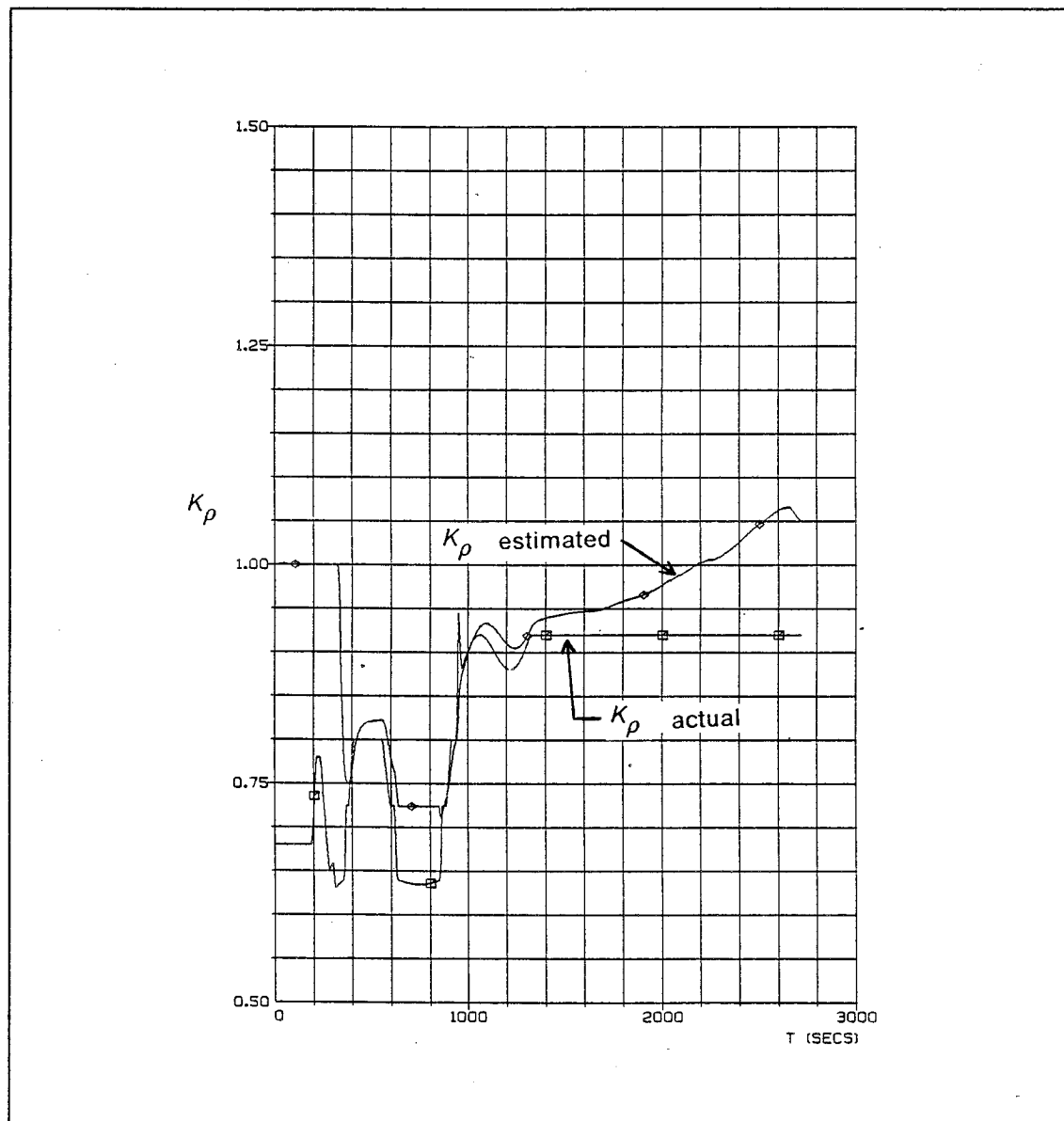


Figure 24. Time Response of the Density Filter

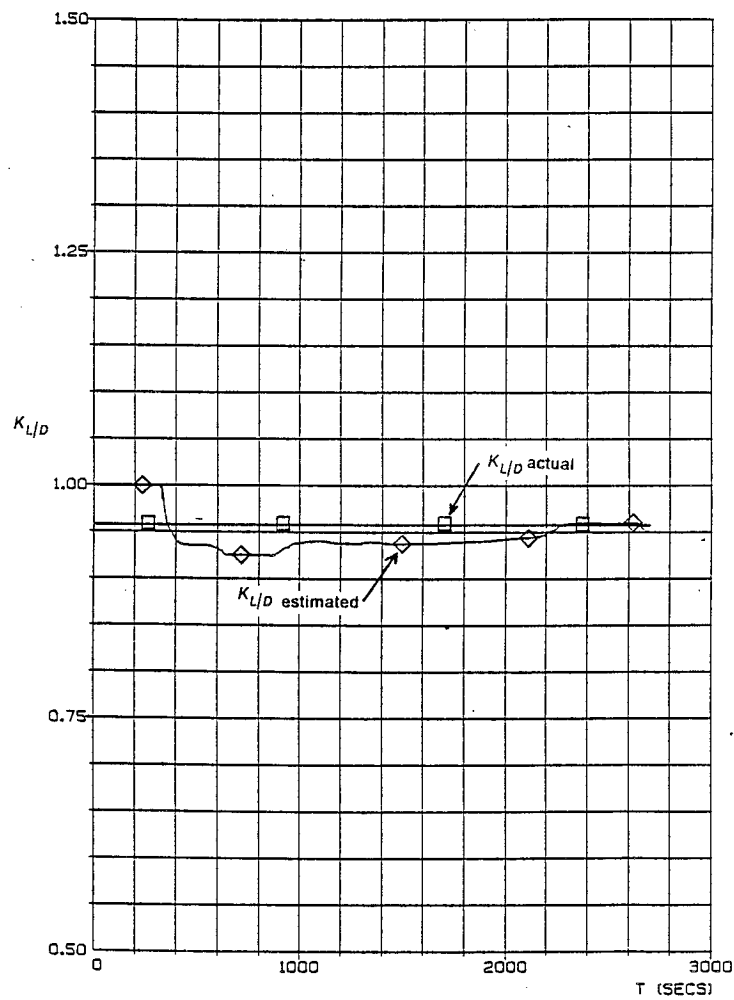


Figure 25. Time Response of the L/D Filter

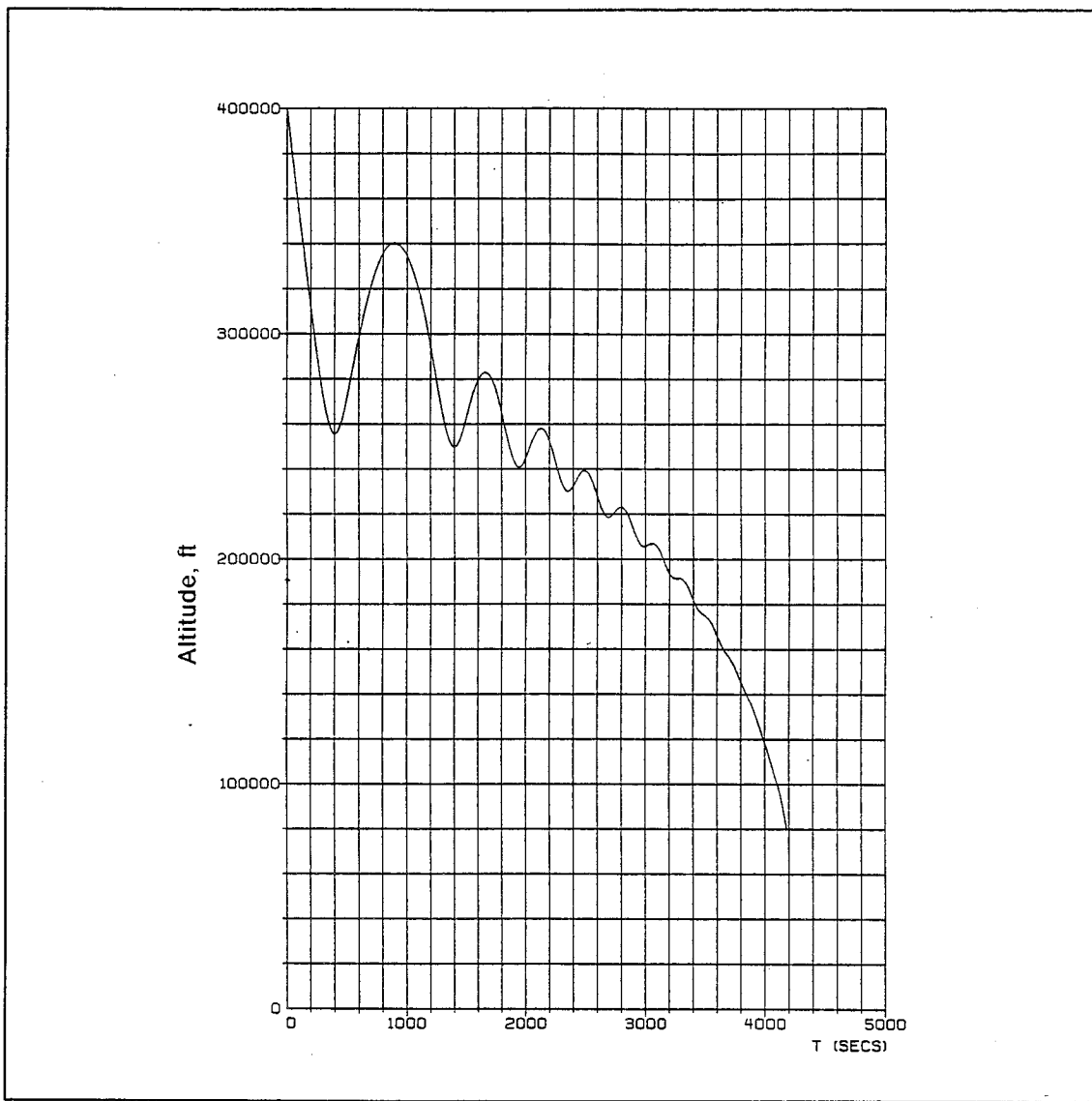


Figure 26. Closed-Loop Altitude History for the Maximum Downrange Case

C - 2

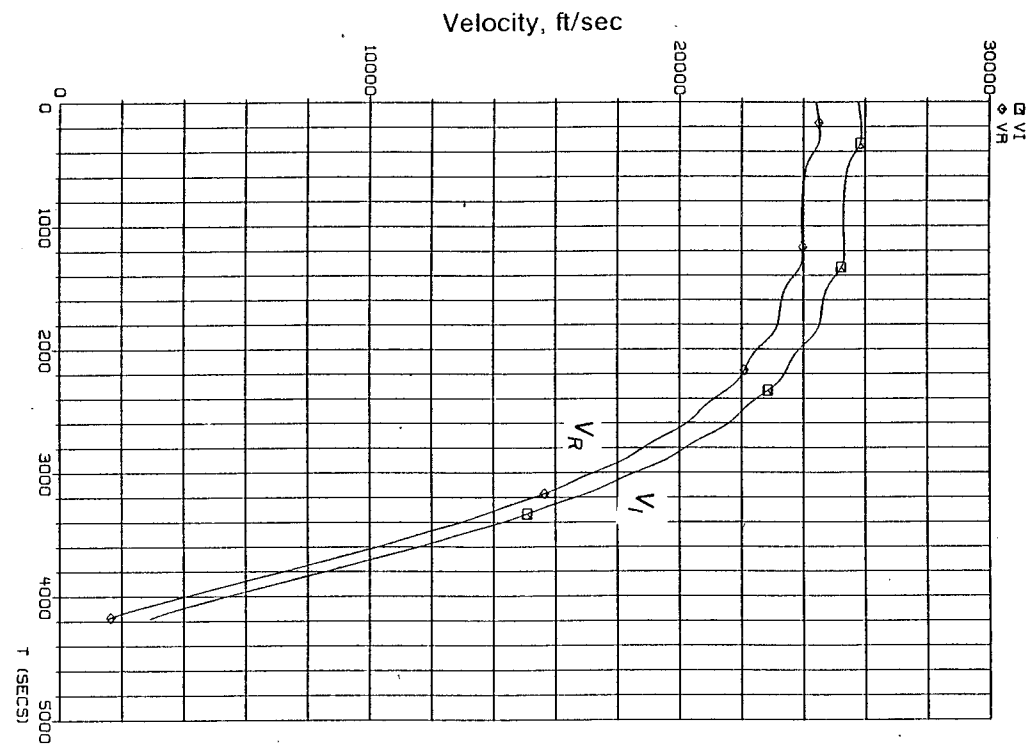


Figure 27. Closed-Loop Velocity History for the Maximum Downrange Case

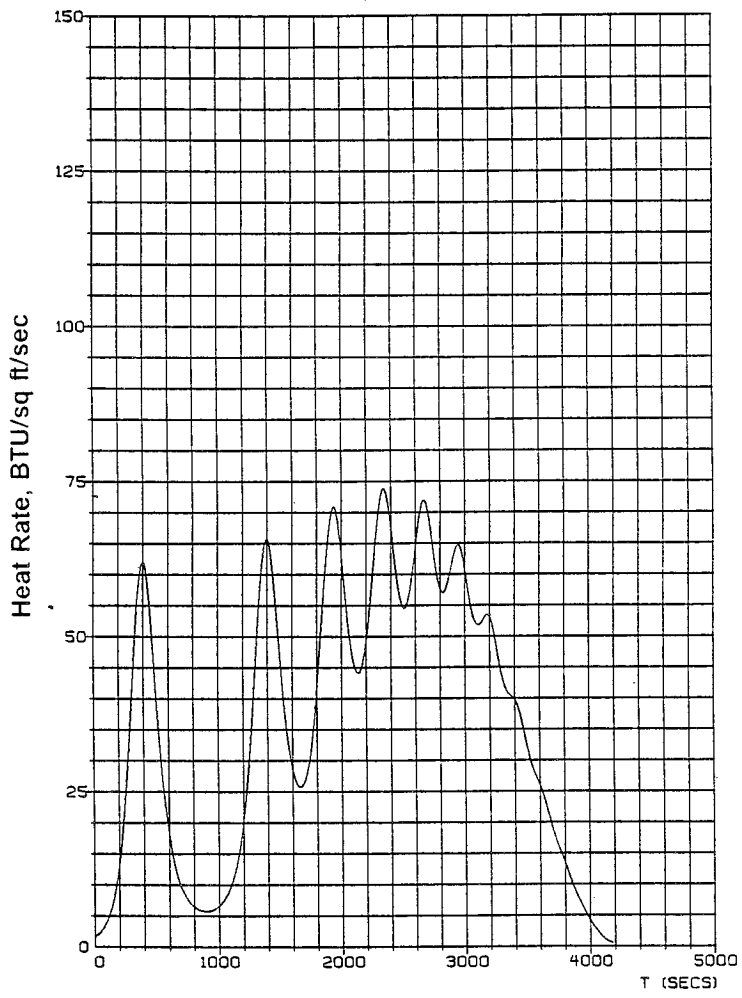


Figure 28. Closed-Loop Heat Rate History for the Maximum Downrange Case

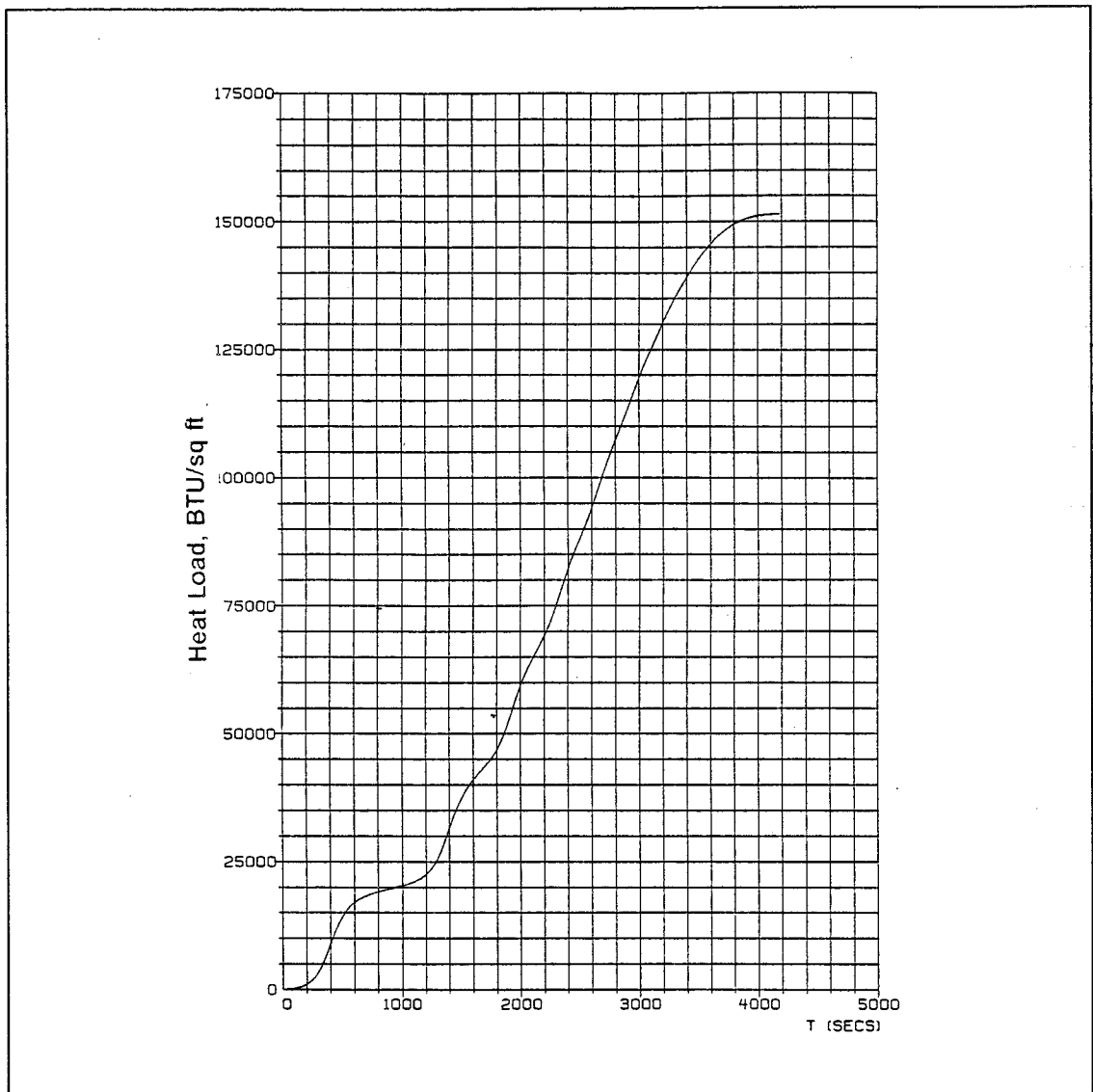


Figure 29. Closed-Loop Heat Load History for the Maximum Downrange Case

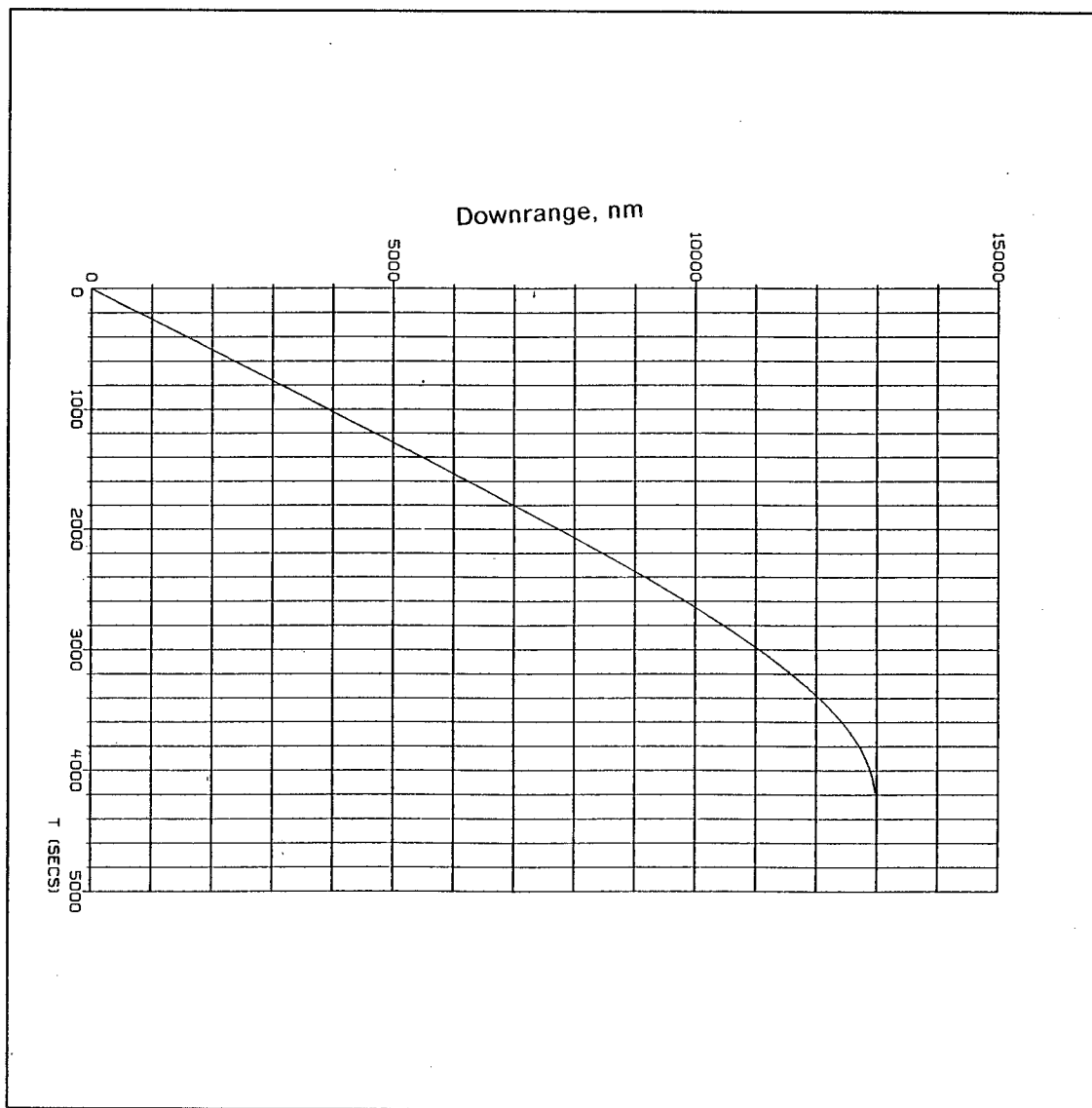


Figure 30. Closed-Loop Downrange History for the Maximum Downrange Case

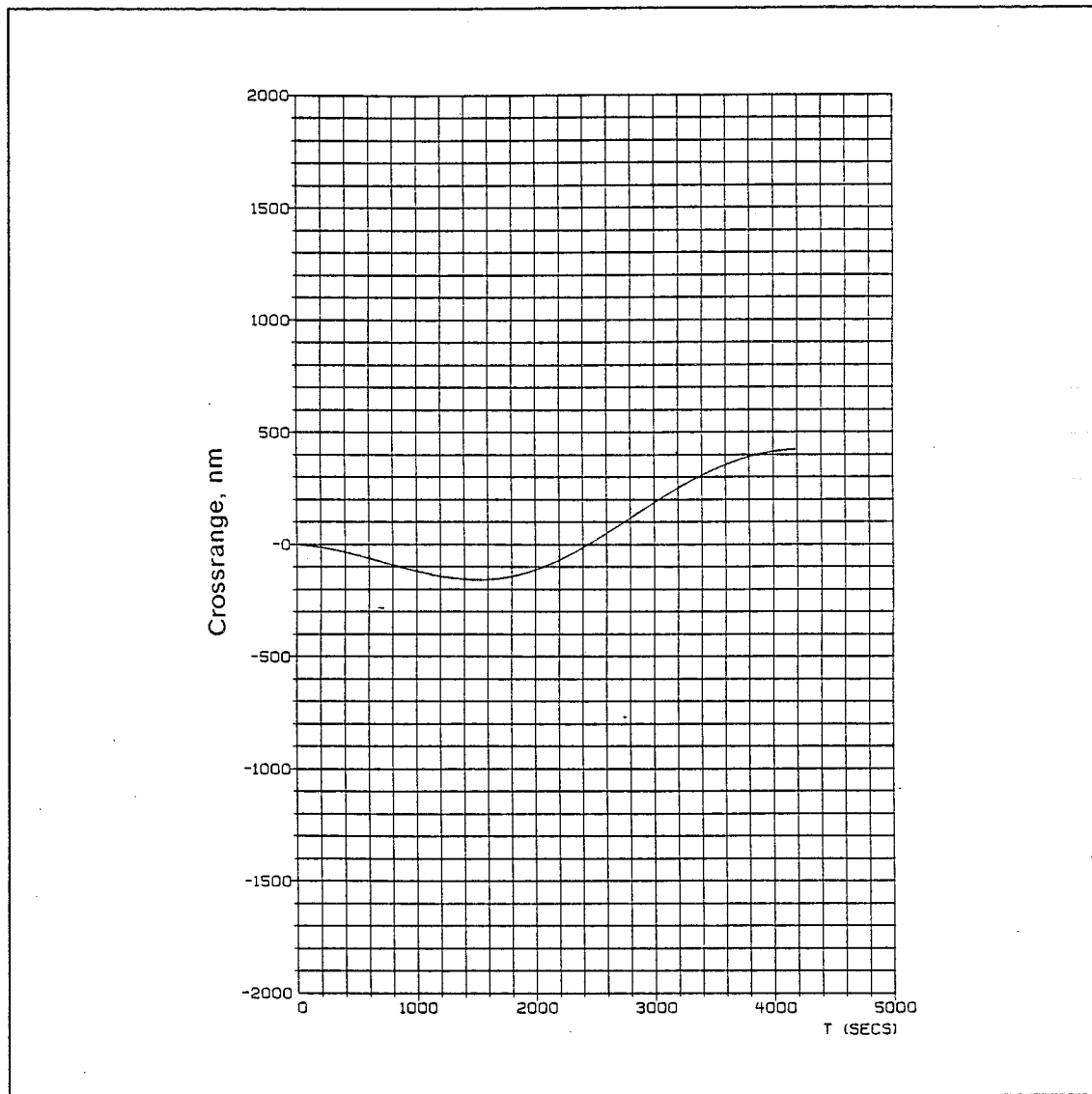


Figure 31. Closed-Loop Crossrange History for the Maximum Downrange Case

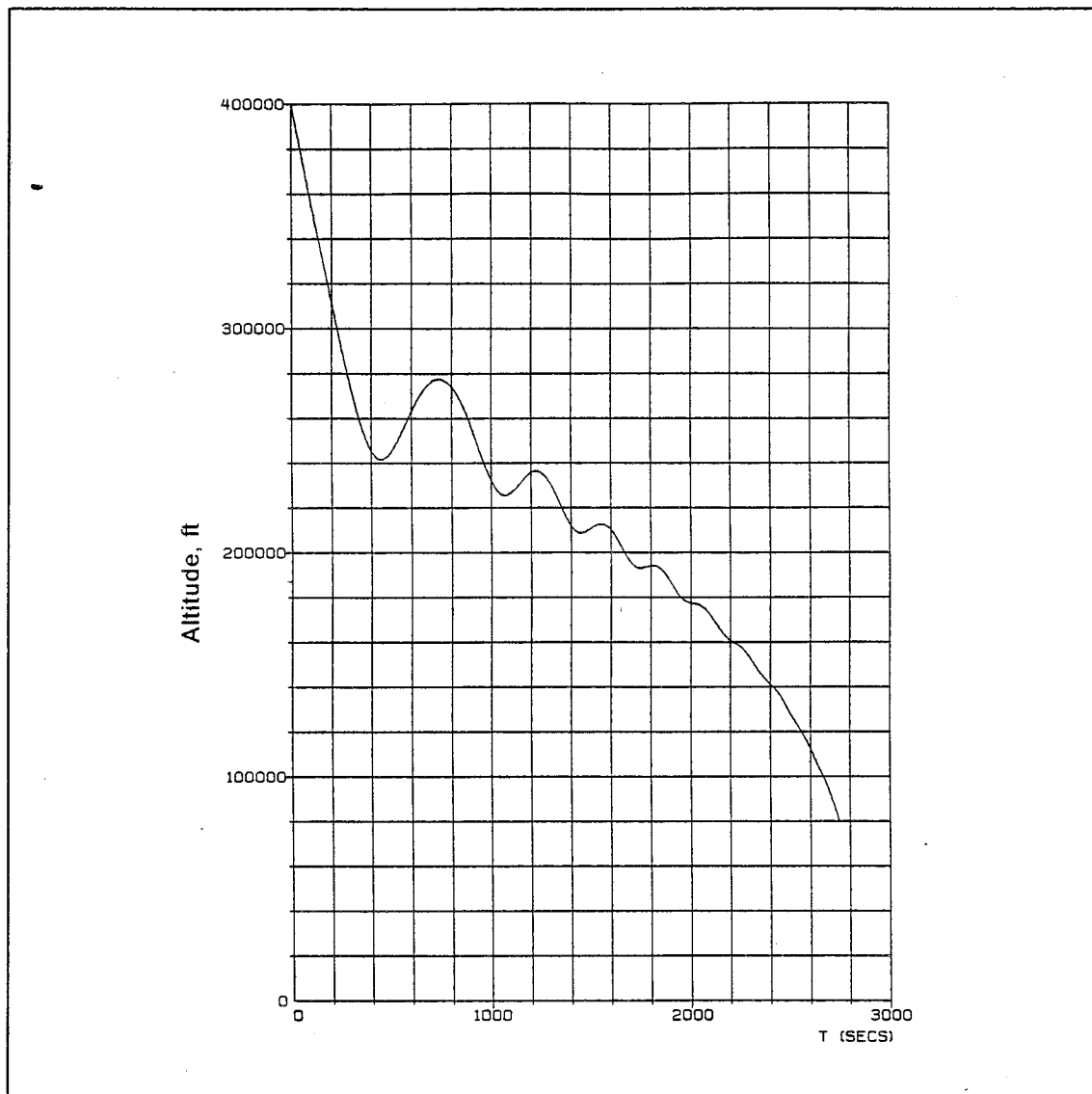


Figure 32. Closed-Loop Altitude History for the Maximum Crossrange Case

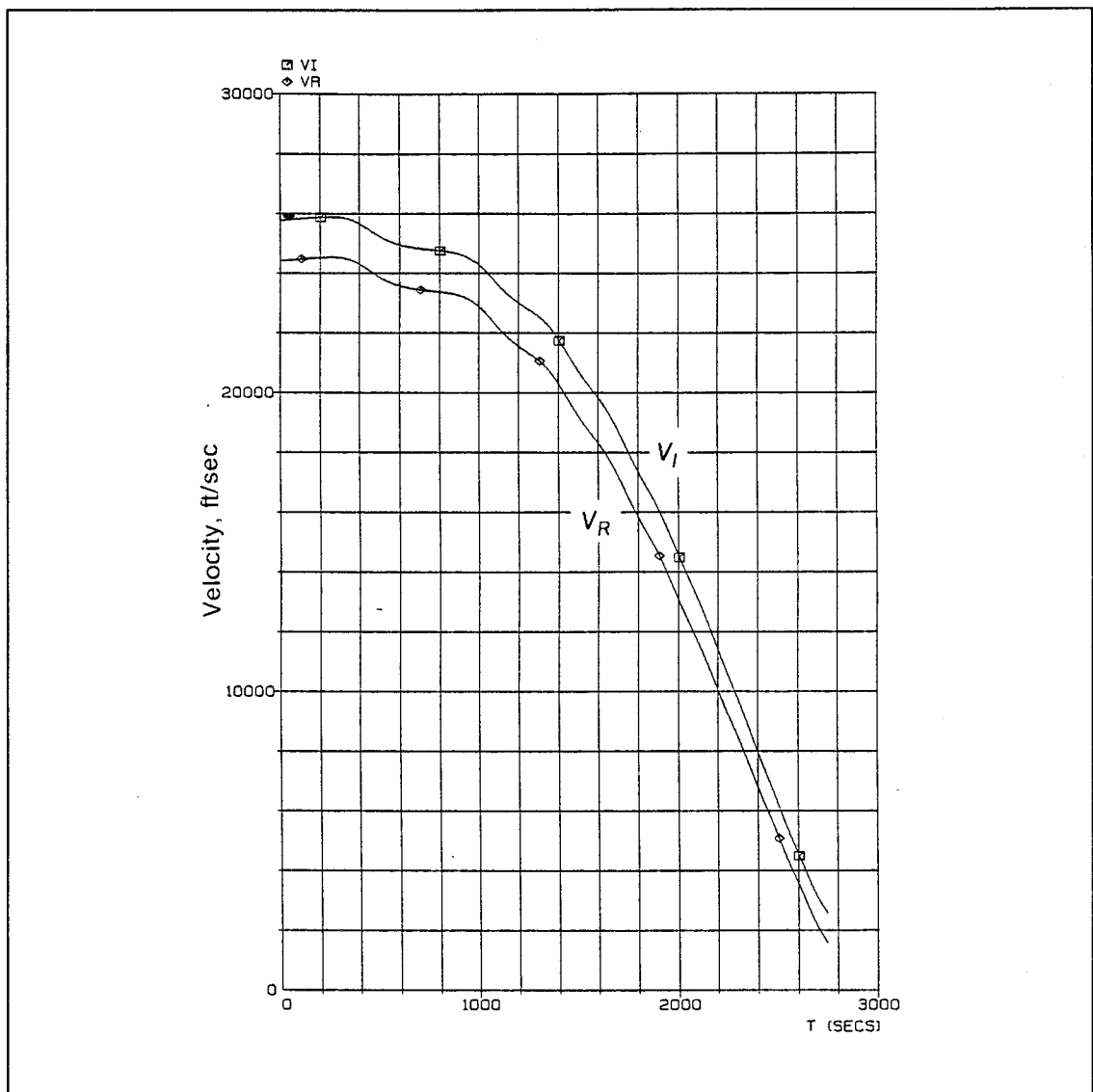


Figure 33. Closed-Loop Velocity History for the Maximum Crossrange Case

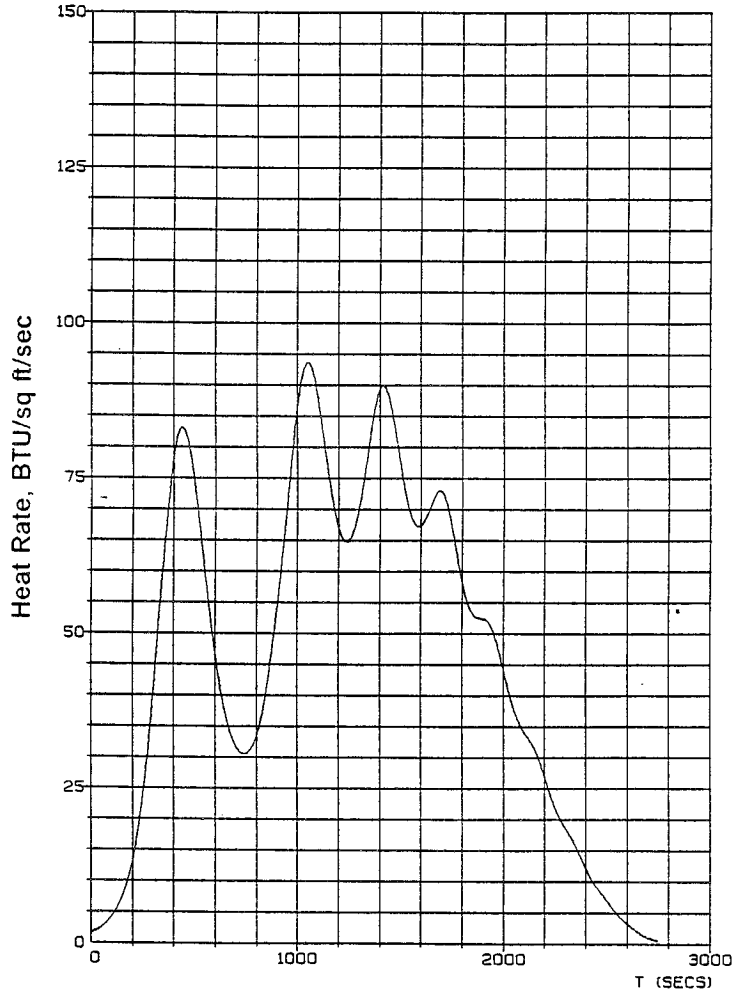


Figure 34. Closed-Loop Heat Rate History for the Maximum Crossrange Case

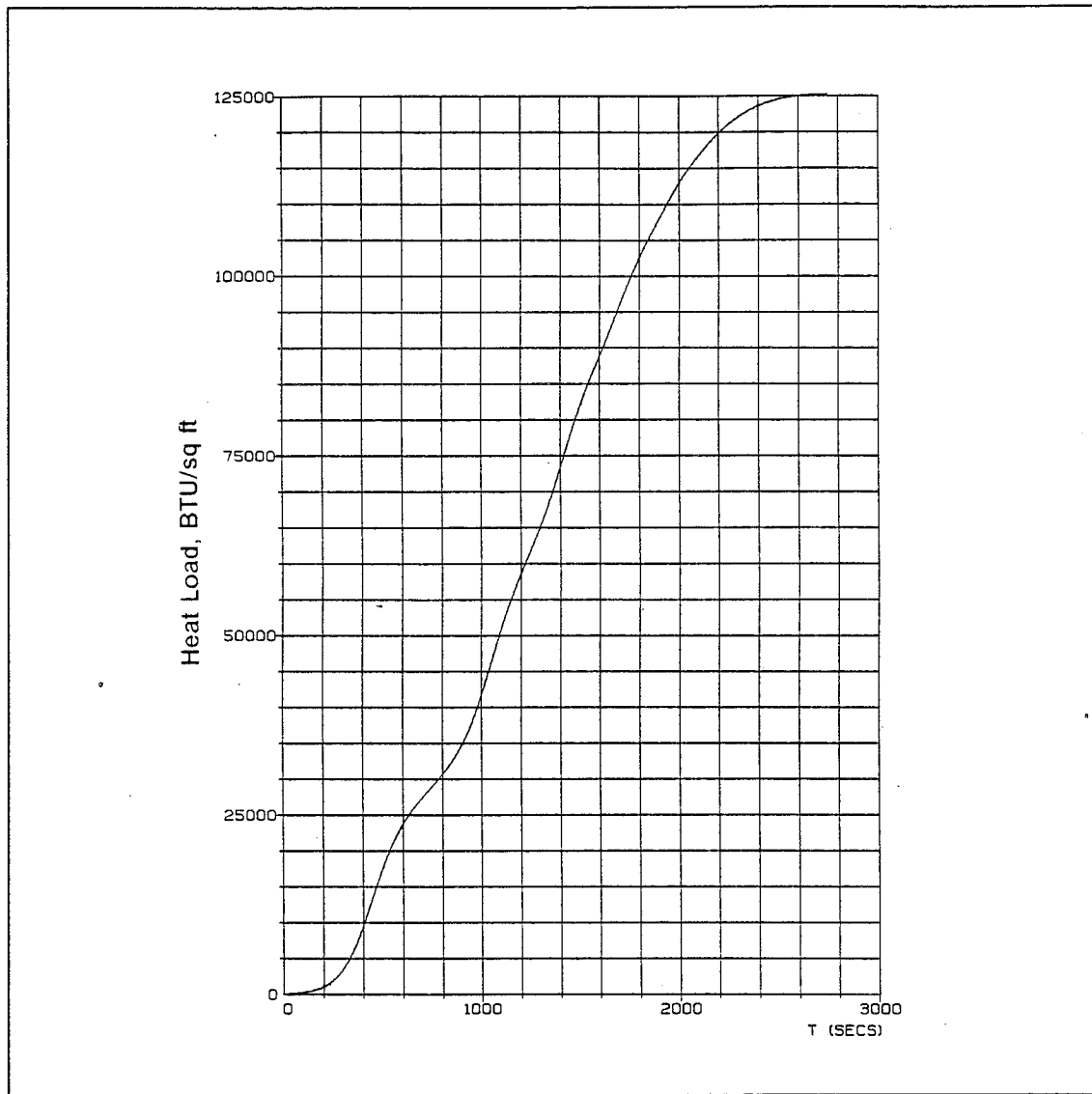


Figure 35. Closed-Loop Heat Load History for the Maximum Crossrange Case

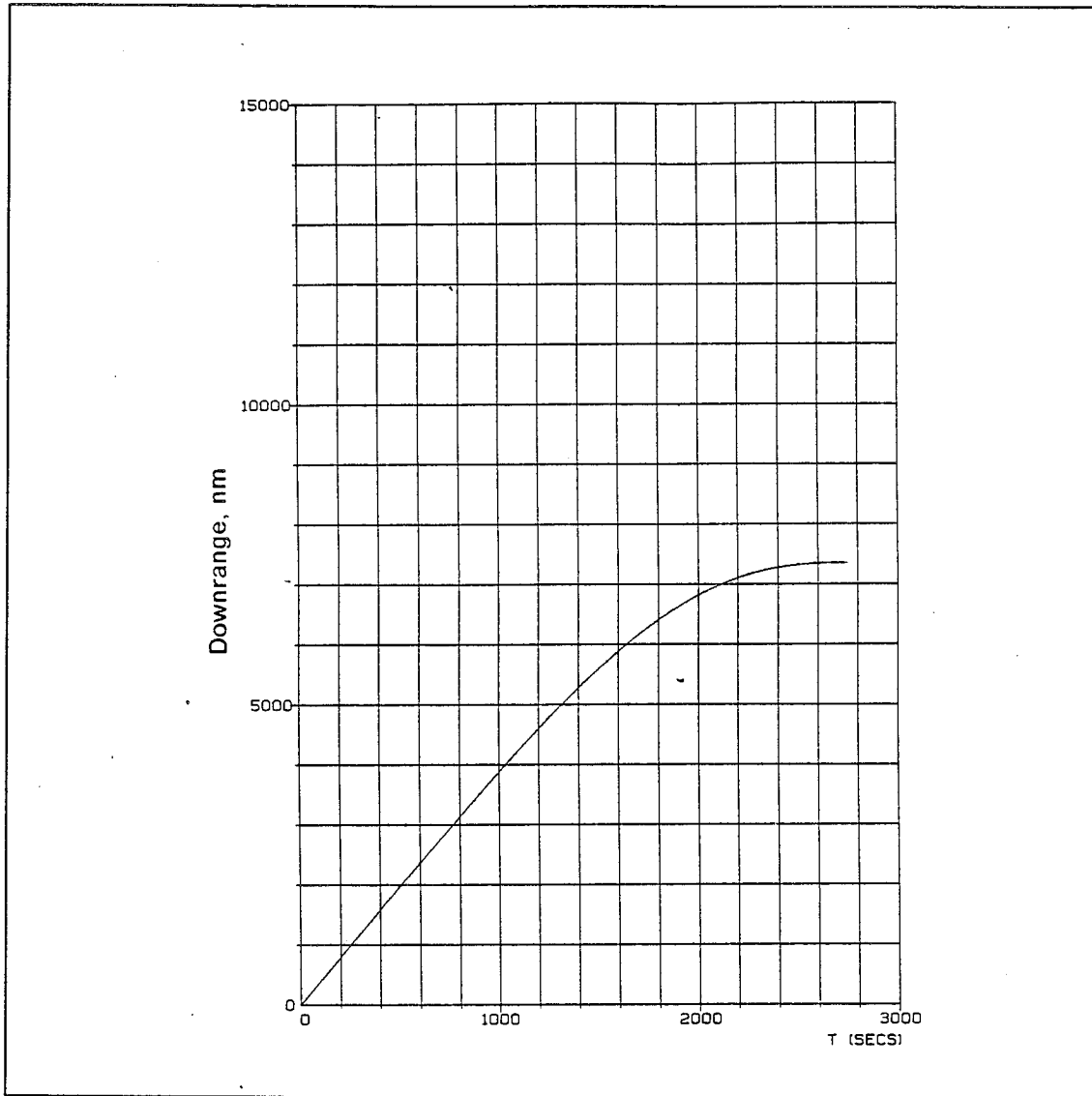


Figure 36. Closed-Loop Downrange History for the Maximum Crossrange Case

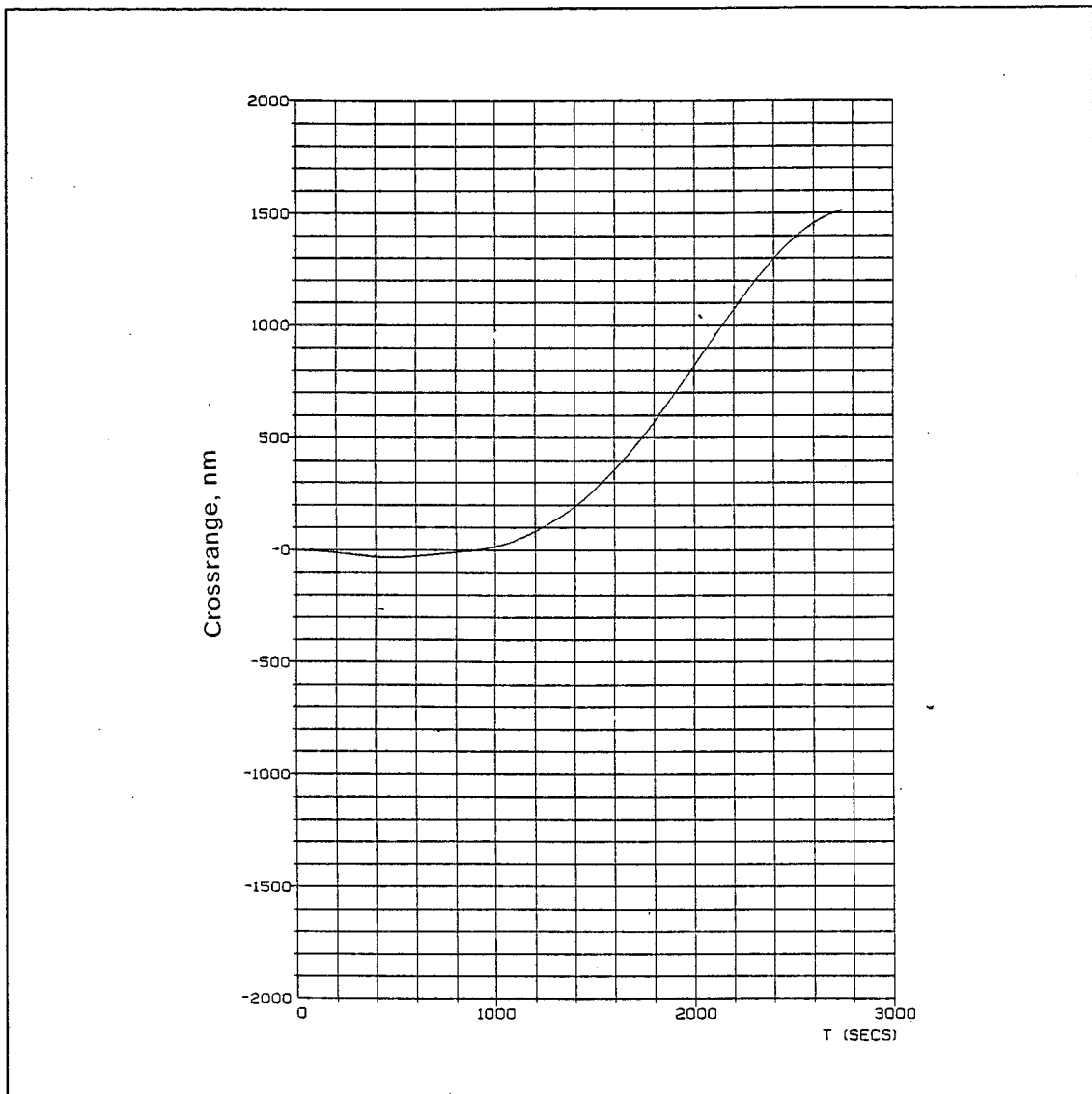


Figure 37. Closed-Loop Crossrange History for the Maximum Crossrange Case

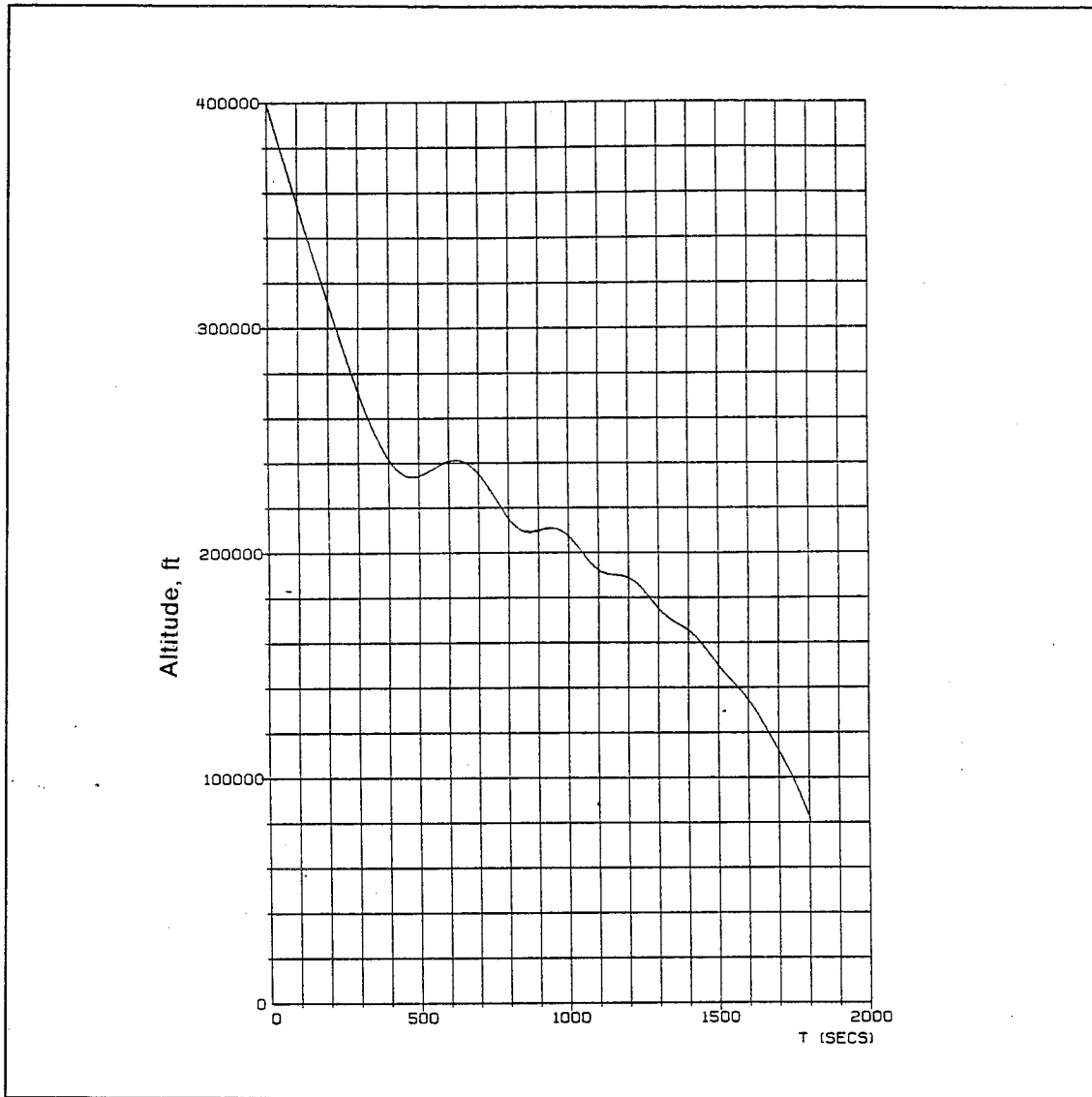


Figure 38. Closed-Loop Altitude History for the Minimum Downrange Case

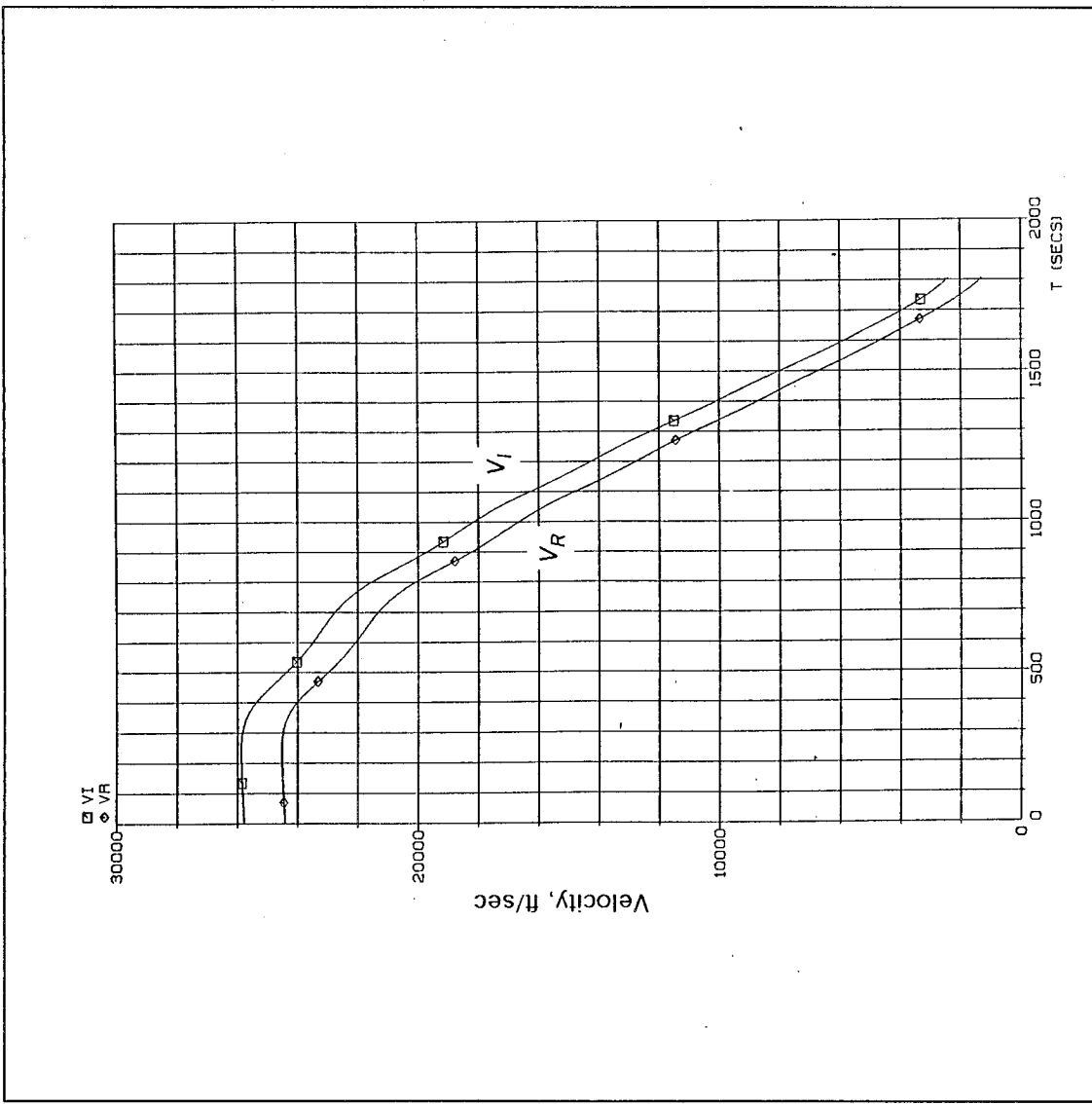


Figure 39. Closed-Loop Velocity History for the Minimum Downrange Case

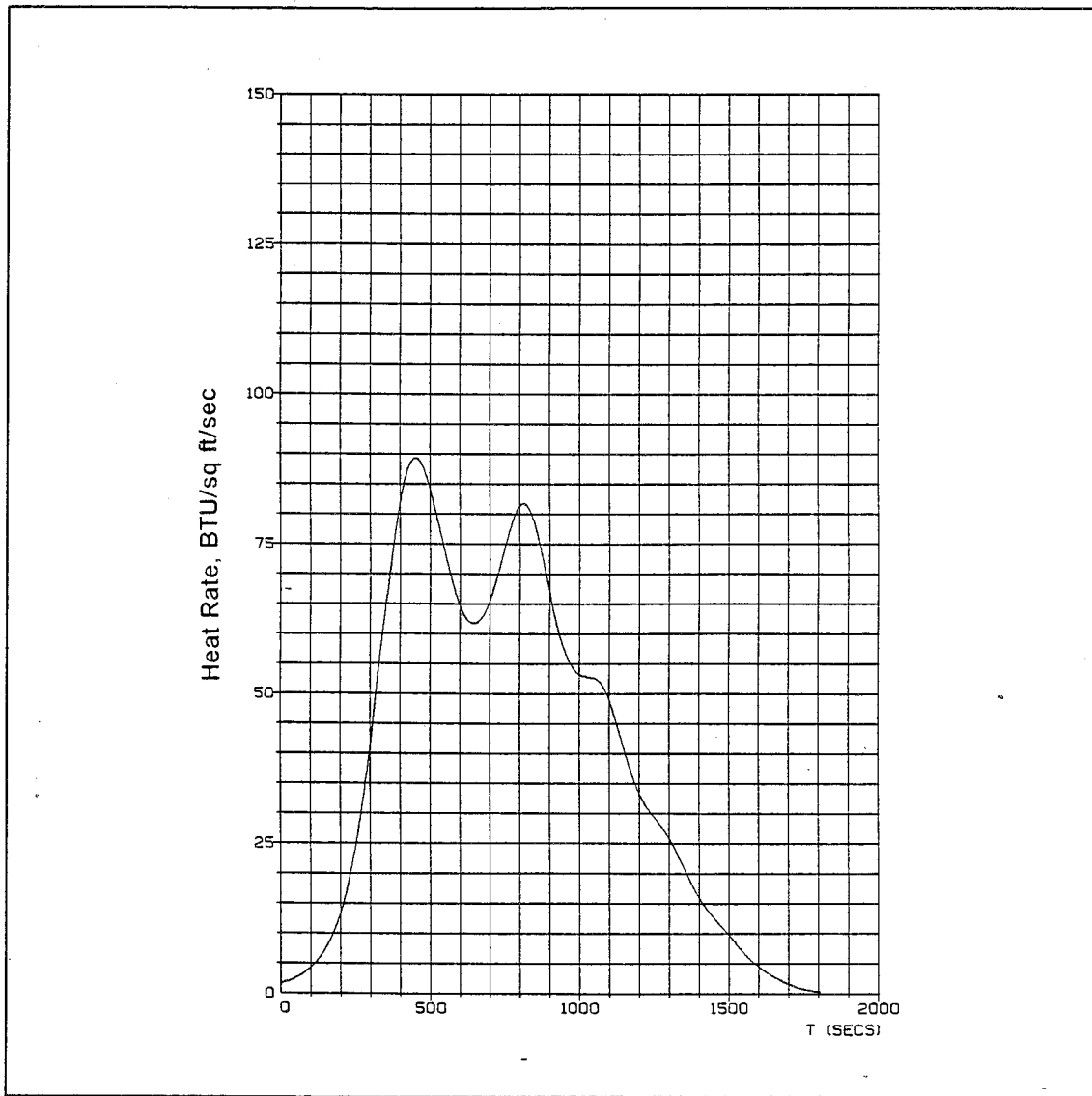


Figure 40. Closed-Loop Heat Rate History for the Minimum Downrange Case

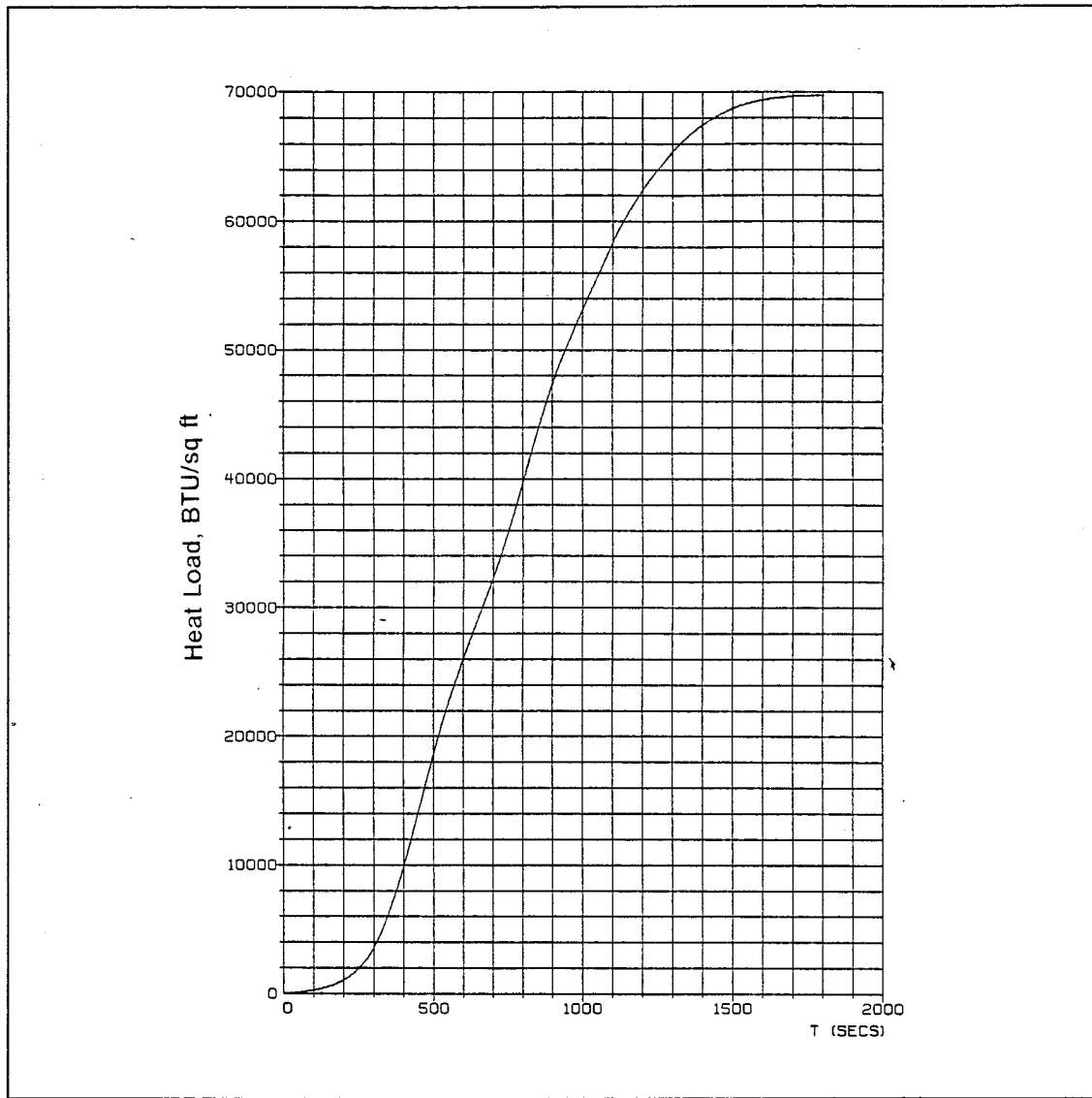


Figure 41. Closed-Loop Heat Load History for the Minimum Downrange Case

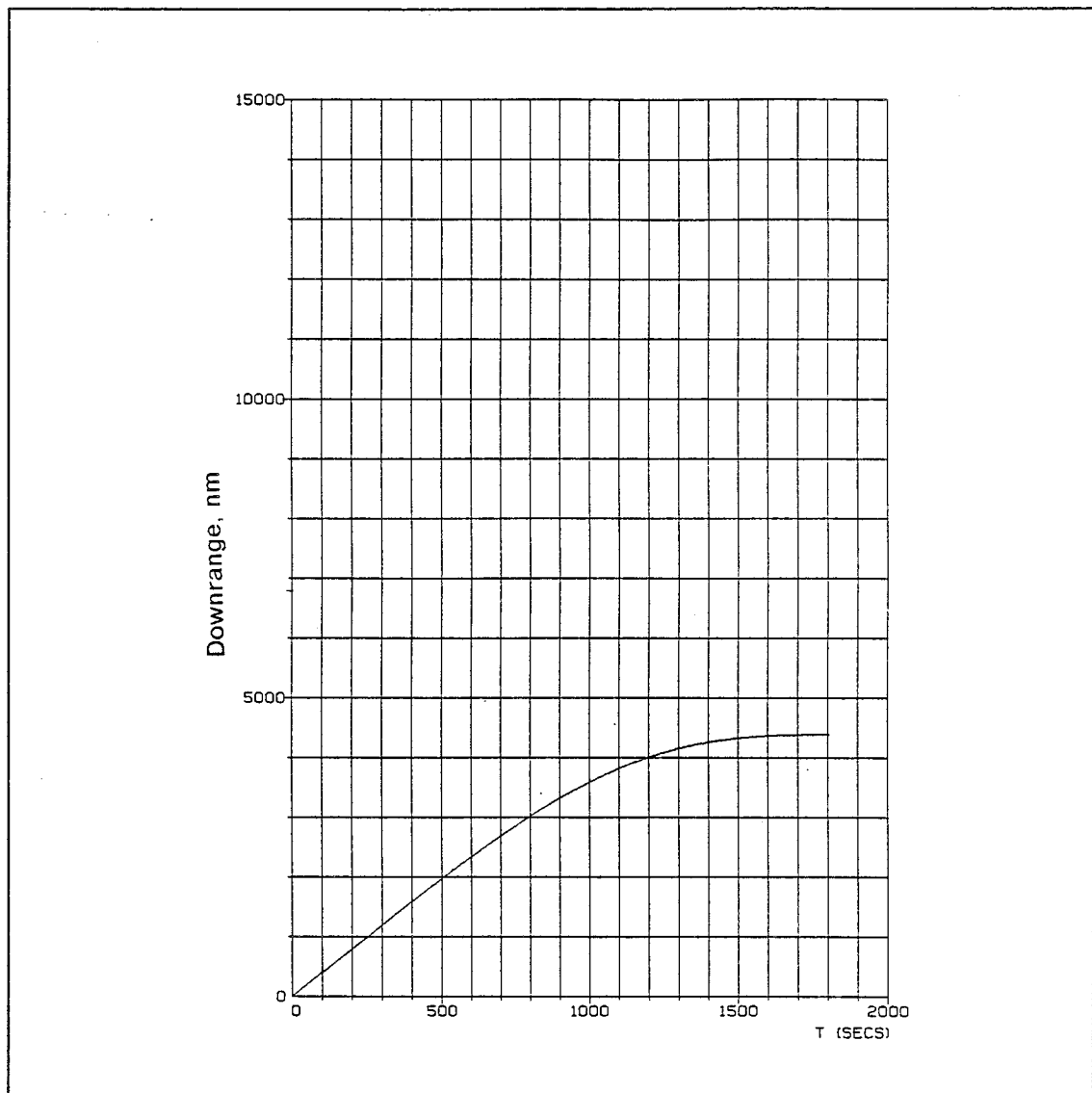


Figure 42. Closed-Loop Downrange History for the Minimum Downrange Case

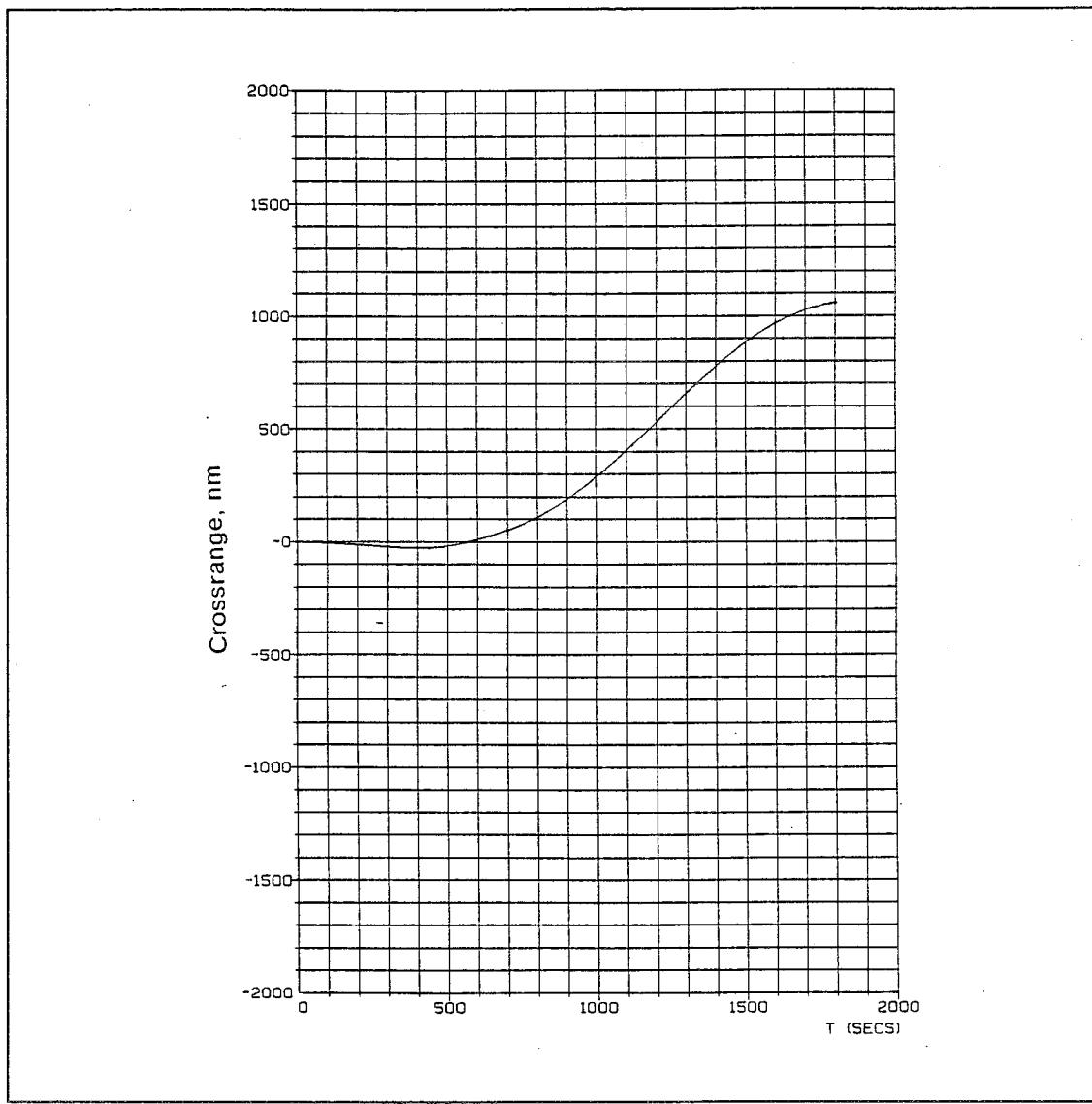


Figure 43. Closed-Loop Crossrange History for the Minimum Downrange Case

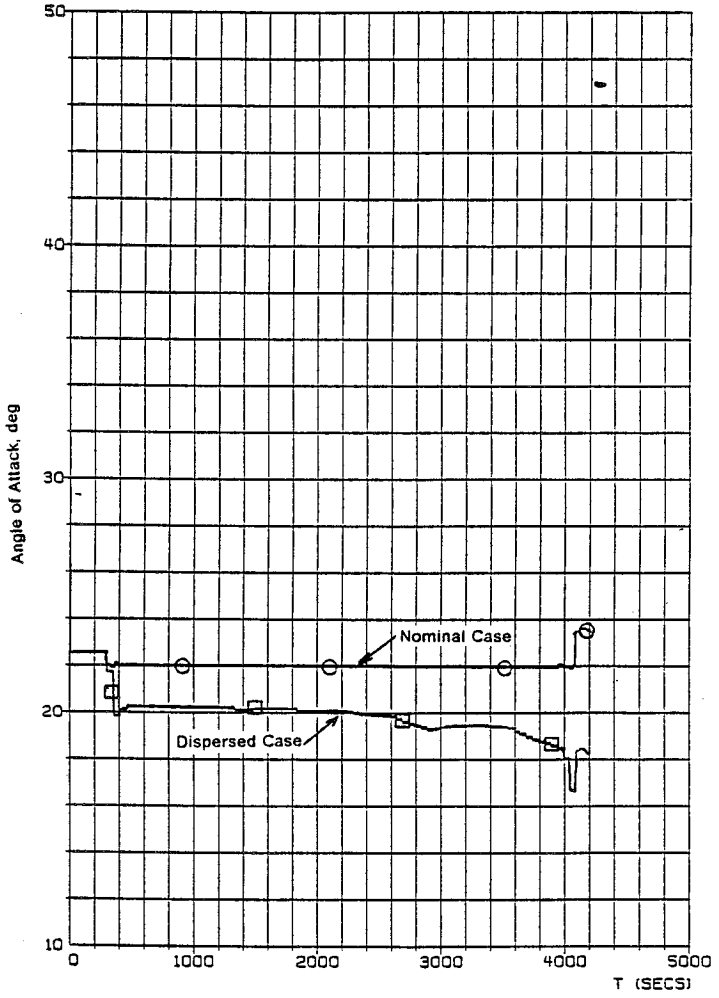


Figure 44. Angle of Attack Comparison for the Maximum Downrange Case

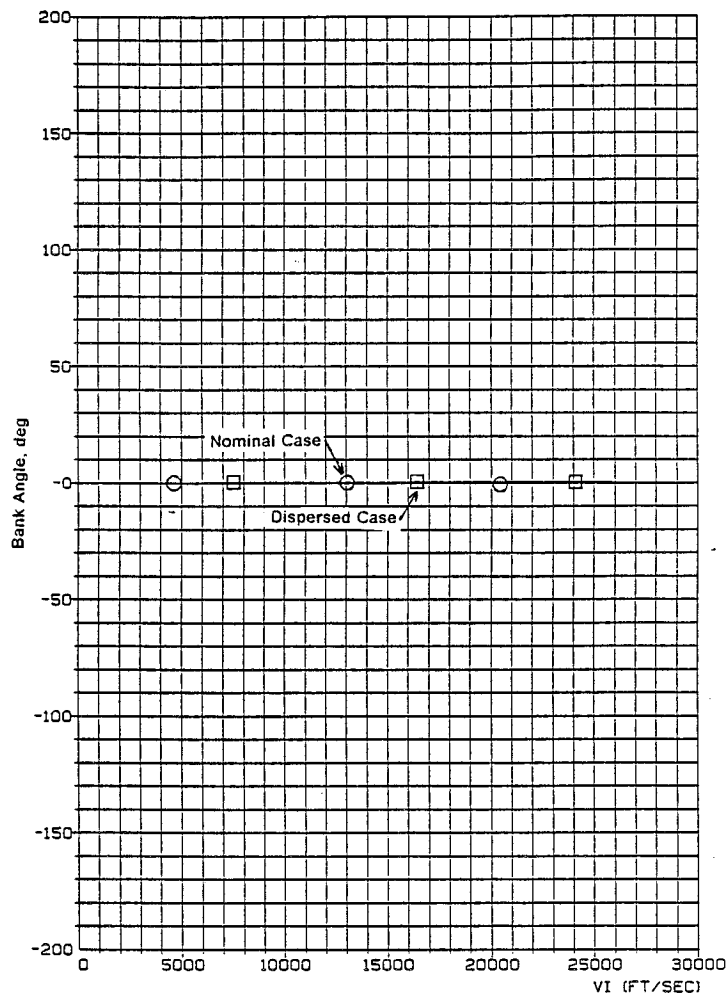


Figure 45. Bank Angle Comparison for the Maximum Downrange Case

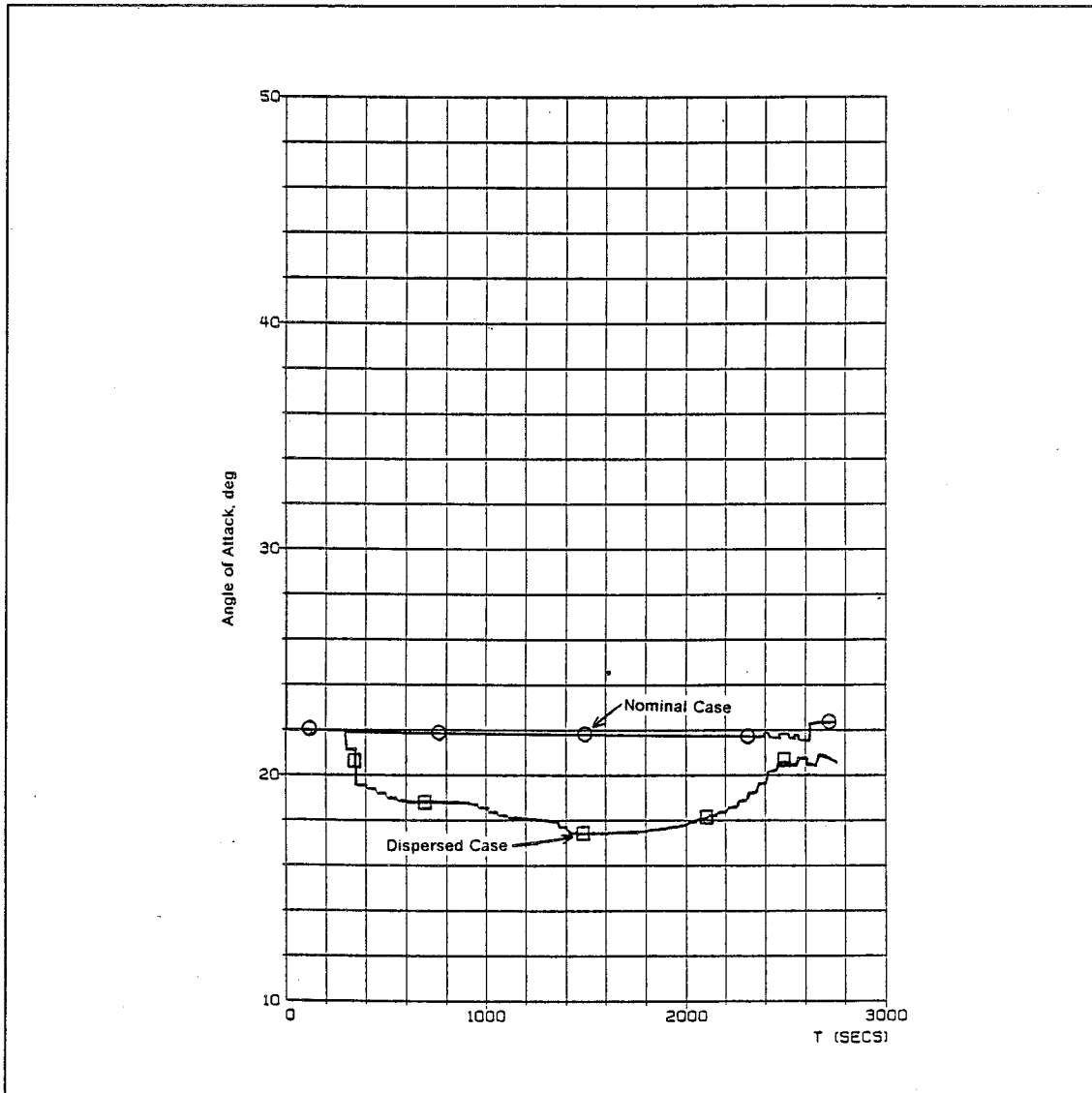


Figure 46. Angle of Attack Comparison for the Maximum Crossrange Case

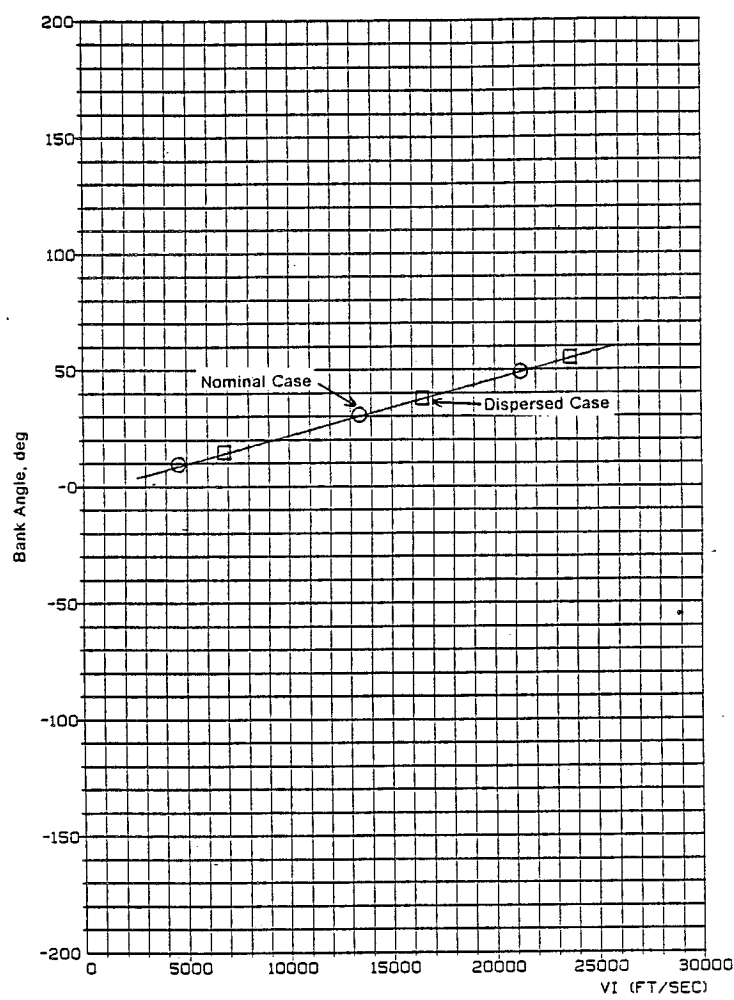


Figure 47. Bank Angle Comparison for the Maximum Crossrange Case

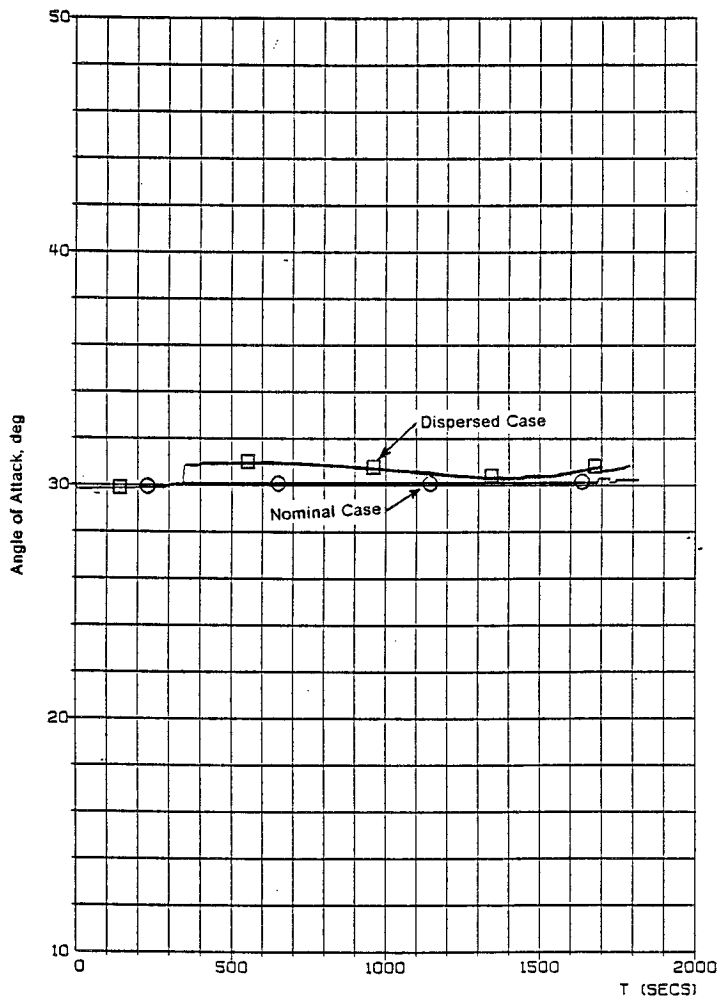


Figure 48. Angle of Attack Comparison for the Minimum Downrange Case

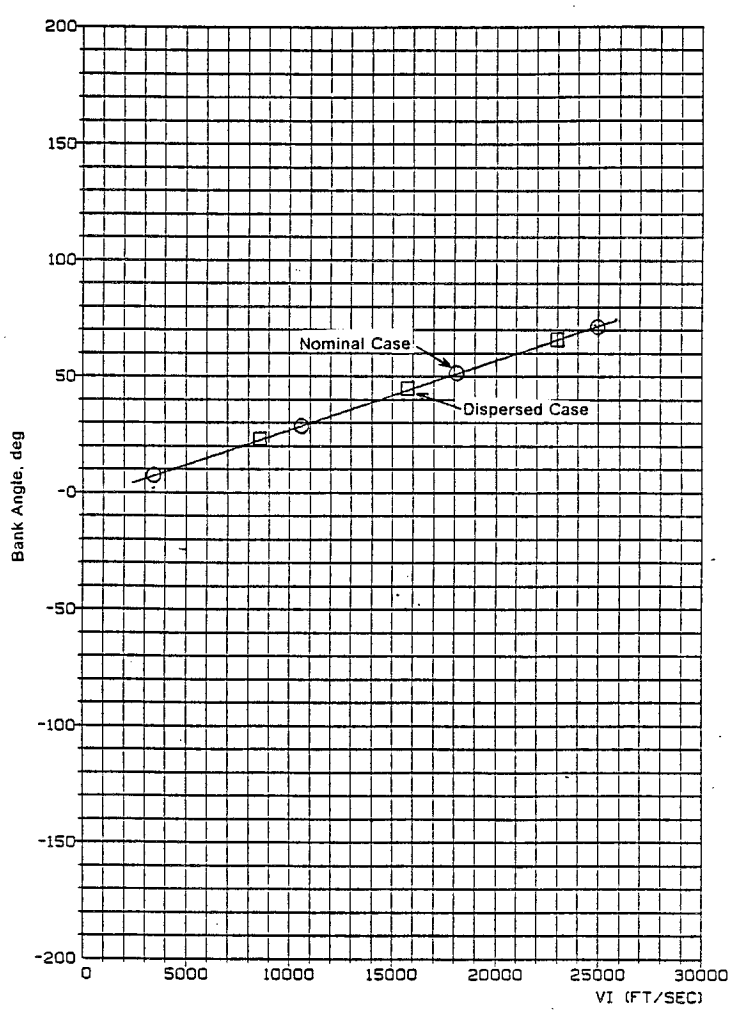


Figure 49. Bank Angle Comparison for the Minimum Downrange Case

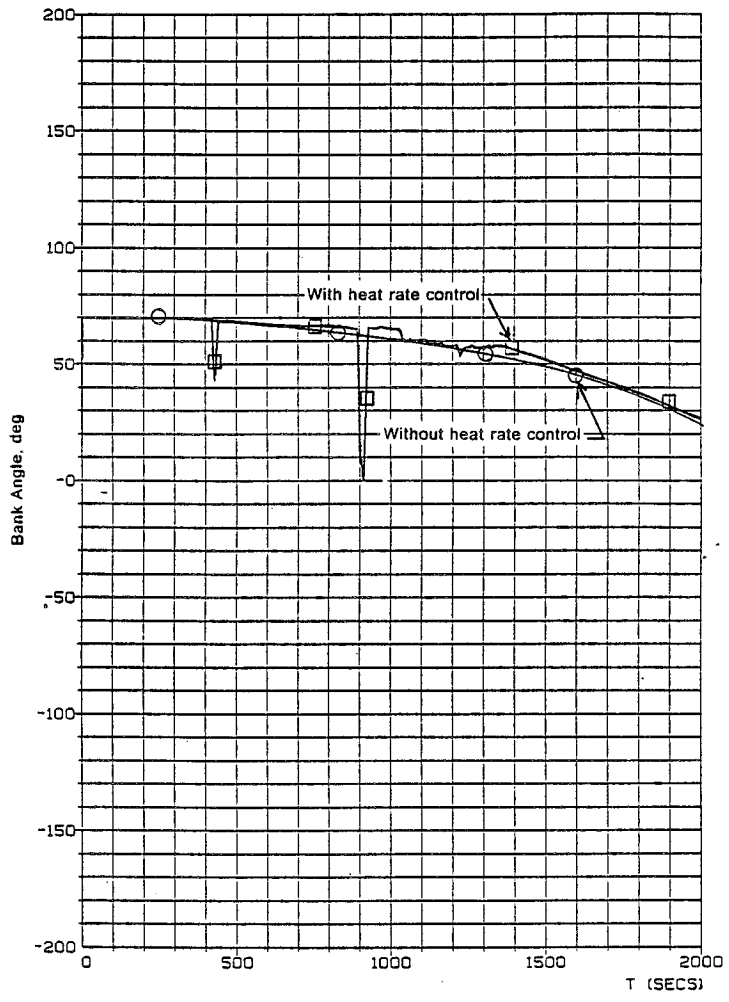


Figure 50. Bank Angle Versus Time Comparison for Heat Rate Control

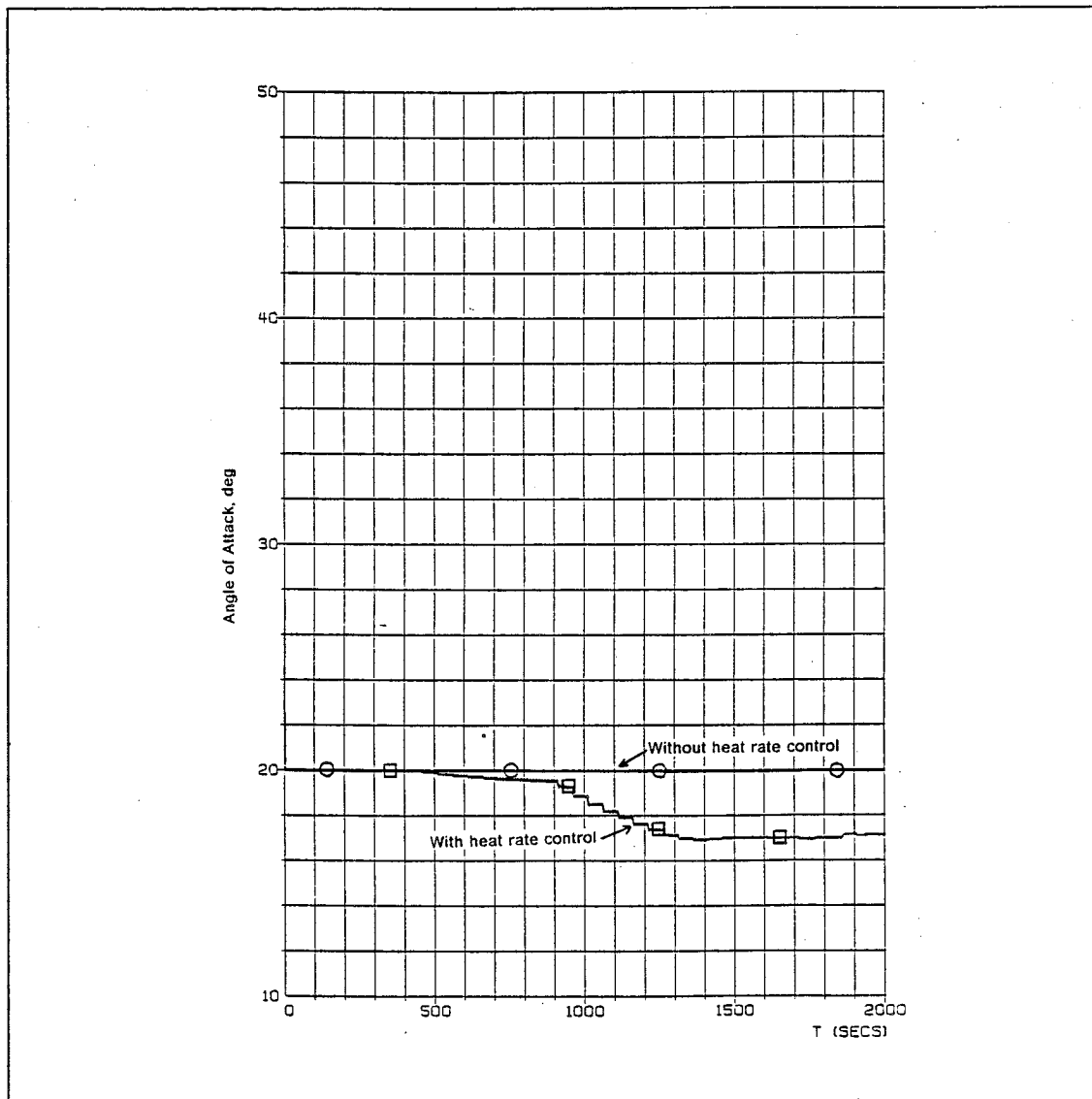


Figure 51. Angle of Attack Versus Time Comparison for Heat Rate Control

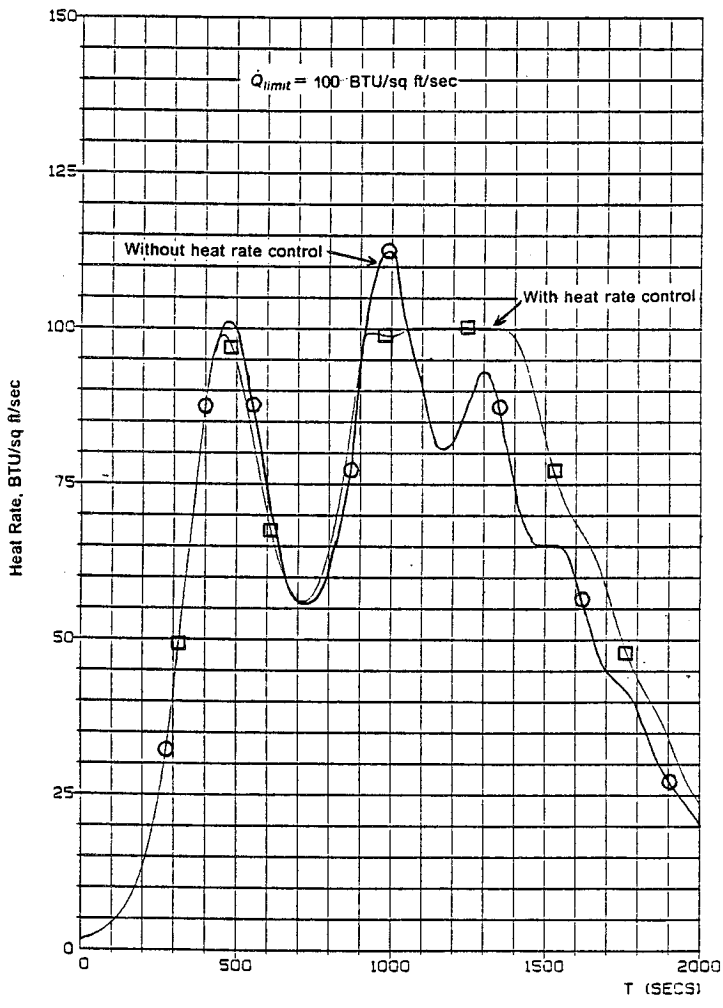


Figure 52. Heat Rate Versus Time Comparison for Heat Rate Control

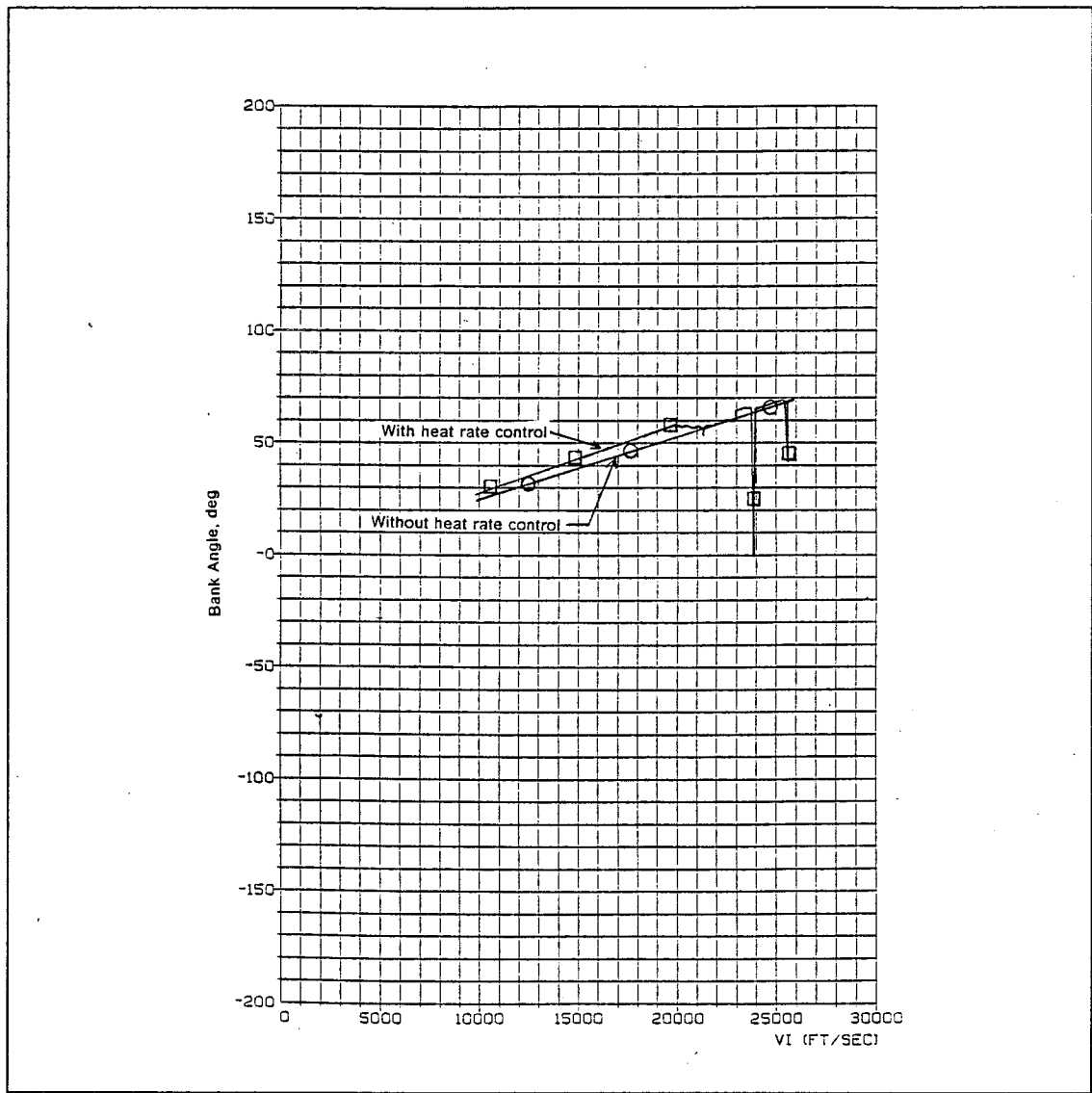


Figure 53. Bank Angle Versus Velocity Comparison for Heat Rate Control

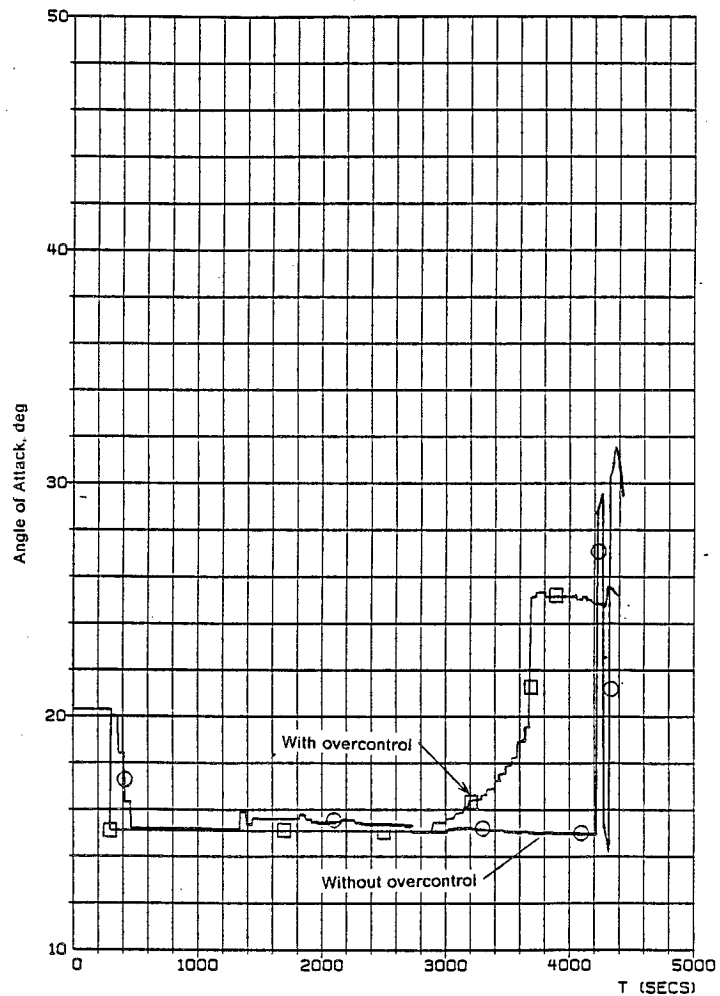


Figure 54. Angle of Attack Versus Time Comparison with Overcontrol

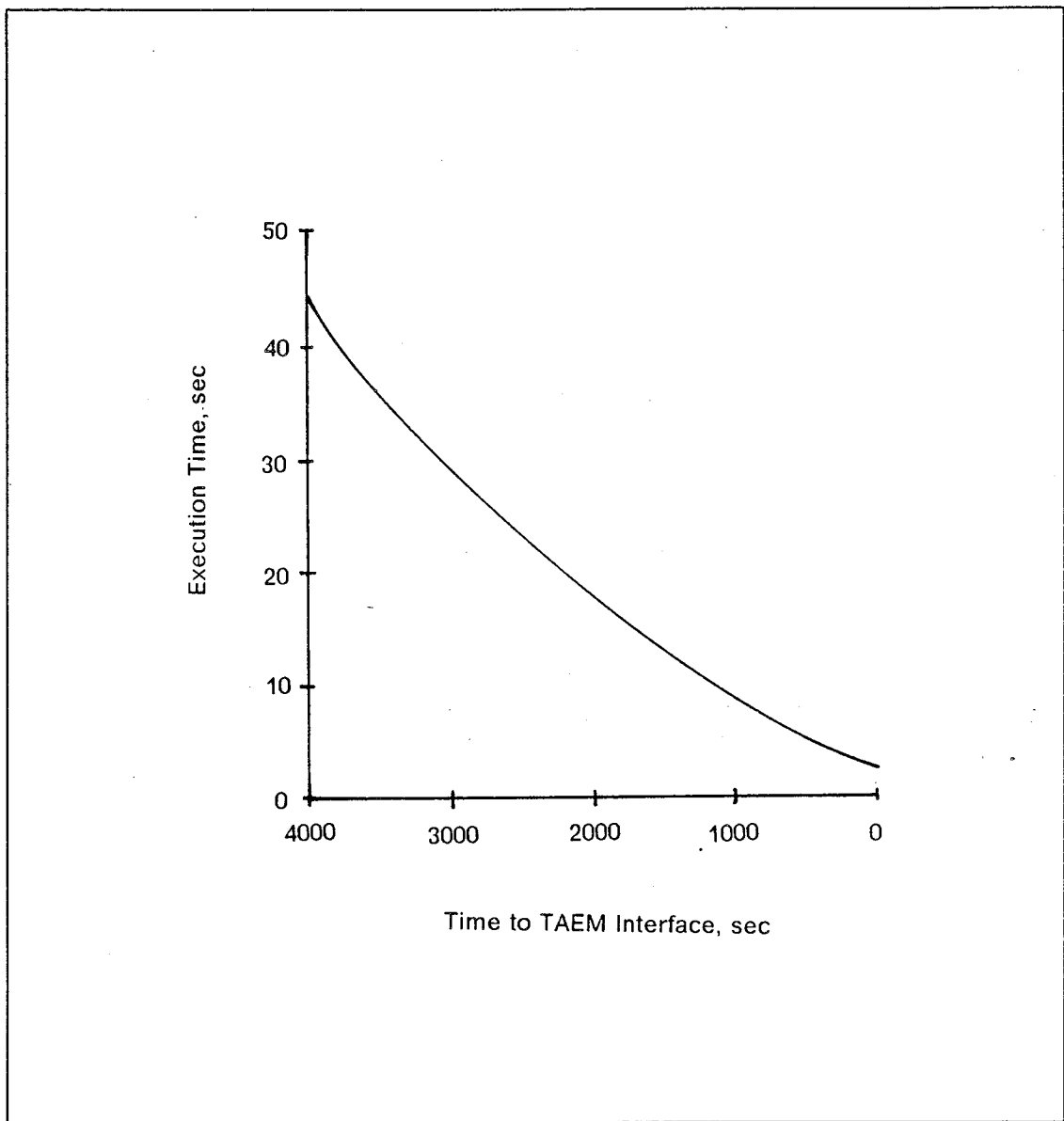


Figure 55. Required Execution Time for the Predictor-Corrector

APPENDIX A. ERV AERODYNAMICS MODEL

The aerodynamics of the ERV were reported in Reference [14], and the longitudinal performance coefficients, C_L and L/D, are shown in Figures 20 on page 97 and 21 on page 98. Figure 22 on page 99 shows a typical L/D versus angle of attack profile. This profile is for a Mach Number of 10, but across the flow regimes, the maximum L/D always occurs at an angle of attack of approximately 15 degrees. This data was incorporated into the aerodynamic model of the simulator and into the aerodynamic model of the predictor. It is seen that the aerodynamic flow regimes are a function of:

1. Mach Number, M
2. Viscous Interaction Parameter, \bar{V}
3. Altitude, h

The Mach Number, M , is computed from,

$$M = \frac{V_R}{C_s} \quad (99)$$

where the speed of sound, C_s , is computed from,

$$C_s = \sqrt{\gamma \frac{R}{M_0} T_M} \quad (100)$$

The viscous interaction parameter, \bar{V} , is computed from,

$$\bar{V} = M \sqrt{\frac{C'}{Re}} \quad (101)$$

where,

$$C' = \left(\frac{T'}{T_{static}} \right)^{0.5} \left[\frac{T_{static} + 122.1 \times 10^{-(5/T_{static})}}{T' + 122.1 \times 10^{-(5/T')}} \right]^{1.0} \quad (102)$$

and,

$$\frac{T'}{T_{static}} = 0.468 + 0.532 \frac{T_{wall}}{T_{static}} + 0.195 \frac{\gamma - 1}{2} M^2 \quad (103)$$

The Reynolds Number, Re , is calculated from,

$$Re = \frac{\rho V_R \bar{c}}{\mu} \quad (104)$$

where the coefficient of viscosity for air, μ , is given by,

$$\mu = \frac{\beta T_{static}^{3/2}}{S + T_{static}} \quad (105)$$

APPENDIX B. ALGORITHM PROGRAM LISTINGS

Compiled listings of the flight software principal functions for the predictor-corrector guidance algorithm as coded for use in the 6-DOF Aeroassist Flight Experiment Simulator (AFESIM) follow. The algorithms are coded in the HAL/S computer language. The principal functions are:

1. IL_LOAD - Values for all constants and I-loads
2. FSW_SEQ - Flight Software Sequencer
3. ORB_NAV - Orbit Navigation Algorithm
4. AERO_GUID - Predictor-Corrector Guidance Algorithm

At the beginning of each principal function is a description of the function and the input/output parameters. At the end of each principal function is a cross reference table listing the program line at which each variable is referenced or computed.

STMT	SOURCE	CURRENT SCOPE
211 M IL_LOAD;		IL_LOAD
211 M PROCEDURE;		IL_LOAD
C ----- C FUNCTION: VALUES OF I-LOADS AND CONSTANTS C INPUTS: NONE C OUTPUTS: ALL I-LOADS AND CONSTANTS LISTED C COMMENTS: NONE C -----		IL_LOAD IL_LOAD IL_LOAD IL_LOAD IL_LOAD IL_LOAD
C ----- C MATH CONSTANTS AND CONVERSION FACTORS C -----		IL_LOAD IL_LOAD IL_LOAD
212 M DECLARE PI SCALAR DOUBLE CONSTANT(3.1415926535897932385);		IL_LOAD
213 M DECLARE DEG_TO_SEC SCALAR DOUBLE CONSTANT(3600);		IL_LOAD
214 M DECLARE SEC_TO_DEG SCALAR DOUBLE CONSTANT(1 / DEG_TO_SEC);		IL_LOAD
215 M DECLARE DEG_TO_RAD SCALAR DOUBLE CONSTANT(PI / 180);		IL_LOAD
216 M DECLARE RAD_TO_DEG SCALAR DOUBLE CONSTANT(1 / DEG_TO_RAD);		IL_LOAD
217 M DECLARE SEC_TO_RAD SCALAR DOUBLE CONSTANT(DEG_TO_RAD / 3600);		IL_LOAD
218 M DECLARE RAD_TO_SEC SCALAR DOUBLE CONSTANT(1 / SEC_TO_RAD);		IL_LOAD
219 M DECLARE FT_TO_M SCALAR DOUBLE CONSTANT(0.3048);		IL_LOAD
220 M DECLARE M_TO_FT SCALAR DOUBLE CONSTANT(1 / FT_TO_M);		IL_LOAD
221 M DECLARE FT_TO_NM SCALAR DOUBLE CONSTANT(FT_TO_M / 1852);		IL_LOAD
222 M DECLARE NM_TO_FT SCALAR DOUBLE CONSTANT(1 / FT_TO_NM);		IL_LOAD
223 M DECLARE G_TO_FPS2 SCALAR DOUBLE CONSTANT(9.80665 M_TO_FT);		IL_LOAD
224 M DECLARE FPS2_TO_G SCALAR DOUBLE CONSTANT(1 / G_TO_FPS2);		IL_LOAD
225 M DECLARE LBM_TO_KG SCALAR DOUBLE CONSTANT(.45359237);		IL_LOAD
226 M DECLARE KG_TO_LBM SCALAR DOUBLE CONSTANT(1 / LBM_TO_KG);		IL_LOAD
227 M DECLARE SLUG_TO_KG SCALAR DOUBLE CONSTANT(LBM_TO_KG G_TO_FPS2);		IL_LOAD
228 M DECLARE KG_TO_SLUG SCALAR DOUBLE CONSTANT(KG_TO_LBM FPS2_TO_G);		IL_LOAD
229 M DECLARE LBF_TO_N SCALAR DOUBLE CONSTANT(4.4482216152605);		IL_LOAD
230 M DECLARE N_TO_LBF SCALAR DOUBLE CONSTANT(1 / LBF_TO_N);		IL_LOAD

PREGMING PAGE BLANK NOT FILMED

STMT	SOURCE	CURRENT SCOPE
C ----- C FSW SEQ VARIABLES C -----		IL_LOAD IL_LOAD IL_LOAD
231 M AERO_DAP_CNT = 1;		IL_LOAD
232 M AERO_DAP_PHS = 0;		IL_LOAD
233 M AERO_GUID_CNT = 5;		IL_LOAD
234 M AERO_GUID_PHS = 0;		IL_LOAD
235 M ORB_NAV_CNT = 5;		IL_LOAD
236 M ORB_NAV_PHS = 0;		IL_LOAD
C ----- C EPOCH DATA C -----		IL_LOAD IL_LOAD IL_LOAD
E * 237 M EF_TO_REF_AT_EPOCH = MATRIX S (+1.0, +0.0, +0.0, +0.0, +1.0, +0.0, +0.0, +0.0, +1.0); @DOUBLE,3,3		IL_LOAD
238 M T_EPOCH = 0;		IL_LOAD
C ----- C EARTH PHYSICAL PARAMETERS C -----		IL_LOAD IL_LOAD IL_LOAD
239 M EARTH_FLAT = 1 / 298.3;		IL_LOAD
240 M EARTH_J2 = 1082.7E-6;		IL_LOAD
E * 241 M EARTH_MU = (3.986012E14) / (.3048) ³		IL_LOAD
E * 242 M EARTH_POLE = VECTOR S (2.8991969340471790E-3, -5.1580036678323420E-5, @DOUBLE,3		IL_LOAD
242 M 9.9999579598948170E-1;		IL_LOAD
243 M EARTH_R = (6378166.0) / .3048;		IL_LOAD
244 M EARTH_RATE = 7.292114883223324E-5;		IL_LOAD
E * 245 M ME_NAV = EARTH_RATE EARTH_POLE;		IL_LOAD

HAL/S STD 360-24.20

INTERMETRICS, INC.

APRIL 27, 1987 15:0:48.60

STMT	SOURCE	CURRENT SCOPE
C ----- C PREDICTOR-CORRECTOR I-LOADS (MISSION-SPECIFIC) C -----		IL_LOAD IL_LOAD IL_LOAD
C ----- C TARGET AIM POINT FOR MAXIMUM DOWNRANGE CASE C DOWNRANGE = 13849 N.M. C CROSSRANGE = 497 N.M. C -----		IL_LOAD IL_LOAD IL_LOAD IL_LOAD IL_LOAD
C ----- C INITIAL CONDITIONS: C ----- C LATITUDE -28.071 DEG C LONGITUDE -69.313 DEG C INCLINATION 28.50 DEG C FLIGHT PATH ANGLE -0.996 DEG C INERTIAL VELOCITY 25778.843 FT/SEC C ALTITUDE 400000.0 FT C -----		IL_LOAD IL_LOAD IL_LOAD IL_LOAD IL_LOAD IL_LOAD IL_LOAD IL_LOAD IL_LOAD
C ----- C GEODETIC LATITUDE OF TAEM INTERFACE AIM POINT C -----		IL_LOAD IL_LOAD IL_LOAD
246 M LAT_TARGET = 3.084;		IL_LOAD
C ----- C LONGITUDE OF TAEM INTERFACE AIM POINT C -----		IL_LOAD IL_LOAD IL_LOAD
247 M LONG_TARGET = 157.659;		IL_LOAD
C ----- C INITIAL CONTROL VALUES FOR MAXIMUM DOWNRANGE CASE C -----		IL_LOAD IL_LOAD IL_LOAD
248 M PHI_EI = 0.0;		IL_LOAD
249 M ALPHA_EI = 20.0;		IL_LOAD
C ----- C ESTIMATOR FILTER GAINS (TAU = 25.0 SECONDS) C -----		IL_LOAD IL_LOAD IL_LOAD
250 M K_RHO_FILTER_GAIN = .03921;		IL_LOAD
251 M L_OVER_D_FILTER_GAIN = .03921;		IL_LOAD
C ----- C VEHICLE MASS (SLUGS) C -----		IL_LOAD IL_LOAD IL_LOAD
252 M MASS_NAV = 186.0;		IL_LOAD

HAL/S STO 360-24.20 INTE R M E T R I C S , I N C . APRIL 27, 1987 15:0:48.60

STMT	SOURCE	CURRENT SCOPE
C1	PREDICTOR-CORRECTOR I-LOADS (DESIGN PARAMETERS NOT NORMALLY CHANGED)	I-LOAD
C1	ALTITUDES AT WHICH SURFACE GEOMETRIES, FREEZES COMMAND, TARGETS, AND USES HINNIM TIME STEP FOR INTEGRATION	I-LOAD
253 M1	ALT_EXIT = 400000.0,	I-LOAD
254 M1	ALT_FREEZE_GRID = 100000.0,	I-LOAD
255 M1	ALT_TARGET = 60000.0,	I-LOAD
256 M1	ALT_TARGET = ALT_TARGET + 10000.0,	I-LOAD
257 M1	G_RAN_GUIDANCE = 0.07,	I-LOAD
C1	G-LEVEL AT WHICH TO ACTIVATE GUIDANCE	I-LOAD
C1	GRAVITY MODEL WITH JS TERM	I-LOAD
258 M1	GRAVITY_MODEL = 1,	I-LOAD
C1	REFERENCE AREA OF ERY	I-LOAD
259 M1	S_REF = 177.41	I-LOAD
C1	TIME INCREMENT BETWEEN EXECUTIONS OF PREDICTOR-CORRECTOR EXECUTIVE	I-LOAD
C1	NUMBER OF EXECUTIONS OF PREDICTOR-CORRECTOR EXECUTIVE BETWEEN UPDATES OF COMMANDED ATTITUDE USING PREDICTOR-CORRECTOR	I-LOAD
260 M1	DT_AEROGUID = 1.0,	I-LOAD
C1	GUID_PASSTHM = 50	I-LOAD

ORIGINAL PAGE IS
OF POOR QUALITY

HAL/S STD 360-24.20	INTERMETRICS, INC.	APRIL 27, 1987 15:0:48.60
STMT	SOURCE	CURRENT SCOPE
C ----- C LINEAR BANK WITH VELOCITY PROFILE CONSTANTS C -----		IL_LOAD IL_LOAD IL_LOAD
262 M PHI_DES_MAX = 180.0;		IL_LOAD
263 M PHI_MAX = 90.0;		IL_LOAD
264 M V_FINAL_MAG = 1000.0;		IL_LOAD
265 M V_INITIAL_MAG = 26000.0;		IL_LOAD
266 M V_MAG_CHANGE = V_INITIAL_MAG - V_FINAL_MAG;		IL_LOAD
C ----- C CONSTANT ANGLE OF ATTACK PROFILE CONSTANTS C -----		IL_LOAD IL_LOAD IL_LOAD
267 M ALPHA_MAX = 45.0;		IL_LOAD
268 M ALPHA_MIN = 15.0;		IL_LOAD
C ----- C VARIABLE TIME STEP CONTROL CONSTANTS C -----		IL_LOAD IL_LOAD IL_LOAD
269 M DELTA_T_PRED_GAIN = 200.0;		IL_LOAD
270 M DELTA_T_PRED_MAX = 20.0;		IL_LOAD
271 M DELTA_T_PRED_MIN = 2.0;		IL_LOAD
C ----- C HEAT RATE CONTROL CONSTANTS C -----		IL_LOAD IL_LOAD IL_LOAD
272 M HS = 23500.0;		IL_LOAD
273 M OMEGA_QDOT = 0.10;		IL_LOAD
274 M QDOT_LIMIT = 125.0;		IL_LOAD
275 M RHO_SL = 0.002378;		IL_LOAD
276 M ZETA_QDOT = 1.00;		IL_LOAD
277 M CLOSE IL_LOAD;		IL_LOAD

**** BLOCK SUMMARY ****

COMPOOL VARIABLES USED

HAL/S STD 360-24.20

INTERMETRICS, INC.

APRIL 27, 1987 15:048.60

STMT	SOURCE	CURRENT SCOPE
AERO_DAP_CNT*, AERO_DAP_PHS*, AERO_GUID_CNT*, AERO_GUID_PHS*, ORB_NAV_CNT*, ORB_NAV_PHS*, EF_TO_REF_AT_EPOCH*, T_EPOCH*		
EARTH_FLAT*, EARTH_J2*, EARTH_MU*, EARTH_POLE*, EARTH_RX*, EARTH_RATE*, HE_NAVX, EARTH_RATE, EARTH_POLE, LAT_TARGET*		
LONG_TARGET*, PHI_EIX, ALPHA_EIX, K_RHO_FILTER_GAIN*, L_OVER_D_FILTER_GAIN*, MASS_NAVX, ALT_EXIT*, ALT_FREEZE_GUID*, ALT_TAEM*		
ALT_TAEM_BIAS*, ALT_TAEM, G_RUN_GUIDANCE*, GRAVITY_MODEL*, S_REFX, DT_AEROGUID*, GUID_PASS_LINX, PHI_DES_MAX*, PHI_MAX*		
V_FINAL_MAG*, V_INITIAL_MAG*, V_MAG_CHANGE*, V_INITIAL_MAG, V_FINAL_MAG, ALPHA_MAX*, ALPHA_MIN*, DELTA_T_PRED_GAIN*		
DELTA_T_PRED_MAX*, DELTA_T_PRED_MIN*, HS*, OMEGA_QDOT*, QDOT_LIMIT*, RHO_SL*, ZETA_QDOT*		

HAL/S STD 360-24.20

INTERMETRICS, INC.

APRIL 27, 1987 15:04:48.60

***** COMPILED LAYOUT *****

IL_POOL: EXTERNAL COMPOOL;

IL_LOAD: PROCEDURE;

ORIGINAL PAGE IS
OF POOR QUALITY

HAL/S STD 360-24.20

INTERMETRICS, INC.

APRIL 27, 1987 15:0:48.60

S Y M B O L & C R O S S R E F E R E N C E T A B L E L I S T I N G :

(CROSS REFERENCE FLAG KEY: 4 = ASSIGNMENT, 2 = REFERENCE, 1 = SUBSCRIPT USE, 0 = DEFINITION)

DCL	NAME	TYPE	ATTRIBUTES & CROSS REFERENCE
21	AERO_DAP_CNT	INTEGER	SINGLE, ALIGNED, INITIAL XREF: 0 0021 4 0231 NOT REFERENCED
20	AERO_DAP_PHS	INTEGER	SINGLE, ALIGNED, INITIAL XREF: 0 0020 4 0232 NOT REFERENCED
23	AERO_GUID_CNT	INTEGER	SINGLE, ALIGNED, INITIAL XREF: 0 0023 4 0233 NOT REFERENCED
22	AERO_GUID_PHS	INTEGER	SINGLE, ALIGNED, INITIAL XREF: 0 0022 4 0234 NOT REFERENCED
97	ALPHA_EI	SCALAR	SINGLE, ALIGNED, INITIAL XREF: 0 0097 4 0249 NOT REFERENCED
209	ALPHA_MAX	SCALAR	SINGLE, ALIGNED, INITIAL XREF: 0 0209 4 0267 NOT REFERENCED
209	ALPHA_MIN	SCALAR	SINGLE, ALIGNED, INITIAL XREF: 0 0209 4 0268 NOT REFERENCED
79	ALT_EXIT	SCALAR	SINGLE, ALIGNED, INITIAL XREF: 0 0079 4 0253 NOT REFERENCED
209	ALT_FREEZE_GUID	SCALAR	SINGLE, ALIGNED, INITIAL XREF: 0 0209 4 0254 NOT REFERENCED
209	ALT_TAEM	SCALAR	SINGLE, ALIGNED, INITIAL XREF: 0 0209 4 0255 2 0256
209	ALT_TAEM_BIAS	SCALAR	SINGLE, ALIGNED, INITIAL XREF: 0 0209 4 0256 NOT REFERENCED
215	DEG_TO_RAD	SCALAR	DOUBLE, ALIGNED, STATIC, CONSTANT XREF: 0 0215 2 0216 2 0217
213	DEG_TO_SEC	SCALAR	DOUBLE, ALIGNED, STATIC, CONSTANT XREF: 0 0213 2 0214
209	DELTA_T_PRED_GAIN	SCALAR	SINGLE, ALIGNED, INITIAL XREF: 0 0209 4 0269 NOT REFERENCED
209	DELTA_T_PRED_MAX	SCALAR	SINGLE, ALIGNED, INITIAL XREF: 0 0209 4 0270 NOT REFERENCED
209	DELTA_T_PRED_MIN	SCALAR	SINGLE, ALIGNED, INITIAL XREF: 0 0209 4 0271 NOT REFERENCED
209	DT_AEROGUID	SCALAR	SINGLE, ALIGNED, INITIAL XREF: 0 0209 4 0260 NOT REFERENCED
159	EARTH_FLAT	SCALAR	DOUBLE, ALIGNED, INITIAL XREF: 0 0159 4 0239 NOT REFERENCED
160	EARTH_J2	SCALAR	DOUBLE, ALIGNED, INITIAL XREF: 0 0160 4 0240 NOT REFERENCED
161	EARTH_MU	SCALAR	DOUBLE, ALIGNED, INITIAL XREF: 0 0161 4 0241 NOT REFERENCED
162	EARTH_POLE	3 - VECTOR	DOUBLE, ALIGNED, INITIAL XREF: 0 0162 4 0242 2 0245
163	EARTH_R	SCALAR	DOUBLE, ALIGNED, INITIAL XREF: 0 0163 4 0243 NOT REFERENCED
164	EARTH_RATE	SCALAR	DOUBLE, ALIGNED, INITIAL XREF: 0 0164 4 0244 2 0245
4	EF_TO_REF_AT_EPOCH	3 X 3 MATRIX	DOUBLE, ALIGNED, INITIAL XREF: 0 0004 4 0237 NOT REFERENCED
224	FPS2_TO_G	SCALAR	DOUBLE, ALIGNED, STATIC, CONSTANT XREF: 0 0224 2 0228
219	FT_TO_M	SCALAR	DOUBLE, ALIGNED, STATIC, CONSTANT XREF: 0 0219 2 0220 2 0221
221	FT_TO_NM	SCALAR	DOUBLE, ALIGNED, STATIC, CONSTANT XREF: 0 0221 2 0222
209	G_RUN_GUIDANCE	SCALAR	SINGLE, ALIGNED, INITIAL XREF: 0 0209 4 0257 NOT REFERENCED
223	G_TO_FPS2	SCALAR	DOUBLE, ALIGNED, STATIC, CONSTANT XREF: 0 0223 2 0224 2 0227
165	GRAVITY_MODEL	INTEGER	SINGLE, ALIGNED, INITIAL XREF: 0 0165 4 0258 NOT REFERENCED
209	GUID_PASS_LIM	SCALAR	SINGLE, ALIGNED, INITIAL XREF: 0 0209 4 0261 NOT REFERENCED
209	HS	SCALAR	SINGLE, ALIGNED, INITIAL XREF: 0 0209 4 0272 NOT REFERENCED XREF: 0 0211 NOT REFERENCED
211	IL_LOAD	PROCEDURE	SINGLE, ALIGNED, INITIAL XREF: 0 0168 4 0250 NOT REFERENCED
168	K_RHO_FILTER_GAIN	SCALAR	DOUBLE, ALIGNED, STATIC, CONSTANT XREF: 0 0226 2 0228
226	KG_TO_LBM	SCALAR	DOUBLE, ALIGNED, STATIC, CONSTANT XREF: 0 0228 NOT REFERENCED
228	KG_TO_SLUG	SCALAR	SINGLE, ALIGNED, INITIAL XREF: 0 0171 4 0251 NOT REFERENCED
171	L_OVER_D_FILTER_GAIN	SCALAR	SINGLE, ALIGNED, INITIAL XREF: 0 0209 4 0246 NOT REFERENCED
209	LAT_TARGET	SCALAR	DOUBLE, ALIGNED, STATIC, CONSTANT XREF: 0 0229 2 0230
229	LBF_TO_N	SCALAR	DOUBLE, ALIGNED, STATIC, CONSTANT XREF: 0 0225 2 0226 2 0227
225	LBM_TO_KG	SCALAR	SINGLE, ALIGNED, INITIAL XREF: 0 0209 4 0247 NOT REFERENCED
209	LONG_TARGET	SCALAR	DOUBLE, ALIGNED, STATIC, CONSTANT XREF: 0 0220 2 0223
220	M_TO_FT	SCALAR	SINGLE, ALIGNED, INITIAL XREF: 0 0010 4 0252 NOT REFERENCED
10	MASS_NAV	SCALAR	DOUBLE, ALIGNED, STATIC, CONSTANT XREF: 0 0230 NOT REFERENCED
230	N_TO_LBF	SCALAR	

HAL/S STD 360-24.20 INTERMETRICS, INC. APRIL 27, 1987 15:0:48.60
 DCL NAME TYPE ATTRIBUTES & CROSS REFERENCE
 222 NM_TO_FT SCALAR DOUBLE, ALIGNED, STATIC, CONSTANT XREF: 0 0222
 NOT REFERENCED
 209 QMEGA_QDOT SCALAR SINGLE, ALIGNED, INITIAL XREF: 0 0209 4 0273 NOT REFERENCED
 35 ORB_NAV_CNT INTEGER SINGLE, ALIGNED, INITIAL XREF: 0 0035 4 0235 NOT REFERENCED
 34 ORB_NAV_PHS INTEGER SINGLE, ALIGNED, INITIAL XREF: 0 0034 4 0236 NOT REFERENCED
 209 PHI_DES_MAX SCALAR SINGLE, ALIGNED, INITIAL XREF: 0 0209 4 0262 NOT REFERENCED
 98 PHI_EI SCALAR SINGLE, ALIGNED, INITIAL XREF: 0 0098 4 0248 NOT REFERENCED
 209 PHI_MAX SCALAR SINGLE, ALIGNED, INITIAL XREF: 0 0209 4 0263 NOT REFERENCED
 212 PI SCALAR DOUBLE, ALIGNED, STATIC, CONSTANT XREF: 0 0212 2 0215
 209 QDOT_LIMIT SCALAR SINGLE, ALIGNED, INITIAL XREF: 0 0209 4 0274 NOT REFERENCED
 216 RAD_TO_DEG SCALAR DOUBLE, ALIGNED, STATIC, CONSTANT XREF: 0 0216
 NOT REFERENCED
 218 RAD_TO_SEC SCALAR DOUBLE, ALIGNED, STATIC, CONSTANT XREF: 0 0218
 NOT REFERENCED
 209 RHO_SL SCALAR SINGLE, ALIGNED, INITIAL XREF: 0 0209 4 0275 NOT REFERENCED
 174 S_REF SCALAR SINGLE, ALIGNED, INITIAL XREF: 0 0174 4 0259 NOT REFERENCED
 214 SEC_TO_DEG SCALAR DOUBLE, ALIGNED, STATIC, CONSTANT XREF: 0 0214
 NOT REFERENCED
 217 SEC_TO_RAD SCALAR DOUBLE, ALIGNED, STATIC, CONSTANT XREF: 0 0217 2 0218
 227 SLUG_TO_KG SCALAR DOUBLE, ALIGNED, STATIC, CONSTANT XREF: 0 0227
 NOT REFERENCED
 6 T_EPOCH SCALAR DOUBLE, ALIGNED, INITIAL XREF: 0 0006 4 0238 NOT REFERENCED
 209 V_FINAL_MAG SCALAR SINGLE, ALIGNED, INITIAL XREF: 0 0209 4 0264 2 0266
 209 V_INITIAL_MAG SCALAR SINGLE, ALIGNED, INITIAL XREF: 0 0209 4 0265 2 0266
 209 V_MAG_CHANGE SCALAR SINGLE, ALIGNED, INITIAL XREF: 0 0209 4 0266 NOT REFERENCED
 176 HE_NAV 3 - VECTOR SINGLE, ALIGNED, INITIAL XREF: 0 0176 4 0245 NOT REFERENCED
 209 ZETA_QDOT SCALAR SINGLE, ALIGNED, INITIAL XREF: 0 0209 4 0276 NOT REFERENCED

ORIGINAL
 OF POOR QUALITY

HAL/S STD 360-24.20

INTERMETRICS, INC.

APRIL 27, 1987 15:1:9.08

STMT	SOURCE	CURRENT SCOPE
518 M FSM_SEQ;		FSH_SEQ
518 M PROCEDURE;		FSH_SEQ
C -----		FSH_SEQ
C FUNCTION: EXECUTE FLIGHT SOFTWARE PRINCIPAL FUNCTIONS AT		FSH_SEQ
C PROPER RATE AND IN PROPER ORDER WHEN FUNCTIONS ACTIVE		FSH_SEQ
C INPUTS: ORB_NAV_ACT - ORBIT NAVIGATION ACTIVE FLAG		FSH_SEQ
C AERO_GUID_ACT - PREDICTOR-CORRECTOR ACTIVE FLAG		FSH_SEQ
C AERO_DAP_ACT - DIGITAL AUTOPILOT ACTIVE FLAG		FSH_SEQ
C OUTPUTS: NONE		FSH_SEQ
C COMMENTS: NONE		FSH_SEQ
C -----		FSH_SEQ
C -----		FSH_SEQ
C LOCAL VARIABLES		FSH_SEQ
C -----		FSH_SEQ
519 M DECLARE FSH_PASS INTEGER DOUBLE INITIAL(0);		FSH_SEQ

ORIGINAL PAGE IS
OF POOR QUALITY

HAL/S STD 360-24.20 I N T E R M E T R I C S , I N C . APRIL 27, 1987 15:1:9.08

STMT	SOURCE	CURRENT SCOPE
E 520 M IF ORB_NAV_ACT = ON AND MOD(FSM_PASS, ORB_NAV_CNT) = ORB_NAV_PHS THEN		FSH_SEQ
521 M CALL ORB_NAV;		FSH_SEQ
E 522 M IF AERO_GUID_ACT = ON AND MOD(FSM_PASS, AERO_GUID_CNT) = AERO_GUID_PHS THEN		FSH_SEQ
523 M CALL AERO_GUID;		FSH_SEQ
E 524 M IF AERO_DAP_ACT = ON AND MOD(FSM_PASS, AERO_DAP_CNT) = AERO_DAP_PHS THEN		FSH_SEQ
525 M CALL AERO_DAP;		FSH_SEQ
526 M FSM_PASS = FSM_PASS + 1;		FSH_SEQ
527 M CLOSE FSH_SEQ;		FSH_SEQ
**** B L O C K S U M M A R Y ****		
EXTERNAL PROCEDURES CALLED		
ORB_NAV, AERO_GUID, AERO_DAP		
COMPOOL VARIABLES USED		
ORB_NAV_ACT, ORB_NAV_CNT, ORB_NAV_PHS, AERO_GUID_ACT, AERO_GUID_CNT, AERO_GUID_PHS, AERO_DAP_ACT, AERO_DAP_CNT, AERO_DAP_PHS		

HAL/S STD 360-24.20

INTERMETRICS, INC.

APRIL 27, 1987 15:1:9.08

**** COMPI LATION L A Y O U T ****

IL_POOL: EXTERNAL COMPOOL;
FSM_POOL: EXTERNAL COMPOOL;
ORB_NAV: EXTERNAL PROCEDURE;
AERO_GUID: EXTERNAL PROCEDURE;
AERO_DAP: EXTERNAL PROCEDURE;
FSW_SEQ: PROCEDURE;

HAL/S STD 360-24.20

INTERMETRICS, INC.

APRIL 27, 1987 15:1:9.08

SYMBOL & CROSS REFERENCE TABLE LISTING:

(CROSS REFERENCE FLAG KEY: 4 = ASSIGNMENT, 2 = REFERENCE, 1 = SUBSCRIPT USE, 0 = DEFINITION)

DCL	NAME	TYPE	ATTRIBUTES & CROSS REFERENCE
517	AERO_DAP	PROCEDURE	
255	AERO_DAP_ACT	BIT(1)	EXTERNAL, VERSION=1 XREF: 0 0517 2 0525
21	AERO_DAP_CNT	INTEGER	ALIGNED, INITIAL XREF: 0 0255 2 0524
20	AERO_DAP_PHS	INTEGER	SINGLE, ALIGNED, INITIAL XREF: 0 0021 2 0524
516	AERO_GUID	PROCEDURE	SINGLE, ALIGNED, INITIAL XREF: 0 0020 2 0524
256	AERO_GUID_ACT	BIT(1)	EXTERNAL, VERSION=1 XREF: 0 0516 2 0523
23	AERO_GUID_CNT	INTEGER	ALIGNED, INITIAL XREF: 0 0256 2 0522
22	AERO_GUID_PHS	INTEGER	SINGLE, ALIGNED, INITIAL XREF: 0 0023 2 0522
519	FSM_PASS	INTEGER	SINGLE, ALIGNED, INITIAL XREF: 0 0022 2 0522
			DOUBLE, ALIGNED, STATIC, INITIAL XREF: 0 0519 2 0520 2 0522 2 0524
			6 0526
518	FSM_SEQ	PROCEDURE	XREF: 0 0518 NOT REFERENCED
515	ORB_NAV	PROCEDURE	EXTERNAL, VERSION=1 XREF: 0 0515 2 0521
262	ORB_NAV_ACT	BIT(1)	ALIGNED, INITIAL XREF: 0 0262 2 0520
35	ORB_NAV_CNT	INTEGER	SINGLE, ALIGNED, INITIAL XREF: 0 0035 2 0520
34	ORB_NAV_PHS	INTEGER	SINGLE, ALIGNED, INITIAL XREF: 0 0034 2 0520

ORIGINAL PAGE IS
OF POOR QUALITY

HAL/S STD 360-24.20

INTERMETRICS, INC.

APRIL 27, 1987 11:19:28.56

STM

SOURCE

CURRENT SCOPE

523 MI ORB NAV:

| ORB NAV

523 MI PROCEDURE,

1 ORB NAV

```

C| FUNCTION: MAINTAIN ESTIMATE OF VEHICLE STATE VECTOR AND COMPUTE
C| STATE VECTOR DERIVED PARAMETERS
C| INPUTS: T_ATTITUDE - TIME TAG OF STATE VECTOR
C|          RI - POSITION VECTOR
C|          VI - VELOCITY VECTOR
C|          AI - ACCELERATION VECTOR,
C|          QIB - ATTITUDE QUATERNION
C|          PHI - BANK ANGLE
C| OUTPUTS: T_NAV - TIME TAG OF STATE VECTOR
C|          R_NAV - POSITION VECTOR
C|          V_NAV - VELOCITY VECTOR
C|          A_NAV - ACCELERATION VECTOR
C|          Q_B_TO_I - ATTITUDE QUATERNION
C|          R_NAV_MAG - MAGNITUDE OF POSITION VECTOR
C|          UNIT_R - UNIT VECTOR IN DIRECTION OF POSITION VECTOR
C|          ALT_NAV - ALTITUDE ABOVE FISHER ELLIPSOID
C|          V_NAV_MAG - MAGNITUDE OF VELOCITY VECTOR
C|          V_REL_NAV - RELATIVE VELOCITY VECTOR
C|          V_REL_MAG - MAGNITUDE OF RELATIVE VELOCITY VECTOR
C|          RDOT_NAV - RADIAL VELOCITY MAGNITUDE
C|          G_LOAD - SENSED ACCELERATION MAGNITUDE IN G'S
C|          ALPHA_NAV - ANGLE OF ATTACK
C|          BETA_NAV - SIDESLIP ANGLE
C|          PHI_NAV - BANK ANGLE
C|          ENTRY_COMPLETE - TAEM INTERFACE FLAG
C| COMMENTS: PERFECT NAVIGATION IS ASSUMED, SO THE STATE VECTOR FROM
C|           FROM THE ENVIRONMENT MODEL IS COPIED.

```

C| -----
C| LOCAL VARIABLES
C| -----

ORB_NAV

524 M1 DECLARE VREL BODY VECTOR(3) SINGLE INITIAL(0)

I ORB NAV

HAL/S STD 360-24.20

INTERMETRICS, INC.

APRIL 27, 1987 11:19:28.56

STMT	SOURCE	CURRENT SCOPE
C -----		ORB_NAV
C COMPUTE STATE VECTOR DERIVED PARAMETERS		ORB_NAV
C -----		ORB_NAV
531 M T_NAV = T_IMU_NAV;		ORB_NAV
E -----		
532 M R_NAV_MAG = ABVAL(R_NAV);		ORB_NAV
E -----		
533 M UNIT_R = R_NAV / R_NAV_MAG;		ORB_NAV
E -----		
534 M ALT_NAV = R_NAV_MAG - (1 - EARTH_FLAT) EARTH_R / SQRT(1 + ((1 - EARTH_FLAT) ² - 1) (1 - (UNIT_R .		ORB_NAV
E EARTH_POLE ²));		ORB_NAV
E -----		
535 M V_NAV_MAG = ABVAL(V_NAV);		ORB_NAV
E -----		
536 M V_REL_NAV = V_NAV - (HE_NAV * R_NAV);		ORB_NAV
E -----		
537 M V_REL_MAG = ABVAL(V_REL_NAV);		ORB_NAV
E -----		
538 M RDOT_NAV = V_NAV . UNIT_R;		ORB_NAV
E -----		
539 M G_LOAD = ABVAL(A_NAV) FPS2_TO_G;		ORB_NAV
C -----		
C ANGLE OF ATTACK AND SIDESLIP ANGLE		ORB_NAV
C -----		ORB_NAV
E -----		
540 M VREL_BODY = SQFORM(SQPOSE(Q_B_TO_I), V_REL_NAV);		ORB_NAV
541 M ALPHA_NAV = SARCTAN2(VREL_BODY , VREL_BODY) RAD_TO_DEG;		ORB_NAV
S 3 1		
542 M BETA_NAV = ARCSIN(VREL_BODY / V_REL_MAG) RAD_TO_DEG;		ORB_NAV
S 2		
C -----		
C FLAG SIGNALING TAEM INTERFACE OR SKIP OUT		ORB_NAV
C -----		ORB_NAV
543 M IF ((ALT_NAV > ALT_EXIT) AND (RDOT_NAV > 0)) OR (ALT_NAV < ALT_TAEM) THEN		ORB_NAV
E -----		
544 M AERO_BRAKE_COMPLETE = TRUE;		ORB_NAV

HAL/S STD 360-24.20

INTERMETRICS, INC.

APRIL 27, 1987 11:19:28.56

STMT

SOURCE

CURRENT SCOPE

545 H| CLOSE ORB_NAV;

| ORB_NAV

**** BLOCK SUMMARY ****

EXTERNAL FUNCTIONS INVOKED
SQFORM, SQPOSE, SARCTAN2

COMMON VARIABLES USED

T_IMU_NAV*, T_ATTITUDE, R_NAV*, RI, V_NAV*, VI, A_NAV*, AI, Q_B_TO_I*, QIB, PHI_NAV*, PHI, T_NAV*, T_IMU_NAV, R_NAV_MAG*, R_NAV_UNIT_R*, R_NAV_MAG, ALT_NAV*, EARTH_FLAT, EARTH_R, UNIT_R, EARTH_POLE, V_NAV_MAG*, V_NAV, V_REL_NAV*, HE_NAV, V_REL_MAG*, V_REL_NAV, RDOT_NAV*, G_LOAD, A_NAV, FFS2_TO_G, Q_B_TO_I, ALPHA_NAV*, RAD_TO_DEG, BETA_NAV*, V_REL_MAG, ALT_NAV, ALT_EXIT_RDOT_NAV, ALT_TAEM, AERO BRAKE_COMPLETE*

HAL/S STD 360-24.20

INTERMETRICS, INC.

APRIL 27, 1987 11:19:28.56

**** COMPI LATION L A Y O U T ****

ENV_POOL: EXTERNAL COMPOOL;
FSH_POOL: EXTERNAL COMPOOL;
IL_POOL: EXTERNAL COMPOOL;
DQFORM: EXTERNAL FUNCTION;
Q_ERR_ANG: EXTERNAL FUNCTION;
SARCTAN2: EXTERNAL FUNCTION;
SQFORM: EXTERNAL FUNCTION;
SQMULT: EXTERNAL FUNCTION;
SQPOSE: EXTERNAL FUNCTION;
SRV_TO_QIL: EXTERNAL FUNCTION;
ORB_NAV: PROCEDURE;

SYMBOL & CROSS REFERENCE TABLE LISTING:

(CROSS REFERENCE FLAG KEY: 4 = ASSIGNMENT, 2 = REFERENCE, 1 = SUBSCRIPT USE, 0 = DEFINITION)

DCL	NAME	TYPE	ATTRIBUTES & CROSS REFERENCE
88	A_NAV	3 - VECTOR	DOUBLE, ALIGNED, INITIAL XREF: 0 0088 4 0528 2 0539
78	AERO BRAKE_COMPLETE	BIT(1)	ALIGNED, INITIAL XREF: 0 0078 4 0544 NOT REFERENCED
1	AI	3 - VECTOR	DOUBLE, ALIGNED, INITIAL XREF: 0 0001 2 0528
75	ALPHA_NAV	SCALAR	SINGLE, ALIGNED, INITIAL XREF: 0 0075 4 0541 NOT REFERENCED
384	ALT_EXIT	SCALAR	SINGLE, ALIGNED, INITIAL XREF: 0 0384 2 0543
80	ALT_NAV	SCALAR	DOUBLE, ALIGNED, INITIAL XREF: 0 0080 4 0534 2 0543
514	ALT_TAEM	SCALAR	SINGLE, ALIGNED, INITIAL XREF: 0 0514 2 0543
76	BETA_NAV	SCALAR	SINGLE, ALIGNED, INITIAL XREF: 0 0076 4 0542 NOT REFERENCED
518	CARG	SCALAR	SINGLE, ALIGNED, INPUT-PARM XREF: 0 0518
516	DGFORM	3 - VECTOR FUNCTION	DOUBLE, INITIAL, EXTERNAL, VERSION=2 XREF: 0 0516 NOT REFERENCED
464	EARTH_FLAT	SCALAR	DOUBLE, ALIGNED, INITIAL XREF: 0 0464 2 0534
467	EARTH_POLE	3 - VECTOR	DOUBLE, ALIGNED, INITIAL XREF: 0 0467 2 0534
468	EARTH_R	SCALAR	DOUBLE, ALIGNED, INITIAL XREF: 0 0468 2 0534
15	FPS2_TO_G	SCALAR	DOUBLE, ALIGNED, CONSTANT XREF: 0 0015 2 0019 2 0539
83	G_LOAD	SCALAR	DOUBLE, ALIGNED, INITIAL XREF: 0 0083 4 0539 NOT REFERENCED XREF: 0 0523 NOT REFERENCED
523	ORB_NAV	PROCEDURE	SINGLE, ALIGNED, INPUT-PARM XREF: 0 0520
520	P	4 - VECTOR	SINGLE, ALIGNED, INITIAL XREF: 0 0001 2 0530
1	PHI	SCALAR	SINGLE, ALIGNED, INITIAL XREF: 0 0077 4 0530 NOT REFERENCED
77	PHI_NAV	SCALAR	SINGLE, ALIGNED, INPUT-PARM XREF: 0 0521
521	Q	4 - VECTOR	SINGLE, ALIGNED, INPUT-PARM XREF: 0 0519
519	Q	4 - VECTOR	SINGLE, ALIGNED, INPUT-PARM XREF: 0 0517
517	Q	4 - VECTOR	SINGLE, ALIGNED, INPUT-PARM XREF: 0 0520
520	Q	4 - VECTOR	SINGLE, ALIGNED, INPUT-PARM XREF: 0 0516
516	Q	4 - VECTOR	SINGLE, ALIGNED, INITIAL XREF: 0 0064 4 0529 2 0540
64	Q_B_TO_I	4 - VECTOR	SINGLE, INITIAL, EXTERNAL, VERSION=2 XREF: 0 0517 NOT REFERENCED
517	Q_ERR_ANG	3 - VECTOR FUNCTION	DOUBLE, ALIGNED, INITIAL XREF: 0 0001 2 0529
1	QIB	4 - VECTOR	SINGLE, ALIGNED, INPUT-PARM XREF: 0 0522
522	R	3 - VECTOR	DOUBLE, ALIGNED, INITIAL XREF: 0 0087 4 0526 2 0532 2 0533 2 0536
87	R_NAV	3 - VECTOR	DOUBLE, ALIGNED, INITIAL XREF: 0 0089 4 0532 2 0533 2 0534
89	R_NAV_MAG	SCALAR	DOUBLE, ALIGNED, CONSTANT XREF: 0 0007 2 0541 2 0542
7	RAD_TO_DEG	SCALAR	DOUBLE, ALIGNED, INITIAL XREF: 0 0090 4 0538 2 0543
90	RDOT_NAV	SCALAR	DOUBLE, ALIGNED, INITIAL XREF: 0 0001 2 0526
1	RI	3 - VECTOR	SINGLE, INITIAL, EXTERNAL, VERSION=2 XREF: 0 0518 2 0541
518	SARCTAN2	SCALAR FUNCTION	SINGLE, ALIGNED, INPUT-PARM XREF: 0 0518
518	SARG	SCALAR	SINGLE, INITIAL, EXTERNAL, VERSION=3 XREF: 0 0519 2 0540
519	SQFORM	3 - VECTOR FUNCTION	SINGLE, INITIAL, EXTERNAL, VERSION=3 XREF: 0 0520 NOT REFERENCED
520	SQKULT	4 - VECTOR FUNCTION	SINGLE, INITIAL, EXTERNAL, VERSION=3 XREF: 0 0521 2 0540
521	SQPOSE	4 - VECTOR FUNCTION	SINGLE, INITIAL, EXTERNAL, VERSION=3 XREF: 0 0522 NOT REFERENCED
522	SRV_TO_QIL	4 - VECTOR FUNCTION	DOUBLE, ALIGNED, INITIAL XREF: 0 0001 2 0525
1	T_ATTITUDE	SCALAR	DOUBLE, ALIGNED, INITIAL XREF: 0 0067 4 0525 2 0531
67	T_IMU_NAV	SCALAR	DOUBLE, ALIGNED, INITIAL XREF: 0 0092 4 0531 NOT REFERENCED
92	T_NAV	SCALAR	DOUBLE, ALIGNED, INPUT-PARM XREF: 0 0516
516	U	3 - VECTOR	SINGLE, ALIGNED, INPUT-PARM XREF: 0 0519
519	U	3 - VECTOR	DOUBLE, ALIGNED, INITIAL XREF: 0 0093 4 0533 2 0534 2 0538
93	UNIT_R	3 - VECTOR	

ORIGINAL PAGE IS
OF POOR QUALITY

HAL/S STD 360-24.20

INTERMETRICS, INC.

APRIL 27, 1987 11:19:28.56

DCL	NAME	TYPE	ATTRIBUTES & CROSS REFERENCE
522	V	3 - VECTOR	SINGLE, ALIGNED, INPUT-PARM XREF: 0 0522
94	V_NAV	3 - VECTOR	DOUBLE, ALIGNED, INITIAL XREF: 0 0094 4 0527 2 0535 2 0536 2 0538
95	V_NAV_MAG	SCALAR	DOUBLE, ALIGNED, INITIAL XREF: 0 0095 4 0535 NOT REFERENCED
96	V_REL_MAG	SCALAR	DOUBLE, ALIGNED, INITIAL XREF: 0 0096 4 0537 2 0542
97	V_REL_NAV	3 - VECTOR	DOUBLE, ALIGNED, INITIAL XREF: 0 0097 4 0536 2 0537 2 0540
1	VI	3 - VECTOR	DOUBLE, ALIGNED, INITIAL XREF: 0 0001 2 0527
524	VREL_BODY	3 - VECTOR	SINGLE, ALIGNED, STATIC, INITIAL XREF: 0 0524 4 0540 2 0541 2 0542
481	WE_NAV	3 - VECTOR	SINGLE, ALIGNED, INITIAL XREF: 0 0481 2 0536

HAL/S STD 360-24.20

INTERMETRICS, INC.

APRIL 27, 1987 14:13:28.85

STMT	SOURCE	CURRENT SCOPE
515 M AERO_GUID:		AERO_GUID
515 M PROCEDURE;		AERO_GUID
C -----		AERO_GUID
C DATE: 4/1/87		AERO_GUID
C FUNCTION: NUMERIC PREDICTOR/CORRECTOR ENTRY GUIDANCE ALGORITHM		AERO_GUID
C FOR THE ENTRY RESEARCH VEHICLE (ERV).		AERO_GUID
C INPUTS: A_NAV - SENSED INERTIAL ACCELERATION VECTOR		AERO_GUID
C ALPHA_NAV - ANGLE OF ATTACK		AERO_GUID
C ALT_NAV - ALTITUDE ABOVE FISHER ELLIPSOID		AERO_GUID
C G_LOAD - SENSED ACCELERATION MAGNITUDE IN G'S		AERO_GUID
C R_NAV - INERTIAL POSITION VECTOR		AERO_GUID
C T_GMT - GREENWICH MEAN TIME		AERO_GUID
C V_NAV - INERTIAL VELOCITY VECTOR		AERO_GUID
C V_NAV_MAG - INERTIAL VELOCITY MAGNITUDE		AERO_GUID
C V_REL_MAG - RELATIVE VELOCITY MAGNITUDE		AERO_GUID
C V_REL_NAV - RELATIVE VELOCITY VECTOR		AERO_GUID
C OUTPUTS: ALPHA_CMD - COMMANDED ANGLE OF ATTACK		AERO_GUID
C PHI_CMD - COMMANDED BANK ANGLE		AERO_GUID
C DESIGNED BY: K. SPRATLIN		AERO_GUID
C C.S. DRAPER LABORATORY, INC.		AERO_GUID
C MAIL STOP 2B		AERO_GUID
C 555 TECHNOLOGY SQUARE		AERO_GUID
C CAMBRIDGE, MA 02139		AERO_GUID
C (617) 258-2441		AERO_GUID
C -----		AERO_GUID

ORIGINAL PAGE IS
OF POOR QUALITY

STMT	SOURCE	CURRENT SCOPE
C ----- C LOCAL VARIABLES C -----		AERO_GUID AERO_GUID AERO_GUID
516 M DECLARE ALPHA_DES SCALAR SINGLE;		AERO_GUID
517 M DECLARE CL_EST SCALAR SINGLE;		AERO_GUID
518 M DECLARE COSPHI_QDOT SCALAR SINGLE INITIAL(-1.0);		AERO_GUID
519 M DECLARE DELTA_T_PRED SCALAR SINGLE;		AERO_GUID
520 M DECLARE EF_FROM_REF_AT_EPOCH MATRIX(3, 3) DOUBLE;		AERO_GUID
521 M DECLARE GUID_PASS INTEGER SINGLE;		AERO_GUID
522 M DECLARE I_TARGET_EF VECTOR(3) DOUBLE;		AERO_GUID
523 M DECLARE INITIALIZE_GUIDANCE BOOLEAN INITIAL(TRUE);		AERO_GUID
524 M DECLARE PHI_DES SCALAR SINGLE;		AERO_GUID
525 M DECLARE RHO_NAV SCALAR SINGLE;		AERO_GUID
C ----- C ATMOSPHERIC PROPERTIES STRUCTURE C -----		AERO_GUID AERO_GUID AERO_GUID
526 M STRUCTURE ATOMSPROP:		AERO_GUID
526 M 1 H SCALAR SINGLE,		AERO_GUID
526 M 1 RHO SCALAR SINGLE,		AERO_GUID
526 M 1 TS SCALAR SINGLE,		AERO_GUID
526 M 1 TM SCALAR SINGLE;		AERO_GUID

ORIGINAL PAGE IS
OF POOR QUALITY

STMT	SOURCE	CURRENT SCOPE
EI	IF (INITIALIZE_GUIDANCE = TRUE) THEN	AERO_GUIDO
CI	FIRST-PASS INITIALIZATION	AERO_GUIDO
528 MI	CALL INITIAL_GUIDO;	AERO_GUIDO
EI	INITIALIZE_GUIDANCE = FALSE;	AERO_GUIDO
531 MI	END;	AERO_GUIDO
532 MI	IF (G_LOAD > G_RIM_GUIDANCE) THEN	AERO_GUIDO
CI	RUN GUIDANCE	AERO_GUIDO
533 MI	DO;	AERO_GUIDO
CI	RUN LD AND DENSITY ESTIMATORS	AERO_GUIDO
534 MI	CALL FILTERS;	AERO_GUIDO
CI	RUN PREDICTOR/CORRECTOR AT CORRECT RATE	AERO_GUIDO
535 MI	IF (GUID_PASS = 0) AND (ALT_NAV > ALT_FREEZE_GUID) THEN	AERO_GUIDO
536 MI	CALL CORRECTOR;	AERO_GUIDO
CI	COUNT GUIDANCE_PASSES	AERO_GUIDO
537 MI	GUID_PASS = GUID_PASS + 1;	AERO_GUIDO
538 MI	IF (GUID_PASS >= GUID_PASS_LIM) THEN	AERO_GUIDO
539 MI	GUID_PASS = 0;	AERO_GUIDO

HAL/S STD 360-24.20

I N T E R M E T R I C S , I N C .

APRIL 27, 1987 14:13:28.85

STMT	SOURCE	CURRENT SCOPE
C ----- C COMPUTE BANK MAGNITUDE FOR HEAT RATE CONTROL C -----		AERO_GUID AERO_GUID AERO_GUID
540 M 1 CALL HEAT_RATE_CONTROL; C ----- C UPDATE COMMANDED ATTITUDE C -----		AERO_GUID AERO_GUID AERO_GUID
541 M 1 CALL ATTITUDE_COMMAND;		AERO_GUID
542 M END;		AERO_GUID

STMT	SOURCE	CURRENT SCOPE
543 MI INITIAL_GUID;	INITIAL_GUID;	INITIAL_GUID
543 MI PROCEDURE;	INITIAL_GUID;	INITIAL_GUID
543 MI FUNCTION: GUIDANCE FIRST-PASS INITIALIZATION	INITIAL_GUID;	INITIAL_GUID
543 MI LOCAL_VARIABLES	INITIAL_GUID;	INITIAL_GUID
544 MI DECLARE LAT SCALAR SINGLE;	INITIAL_GUID;	INITIAL_GUID
545 MI DECLARE LONG SCALAR SINGLE;	INITIAL_GUID;	INITIAL_GUID
546 MI DECLARE X SCALAR SINGLE;	INITIAL_GUID;	INITIAL_GUID
546 MI DECLARE Y SCALAR SINGLE;	INITIAL_GUID;	INITIAL_GUID
546 MI DECLARE Z SCALAR SINGLE;	INITIAL_GUID;	INITIAL_GUID
547 MI * ORIENTATION OF EARTH AT EPPOCH	INITIAL_GUID;	INITIAL_GUID
547 MI EF_FORM_REF_AT_EPPOCH = TRANSPPOSE(EF_TO_REF_AT_EPPOCH);	INITIAL_GUID;	INITIAL_GUID
547 MI * *	INITIAL_GUID;	INITIAL_GUID
549 MI GUID_PASS = 0;	INITIAL_GUID;	INITIAL_GUID
550 MI GUID_COUNT_FOR_PRD_CORR	INITIAL_GUID;	INITIAL_GUID
551 MI ALPHA_DES = ALPHA_EI;	INITIAL_GUID;	INITIAL_GUID
552 MI PHI_DES = PHI_EI;	INITIAL_GUID;	INITIAL_GUID
553 MI INITIAL ATTITUDE COMMAND	INITIAL_GUID;	INITIAL_GUID
554 MI ALPHA_CMD = MIDVAL(ALPHA_MIN, ALPHA_EI, ALPHA_MAX);	INITIAL_GUID;	INITIAL_GUID
554 MI PHI_CMD = MIDVAL((PHI_MAX), PHI_EI, PHI_MAX);	INITIAL_GUID;	INITIAL_GUID
555 MI CONVERT TARGET LONGITUDE AND LATITUDE TO RADIAN	INITIAL_GUID;	INITIAL_GUID

```

*** B L O C K S U M M A R Y ***
HAL/S STD 360-24.20 INTEGRICS, INC. APRIL 27, 1987 14:13:28.85

      SOURCE          CURRENT SCOPE
555 H1 LONG = LONG_TARGET_DEG_TO_RADS
| INITIAL_GUID
| INITIAL_GUID
| INITIAL_GUID
| INITIAL_GUID
| INITIAL_GUID
| INITIAL_SCOPE
556 H1 LAT = LAT_TARGET_DEG_TO_RADS
| INITIAL_GUID
| INITIAL_GUID
| INITIAL_GUID
| INITIAL_GUID
| INITIAL_GUID
| INITIAL_SCOPE
557 H1 LAT = ARCTICNATL(LAT) (1 - EARTH_FLAT)
| INITIAL_GUID
| INITIAL_GUID
| INITIAL_GUID
| INITIAL_GUID
| INITIAL_GUID
| INITIAL_SCOPE
558 H1 COHPUTE UNIT TARGET VECTOR IN EARTH-FIXED COORDINATES
| INITIAL_GUID
| INITIAL_GUID
| INITIAL_GUID
| INITIAL_GUID
| INITIAL_GUID
| INITIAL_SCOPE
559 H1 X = 1 - Z
| INITIAL_GUID
| INITIAL_GUID
| INITIAL_GUID
| INITIAL_GUID
| INITIAL_GUID
| INITIAL_SCOPE
560 H1 IF (X <= 0) THEN
| INITIAL_GUID
| INITIAL_GUID
| INITIAL_GUID
| INITIAL_GUID
| INITIAL_GUID
| INITIAL_SCOPE
561 H1 X = 0
| INITIAL_GUID
| INITIAL_GUID
| INITIAL_GUID
| INITIAL_GUID
| INITIAL_GUID
| INITIAL_SCOPE
562 H1 ELSE
| INITIAL_GUID
| INITIAL_GUID
| INITIAL_GUID
| INITIAL_GUID
| INITIAL_GUID
| INITIAL_SCOPE
562 H1 X = SQRT(X) COS(LONG)
| INITIAL_GUID
| INITIAL_GUID
| INITIAL_GUID
| INITIAL_GUID
| INITIAL_GUID
| INITIAL_SCOPE
563 H1 Y = 1 - X
| INITIAL_GUID
| INITIAL_GUID
| INITIAL_GUID
| INITIAL_GUID
| INITIAL_GUID
| INITIAL_SCOPE
564 H1 IF (Y <= 0) THEN
| INITIAL_GUID
| INITIAL_GUID
| INITIAL_GUID
| INITIAL_GUID
| INITIAL_GUID
| INITIAL_SCOPE
565 H1 Y = 0
| INITIAL_GUID
| INITIAL_GUID
| INITIAL_GUID
| INITIAL_GUID
| INITIAL_GUID
| INITIAL_SCOPE
566 H1 ELSE
| INITIAL_GUID
| INITIAL_GUID
| INITIAL_GUID
| INITIAL_GUID
| INITIAL_GUID
| INITIAL_SCOPE
566 H1 Y = SQR(TYY) SIGN(LONG)
| INITIAL_GUID
| INITIAL_GUID
| INITIAL_GUID
| INITIAL_GUID
| INITIAL_GUID
| INITIAL_SCOPE
567 H1 I_TARGET_EF = UNIT(VECTOR (X, Y, Z))
| INITIAL_GUID
| INITIAL_GUID
| INITIAL_GUID
| INITIAL_GUID
| INITIAL_GUID
| INITIAL_SCOPE
568 H1 K_RHO_NAV = 1.0
| INITIAL_GUID
| INITIAL_GUID
| INITIAL_GUID
| INITIAL_GUID
| INITIAL_GUID
| INITIAL_SCOPE
569 H1 K_LOD_NAV = 1.0
| INITIAL_GUID
| INITIAL_GUID
| INITIAL_GUID
| INITIAL_GUID
| INITIAL_GUID
| INITIAL_SCOPE
570 H1 CLOSE_INITIAL_GUID
| INITIAL_GUID
| INITIAL_GUID
| INITIAL_GUID
| INITIAL_GUID
| INITIAL_GUID
| INITIAL_SCOPE

```

HAL/S STD 360-24.20

INTERMETRICS, INC.

APRIL 27, 1987 14:13:28.85

STMT

SOURCE

CURRENT SCOPE

COMPOOL VARIABLES USED

EF_TO_REF_AT_EPOCH, ALPHA_EI, PHI_EI, ALPHA_CMD*, ALPHA_MIN, ALPHA_MAX, PHI_CMD*, PHI_MAX, LONG_TARGET, DEG_TO_RAD, LAT_TARGET
EARTH_FLAT, K_RHD_NAV*, K_LOD_NAV*

OUTER VARIABLES USED

EF_FROM_REF_AT_EPOCH*, GUID_PASS*, ALPHA_DES*, PHI_DES*, I_TARGET_EF*

© INTERMETRICS
COMPOOL PAGE 15

HAL/S STD 360-26.20

INTERMETRICS, INC.

APRIL 27, 1987 14:13:28.85

STMT	SOURCE	CURRENT SCOPE
571 M FILTERS:		FILTERS
571 M PROCEDURE;		FILTERS
C ----- C FUNCTION: IN-FLIGHT ACCELERATION MEASUREMENT FILTERING C -----		FILTERS FILTERS FILTERS
C ----- C LOCAL VARIABLES C -----		FILTERS FILTERS FILTERS
572 M DECLARE A_DRAG_MAG SCALAR SINGLE;		FILTERS
573 M DECLARE A_LIFT_MAG SCALAR SINGLE;		FILTERS
574 M DECLARE ATOMS ATMOSPROP-STRUCTURE;		FILTERS
575 M DECLARE CD_NOM SCALAR SINGLE;		FILTERS
576 M DECLARE CL_NOM SCALAR SINGLE;		FILTERS
577 M DECLARE LOD_MEAS SCALAR SINGLE;		FILTERS
578 M DECLARE LOD_NOM SCALAR SINGLE;		FILTERS
579 M DECLARE MACH SCALAR SINGLE;		FILTERS
580 M DECLARE RHO_MEAS SCALAR SINGLE;		FILTERS
581 M DECLARE V_BAR SCALAR SINGLE;		FILTERS
C ----- C LOOK UP OF NOMINAL DENSITY AND L/D C -----		FILTERS FILTERS FILTERS
E 582 M CALL USATHOS62(R_NAV, EARTH_POLE) ASSIGN(ATMOS);		FILTERS
E 583 M CALL AERO_PARAMETERS(V_REL_MAG, ATMOS) ASSIGN(V_BAR, MACH);		FILTERS
584 M CALL LOOKUP(ALPHA_NAV, ATMOS.H, V_BAR, MACH) ASSIGN(CL_NOM, CD_NOM);		FILTERS
585 M LOD_NOM = CL_NOM / CD_NOM;		FILTERS
C ----- C COMPUTE DRAG AND LIFT ACCELERATION C -----		FILTERS FILTERS FILTERS
E 586 M A_DRAG_MAG = -(A_NAV . V_REL_NAV) / V_REL_MAG;		FILTERS

STMT	SOURCE	CURRENT SCOPE
E 587 M A_LIFT_MAG = SQRT(A_NAV . A_NAV - A_DRAG_MAG A_DRAG_MAG);		FILTERS
C ----- C COMPUTE MEASURED L/D AND DENSITY C -----		FILTERS FILTERS FILTERS
588 M LOD_MEAS = A_LIFT_MAG / A_DRAG_MAG;		FILTERS
E 589 M RHO_MEAS = 2 A_DRAG_MAG MASS_NAV / (CD_NOM S_REF V_REL_MAG); ²		FILTERS
C ----- C FILTER MEASURED L/D AND DENSITY RATIOS C -----		FILTERS FILTERS FILTERS
590 M K_LOD_NAV = (1 - L_OVER_D_FILTER_GAIN) K_LOD_NAV + L_OVER_D_FILTER_GAIN (LOD_MEAS / LOD_NOM);		FILTERS
591 M K_RHO_NAV = (1 - K_RHO_FILTER_GAIN) K_RHO_NAV + K_RHO_FILTER_GAIN (RHO_MEAS / ATOMOS.RHO);		FILTERS
C ----- C COMPUTE FILTERED MEASURED DENSITY C -----		FILTERS FILTERS FILTERS
592 M RHO_NAV = K_RHO_NAV ATOMOS.RHO;		FILTERS
C ----- C COMPUTE FILTERED ESTIMATED CL C -----		FILTERS FILTERS FILTERS
593 M CL_EST = K_LOD_NAV CL_NOM;		FILTERS
594 M CLOSE FILTERS;		FILTERS

**** BLOCK SUMMARY ****

OUTER PROCEDURES CALLED
LOOKUP, AERO_PARAMETERS, USATMOS62

COMPOOL VARIABLES USED

R_NAV, EARTH_POLE, V_REL_MAG, ALPHA_NAV, A_NAV, V_REL_NAV, MASS_NAV, S_REF, K_LOD_NAV*, L_OVER_D_FILTER_GAIN, K_LOD_NAV
K_RHO_NAV*, K_RHO_FILTER_GAIN, K_RHO_NAV

OUTER VARIABLES USED
RHO_NAV*, CL_EST*OUTER STRUCTURE TEMPLATES USED
ATMOSPROP

HAL/S STD 360-24.20

INTERMETRICS, INC.

APRIL 27, 1987 14:13:28.85

STMT	SOURCE	CURRENT SCOPE
595 M HEAT_RATE_CONTROL:		HEAT_RATE_CONTROL
595 M PROCEDURE;		HEAT_RATE_CONTROL
C -----		HEAT_RATE_CONTROL
C FUNCTION: CONTROL PEAK HEAT RATE		HEAT_RATE_CONTROL
C -----		HEAT_RATE_CONTROL
C -----		HEAT_RATE_CONTROL
C LOCAL VARIABLES		HEAT_RATE_CONTROL
C -----		HEAT_RATE_CONTROL
596 M DECLARE COSPHI_1 SCALAR SINGLE;		HEAT_RATE_CONTROL
597 M DECLARE COSPHI_2 SCALAR SINGLE;		HEAT_RATE_CONTROL
598 M DECLARE FIRST_PASS BOOLEAN INITIAL(TRUE);		HEAT_RATE_CONTROL
599 M DECLARE HS_2 SCALAR SINGLE;		HEAT_RATE_CONTROL
600 M DECLARE K_QDOT SCALAR SINGLE;		HEAT_RATE_CONTROL
601 M DECLARE K_QDOT_RATE SCALAR SINGLE;		HEAT_RATE_CONTROL
602 M DECLARE K1_GAIN SCALAR SINGLE;		HEAT_RATE_CONTROL
603 M DECLARE K1_QDOT SCALAR SINGLE;		HEAT_RATE_CONTROL
604 M DECLARE OMEGA_QDOT_SQUARED SCALAR SINGLE;		HEAT_RATE_CONTROL
605 M DECLARE QBAR SCALAR SINGLE;		HEAT_RATE_CONTROL
606 M DECLARE QDOT SCALAR SINGLE;		HEAT_RATE_CONTROL
607 M DECLARE QDOT_PAST SCALAR SINGLE;		HEAT_RATE_CONTROL
608 M DECLARE QDOT_RATE SCALAR SINGLE;		HEAT_RATE_CONTROL
609 M DECLARE TWO_ZETA_OMEGA SCALAR SINGLE;		HEAT_RATE_CONTROL
E		
610 M QDOT = 17700.0 SQRT(RHO_NAV) (V_REL_MAG / 10000) ^{3.05} ;		HEAT_RATE_CONTROL
E		
611 M IF (FIRST_PASS = TRUE) THEN		HEAT_RATE_CONTROL
612 M DO;		HEAT_RATE_CONTROL
E		
613 M 1 FIRST_PASS = FALSE;		HEAT_RATE_CONTROL
C -----		HEAT_RATE_CONTROL
C HEAT RATE CONTROL CONSTANTS		HEAT_RATE_CONTROL

STMT	SOURCE	CURRENT SCOPE
C -----		HEAT_RATE_CONTROL
614 M 1 HS_2 = 2 HS;		HEAT_RATE_CONTROL
615 M 1 K1_GAIN = S_REF SQRT(RHO_SL) 17700.0 / (HS_2 MASS_NAV);		HEAT_RATE_CONTROL
616 M 1 OMEGA_QDOT_SQUARED = OMEGA_QDOT OMEGA_QDOT;		HEAT_RATE_CONTROL
617 M 1 TWO_ZETA_OMEGA = 2 ZETA_QDOT OMEGA_QDOT;		HEAT_RATE_CONTROL
C -----		HEAT_RATE_CONTROL
C FIRST PASS INITIALIZATION		HEAT_RATE_CONTROL
C -----		HEAT_RATE_CONTROL
618 M 1 QDOT_RATE = 0;		HEAT_RATE_CONTROL
619 M END;		HEAT_RATE_CONTROL
620 M ELSE		HEAT_RATE_CONTROL
620 M QDOT_RATE = (QDOT - QDOT_PAST) / DT_AEROGLID;		HEAT_RATE_CONTROL
621 M QDOT_PAST = QDOT;		HEAT_RATE_CONTROL
622 M IF (QDOT > .5 QDOT_LIMIT) THEN		HEAT_RATE_CONTROL
623 M DO;		HEAT_RATE_CONTROL
C -----		HEAT_RATE_CONTROL
C ESTIMATED DYNAMIC PRESSURE		HEAT_RATE_CONTROL
C -----		HEAT_RATE_CONTROL
624 M 1 QBAR = .5 RHO_NAV V_REL_MAG V_REL_MAG;		HEAT_RATE_CONTROL
C -----		HEAT_RATE_CONTROL
C HEAT RATE CONTROL GAINS		HEAT_RATE_CONTROL
C -----		HEAT_RATE_CONTROL
E 625 M 1 K1_QDOT = K1_GAIN CL_EST (V_REL_MAG / 10000.0) ^{3.05} EXP(-(ALT_NAV / HS_2));		HEAT_RATE_CONTROL
626 M 1 K_QDOT = OMEGA_QDOT_SQUARED / K1_QDOT;		HEAT_RATE_CONTROL
627 M 1 K_QDOT_RATE = TWO_ZETA_OMEGA / K1_QDOT;		HEAT_RATE_CONTROL
C -----		HEAT_RATE_CONTROL
C HEAT RATE CONTROL EQUATION		HEAT_RATE_CONTROL
C -----		HEAT_RATE_CONTROL
628 M 1 COSPHI_1 = K_QDOT_RATE QDOT_RATE / QBAR;		HEAT_RATE_CONTROL
629 M 1 COSPHI_2 = K_QDOT (QDOT - QDOT_LIMIT) / QBAR;		HEAT_RATE_CONTROL
630 M 1 COSPHI_QDOT = COSPHI_1 + COSPHI_2;		HEAT_RATE_CONTROL

HAL/S STD 360-24.20

INTERMETRICS, INC.

APRIL 27, 1987 14:13:28.85

STMT	SOURCE	CURRENT SCOPE
631 M END;		HEAT_RATE_CONTROL
632 M ELSE		HEAT_RATE_CONTROL
632 M COSPHI_QDOT = -1.0;		HEAT_RATE_CONTROL
633 M CLOSE HEAT_RATE_CONTROL;		HEAT_RATE_CONTROL

**** BLOCK SUMMARY ****

COMPOOL VARIABLES USED

V_REL_MAG, HS, S_REF, RHO_SL, MASS_NAV, OMEGA_QDOT, ZETA_QDOT, DT_AEROGUID, QDOT_LIMIT, ALT_NAV

OUTER VARIABLES USED

RHO_NAV, CL_EST, COSPHI_QDOT*

ORIGINAL PAGE IS
OF POOR QUALITY

HAL/S STD 360-24.20 I N T E R M E T R I C S , I N C . APRIL 27, 1987 14:13:28.85

STMT	SOURCE	CURRENT SCOPE
634 M ATTITUDE_COMMAND;		ATTITUDE_COMMAND
634 M PROCEDURE;		ATTITUDE_COMMAND
C -----		ATTITUDE_COMMAND
C LOAD ALPHA COMMAND		ATTITUDE_COMMAND
C -----		ATTITUDE_COMMAND
635 M ALPHA_CMD = ALPHA_DES;		ATTITUDE_COMMAND
C -----		ATTITUDE_COMMAND
C COMPUTE AND LIMIT PHI COMMAND		ATTITUDE_COMMAND
C -----		ATTITUDE_COMMAND
636 M PHI_CMD = PHI_DES ABS(V_NAV_MAG - V_FINAL_MAG) / V_MAG_CHANGE;		ATTITUDE_COMMAND
637 M PHI_CMD = MIDVAL((-PHI_MAX), PHI_CMD, PHI_MAX);		ATTITUDE_COMMAND
C -----		ATTITUDE_COMMAND
C ADJUST COMMANDED BANK ANGLE FOR HEAT RATE CONTROL		ATTITUDE_COMMAND
C -----		ATTITUDE_COMMAND
638 M IF (COSPHI_QDOT > 0) THEN		ATTITUDE_COMMAND
639 M DO;		ATTITUDE_COMMAND
640 M TEMPORARY COSPHI_CMD SCALAR SINGLE;		ATTITUDE_COMMAND
641 M COSPHI_CMD = COS(PHI_CMD DEG_TO_RAD) + COSPHI_QDOT;		ATTITUDE_COMMAND
642 M COSPHI_CMD = MIDVAL(-1.0, COSPHI_CMD, +1.0);		ATTITUDE_COMMAND
643 M PHI_CMD = SIGN(PHI_CMD) ARCCOS(COSPHI_CMD) RAD_TO_DEG;		ATTITUDE_COMMAND
644 M END;		ATTITUDE_COMMAND
C -----		ATTITUDE_COMMAND
C LIMIT ALPHA AND PHI COMMANDS		ATTITUDE_COMMAND
C -----		ATTITUDE_COMMAND
645 M ALPHA_CMD = MIDVAL(ALPHA_MIN, ALPHA_CMD, ALPHA_MAX);		ATTITUDE_COMMAND
646 M PHI_CMD = MIDVAL((-PHI_MAX), PHI_CMD, PHI_MAX);		ATTITUDE_COMMAND
647 M CLOSE ATTITUDE_COMMAND;		ATTITUDE_COMMAND

**** B L O C K S U M M A R Y ****

COMMON VARIABLES USED
ALPHA_CMD*, PHI_CMD*, V_NAV_MAG, V_FINAL_MAG, V_MAG_CHANGE, PHI_MAX, PHI_CMD, DEG_TO_RAD, RAD_TO_DEG, ALPHA_MIN, ALPHA_CMD
ALPHA_MAX

OUTER VARIABLES USED
ALPHA_DES, PHI_DES, COSPHI_QDOT

HAL/S STD 360-24.20

INTERMETRICS, INC.

APRIL 27, 1987 14:13:28.85

STMT	SOURCE	CURRENT SCOPE
648 M CORRECTOR;		CORRECTOR
648 M PROCEDURE;		CORRECTOR
C ----- C FUNCTION: PREDICTOR/CORRECTOR SEQUENCER C -----		CORRECTOR CORRECTOR CORRECTOR
C ----- C LOCAL VARIABLES C -----		CORRECTOR CORRECTOR CORRECTOR
649 M DECLARE ALPHA_TRY SCALAR SINGLE;		CORRECTOR
650 M DECLARE DELTA_ALPHA SCALAR SINGLE CONSTANT(3);		CORRECTOR
651 M DECLARE DELTA_PHI SCALAR SINGLE CONSTANT(3);		CORRECTOR
652 M DECLARE DETERM SCALAR SINGLE INITIAL(0);		CORRECTOR
653 M DECLARE DDRE_DA SCALAR SINGLE;		CORRECTOR
654 M DECLARE DDRE_DP SCALAR SINGLE;		CORRECTOR
655 M DECLARE DCRE_DA SCALAR SINGLE;		CORRECTOR
656 M DECLARE DCRE_DP SCALAR SINGLE;		CORRECTOR
657 M DECLARE CRE SCALAR SINGLE;		CORRECTOR
658 M DECLARE CR_ERROR ARRAY(3) SCALAR SINGLE;		CORRECTOR
659 M DECLARE CR_ERR SCALAR SINGLE;		CORRECTOR
660 M DECLARE PHI_TRY SCALAR SINGLE;		CORRECTOR
661 M DECLARE PRED_EXIT BOOLEAN;		CORRECTOR
662 M DECLARE DR_ERROR ARRAY(3) SCALAR SINGLE;		CORRECTOR
663 M DECLARE DR_ERR SCALAR SINGLE;		CORRECTOR
664 M DECLARE DRE SCALAR SINGLE;		CORRECTOR
665 M DO FOR TEMPORARY I = 1 TO 3;		CORRECTOR
666 M I DO CASE I;		CORRECTOR
667 M 2 DO;		CORRECTOR CASE 1
668 M 3 ALPHA_TRY = ALPHA_DES;		CORRECTOR
669 M 3 PHI_TRY = PHI_DES;		CORRECTOR

HAL/S STD 360-24.20

INTERMETRICS, INC.

APRIL 27, 1987 14:13:28.85

STMT	SOURCE	CURRENT SCOPE
670 M 2 END;		CORRECTOR
671 M 2 DO\$		CORRECTOR CASE 2
672 M 3 ALPHA_TRY = ALPHA_DES + DELTA_ALPHA;		CORRECTOR
673 M 3 PHI_TRY = PHI_DES;		CORRECTOR
674 M 2 END;		CORRECTOR
675 M 2 DO\$		CORRECTOR CASE 3
676 M 3 ALPHA_TRY = ALPHA_DES;		CORRECTOR
677 M 3 PHI_TRY = PHI_DES + DELTA_PHI;		CORRECTOR
678 M 2 END;		CORRECTOR
679 M 1 END;		CORRECTOR DO CASE END
C ----- C CALL PREDICTOR WITH DESIRED CONTROL HISTORY C -----		
680 M 1 CALL PREDICTOR;		CORRECTOR
C ----- C STORE FINAL STATE ERRORS C -----		
681 M 1 DR_ERROR = DR_ERR;		CORRECTOR
S I		
682 M 1 CR_ERROR = CR_ERR;		CORRECTOR
S I		
683 M END;		CORRECTOR
C ----- C COMPUTE PARTIALS C -----		
684 M DDRE_DA = (DR_ERROR - DR_ERROR) / DELTA_ALPHA;		CORRECTOR
S 2 1		
685 M DCRE_DP = (CR_ERROR - CR_ERROR) / DELTA_PHI;		CORRECTOR
S 3 1		
686 M DCRE_DA = (CR_ERROR - CR_ERROR) / DELTA_ALPHA;		CORRECTOR
S 2 1		
687 M DCRE_DP = (CR_ERROR - CR_ERROR) / DELTA_PHI;		CORRECTOR
S 3 1		

STMT	SOURCE	CURRENT SCOPE
688 M DRE = DR_ERROR ; S 1		CORRECTOR
689 M CRE = CR_ERROR ; S 1		CORRECTOR
C ----- C SOLVE SET OF 2 SIMULTANEOUS EQUATIONS C -----		CORRECTOR CORRECTOR CORRECTOR
690 M DETERM = DCRE_DP DDRE_DA - DDRE_DP DCRE_DA;		CORRECTOR
691 M IF (DETERM ~= 0) THEN		CORRECTOR
692 M DO;		CORRECTOR
693 M 1 ALPHA_DES = ALPHA_DES + (DDRE_DP CRE - DCRE_DP DRE) / DETERM;		CORRECTOR
694 M 1 ALPHA_DES = MIDVAL(ALPHA_MIN, ALPHA_DES, ALPHA_MAX);		CORRECTOR
695 M 1 PHI_DES = PHI_DES - (DDRE_DA CRE - DCRE_DA DRE) / DETERM;		CORRECTOR
696 M 1 PHI_DES = MIDVAL(-PHI_DES_MAX, PHI_DES, PHI_DES_MAX);		CORRECTOR
697 M END;		CORRECTOR

HAL/S STD 360-24.20

INTERMETRICS, INC.

APRIL 27, 1987 14:13:28.85

HAL/S STD 360-24.20

INTERMETRICS, INC.

APRIL 27, 1987 14:13:28.85

STMT	SOURCE	CURRENT SCOPE
698 M PREDICTOR:		PREDICTOR
698 M PROCEDURE;		PREDICTOR
C ----- C FUNCTION: NUMERIC PREDICTOR ALGORITHM C -----		PREDICTOR PREDICTOR PREDICTOR
C ----- C LOCAL FUNCTION C -----		PREDICTOR PREDICTOR PREDICTOR
699 M DECLARE EARTH_FIXED_FROM_REFERENCE FUNCTION MATRIX(3, 3) DOUBLE;		PREDICTOR
C ----- C LOCAL VARIABLES C -----		PREDICTOR PREDICTOR PREDICTOR
700 M DECLARE TOTAL_TIME_STEPS INTEGER SINGLE;		PREDICTOR
701 M DECLARE A_PRED VECTOR(3) DOUBLE;		PREDICTOR
702 M DECLARE A_PRED_MAG SCALAR SINGLE;		PREDICTOR
703 M DECLARE ALPHA_PRED SCALAR SINGLE;		PREDICTOR
704 M DECLARE ATMOS ATMOSPROP-STRUCTURE;		PREDICTOR
705 M DECLARE CD_PRED SCALAR SINGLE;		PREDICTOR
706 M DECLARE CL_PRED SCALAR SINGLE;		PREDICTOR
707 M DECLARE DOT SCALAR DOUBLE;		PREDICTOR
708 M DECLARE EF_FROM_REF MATRIX(3, 3) DOUBLE;		PREDICTOR
709 M .DECLARE I_INPLANE VECTOR(3) DOUBLE;		PREDICTOR
710 M .DECLARE I_NORMAL VECTOR(3) DOUBLE;		PREDICTOR
711 M .DECLARE INTEG_LOOP SCALAR SINGLE;		PREDICTOR
712 M .DECLARE IR_E VECTOR(3) DOUBLE;		PREDICTOR
713 M .DECLARE LOD_PRED SCALAR SINGLE;		PREDICTOR
714 M .DECLARE MACH_PRED SCALAR SINGLE;		PREDICTOR
715 M .DECLARE PHI_PRED SCALAR SINGLE;		PREDICTOR
716 M .DECLARE R_PRED VECTOR(3) DOUBLE;		PREDICTOR
717 M .DECLARE R_MAG_PRED SCALAR DOUBLE;		PREDICTOR
718 M .DECLARE RDOT_PRED SCALAR SINGLE;		PREDICTOR

HAL/S STD 360-24.20	INTERMETRICS, INC.	APRIL 27, 1987 14:13:28.85
STMT	SOURCE	CURRENT SCOPE
719 M DECLARE T_PRED SCALAR DOUBLE;		PREDICTOR
720 M DECLARE V_BAR_PRED SCALAR SINGLE;		PREDICTOR
721 M DECLARE V_MAG_PRED SCALAR DOUBLE;		PREDICTOR
722 M DECLARE V_PRED VECTOR(3) DOUBLE;		PREDICTOR
723 M DECLARE V_REL_MAG_PRED SCALAR SINGLE;		PREDICTOR
724 M DECLARE V_REL_PRED VECTOR(3) SINGLE;		PREDICTOR
725 M DECLARE VR_E VECTOR(3) DOUBLE;		PREDICTOR
C ----- C INITIALIZE PREDICTOR STATE VECTOR C -----		PREDICTOR PREDICTOR PREDICTOR
726 M T_PRED = T_GMT;		PREDICTOR
E - - 727 M R_PRED = R_NAV;		PREDICTOR
E - - 728 M R_MAG_PRED = ABVAL(R_PRED);		PREDICTOR
E - - 729 M V_PRED = V_NAV;		PREDICTOR
E - - 730 M V_MAG_PRED = ABVAL(V_PRED);		PREDICTOR
E - - 731 M V_REL_PRED = V_PRED - (HE_NAV * R_PRED);		PREDICTOR
E - - 732 M V_REL_MAG_PRED = ABVAL(V_REL_PRED);		PREDICTOR
C ----- C ANGLE OF ATTACK FOR PREDICTION C -----		PREDICTOR PREDICTOR PREDICTOR
733 M ALPHA_PRED = ALPHA_TRY;		PREDICTOR
C ----- C INITIALIZE 1962 U.S. STANDARD ATMOSPHERE C -----		PREDICTOR PREDICTOR PREDICTOR
E - - 734 M CALL USATHOS62(R_PRED, EARTH_POLE) ASSIGN(ATMOS); +-----		PREDICTOR
C ----- C FORCE 1ST TIME STEP TO BE MINIMUM TIME STEP C -----		PREDICTOR PREDICTOR PREDICTOR

HAL/S STD 360-24.20

INTERMETRICS, INC.

APRIL 27, 1987 14:13:28.85

STMT	SOURCE	CURRENT SCOPE
E		
735 M A_PRED = VECTOR (999999., 999999., 999999.); S @SINGLE,3		PREDICTOR
C ----- C PREDICTOR LOOP C -----		PREDICTOR PREDICTOR PREDICTOR
736 M DO FOR TEMPORARY TIME_INCREMENT = 1 TO 5000; C ----- C COMPUTE TIME STEP FOR 4TH ORDER RUNGA-KUTTA INTEGRATION C -----		PREDICTOR PREDICTOR PREDICTOR
737 M 1 TOTAL_TIME_STEPS = TIME_INCREMENT;		PREDICTOR
738 M 1 IF (ATMOS.H <= ALT_TAEM_BIAS) THEN		PREDICTOR
739 M 1 DELTA_T_PRED = DELTA_T_PRED_MIN;		PREDICTOR
740 M 1 ELSE		PREDICTOR
740 M 1 DO; E		PREDICTOR
741 M 2 A_PRED_MAG = ABVAL(A_PRED);		PREDICTOR
742 M 2 IF (A_PRED_MAG ~= 0) THEN		PREDICTOR
743 M 2 DELTA_T_PRED = DELTA_T_PRED_GAIN / A_PRED_MAG;		PREDICTOR
744 M 2 ELSE		PREDICTOR
744 M 2 DELTA_T_PRED = DELTA_T_PRED_MAX;		PREDICTOR
745 M 2 DELTA_T_PRED = MIDVAL(DELTA_T_PRED_MIN, DELTA_T_PRED, DELTA_T_PRED_MAX);		PREDICTOR
746 M 1 END;		PREDICTOR
C ----- C AERODYNAMIC PROPERTIES LOOK-UP C -----		PREDICTOR PREDICTOR PREDICTOR
E		
747 M 1 CALL AERO_PARAMETERS(V_REL_MAG_PRED, ATMOS) ASSIGN(V_BAR_PRED, MACH_PRED); + 748 M 1 CALL LOOKUP(ALPHA_PRED, ATMOS.H, V_BAR_PRED, MACH_PRED) ASSIGN(CL_PRED, CD_PRED);		PREDICTOR PREDICTOR
C ----- C ESTIMATED L/D C -----		PREDICTOR PREDICTOR PREDICTOR
749 M 1 LOD_PRED = K_LOD_NAV CL_PRED / CD_PRED;		PREDICTOR

ORIGINAL PAGE
 COLOR PHOTOGRAPH

HAL/S STD 360-24.20

INTERMETRICS, INC.

APRIL 27, 1987 14:13:28.85

STMT	SOURCE	CURRENT SCOPE
C -----		
C EQUATIONS OF MOTION FOR ERV ENTRY		PREDICTOR
C -----		PREDICTOR
750 M 1 DO FOR INTEG_LOOP = 1 TO 4;		PREDICTOR
751 M 2 TEMPORARY AERO_ACCEL VECTOR(3) SINGLE;		PREDICTOR
752 M 2 TEMPORARY CPHI SCALAR SINGLE;		PREDICTOR
753 M 2 TEMPORARY DRAG_ACCEL SCALAR SINGLE;		PREDICTOR
754 M 2 TEMPORARY GRAV_ACCEL VECTOR(3) DOUBLE;		PREDICTOR
755 M 2 TEMPORARY HS_NORM_PRED SCALAR SINGLE;		PREDICTOR
756 M 2 TEMPORARY I_LAT VECTOR(3) SINGLE;		PREDICTOR
757 M 2 TEMPORARY I_LIFT VECTOR(3) SINGLE;		PREDICTOR
758 M 2 TEMPORARY I_VEL VECTOR(3) SINGLE;		PREDICTOR
759 M 2 TEMPORARY LIFT_ACCEL SCALAR SINGLE;		PREDICTOR
760 M 2 TEMPORARY RHO_PRED SCALAR SINGLE;		PREDICTOR
761 M 2 TEMPORARY SPHI SCALAR SINGLE;		PREDICTOR
762 M 2 TEMPORARY U_PRED VECTOR(3) DOUBLE;		PREDICTOR
763 M 2 TEMPORARY Z_PRED SCALAR DOUBLE;		PREDICTOR
C -----		
C ESTIMATED DENSITY		PREDICTOR
C -----		PREDICTOR
764 M 2 RHO_PRED = K_RHO_NAV ATMOS.RHO;		PREDICTOR
C -----		
C BANK ANGLE MODEL		PREDICTOR
C -----		PREDICTOR
765 M 2 PHI_PRED = PHI_TRY ABS(V_MAG_PRED - V_FINAL_MAG) / V_MAG_CHANGE;		PREDICTOR
766 M 2 PHI_PRED = MIDVAL((-PHI_MAX), PHI_PRED, PHI_MAX) DEG_TO_RAD;		PREDICTOR
767 M 2 CPHI = COS(PHI_PRED);		PREDICTOR
768 M 2 SPHI = SIN(PHI_PRED);		PREDICTOR
C -----		
C AERODYNAMIC ACCELERATION		PREDICTOR
C -----		PREDICTOR

ORIGINAL PAGE IS
OF POOR QUALITY

HAL/S STD 360-24.20

INTERMETRICS, INC.

APRIL 27, 1987 14:13:28.85

STMT	SOURCE	CURRENT SCOPE
E 769 M 2	DRAG_ACCEL = .5 RHO_PRED V_REL_MAG_PRED ² CD_PRED S_REF / MASS_NAV;	PREDICTOR
770 M 2	LIFT_ACCEL = LOD_PRED DRAG_ACCEL;	PREDICTOR
E 771 M 2	I_VEL = V_REL_PRED / V_REL_MAG_PRED;	PREDICTOR
E 772 M 2	I_LAT = UNIT(I_VEL * R_PRED);	PREDICTOR
E 773 M 2	I_LIFT = UNIT(I_LAT * I_VEL) CPHI + I_LAT SPHI;	PREDICTOR
E 774 M 2	AERO_ACCEL = LIFT_ACCEL I_LIFT - DRAG_ACCEL I_VEL;	PREDICTOR
C -----		PREDICTOR
C GRAVITY ACCELERATION WITH J2 TERM		PREDICTOR
C -----		PREDICTOR
E 775 M 2	U_PRED = R_PRED / R_MAG_PRED;	PREDICTOR
E 776 M 2	Z_PRED = U_PRED . EARTH_POLE;	PREDICTOR
E 777 M 2	U_PRED = U_PRED + (3 EARTH_J2 / 2) (EARTH_R / R_MAG_PRED) ² ((1 - 5 Z_PRED ²) U_PRED + 2	PREDICTOR
E 777 M 2	Z_PRED EARTH_POLE);	PREDICTOR
E 778 M 2	GRAV_ACCEL = -(EARTH_MU / R_MAG_PRED) ² U_PRED;	PREDICTOR
C -----		PREDICTOR
C TOTAL ACCELERATION		PREDICTOR
C -----		PREDICTOR
E 779 M 2	A_PRED = AERO_ACCEL + GRAV_ACCEL;	PREDICTOR
C -----		PREDICTOR
C CALL RUNGA-KUTTA INTEGRATOR		PREDICTOR
C -----		PREDICTOR
780 M 2	CALL INTEGRATOR;	PREDICTOR
C -----		PREDICTOR
C STATE PARAMETERS		PREDICTOR
C -----		PREDICTOR
E 781 M 2	R_MAG_PRED = ABVAL(R_PRED);	PREDICTOR

HAL/S STD 360-24.20 I N T E R M E T R I C S , I N C . APRIL 27, 1987 14:13:28.05

STMT	SOURCE	CURRENT SCOPE
E		
782 M 2 V_MAG_PRED = ABVAL(V_PRED);		PREDICTOR
C -----		
C RELATIVE VELOCITY		PREDICTOR
; C -----		PREDICTOR
E		
783 M 2 V_REL_PRED = V_PRED - (WE_NAV * R_PRED);		PREDICTOR
E		
784 M 2 V_REL_MAG_PRED = ABVAL(V_REL_PRED);		PREDICTOR
C -----		
C 1962 U.S. STANDARD ATMOSPHERE		PREDICTOR
C -----		PREDICTOR
E		
785 M 2 CALL USATHMOS62(R_PRED, EARTH_POLE) ASSIGN(ATMOS);		PREDICTOR
786 M 1 END;		PREDICTOR
C -----		
C STATE PARAMETERS		PREDICTOR
C -----		PREDICTOR
787 M 1 T_PRED = T_PRED + DELTA_T_PRED;		PREDICTOR
E		
788 M 1 RDOT_PRED = V_PRED . R_PRED / R_MAG_PRED;		PREDICTOR
C -----		
C CHECK FOR ATMOSPHERIC EXIT		PREDICTOR
C -----		PREDICTOR
789 M 1 IF ((ATMOS.H > 400000) AND (RDOT_PRED > 0)) THEN		PREDICTOR
E		
790 M 1 PRED_EXIT = TRUE;		PREDICTOR
E		
791 M 1 IF (PRED_EXIT = TRUE) THEN		PREDICTOR
792 M 1 EXIT;		PREDICTOR
C -----		
C CHECK FOR TAEM INTERFACE		PREDICTOR
C -----		PREDICTOR
793 M 1 IF (ATMOS.H <= ALT_TAEM) THEN		PREDICTOR
794 M 1 EXIT;		PREDICTOR
795 M 1 END;		PREDICTOR

HAL/S STD 360-24.20	INTERMETRICS, INC.	APRIL 27, 1987	14:13:28.85
STMT	SOURCE	CURRENT SCOPE	
C -----		PREDICTOR	
C COMPUTE DONNRANGE AND CROSSRANGE ERRORS		PREDICTOR	
C -----		PREDICTOR	
E * 796 M EF_FROM_REF = EARTH_FIXED_FROM_REFERENCE(T_PRED);		PREDICTOR	
E - * - 797 M IR_E = UNIT(EF_FROM_REF R_PRED);		PREDICTOR	
E - * - 798 M VR_E = EF_FROM_REF (V_PRED - WE_NAV * R_PRED);		PREDICTOR	
E - - - 799 M I_NORMAL = UNIT(IR_E * VR_E);		PREDICTOR	
E - - - 800 M I_INPLANE = UNIT(I_TARGET_EF - (I_TARGET_EF . I_NORMAL) I_NORMAL);		PREDICTOR	
E - - - 801 M DOT = I_INPLANE . I_TARGET_EF;		PREDICTOR	
802 M IF (ABS(DOT) > 1) THEN		PREDICTOR	
803 M DOT = SIGN(DOT);		PREDICTOR	
E 804 M CR_ERR = EARTH_R_FT_TO_NM ARCCOS(DOT) SIGN((I_INPLANE * I_TARGET_EF) . (I_NORMAL * I_INPLANE));		PREDICTOR	
E - - - 805 M DOT = IR_E . I_INPLANE;		PREDICTOR	
806 M IF (ABS(DOT) > 1) THEN		PREDICTOR	
807 M DOT = SIGN(DOT);		PREDICTOR	
E 808 M DR_ERR = EARTH_R_FT_TO_NM ARCCOS(DOT) SIGN((IR_E * I_INPLANE) . I_NORMAL);		PREDICTOR	

ORIGINAL PAGE IS
OF POOR QUALITY

HAL/S STD 360-24.20

INTERMETRICS, INC.

APRIL 27, 1987 14:13:28.85

STMT	SOURCE	CURRENT SCOPE
809 M INTEGRATOR:		INTEGRATOR
809 M PROCEDURE;		INTEGRATOR
C -----		INTEGRATOR
C FUNCTION: 4TH ORDER RUNGA-KUTTA INTEGRATOR ALGORITHM		INTEGRATOR
C -----		INTEGRATOR
C -----		INTEGRATOR
C LOCAL VARIABLES		INTEGRATOR
C -----		INTEGRATOR
810 M DECLARE ACCUM_ACCEL VECTOR(3) DOUBLE;		INTEGRATOR
811 M DECLARE ACCUM_VEL VECTOR(3) DOUBLE;		INTEGRATOR
812 M DECLARE ORIG_POS VECTOR(3) DOUBLE;		INTEGRATOR
813 M DECLARE ORIG_VEL VECTOR(3) DOUBLE;		INTEGRATOR
814 M DO CASE INTEG_LOOP;		INTEGRATOR
815 M 1 DO;		INTEGRATOR CASE 1
E 816 M 2 ORIG_POS = R_PRED;		INTEGRATOR
E 817 M 2 ORIG_VEL = V_PRED;		INTEGRATOR
E 818 M 2 ACCUM_VEL = V_PRED;		INTEGRATOR
E 819 M 2 ACCUM_ACCEL = A_PRED;		INTEGRATOR
E 820 M 2 R_PRED = ORIG_POS + .5 DELTA_T_PRED V_PRED;		INTEGRATOR
E 821 M 2 V_PRED = ORIG_VEL + .5 DELTA_T_PRED A_PRED;		INTEGRATOR
822 M 1 END;		INTEGRATOR
823 M 1 DO;		INTEGRATOR CASE 2
E 824 M 2 ACCUM_VEL = ACCUM_VEL + 2 V_PRED;		INTEGRATOR
E 825 M 2 ACCUM_ACCEL = ACCUM_ACCEL + 2 A_PRED;		INTEGRATOR

HAL/S STD 360-24.20

INTERMETRICS, INC.

APRIL 27, 1987 14:13:28.85

STMT	SOURCE	CURRENT SCOPE
E 826 M 2	R_PRED = ORIG_POS + .5 DELTA_T_PRED V_PRED;	INTEGRATOR
E 827 M 2	V_PRED = ORIG_VEL + .5 DELTA_T_PRED A_PRED;	INTEGRATOR
828 M 1	END;	INTEGRATOR
829 M 1	DO;	INTEGRATOR CASE 3
E 830 M 2	ACCUM_VEL = ACCUM_VEL + 2 V_PRED;	INTEGRATOR
E 831 M 2	ACCUM_ACCEL = ACCUM_ACCEL + 2 A_PRED;	INTEGRATOR
E 832 M 2	R_PRED = ORIG_POS + DELTA_T_PRED V_PRED;	INTEGRATOR
E 833 M 2	V_PRED = ORIG_VEL + DELTA_T_PRED A_PRED;	INTEGRATOR
834 M 1	END;	INTEGRATOR
835 M 1	DO;	INTEGRATOR CASE 4
E 836 M 2	R_PRED = ORIG_POS + (ACCUM_VEL + V_PRED) DELTA_T_PRED / 6;	INTEGRATOR
E 837 M 2	V_PRED = ORIG_VEL + (ACCUM_ACCEL + A_PRED) DELTA_T_PRED / 6;	INTEGRATOR
838 M 1	END;	INTEGRATOR
839 M END;		INTEGRATOR DO CASE END
840 M CLOSE INTEGRATOR;		INTEGRATOR

**** BLOCK SUMMARY ****

OUTER VARIABLES USED
 INTEG_LOOP, R_PRED, V_PRED, A_PRED, R_PRED*, DELTA_T_PRED, V_PRED*

ORIGINAL PAGE IS
OF POOR QUALITY

HAL/S STD 360-24.20

INTERMETRICS, INC.

APRIL 27, 1987 14:13:28.85

STMT	SOURCE	CURRENT SCOPE
841 M EARTH_FIXED_FROM_REFERENCE;		EARTH_FIXED_FROM_REFER
841 M FUNCTION(T) MATRIX(3, 3) DOUBLE;		EARTH_FIXED_FROM_REFER
C -----		EARTH_FIXED_FROM_REFER
C DATE: 01/01/80		EARTH_FIXED_FROM_REFER
C FUNCTION: COMPUTE (LEFT) REFERENCE INERTIAL TO EARTH-FIXED		EARTH_FIXED_FROM_REFER
C TRANSFORMATION MATRIX OR VARIOUS APPROXIMATIONS THEREOF.		EARTH_FIXED_FROM_REFER
C INPUTS: T - THE NUMBER OF SECONDS ELAPSED SINCE TIME ORIGIN		EARTH_FIXED_FROM_REFER
C OUTPUTS: EARTH-FIXED FROM REFERENCE ROTATION MATRIX		EARTH_FIXED_FROM_REFER
C COMMENTS: NONE		EARTH_FIXED_FROM_REFER
C REFERENCE: UNDOCUMENTED		EARTH_FIXED_FROM_REFER
C -----		EARTH_FIXED_FROM_REFER
842 M DECLARE T SCALAR DOUBLE;		EARTH_FIXED_FROM_REFER
843 M DECLARE CLAMBDA SCALAR DOUBLE;		EARTH_FIXED_FROM_REFER
844 M DECLARE SLAMBDA SCALAR DOUBLE;		EARTH_FIXED_FROM_REFER
845 M CLAMBDA = COS(T - T_EPOCH) EARTH_RATE);		EARTH_FIXED_FROM_REFER
846 M SLAMBDA = SIN(T - T_EPOCH) EARTH_RATE);		EARTH_FIXED_FROM_REFER
847 M RETURN MATRIX (CLAMBDA, SLAMBDA, 0, -SLAMBDA, CLAMBDA, 0, 0, 0, 1)		EARTH_FIXED_FROM_REFER
SI @DOUBLE,3,3		
E * 847 M EF_FROM_REF_AT_EPOCH);		EARTH_FIXED_FROM_REFER
848 M CLOSE EARTH_FIXED_FROM_REFERENCE;		EARTH_FIXED_FROM_REFER
***** BLOCK SUMMARY *****		
COMPOOL VARIABLES USED		
T_EPOCH, EARTH_RATE		
OUTER VARIABLES USED		
EF_FROM_REF_AT_EPOCH		

HAL/S STD 360-24.20

INTERMETRICS, INC.

APRIL 27, 1987 14:13:28.85

STMT

SOURCE

CURRENT SCOPE

849 M| CLOSE PREDICTOR;

| PREDICTOR

**** BLOCK SUMMARY ****

OUTER PROCEDURES CALLED
USATHOS62, AERO_PARAMETERS, LOOKUP

COMPOOL VARIABLES USED
T_GMT, R_NAV, V_NAV, HE_NAV, EARTH_POLE, ALT_TAEM_BIAS, DELTA_T_PRED_MIN, DELTA_T_PRED_GAIN, DELTA_T_PRED_MAX, K_LOD_NAV
K_RHO_NAV, V_FINAL_MAG, V_MAG_CHANGE, PHI_MAX, DEG_TO_RAD, S_REF, MASS_NAV, EARTH_J2, EARTH_R, EARTH_MU, ALT_TAEM, FT_TO_NM

OUTER VARIABLES USED
ALPHA_TRY, DELTA_T_PRED*, DELTA_T_PRED, PHI_TRY, PRED_EXIT*, PRED_EXIT, I_TARGET_EF, CR_ERR*, DR_ERR*

OUTER STRUCTURE TEMPLATES USED
ATMOSPROP

HAL/S STD 360-24.20

INTERMETRICS, INC.

APRIL 27, 1987 14:13:28.85

STMT

SOURCE

CURRENT SCOPE

850 M| CLOSE CORRECTOR;

| CORRECTOR

**** BLOCK SUMMARY ****

COMPOOL VARIABLES USED
ALPHA_MIN, ALPHA_MAX, PHI_DES_MAX

OUTER VARIABLES USED
ALPHA_DES, PHI_DES, ALPHA_DES*, PHI_DES*

184

STMT	SOURCE	APRIL 27, 1987 14:13:28.85	CURRENT SCOPE
851 M AERO_PARAMETERS;			AERO_PARAMETERS
851 M PROCEDURE(V_REL_MAG, ATMOS) ASSIGN(V_BAR, MACH);			AERO_PARAMETERS
C ----- C FUNCTION: COMPUTE AERODYNAMIC FLOW REGIME PARAMETERS C -----			AERO_PARAMETERS AERO_PARAMETERS AERO_PARAMETERS
C ----- C LOCAL VARIABLES C -----			AERO_PARAMETERS AERO_PARAMETERS AERO_PARAMETERS
852 M DECLARE V_REL_MAG SCALAR SINGLE;			AERO_PARAMETERS
853 M DECLARE ATMOS ATMOSPROP-STRUCTURE;			AERO_PARAMETERS
854 M DECLARE MACH SCALAR SINGLE;			AERO_PARAMETERS
855 M DECLARE V_BAR SCALAR SINGLE;			AERO_PARAMETERS
856 M DECLARE C_PRIME SCALAR SINGLE;			AERO_PARAMETERS
857 M DECLARE GAMMA_VBAR SCALAR SINGLE;			AERO_PARAMETERS
858 M DECLARE REYNOLDS_NUMBER SCALAR SINGLE;			AERO_PARAMETERS
859 M DECLARE SPEED_OF_SOUND SCALAR SINGLE;			AERO_PARAMETERS
860 M DECLARE T_PRIME SCALAR SINGLE;			AERO_PARAMETERS
861 M DECLARE T_WALL SCALAR SINGLE;			AERO_PARAMETERS
862 M DECLARE VISCOSITY SCALAR SINGLE;			AERO_PARAMETERS
C ----- C LOCAL CONSTANTS C -----			AERO_PARAMETERS AERO_PARAMETERS AERO_PARAMETERS
863 M DECLARE C_BAR SCALAR SINGLE CONSTANT(25.0);			AERO_PARAMETERS
864 M DECLARE DEG_R_TO_DEG_K SCALAR SINGLE CONSTANT(9 / 5);			AERO_PARAMETERS
865 M DECLARE GAMMA SCALAR SINGLE CONSTANT(1.4);			AERO_PARAMETERS
E 866 M DECLARE UNIV_GAS_CONST SCALAR SINGLE CONSTANT(8.31432 10. ³);			AERO_PARAMETERS
867 M DECLARE MOLE_WT_ZERO SCALAR SINGLE CONSTANT(28.9644);			AERO_PARAMETERS
868 M DECLARE SPEED_OF_SOUND_CONST SCALAR SINGLE CONSTANT(SQRT(GAMMA UNIV_GAS_CONST / MOLE_WT_ZERO));			AERO_PARAMETERS

ORIGINAL PAGE IS
OF POOR QUALITY

HAL/S STD 360-24.20

I N T E R M E T R I C S , I N C .

APRIL 27, 1987 14:13:28.85

STMT

SOURCE

CURRENT SCOPE

C| -----
C| MACH NUMBER
C| -----

| AERO_PARAMETERS
| AERO_PARAMETERS
| AERO_PARAMETERS

869 M| SPEED_OF_SOUND = SPEED_OF_SOUND_CONST M_TO_FT SQRT(ATMOS.TM);

| AERO_PARAMETERS

870 M| IF SPEED_OF_SOUND = 0 THEN

| AERO_PARAMETERS

871 M| MACH = 0;

| AERO_PARAMETERS

872 M| ELSE

| AERO_PARAMETERS

872 M| MACH = V_REL_MAG / SPEED_OF_SOUND;

| AERO_PARAMETERS

C| -----
C| REYNOLDS NUMBER
C| -----

| AERO_PARAMETERS
| AERO_PARAMETERS
| AERO_PARAMETERS

E| 873 M| VISCOSITY = 1.458 10⁻⁶ KG_TO_SLUG ATMOS.TS^{1.5} / ((110.4 + ATMOS.TS) M_TO_FT);

| AERO_PARAMETERS

874 M| IF (VISCOSITY = 0 OR ATMOS.H > 300000) THEN

| AERO_PARAMETERS

875 M| REYNOLDS_NUMBER = 0;

| AERO_PARAMETERS

876 M| ELSE

| AERO_PARAMETERS

876 M| REYNOLDS_NUMBER = ATMOS.RHO V_REL_MAG C_BAR / VISCOSITY;

| AERO_PARAMETERS

C| -----
C| VISCOS Parameter
C| -----

| AERO_PARAMETERS
| AERO_PARAMETERS
| AERO_PARAMETERS

877 M| IF REYNOLDS_NUMBER = 0 THEN

| AERO_PARAMETERS

878 M| V_BAR = 0;

| AERO_PARAMETERS

879 M| ELSE

| AERO_PARAMETERS

HAL/S STD 360-24.20

INTERMETRICS, INC.

APRIL 27, 1987 14:13:28.85

STMT	SOURCE	CURRENT SCOPE
879 M 1 DO;		AERO_PARAMETERS
C ----- C T_WALL FOR VISCOS PARAMETER C -----		AERO_PARAMETERS AERO_PARAMETERS AERO_PARAMETERS
880 M 1 IF (ATMOS.H < 249000) THEN		AERO_PARAMETERS
881 M 1 T_WALL = 2178.0 DEG_R_TO_DEG_K;		AERO_PARAMETERS
882 M 1 ELSE IF (ATMOS.H >= 249000) AND (ATMOS.H < 360000) THEN		AERO_PARAMETERS
883 M 1 T_WALL = (5913.0 - 0.015 ATMOS.H) DEG_R_TO_DEG_K;		AERO_PARAMETERS
884 M 1 ELSE IF (ATMOS.H >= 360000) THEN		AERO_PARAMETERS
885 M 1 T_WALL = 504.0 DEG_R_TO_DEG_K;		AERO_PARAMETERS
C ----- C GAMMA FOR VISCOS PARAMETER C -----		AERO_PARAMETERS AERO_PARAMETERS AERO_PARAMETERS
886 M 1 IF (ATMOS.H < 100000) THEN		AERO_PARAMETERS
887 M 1 GAMMA_VBAR = 1.4;		AERO_PARAMETERS
888 M 1 ELSE IF (ATMOS.H >= 100000) AND (ATMOS.H < 170000) THEN		AERO_PARAMETERS
889 M 1 GAMMA_VBAR = 1.7 - 3.00E-6 ATMOS.H;		AERO_PARAMETERS
890 M 1 ELSE IF (ATMOS.H >= 170000) AND (ATMOS.H < 225000) THEN		AERO_PARAMETERS
891 M 1 GAMMA_VBAR = 1.375 - 1.09E-6 ATMOS.H;		AERO_PARAMETERS
892 M 1 ELSE IF (ATMOS.H >= 225000) AND (ATMOS.H < 300000) THEN		AERO_PARAMETERS
893 M 1 GAMMA_VBAR = 1.220 - 4.00E-7 ATMOS.H;		AERO_PARAMETERS
894 M 1 ELSE IF (ATMOS.H >= 300000) THEN		AERO_PARAMETERS
895 M 1 GAMMA_VBAR = 1.1;		AERO_PARAMETERS
C ----- C T_PRIME AND C_PRIME FOR VISCOS PARAMETER C -----		AERO_PARAMETERS AERO_PARAMETERS AERO_PARAMETERS
E 896 M 1 T_PRIME = (.468 + .532 T_WALL / ATMOS.TS + .195 (GAMMA_VBAR - 1) MACH ² / 2) ATMOS.TS;		AERO_PARAMETERS
E 897 M 1 C_PRIME = (T_PRIME / ATMOS.TS) ^{.5} ((ATMOS.TS + 122.1 10 ⁻⁵) / (T_PRIME + 122.1 10 ⁻⁵)) / (5/T_PRIME);		AERO_PARAMETERS
E 897 M 1)) ;		AERO_PARAMETERS

ORIGINAL PAGE IS
OF POOR QUALITY

HAL/S STD 360-24.20 I N T E R M E T R I C S , I N C . APRIL 27, 1987 14:13:28.85

STMT	SOURCE	CURRENT SCOPE
E		AERO_PARAMETERS
898 M 1 V_BAR = MACH (C_PRIME / REYNOLDS_NUMBER) ^{.5}		AERO_PARAMETERS
899 M END;		AERO_PARAMETERS
900 M CLOSE AERO_PARAMETERS;		AERO_PARAMETERS

***** B L O C K S U M M A R Y *****

COMPOOL VARIABLES USED
M_TO_FT, KG_TO_SLUG

OUTER STRUCTURE TEMPLATES USED
ATMOSPROP

HAL/S STD 360-24.20

INTERMETRICS, INC.

APRIL 27, 1987 14:13:28.85

STMT	SOURCE	CURRENT SCOPE
901 M LOOKUP:		LOOKUP
901 M PROCEDURE(ALPHA, ALT, V_BAR, MACH) ASSIGN(CL, CD);		LOOKUP
C -----		
C FUNCTION: LOOK-UP OF CL AND CD VERSUS ALPHA, ALTITUDE, VISCOUS		LOOKUP
C PARAMETER, AND MACH NUMBER.		LOOKUP
C INPUTS: ALPHA - ANGLE OF ATTACK (DEG)		LOOKUP
C ALTITUDE - ALTITUDE ABOVE FISHER ELLIPSOID (FT)		LOOKUP
C V_BAR - VISCOUS PARAMETER		LOOKUP
C MACH - MACH NUMBER		LOOKUP
C OUTPUT: CD - DRAG COEFFICIENT		LOOKUP
C CL - LIFT COEFFICIENT		LOOKUP
C FLOW_REGIME: 1 = USE ALTITUDE DATA		LOOKUP
C 2 = USE V_BAR DATA		LOOKUP
C 3 = USE MACH DATA		LOOKUP
C REFERENCE: NOT DOCUMENTED		LOOKUP
C -----		LOOKUP
C -----		LOOKUP
C INPUT AND OUTPUT VARIABLES		LOOKUP
C -----		LOOKUP
902 M DECLARE ALPHA SCALAR SINGLE;		LOOKUP
903 M DECLARE ALT SCALAR SINGLE;		LOOKUP
904 M DECLARE CD SCALAR SINGLE;		LOOKUP
905 M DECLARE CL SCALAR SINGLE;		LOOKUP
906 M DECLARE MACH SCALAR SINGLE;		LOOKUP
907 M DECLARE V_BAR SCALAR SINGLE;		LOOKUP
C -----		
C LOCAL VARIABLES		LOOKUP
C -----		LOOKUP
908 M DECLARE ALPHA_FRACT SCALAR SINGLE;		LOOKUP
909 M DECLARE ALPHA_MAX SCALAR SINGLE CONSTANT(50);		LOOKUP
910 M DECLARE ALPHA_MIN SCALAR SINGLE CONSTANT(0);		LOOKUP
911 M DECLARE ALT_L SCALAR SINGLE;		LOOKUP
912 M DECLARE ALT_MAX SCALAR SINGLE CONSTANT(537000);		LOOKUP
913 M DECLARE ALT_MIN SCALAR SINGLE CONSTANT(300000);		LOOKUP
914 M DECLARE ALT_RUN SCALAR SINGLE CONSTANT(ALT_MAX - ALT_MIN);		LOOKUP
915 M DECLARE CD_1 SCALAR SINGLE;		LOOKUP

ORIGINAL PAGE IS
OF POOR QUALITY

STMT	SOURCE	CURRENT SCOPE
916 M1	DECLARE CD_2 SCALAR SINGLE;	CD
917 M1	DECLARE CL_3 SCALAR SINGLE;	CD
918 M1	DECLARE CL_2 SCALAR SINGLE;	CD
919 M1	DECLARE COS_ALPHA SCALAR SINGLE;	CD
920 M1	DECLARE FRACT_SCALAR SINGLE;	CD
921 M1	DECLARE FLOW_REGIME INTEGER SINGLE;	CD
922 M1	DECLARE I INTEGER SINGLE;	CD
923 M1	DECLARE J INTEGER SINGLE;	CD
924 M1	DECLARE MACH_SCALAR SINGLE;	CD
925 M1	DECLARE MACH_MAX SCALAR SINGLE CONSTANT(10);	CD
926 M1	DECLARE MACH_MIN SCALAR SINGLE CONSTANT(2);	CD
927 M1	DECLARE SIN_ALPHA SCALAR SINGLE;	CD
928 M1	DECLARE V_BAR_SCALAR SINGLE;	CD
929 M1	DECLARE V_BAR_MAX_SCALAR SINGLE CONSTANT(0.0744);	CD
930 M1	DECLARE V_BAR_MIN_SCALAR SINGLE CONSTANT(0.0050);	CD
931 M1	DECLARE V_BAR_TABLE ARRAY(8) SCALAR SINGLE CONSTANT(.0050, .0103, .0148, .0208, .0245, .0373);	CD
932 M1	.0570, .0744);	CD

HAL/S STID 360-24.20 INTREROMETRICS, INC. APRIL 27, 1987 14:13:28.85

H&L/S STD 360-24.20

I N T E R M E T R I C S , I N C .

APRIL 27, 1987 14:13:28.85

STMT

SOURCE

CURRENT SCOPE

C| -----
C| ERV AERODYNAMIC DATA TABLES NOT LISTED
C| -----

| LOOKUP
| LOOKUP
| LOOKUP

949 MI 2 ALT_L = MIDVAL(ALT_MIN, ALT, ALT_MAX);
 | LOOKUP
 | SOURCE
CURRENT SCOPE
CI DETERMINE INDEX OF ANGLE OF ATTACK
CI LOOKUP
938 MI J = MIDVAL(1, (TRUNCATE(ALPHA) + 1), 50);
LOOKUP
ALPHA_FRACT = (ALPHA - TRUNCATE(ALPHA));
LOOKUP
DETERMINE FLOW REGIME TO USE FOR LOOK UP
CI
931 MI ELSE IF (ALT >= ALT_MIN) THEN
LOOKUP
FLOW_REGIME = 1;
942 MI ELSE FLOW_REGIME = 3;
LOOKUP
ELSE IF (MACH <= MACH_MAX) THEN
LOOKUP
FLOW_REGIME = 2;
945 MI DO CASE FLOW_REGIME;
LOOKUP

CI INTERPOLATE FOR ALPHA USING CORRECT TABLES
CI
947 MI 1 DO1
LOOKUP
CASE 1
ALTITUDE DATA
CI
948 MI 2 ALT_L = MIDVAL(ALT_MIN, ALT, ALT_MAX);
LOOKUP
SOURCE
CURRENT SCOPE

CI ALTITUDE DATA
CI
949 SI CL_L = CL_ALT_{1,j} + (CL_ALT_{1,j+1} - CL_ALT_{1,j}) ALPHA_FRACT₁
LOOKUP
CL_L = CL_ALT_{2,j} + (CL_ALT_{2,j+1} - CL_ALT_{2,j}) ALPHA_FRACT₂
950 SI CL_L = CL_ALT_{2,j} + (CL_ALT_{2,j+1} - CL_ALT_{2,j}) ALPHA_FRACT₂
LOOKUP
CL_L = CL_ALT_{1,j} + (CL_ALT_{1,j+1} - CL_ALT_{1,j}) ALPHA_FRACT₁
951 MI 2 CD_L = CD_ALT_{1,j} + (CD_ALT_{1,j+1} - CD_ALT_{1,j}) ALPHA_FRACT₁
LOOKUP
CD_L = CD_ALT_{2,j} + (CD_ALT_{2,j+1} - CD_ALT_{2,j}) ALPHA_FRACT₂
952 MI 2 CD_L = CD_ALT_{2,j} + (CD_ALT_{2,j+1} - CD_ALT_{2,j}) ALPHA_FRACT₂
LOOKUP

953 MI 2 FRACT = (ALT_L - ALT_MIN) / ALT_RUNS
LOOKUP
END1

ORIGINAL PAGE IS
OF POOR QUALITY

STATE	SOURCE	CURRENT SCOPE
955 M 1 DO,	LOOKUP LOOKUP LOOKUP CASE 2	
956 M 2 V_BAR_L = MIDVAL(V_BAR_MIN, V_BAR, V_BAR_MAX);	LOOKUP LOOKUP LOOKUP	
957 M 2 DO FOR TEMPORARY K = 7 TO 1 BY -1;	LOOKUP LOOKUP	
958 M 3 I = K;	LOOKUP LOOKUP	
959 M 3 IF (V_BAR_L <= V_BAR_TABLE) THEN EXIT;	LOOKUP LOOKUP	
960 M 2 END;	LOOKUP LOOKUP	
961 M 2 CD_1 = CL_VISC_I,j + (CL_VISC_I,j+1 - CL_VISC_I,j) ALPHA_FRACT;	LOOKUP LOOKUP	
962 M 2 CL_2 = CL_VISC_I,j + (CL_VISC_I,j+1 - CL_VISC_I,j) ALPHA_FRACT;	LOOKUP LOOKUP	
963 M 2 CL_2 = CL_VISC_I,j + (CL_VISC_I,j+1 - CL_VISC_I,j) ALPHA_FRACT;	LOOKUP LOOKUP	
964 M 2 CD_1 = CD_VISC_I,j + (CD_VISC_I,j+1 - CD_VISC_I,j) ALPHA_FRACT;	LOOKUP LOOKUP	
965 M 2 CD_2 = CD_VISC_I,j + (CD_VISC_I,j+1 - CD_VISC_I,j) ALPHA_FRACT;	LOOKUP LOOKUP	
966 M 2 FRACT = (V_BAR_L - V_BAR_TABLE) / (V_BAR_TABLE - V_BAR_TABLE);	LOOKUP LOOKUP	
967 M 1 END;	MACH DATA ----- C -----	
968 M 1 DO,	LOOKUP CASE 3	
969 M 2 MACH_L = MIDVAL(MACH_MIN, MACH, MACH_MAX);	LOOKUP LOOKUP	
970 M 2 I = MIDVAL(2, (TRUNCATE(MACH_L / 2)), 4);	LOOKUP LOOKUP	
971 M 2 CL_2 = CL_MACH_I,j + (CL_MACH_I,j+1 - CL_MACH_I,j) ALPHA_FRACT;	LOOKUP LOOKUP	
972 M 2 CL_2 = CL_MACH_I,j + (CL_MACH_I,j+1 - CL_MACH_I,j) ALPHA_FRACT;	LOOKUP LOOKUP	
973 M 2 CD_1 = CD_MACH_I,j + (CD_MACH_I,j+1 - CD_MACH_I,j) ALPHA_FRACT;	LOOKUP LOOKUP	

HAL/S STD 360-24.20 INTERMETRICS, INC.

APRIL 27, 1987 14:13:28.85

STMT	SOURCE	CURRENT SCOPE
974 M 2 CD_2 = CD_MACH _{I+1,J} + (CD_MACH _{I+1,J+1} - CD_MACH _{I+1,J}) ALPHA_FRACT;	LOOKUP	
975 M 2 FRACT = (MACH_L / 2 - I);	LOOKUP	
976 M 1 END;	LOOKUP	
977 M END;	LOOKUP DO CASE END	
C -----	LOOKUP	
C INTERPOLATE BETWEEN TABLES	LOOKUP	
C -----	LOOKUP	
978 M CL = CL_1 + (CL_2 - CL_1) FRACT;	LOOKUP	
979 M CD = CD_1 + (CD_2 - CD_1) FRACT;	LOOKUP	
980 M CLOSE LOOKUP;	LOOKUP	

HAL/S STD 360-24.20

INTERMETRICS, INC.

APRIL 27, 1987 14:13:28.85

STMT	SOURCE	CURRENT SCOPE
981 M USATMOS62;		USATMOS62
981 M PROCEDURE(R, POLE) ASSIGN(ATMOS);		USATMOS62
C -----		USATMOS62
C DATE: 12/28/81		USATMOS62
C FUNCTION: COMPUTES THE DENSITY OF THE ATMOSPHERE (0-150KM)		USATMOS62
C AT A SPECIFIED ALTITUDE USING THE 1962 U.S.STANDARD		USATMOS62
C ATMOSPHERE MODEL.		USATMOS62
C INPUTS: R - INERTIAL POSITION VECTOR (FT)		USATMOS62
C POLE - INERTIAL NORTH POLE (ND)		USATMOS62
C OUTPUTS: ATMOS.H - ALTITUDE (FT)		USATMOS62
C ATMOS.RHO - DENSITY (LBM/FT**3)		USATMOS62
C ATMOS.TS - STATIC TEMPERATURE OF AIR (DEG K)		USATMOS62
C ATMOS.TM - MOLECULAR TEMPERATURE OF AIR (DEG K)		USATMOS62
C NOMENCLATURE: A - EARTH EQUATORIAL RADIUS (M)		USATMOS62
C F - EARTH FLATTENING (ND)		USATMOS62
C RO - EARTH RADIUS (PHI = 45 DEGS) (M)		USATMOS62
C PHI - GEOGRAPHIC LATITUDE (DEGS)		USATMOS62
C PSI - GEOCENTRIC LATITUDE (DEGS)		USATMOS62
C GO - SEA-LEVEL GRAVITY (M/S/S)		USATMOS62
C MO - MEAN MOLECULAR WEIGHT OF AIR (ND)		USATMOS62
C RR - UNIVERSAL GAS CONSTANT		USATMOS62
C (JOULES / (DEG K) / (KG-MOL))		USATMOS62
C -----		USATMOS62
982 M DECLARE ATMOS ATMOSPROP-STRUCTURE;		USATMOS62
983 M DECLARE R VECTOR(3) DOUBLE;		USATMOS62
984 M DECLARE POLE VECTOR(3) DOUBLE;		USATMOS62
985 M DECLARE GO SCALAR SINGLE CONSTANT(9.80665);		USATMOS62
986 M DECLARE MO SCALAR SINGLE CONSTANT(28.9644);		USATMOS62
987 M DECLARE RR SCALAR SINGLE CONSTANT(8314.32);		USATMOS62
988 M DECLARE K2 SCALAR SINGLE CONSTANT(GO MO / RR);		USATMOS62
989 M DECLARE M_TO_FT SCALAR DOUBLE CONSTANT(1 / .3048);		USATMOS62
990 M DECLARE KG_TO_LBM SCALAR SINGLE CONSTANT(1 / .45359237);		USATMOS62
991 M DECLARE A SCALAR DOUBLE CONSTANT(6378178);		USATMOS62
992 M DECLARE F SCALAR DOUBLE CONSTANT(1 / 298.32);		USATMOS62

HAL/S STD 360-24.20 INTERMETRICS, INC. APRIL 27, 1987 14:13:28.85

STMT	SOURCE	CURRENT SCOPE
E 993 M	DECLARE R0 SCALAR SINGLE CONSTANT(A SQRT((1 + (1 - F)) / (1 + (1 - F))));	USATMOS62
994 M	DECLARE I INTEGER SINGLE;	USATMOS62
995 M	DECLARE NSEGS INTEGER SINGLE CONSTANT(12);	USATMOS62
996 M	DECLARE H_BASE ARRAY(NSEGS + 1) SCALAR SINGLE CONSTANT(0, 11000, 20000, 32000, 47000, 52000,	USATMOS62
996 M	61000, 79000, 90000, 100000, 110000, 120000, 150000);	USATMOS62
997 M	DECLARE TM_BASE ARRAY(NSEGS + 1) SCALAR SINGLE CONSTANT(288.15, 216.65, 216.65, 228.65, 270.65,	USATMOS62
997 M	270.65, 252.65, 180.65, 180.65, 210.65, 260.65, 360.65, 960.65);	USATMOS62
998 M	DECLARE T_BASE ARRAY(NSEGS + 1) SCALAR SINGLE CONSTANT(288.15, 216.65, 216.65, 228.65, 270.65,	USATMOS62
998 M	270.65, 252.65, 180.65, 180.65, 210.02, 257.00, 349.49, 892.79);	USATMOS62
999 M	DECLARE RH0_BASE ARRAY(NSEGS + 1) SCALAR SINGLE CONSTANT(1.2250, 0.36392, 0.088035, 0.013225,	USATMOS62
999 M	0.0014275, 0.00075943, 0.00025109, 0.00002001, 0.000003170, 0.0000004974, 0.00000009829,	USATMOS62
999 M	0.00000002436, 0.00000001836);	USATMOS62
1000 M	DECLARE DTMHD ARRAY(NSEGS) SCALAR SINGLE INITIAL(-.0065, .0000, .0010, .0028, .0000, -.0020, -	USATMOS62
1000 M	.0040, .0000, .0030, .0050, .0100, .0200);	USATMOS62
1001 M	DECLARE DTDH ARRAY(NSEGS) SCALAR SINGLE INITIAL(-.006500, .000000, .001000, .0028000, .0000000000	USATMOS62
1001 M	, -.002000, -.004000, .000000, .002937, .0046980, .009249000, .018110);	USATMOS62
1002 M	DECLARE SCALAR DOUBLE,	USATMOS62
1002 M	R_MAG, H, SPSI;	USATMOS62
1003 M	DECLARE SCALAR SINGLE,	USATMOS62
1003 M	DH, EXP0, ALTADJ, ALTRATIO, GRAVRATIO, TEMPRATIO;	USATMOS62
C	-----	USATMOS62
C	DETERMINE ALTITUDE ABOVE FISHER ELLIPSOID	USATMOS62
C	-----	USATMOS62
E		USATMOS62
1004 M	R_MAG = ABVAL(R);	USATMOS62
E		USATMOS62
1005 M	SPSI = (R / R_MAG) . POLE;	USATMOS62

```

      SOURCE          CURRENT SCOPE
      -----          -----
      E| H = (R_MAE / M_TO_FT) - A (1 - F) / SQR(1 - F (2 - F) (1 - S_P))2
      C| DETERMINE DENSITY, STATIC TEMPERATURE, AND MOLECULAR TEMPERATURE
      C| USATMOS62
      1006 H| ATMSO.H = H M_TO_FT;
      C| USATMOS62
      1007 H| ATMSO.H = H M_TO_FT;
      C| USATMOS62
      E| H = (R_MAE / M_TO_FT) - A (1 - F) / SQR(1 - F (2 - F) (1 - S_P))2
      C| DETERMINE DENSITY, STATIC TEMPERATURE, AND MOLECULAR TEMPERATURE
      C| USATMOS62
      1008 H| IF (H > 150000) THEN
      C| USATMOS62
      1009 H| ATMSO.RHO = 0;
      C| USATMOS62
      1010 H| ELSE
      C| USATMOS62
      1010 H| DO1
      C| USATMOS62
      1011 H| GRVARRATIO = R0 / (R0 + H);
      C| USATMOS62
      1012 H| IF (H < 90000) THEN
      C| USATMOS62
      1013 H| H = GRVARRATIO H;
      C| USATMOS62
      1014 H| E| GRVARRATIO = GRVARRATIO2
      C| USATMOS62
      1015 H| DO FOR TEMPORARY N = 1 TO NSEGS;
      C| USATMOS62
      1016 H| 2| I = N;
      C| USATMOS62
      1017 H| 2| IF (H < H_BASE ) THEN
      C| USATMOS62
      1018 H| 2| EXIT;
      C| USATMOS62
      1019 H| 1| END;
      C| USATMOS62
      1020 H| 1| DH = H - H_BASE ;
      C| USATMOS62
      1021 H| 1| ATMSO.TM = TM_BASE + DH_DTM ;
      C| USATMOS62
      1022 H| 1| ATMSO.TS = T_BASE + DH_DTH ;
      C| USATMOS62
      1023 H| 1| IF (H < 90000) THEN
      C| USATMOS62
      1024 H| 1| DO1
      C| USATMOS62
  
```

HAL/S STD 360-24.20

INTERMETRICS, INC.

APRIL 27, 1987 14:13:28.85

STMT	SOURCE	CURRENT SCOPE
1025 M 2 S	IF (DTMDH = 0) THEN I	USATMOS62
1026 M 2 S	ATMOS.RHO = RHO_BASE EXP(-K2 DH / TM_BASE); I I	USATMOS62
1027 M 2	ELSE	USATMOS62
1027 M 2	DO;	USATMOS62
1028 M 3 S	EXPO = 1 + K2 / DTMDH ; I	USATMOS62
E 1029 M 3 S	ATMOS.RHO = RHO_BASE (TM_BASE / ATMOS.TM) EXPO I I I	USATMOS62
1030 M 2	END;	USATMOS62
1031 M 1	END;	USATMOS62
1032 M 1	ELSE	USATMOS62
1032 M 1	DO;	USATMOS62
1033 M 2 S	ALTADJ = R0 + H_BASE - TM_BASE / DTMDH ; I I I	USATMOS62
1034 M 2 S	ALTRATIO = (R0 + H) / (R0 + H_BASE); I	USATMOS62
1035 M 2 S	TEMPRATIO = TM_BASE / ATMOS.TM; I	USATMOS62
E 1036 M 2 S	EXPO = ((K2 / DTMDH) (R0 / ALTADJ)) ² I	USATMOS62
1037 M 2 S	ATMOS.RHO = RHO_BASE TEMPRATIO EXP((K2 / DTMDH) GRAVRATIO ALTRATIO (DH / ALTADJ)) I I	USATMOS62
E 1037 M 2	(TEMPRATIO ALTRATIO) EXPO	USATMOS62
1038 M 1	END;	USATMOS62
E 1039 M 1	ATMOS.RHO = ATMOS.RHO (KG_TO_LBM / (M_TO_FT ³ G_TO_FPS2));	USATMOS62
1040 M	END;	USATMOS62
1041 M	CLOSE USATMOS62;	USATMOS62

HAL/S STD 360-24.20

INTERMETRICS, INC.

APRIL 27, 1987 14:13:28.85

STMT

SOURCE

CURRENT SCOPE

**** BLOCK SUMMARY ****

COMPOOL VARIABLES USED
G_TO_FPS2

OUTER STRUCTURE TEMPLATES USED
ATMOSPROP

HAL/S STD 360-24.20

INTERMETRICS, INC.

APRIL 27, 1987 14:13:28.85

STMT

SOURCE

CURRENT SCOPE

1042 M| CLOSE AERO_GUID;

| AERO_GUID

****B L O C K S U M M A R Y ****

COMPOOL VARIABLES USED

G_LOAD, G_RUN_GUIDANCE, ALT_NAV, ALT_FREEZE_GUID, GUID_PASS_LIM

C - 3

HAL/S STD 360-24.20

I N T E R M E T R I C S , I N C .

APRIL 27, 1987 14:13:28.85

***** C O M P I L A T I O N L A Y O U T *****
FSM_POOL: EXTERNAL COMPOOL;
IL_POOL: EXTERNAL COMPOOL;
AERO_GUID: PROCEDURE;
INITIAL_GUID: PROCEDURE;
FILTERS: PROCEDURE;
HEAT_RATE_CONTROL: PROCEDURE;
ATTITUDE_COMMAND: PROCEDURE;
CORRECTOR: PROCEDURE;
PREDICTOR: PROCEDURE;
INTEGRATOR: PROCEDURE;
EARTH_FIXED_FROM_REFERENCE: FUNCTION;
AERO_PARAMETERS: PROCEDURE;
LOOKUP: PROCEDURE;
USATMOS62: PROCEDURE;

201

SYMBOL & CROSS REFERENCE TABLE LISTING:

(CROSS REFERENCE FLAG KEY: 4 = ASSIGNMENT, 2 = REFERENCE, 1 = SUBSCRIPT USE, 0 = DEFINITION)

DCL	NAME	TYPE	STRUCTURE TEMPLATE	ATTRIBUTES & CROSS REFERENCE
526	ATMOSPROP			ALIGNED XREF: 0 0526 2 0574 2 0582 2 0583 2 0584 2 0591 2 0592 2 0704 2 0734 2 0738 2 0747 2 0748 2 0764 2 0785 2 0789 2 0793 2 0853 2 0869 2 0873 2 0874 2 0876 2 0880 2 0882 2 0883 2 0884 2 0886 2 0888 2 0889 2 0890 2 0891 2 0892 2 0893 2 0894 2 0896 2 0897 2 0982 2 1007 2 1009 2 1021 2 1022 2 1026 2 1029 2 1035 2 1037 2 1039 SINGLE, ALIGNED XREF: 0 0526 2 0584 2 0738 2 0748 2 0789 2 0793 2 0874 2 0880 2 0882 2 0883 2 0884 2 0886 2 0888 2 0889 2 0890 2 0891 2 0892 2 0893 2 0894 4 1007 SINGLE, ALIGNED XREF: 0 0526 2 0591 2 0592 2 0764 2 0876 4 1009 4 1026 4 1029 4 1037 6 1039 SINGLE, ALIGNED XREF: 0 0526 2 0873 2 0896 2 0897 4 1022 SINGLE, ALIGNED XREF: 0 0526 2 0869 4 1021 2 1029 2 1035 DOUBLE, ALIGNED, STATIC, CONSTANT XREF: 0 0991 2 0993 2 1006 SINGLE, ALIGNED, STATIC XREF: 0 0572 4 0586 2 0587 2 0588 2 0589 SINGLE, ALIGNED, STATIC XREF: 0 0573 4 0587 2 0588 DOUBLE, ALIGNED, INITIAL XREF: 0 0087 2 0586 2 0587 DOUBLE, ALIGNED, STATIC XREF: 0 0701 4 0735 2 0741 4 0779 2 0819 2 0821 2 0825 2 0827 2 0831 2 0833 2 0837 SINGLE, ALIGNED, STATIC XREF: 0 0702 4 0741 2 0742 2 0743 DOUBLE, ALIGNED, STATIC XREF: 0 0810 4 0819 6 0825 6 0831 2 0837 DOUBLE, ALIGNED, STATIC XREF: 0 0811 4 0818 6 0824 6 0830 2 0836 SINGLE, TEMPORARY XREF: 0 0751 4 0774 2 0779 XREF: 0 0515 NOT REFERENCED XREF: 2 0583 2 0747 0 0851 SINGLE, ALIGNED, INPUT-PARM XREF: 0 0901 0 0902 2 0938 2 0939 SINGLE, ALIGNED, INITIAL XREF: 0 0352 4 0553 4 0635 6 0645 SINGLE, ALIGNED, STATIC XREF: 0 0516 4 0551 2 0635 2 0668 2 0672 2 0676 6 0693 6 0694 SINGLE, ALIGNED, INITIAL XREF: 0 0401 2 0551 2 0553 SINGLE, ALIGNED, STATIC XREF: 0 0908 4 0939 2 0949 2 0950 2 0951 2 0952 2 0962 2 0963 2 0964 2 0965 2 0971 2 0972 2 0973 2 0974 SINGLE, ALIGNED, INITIAL XREF: 0 0513 2 0553 2 0645 2 0694 SINGLE, ALIGNED, STATIC, CONSTANT XREF: 0 0909 NOT REFERENCED SINGLE, ALIGNED, INITIAL XREF: 0 0513 2 0553 2 0645 2 0694 SINGLE, ALIGNED, STATIC, CONSTANT XREF: 0 0910 NOT REFERENCED SINGLE, ALIGNED, INITIAL XREF: 0 0074 2 0584 SINGLE, ALIGNED, STATIC XREF: 0 0703 4 0733 2 0748 SINGLE, ALIGNED, STATIC XREF: 0 0649 4 0668 4 0672 4 0676 2 0733 SINGLE, ALIGNED, INPUT-PARM XREF: 0 0901 0 0903 2 0941 2 0948
526	H	1	SCALAR	
526	RHO	1	SCALAR	
526	TS	1	SCALAR	
526	TM	1	SCALAR	
991	A		SCALAR	
572	A_DRAG_MAG		SCALAR	
573	A_LIFT_MAG		SCALAR	
87	A_NAV	3 - VECTOR		
701	A_PRED	3 - VECTOR		
702	A_PRED_MAG		SCALAR	
810	ACCUM_ACCEL	3 - VECTOR		
811	ACCUM_VEL	3 - VECTOR		
751	AERO_ACCEL	3 - VECTOR		
515	AERO_GUID		PROCEDURE	
851	AERO_PARAMETERS		PROCEDURE	
901	ALPHA		SCALAR	
352	ALPHA_CMD		SCALAR	
516	ALPHA_DES		SCALAR	
401	ALPHA_EI		SCALAR	
908	ALPHA_FRACT		SCALAR	
513	ALPHA_MAX		SCALAR	
909	ALPHA_MAX		SCALAR	
513	ALPHA_MIN		SCALAR	
910	ALPHA_MIN		SCALAR	
74	ALPHA_NAV		SCALAR	
703	ALPHA_PRED		SCALAR	
649	ALPHA_TRY		SCALAR	
901	ALT		SCALAR	

DCL	NAME	TYPE	ATTRIBUTES & CROSS REFERENCE
513	ALT_FREEZE_GUID	SCALAR	SINGLE, ALIGNED, INITIAL XREF: 0 0513 2 0535
911	ALT_L	SCALAR	SINGLE, ALIGNED, STATIC XREF: 0 0911 4 0948 2 0953
912	ALT_MAX	SCALAR	SINGLE, ALIGNED, STATIC, CONSTANT XREF: 0 0912 2 0914 2 0948
913	ALT_MIN	SCALAR	SINGLE, ALIGNED, STATIC, CONSTANT XREF: 0 0913 2 0914 2 0941 2 0948 2 0953
79	ALT_NAV	SCALAR	DOUBLE, ALIGNED, INITIAL XREF: 0 0079 2 0535 2 0625
914	ALT_RUN	SCALAR	SINGLE, ALIGNED, STATIC XREF: 0 0914 2 0953
513	ALT_TAEM	SCALAR	SINGLE, ALIGNED, INITIAL XREF: 0 0513 2 0793
513	ALT_TAEM_BIAS	SCALAR	SINGLE, ALIGNED, INITIAL XREF: 0 0513 2 0738
1003	ALTADJ	SCALAR	SINGLE, ALIGNED, STATIC XREF: 0 1003 4 1033 2 1036 2 1037
1003	ALTRATIO	SCALAR	SINGLE, ALIGNED, STATIC XREF: 0 1003 4 1034 2 1037
981	ATMOS	STRUCTURE	ATMOSPROP-STRUCTURE, ALIGNED, ASSIGN-PARM XREF: 0 0981 0 0982 4 1007 4 1009 4 1021 4 1022 4 1026 6 1029 2 1035 4 1037 6 1039
851	ATMOS	STRUCTURE	ATMOSPROP-STRUCTURE, ALIGNED, INPUT-PARM XREF: 0 0851 0 0853 2 0869 2 0873 2 0874 2 0880 2 0882 2 0883 2 0884 2 0886 2 0888 2 0889 2 0890 2 0891 2 0892 2 0893 2 0894 2 0896 2 0897
574	ATMOS	STRUCTURE	ATMOSPROP-STRUCTURE, ALIGNED, STATIC XREF: 0 0574 4 0582 2 0583 2 0584 2 0591 2 0592
704	ATMOS	STRUCTURE	ATMOSPROP-STRUCTURE, ALIGNED, STATIC XREF: 0 0704 4 0734 2 0738 2 0747 2 0748 2 0764 4 0785 2 0789 2 0793
634	ATTITUDE_COMMAND	PROCEDURE	XREF: 2 0541 0 0634
863	C_BAR	SCALAR	SINGLE, ALIGNED, STATIC, CONSTANT XREF: 0 0863 2 0876
856	C_PRIME	SCALAR	SINGLE, ALIGNED, STATIC XREF: 0 0856 4 0897 2 0898
901	CD	SCALAR	SINGLE, ALIGNED, ASSIGN-PARM XREF: 0 0901 0 0904 4 0979 NOT REFERENCED
933	CD_ALT	SCALAR ARRAY	ARRAY(2,51), SINGLE, ALIGNED, STATIC, CONSTANT XREF: 0 0935 2 0951 2 0952
937	CD_MACH	SCALAR ARRAY	ARRAY(15,51), SINGLE, ALIGNED, STATIC, CONSTANT XREF: 0 0937 2 0973 2 0974
575	CD_NOM	SCALAR	SINGLE, ALIGNED, STATIC XREF: 0 0575 4 0584 2 0585 2 0589
705	CD_PRED	SCALAR	SINGLE, ALIGNED, STATIC XREF: 0 0705 4 0748 2 0749 2 0769
935	CD_VISC	SCALAR ARRAY	ARRAY(18,51), SINGLE, ALIGNED, STATIC, CONSTANT XREF: 0 0935 2 0964 2 0965
915	CD_1	SCALAR	SINGLE, ALIGNED, STATIC XREF: 0 0915 4 0951 4 0964 4 0973 2 0979
916	CD_2	SCALAR	SINGLE, ALIGNED, STATIC XREF: 0 0916 4 0952 4 0965 4 0974 2 0979
901	CL	SCALAR	SINGLE, ALIGNED, ASSIGN-PARM XREF: 0 0901 0 0905 4 0978 NOT REFERENCED
932	CL_ALT	SCALAR ARRAY	ARRAY(12,51), SINGLE, ALIGNED, STATIC, CONSTANT XREF: 0 0932 2 0949 2 0950
517	CL_EST	SCALAR	SINGLE, ALIGNED, STATIC XREF: 0 0517 4 0593 2 0625
936	CL_MACH	SCALAR ARRAY	ARRAY(15,51), SINGLE, ALIGNED, STATIC, CONSTANT XREF: 0 0936 2 0971 2 0972
576	CL_NOM	SCALAR	SINGLE, ALIGNED, STATIC XREF: 0 0576 4 0584 2 0585 2 0593
706	CL_PRED	SCALAR	SINGLE, ALIGNED, STATIC XREF: 0 0706 4 0748 2 0749
934	CL_VISC	SCALAR ARRAY	ARRAY(18,51), SINGLE, ALIGNED, STATIC, CONSTANT XREF: 0 0934 2 0962 2 0963
917	CL_1	SCALAR	SINGLE, ALIGNED, STATIC XREF: 0 0917 4 0949 4 0962 4 0971 2 0978
918	CL_2	SCALAR	SINGLE, ALIGNED, STATIC XREF: 0 0918 4 0950 4 0963 4 0972 2 0978

HAL/S STD 360-24.20

INTERMETRICS, INC.

APRIL 27, 1987 14:13:28.85

DCL	NAME	TYPE	ATTRIBUTES & CROSS REFERENCE
843	CLAMBDA	SCALAR	
648	CORRECTOR	PROCEDURE	XREF: 2 0536 0 0648
919	COS_ALPHA	SCALAR	SINGLE, ALIGNED, STATIC XREF: 0 0919 NOT USED
640	COSPHI_CMD	SCALAR	SINGLE, TEMPORARY XREF: 0 0640 4 0641 6 0642 2 0643
518	COSPHI_QDOT	SCALAR	SINGLE, ALIGNED, STATIC, INITIAL XREF: 0 0518 4 0630 4 0632 2 0638 2 0641
596	COSPHI_1	SCALAR	SINGLE, ALIGNED, STATIC XREF: 0 0596 4 0628 2 0630
597	COSPHI_2	SCALAR	SINGLE, ALIGNED, STATIC XREF: 0 0597 4 0629 2 0630
752	CPHI	SCALAR	SINGLE, TEMPORARY XREF: 0 0752 4 0767 2 0773
659	CR_ERR	SCALAR	SINGLE, ALIGNED, STATIC XREF: 0 0659 2 0682 4 0804
658	CR_ERROR	SCALAR ARRAY	ARRAY(3), SINGLE, ALIGNED, STATIC XREF: 0 0658 4 0682 2 0686 2 0687 2 0689
657	CRE	SCALAR	SINGLE, ALIGNED, STATIC XREF: 0 0657 4 0689 2 0693 2 0695
655	DCRE_DA	SCALAR	SINGLE, ALIGNED, STATIC XREF: 0 0655 4 0686 2 0690 2 0695
656	DCRE_DP	SCALAR	SINGLE, ALIGNED, STATIC XREF: 0 0656 4 0687 2 0690 2 0693
653	DDRE_DA	SCALAR	SINGLE, ALIGNED, STATIC XREF: 0 0653 4 0684 2 0690 2 0695
654	DDRE_DP	SCALAR	SINGLE, ALIGNED, STATIC XREF: 0 0654 4 0685 2 0690 2 0693
864	DEG_R_TO_DEG_K	SCALAR	SINGLE, ALIGNED, STATIC, CONSTANT XREF: 0 0864 2 0881 2 0883 2 0885
5	DEG_TO_RAD	SCALAR	DOUBLE, ALIGNED, CONSTANT XREF: 0 0005 2 0006 2 0007
204	650	DELTA_ALPHA	SINGLE, ALIGNED, STATIC XREF: 0 0650 2 0672 2 0684 2 0686
651	DELTA_PHI	SCALAR	SINGLE, ALIGNED, STATIC, CONSTANT XREF: 0 0651 2 0677 2 0685 2 0687
519	DELTA_T_PRED	SCALAR	SINGLE, ALIGNED, STATIC XREF: 0 0519 4 0739 4 0743 4 0744 6 0745 2 0787 2 0820 2 0821 2 0826 2 0827 2 0832 2 0833 2 0836 2 0837
513	DELTA_T_PRED_GAIN	SCALAR	SINGLE, ALIGNED, INITIAL XREF: 0 0513 2 0743
513	DELTA_T_PRED_MAX	SCALAR	SINGLE, ALIGNED, INITIAL XREF: 0 0513 2 0744 2 0745
513	DELTA_T_PRED_MIN	SCALAR	SINGLE, ALIGNED, INITIAL XREF: 0 0513 2 0759 2 0765
652	DETERM	SCALAR	SINGLE, ALIGNED, STATIC, INITIAL XREF: 0 0652 4 0690 2 0691 2 0693 2 0695
1003	DH	SCALAR	SINGLE, ALIGNED, STATIC XREF: 0 1003 4 1020 2 1021 2 1022 2 1026 2 1037
707	DOT	SCALAR	DOUBLE, ALIGNED, STATIC XREF: 0 0707 4 0801 2 0802 6 0803 2 0804 4 0805 2 0806 6 0807 2 0808
663	DR_ERR	SCALAR	SINGLE, ALIGNED, STATIC XREF: 0 0663 2 0681 4 0808
662	DR_ERROR	SCALAR ARRAY	ARRAY(3), SINGLE, ALIGNED, STATIC XREF: 0 0662 4 0681 2 0684 2 0685 2 0688
753	DRAG_ACCEL	SCALAR	SINGLE, TEMPORARY XREF: 0 0753 4 0769 2 0770 2 0774
664	DRE	SCALAR	SINGLE, ALIGNED, STATIC XREF: 0 0664 4 0688 2 0693 2 0695
513	DT_AEROGUID	SCALAR	SINGLE, ALIGNED, INITIAL XREF: 0 0513 2 0620
1001	DTDH	SCALAR ARRAY	ARRAY(12), SINGLE, ALIGNED, STATIC, INITIAL XREF: 0 1001 2 1022
1000	DTMDH	SCALAR ARRAY	ARRAY(12), SINGLE, ALIGNED, STATIC, INITIAL XREF: C 1000 2 1021 2 1025 2 1028 2 1033 2 1036 2 1037
699	EARTH_FIXED_FROM_REFERENCE	3 X 3 MATRIX FUNCTION	DOUBLE XREF: 0 0699 2 0796
463	EARTH_FLAT	SCALAR	DOUBLE, ALIGNED, INITIAL XREF: 0 0463 2 0557
464	EARTH_J2	SCALAR	DOUBLE, ALIGNED, INITIAL XREF: 0 0464 2 0777
465	EARTH_MU	SCALAR	DOUBLE, ALIGNED, INITIAL XREF: 0 0465 2 0778
466	EARTH_POLE	3 - VECTOR	DOUBLE, ALIGNED, INITIAL XREF: 0 0466 2 0582 2 0734 2 0776 2 0777 2 0785
467	EARTH_R	SCALAR	DOUBLE, ALIGNED, INITIAL XREF: 0 0467 2 0777 2 0804 2 0808
468	EARTH_RATE	SCALAR	DOUBLE, ALIGNED, INITIAL XREF: 0 0468 2 0845 2 0846

HAL/S STD 360-24.20

INTERMETRICS, INC.

APRIL 27, 1987 14:13:28.85

DCL	NAME	TYPE	ATTRIBUTES & CROSS REFERENCE
708	EF_FROM_REF	3 X 3 MATRIX	DOUBLE, ALIGNED, STATIC XREF: 0 0708 4 0796 2 0797 2 0798
520	EF_FROM_REF_AT_EPOCH	3 X 3 MATRIX	DOUBLE, ALIGNED, STATIC XREF: 0 0520 4 0549 2 0847
308	EF_TO_REF_AT_EPOCH	3 X 3 MATRIX	DOUBLE, ALIGNED, INITIAL XREF: 0 0308 2 0549
1003	EXPO	SCALAR	SINGLE, ALIGNED, STATIC XREF: 0 1003 4 1028 2 1029 4 1036 2 1037
992	F	SCALAR	DOUBLE, ALIGNED, STATIC, CONSTANT XREF: 0 0992 2 0993 2 1006
571	FILTERS	PROCEDURE	XREF: 2 0534 0 0571
598	FIRST_PASS	BIT(1)	ALIGNED, STATIC, INITIAL XREF: 0 0598 2 0611 4 0613
921	FLOW_REGIME	INTEGER	SINGLE, ALIGNED, STATIC XREF: 0 0921 4 0940 4 0942 4 0944 4 0945 2 0946
920	FRACT	SCALAR	SINGLE, ALIGNED, STATIC XREF: 0 0920 4 0953 4 0966 4 0975 2 0978 2 0979
11	FT_TO_NM	SCALAR	DOUBLE, ALIGNED, CONSTANT XREF: 0 0011 2 0012 2 0804 2 0808
82	G_LOAD	SCALAR	DOUBLE, ALIGNED, INITIAL XREF: 0 0082 2 0532
513	G_RUN_GUIDANCE	SCALAR	SINGLE, ALIGNED, INITIAL XREF: 0 0513 2 0532
13	G_TO_FPS2	SCALAR	DOUBLE, ALIGNED, CONSTANT XREF: 0 0013 2 0014 2 0017 2 1039
865	GAMMA	SCALAR	SINGLE, ALIGNED, STATIC, CONSTANT XREF: 0 0865 2 0868
857	GAMMA_VBAR	SCALAR	SINGLE, ALIGNED, STATIC XREF: 0 0857 4 0887 4 0889 4 0891 4 0893 4 0895 2 0896
754	GRAV_ACCEL	3 - VECTOR	DOUBLE, TEMPORARY XREF: 0 0754 4 0778 2 0779
1003	GRAVRATIO	SCALAR	SINGLE, ALIGNED, STATIC XREF: 0 1003 4 1011 2 1013 6 1014 2 1037
521	GUID_PASS	INTEGER	SINGLE, ALIGNED, STATIC XREF: 0 0521 2 0535 6 0537 2 0538 4 0539 4 0550
513	GUID_PASS_LIM	SCALAR	SINGLE, ALIGNED, INITIAL XREF: 0 0513 2 0538
985	G0	SCALAR	SINGLE, ALIGNED, STATIC, CONSTANT XREF: 0 0985 2 0988
1002	H	SCALAR	DOUBLE, ALIGNED, STATIC XREF: 0 1002 4 1006 2 1007 2 1008 2 1011 2 1012 6 1013 2 1017 2 1020 2 1023 2 1034
526	H	SCALAR	**** SEE STRUCTURE TEMPLATE ATOMSPROP
996	H_BASE	SCALAR ARRAY	ARRAY(13), SINGLE, ALIGNED, STATIC, CONSTANT XREF: 0 0996 2 1017 2 1020 2 1033 2 1034
595	HEAT_RATE_CONTROL	PROCEDURE	XREF: 2 0540 0 0595
513	HS	SCALAR	SINGLE, ALIGNED, INITIAL XREF: 0 0513 2 0614
755	HS_NORM_PRED	SCALAR	SINGLE, TEMPORARY XREF: 0 0755 NOT USED
599	HS_2	SCALAR	SINGLE, ALIGNED, STATIC XREF: 0 0599 4 0614 2 0615 2 0625
665	I	INTEGER	SINGLE, TEMPORARY XREF: 0 0665 2 0666 1 0681 1 0682
922	I	INTEGER	SINGLE, ALIGNED, STATIC XREF: 0 0922 4 0958 1 0962 1 0963 1 0964 1 0965 1 0966 4 0970 1 0971 1 0972 1 0973 1 0974 2 0975
994	I	INTEGER	SINGLE, ALIGNED, STATIC XREF: 0 0994 4 1016 1 1020 1 1021 1 1022 1 1025 1 1026 1 1028 1 1029 1 1033 1 1034 1 1035 1 1036 1 1037
709	I_INPLANE	3 - VECTOR	DOUBLE, ALIGNED, STATIC XREF: 0 0709 4 0800 2 0801 2 0804 2 0805 2 0808
756	I_LAT	3 - VECTOR	SINGLE, TEMPORARY XREF: 0 0756 4 0772 2 0773
757	I_LIFT	3 - VECTOR	SINGLE, TEMPORARY XREF: 0 0757 4 0773 2 0774
710	I_NORMAL	3 - VECTOR	DOUBLE, ALIGNED, STATIC XREF: 0 0710 4 0799 2 0800 2 0804 2 0808
522	I_TARGET_EF	3 - VECTOR	DOUBLE, ALIGNED, STATIC XREF: 0 0522 4 0567 2 0800 2 0801 2 0804
758	I_VEL	3 - VECTOR	SINGLE, TEMPORARY XREF: 0 0758 4 0771 2 0772 2 0773 2 0774

HAL/S STD 360-24.20

INTERMETRICS, INC.

APRIL 27, 1987 14:13:28.85

DCL	NAME	TYPE	ATTRIBUTES & CROSS REFERENCE
542	INITIAL_GUID	PROCEDURE	XREF: 2 0529 0 0542
523	INITIALIZE_GUIDANCE	BIT(1)	ALIGNED, STATIC, INITIAL XREF: 0 0523 2 0527 4 0530
711	INTEG_LOOP	SCALAR	SINGLE, ALIGNED, STATIC XREF: 0 0711 4 0750 2 0814
809	INTEGRATOR	PROCEDURE	XREF: 2 0780 0 0809
712	IR_E	3 - VECTOR	DOUBLE, ALIGNED, STATIC XREF: 0 0712 4 0797 2 0799 2 0805 2 0808
923	J	INTEGER	SINGLE, ALIGNED, STATIC XREF: 0 0923 4 0938 1 0949 1 0950 1 0951 1 0952 1 0962 1 0963 1 0964 1 0965 1 0971 1 0972 1 0973 1 0974
957	K	INTEGER	SINGLE, TEMPORARY XREF: 4 0957 2 0958 1 0959
84	K_LOD_NAV	SCALAR	SINGLE, ALIGNED, INITIAL XREF: 0 0084 4 0569 6 0590 2 0593 2 0749
600	K_QDOT	SCALAR	SINGLE, ALIGNED, STATIC XREF: 0 0600 4 0626 2 0629
601	K_QDOT_RATE	SCALAR	SINGLE, ALIGNED, STATIC XREF: 0 0601 4 0627 2 0628
472	K_RHO_FILTER_GAIN	SCALAR	SINGLE, ALIGNED, INITIAL XREF: 0 0472 2 0591
83	K_RHO_NAV	SCALAR	SINGLE, ALIGNED, INITIAL XREF: 0 0083 4 0568 6 0591 2 0592 2 0764
990	KG_TO_LBM	SCALAR	SINGLE, ALIGNED, STATIC, CONSTANT XREF: 0 0990 2 1039
18	KG_TO_SLUG	SCALAR	DOUBLE, ALIGNED, CONSTANT XREF: 0 0018 2 0873
602	K1_GAIN	SCALAR	SINGLE, ALIGNED, STATIC XREF: 0 0602 4 0615 2 0625
603	K1_QDOT	SCALAR	SINGLE, ALIGNED, STATIC XREF: 0 0603 4 0625 2 0626 2 0627
988	K2	SCALAR	SINGLE, ALIGNED, STATIC, CONSTANT XREF: 0 0988 2 1026 2 1028 2 1036 2 1037
475	L_OVER_D_FILTER_GAIN	SCALAR	SINGLE, ALIGNED, INITIAL XREF: 0 0475 2 0590
544	LAT	SCALAR	SINGLE, ALIGNED, STATIC XREF: 0 0544 4 0556 6 0557 2 0558
513	LIFT_ACCEL	SCALAR	SINGLE, ALIGNED, INITIAL XREF: 0 0513 2 0556
759	LOD_MEAS	SCALAR	SINGLE, TEMPORARY XREF: 0 0759 4 0770 2 0774
578	LOD_NOM	SCALAR	SINGLE, ALIGNED, STATIC XREF: 0 0577 4 0588 2 0590
713	LOD_PRED	SCALAR	SINGLE, ALIGNED, STATIC XREF: 0 0578 4 0585 2 0590
545	LONG	SCALAR	SINGLE, ALIGNED, STATIC XREF: 0 0713 4 0749 2 0770
513	LONG_TARGET	SCALAR	SINGLE, ALIGNED, STATIC XREF: 0 0545 4 0555 2 0562 2 0566 SINGLE, ALIGNED, INITIAL XREF: 0 0513 2 0555
901	LOOKUP	PROCEDURE	XREF: 2 0584 2 0748 0 0901
10	M_TO_FT	SCALAR	DOUBLE, ALIGNED, CONSTANT XREF: 0 0010 2 0013 2 0869 2 0873
989	M_TO_FT	SCALAR	DOUBLE, ALIGNED, STATIC, CONSTANT XREF: 0 0989 2 1006 2 1007 2 1039
901	MACH	SCALAR	SINGLE, ALIGNED, INPUT-PARM XREF: 0 0901 0 0906 2 0943 2 0969
579	MACH	SCALAR	SINGLE, ALIGNED, STATIC XREF: 0 0579 4 0583 2 0584
851	MACH	SCALAR	SINGLE, ALIGNED, ASSIGN-PARM XREF: 0 0851 0 0854 4 0871 4 0872 2 0896 2 0898
924	MACH_L	SCALAR	SINGLE, ALIGNED, STATIC XREF: 0 0924 4 0969 2 0970 2 0975
925	MACH_MAX	SCALAR	SINGLE, ALIGNED, STATIC, CONSTANT XREF: 0 0925 2 0943 2 0969
926	MACH_MIN	SCALAR	SINGLE, ALIGNED, STATIC, CONSTANT XREF: 0 0926 2 0969
714	MACH_PRED	SCALAR	SINGLE, ALIGNED, STATIC XREF: 0 0714 4 0747 2 0748
314	MASS_NAV	SCALAR	SINGLE, ALIGNED, INITIAL XREF: 0 0314 2 0589 2 0615 2 0769
867	MOLE_MT_ZERO	SCALAR	SINGLE, ALIGNED, STATIC, CONSTANT XREF: 0 0867 2 0868
986	MO	SCALAR	SINGLE, ALIGNED, STATIC, CONSTANT XREF: 0 0986 2 0988
1015	N	INTEGER	SINGLE, TEMPORARY XREF: 4 1015 2 1016 1 1017
995	NSEGS	INTEGER	SINGLE, ALIGNED, STATIC, CONSTANT XREF: 0 0995 2 0996 2 0997 2 0998 2 0999 2 1000 2 1001 2 1015
513	OMEGA_QDOT	SCALAR	SINGLE, ALIGNED, INITIAL XREF: 0 0513 2 0616 2 0617
604	OMEGA_QDOT_SQUARED	SCALAR	SINGLE, ALIGNED, STATIC XREF: 0 0604 4 0616 2 0626

DCL	NAME	TYPE	ATTRIBUTES & CROSS REFERENCE
812	ORIG_POS	3 - VECTOR	DOUBLE, ALIGNED, STATIC XREF: 0 0812 4 0816 2 0820 2 0826 2 0832 2 0836
813	ORIG_VEL	3 - VECTOR	DOUBLE, ALIGNED, STATIC XREF: 0 0813 4 0817 2 0821 2 0827 2 0833 2 0837
25	PHI_CMD	SCALAR	SINGLE, ALIGNED, INITIAL XREF: 0 0025 4 0554 4 0636 6 0637 2 0661 6 0643 6 0646
524	PHI_DES	SCALAR	SINGLE, ALIGNED, STATIC XREF: 0 0524 4 0552 2 0636 2 0669 2 0673 2 0677 6 0695 6 0696
513	PHI_DES_MAX	SCALAR	SINGLE, ALIGNED, INITIAL XREF: 0 0513 2 0696
402	PHI_EI	SCALAR	SINGLE, ALIGNED, INITIAL XREF: 0 0402 2 0552 2 0554
513	PHI_MAX	SCALAR	SINGLE, ALIGNED, INITIAL XREF: 0 0513 2 0554 2 0637 2 0646 2 0766
715	PHI_PRED	SCALAR	SINGLE, ALIGNED, STATIC XREF: 0 0715 4 0765 6 0766 2 0767 2 0768
660	PHI_TRY	SCALAR	SINGLE, ALIGNED, STATIC XREF: 0 0660 4 0669 4 0673 4 0677 2 0765
981	POLE	3 - VECTOR	DOUBLE, ALIGNED, INPUT-PARM XREF: 0 0981 0 0984 2 1005
661	PRED_EXIT	BIT(1)	ALIGNED, STATIC XREF: 0 0661 4 0790 2 0791 XREF: 2 0680 0 0697
697	PREDICTOR	PROCEDURE	SINGLE, ALIGNED, STATIC XREF: 0 0605 4 0624 2 0628 2 0629
605	QBAR	SCALAR	SINGLE, ALIGNED, STATIC XREF: 0 0606 4 0610 2 0620 2 0621 2 0622 2 0629
606	QDOT	SCALAR	SINGLE, ALIGNED, INITIAL XREF: 0 0513 2 0622 2 0629 SINGLE, ALIGNED, STATIC XREF: 0 0607 2 0620 4 0621
513	QDOT_LIMIT	SCALAR	SINGLE, ALIGNED, STATIC XREF: 0 0608 4 0618 4 0620 2 0628
607	QDOT_PAST	SCALAR	DOUBLE, ALIGNED, INPUT-PARM XREF: 0 0981 0 0983 2 1004 2 1005
608	QDOT_RATE	SCALAR	DOUBLE, ALIGNED, STATIC XREF: 0 1002 4 1004 2 1005 2 1006 2 0778 4 0781 2 0788
981	R	3 - VECTOR	DOUBLE, ALIGNED, INITIAL XREF: 0 0086 2 0582 2 0727 DOUBLE, ALIGNED, STATIC XREF: 0 0716 4 0727 2 0728 2 0731 2 0734 2 0772 2 0775 2 0781 2 0783 2 0785 2 0788 2 0797 2 0798 2 0816 4 0820 4 0826 4 0832 4 0836
1002	R_MAG	SCALAR	DOUBLE, ALIGNED, CONSTANT XREF: 0 0006 2 0643
717	R_MAG_PRED	SCALAR	SINGLE, ALIGNED, STATIC XREF: 0 0718 4 0788 2 0789
86	R_NAV	3 - VECTOR	SINGLE, ALIGNED, STATIC XREF: 0 0858 4 0875 4 0876 2 0877 2 0898
716	R_PRED	3 - VECTOR	*** SEE STRUCTURE TEMPLATE ATMOSPROP ARRAY(13), SINGLE, ALIGNED, STATIC, CONSTANT XREF: 0 0999 2 1026 2 1029 2 1037
6	RAD_TO_DEG	SCALAR	SINGLE, ALIGNED, STATIC XREF: 0 0580 4 0589 2 0591
718	RDOT_PRED	SCALAR	SINGLE, ALIGNED, STATIC XREF: 0 0525 4 0592 2 0610 2 0624
858	REYNOLDS_NUMBER	SCALAR	SINGLE, TEMPORARY XREF: 0 0760 4 0764 2 0769
526	RHO	SCALAR	SINGLE, ALIGNED, INITIAL XREF: 0 0513 2 0615
999	RHO_BASE	SCALAR ARRAY	SINGLE, ALIGNED, STATIC, CONSTANT XREF: 0 0987 2 0988 SINGLE, ALIGNED, STATIC, CONSTANT XREF: 0 0993 2 1011 2 1032 2 1034 2 1036
580	RHO_MEAS	SCALAR	SINGLE, ALIGNED, INITIAL XREF: 0 0478 2 0589 2 0615 2 0769
525	RHO_NAV	SCALAR	SINGLE, ALIGNED, STATIC XREF: 0 0927 NOT USED
760	RHO_PRED	SCALAR	DOUBLE, ALIGNED, STATIC XREF: 0 0844 4 0846 2 0847
513	RHO_SL	SCALAR	SINGLE, ALIGNED, STATIC XREF: 0 0859 4 0869 2 0870 2 0872
987	RR	SCALAR	SINGLE, ALIGNED, STATIC, CONSTANT XREF: 0 0868 2 0869
993	RO	SCALAR	SINGLE, TEMPORARY XREF: 0 0761 4 0768 2 0773
478	S_REF	SCALAR	DOUBLE, ALIGNED, STATIC XREF: 0 1002 4 1005 2 1006
927	SIN_ALPHA	SCALAR	
844	SLAMBDA	SCALAR	
859	SPEED_OF_SOUND	SCALAR	
868	SPEED_OF_SOUND_CONST	SCALAR	
761	SPHI	SCALAR	
1002	SPSI	SCALAR	

HAL/S STD 360-24.20

INTERMETRICS, INC.

APRIL 27, 1987 14:13:28.85

DCL NAME	TYPE	ATTRIBUTES & CROSS REFERENCE
841 T	SCALAR	DOUBLE, ALIGNED, INPUT-PARM XREF: 0 0841 0 0842 2 0845 2 0846
998 T_BASE	SCALAR ARRAY	ARRAY(13), SINGLE, ALIGNED, STATIC, CONSTANT XREF: 0 0998 2 1022
310 T_EPOCH	SCALAR	DOUBLE, ALIGNED, INITIAL XREF: 0 0310 2 0845 2 0846
22 T_GMT	SCALAR	DOUBLE, ALIGNED, INITIAL XREF: 0 0022 2 0726
719 T_PRED	SCALAR	DOUBLE, ALIGNED, STATIC XREF: 0 0719 4 0726 6 0787 2 0796
860 T_PRIME	SCALAR	SINGLE, ALIGNED, STATIC XREF: 0 0860 4 0896 2 0897
861 T_WALL	SCALAR	SINGLE, ALIGNED, STATIC XREF: 0 0861 4 0881 4 0883 4 0885 2 0896
1003 TEMPRATIO	SCALAR	SINGLE, ALIGNED, STATIC XREF: 0 1003 4 1035 2 1037
736 TIME_INCREMENT	INTEGER	SINGLE, TEMPORARY XREF: 4 0736 2 0737
526 TH	SCALAR	*** SEE STRUCTURE TEMPLATE ATMOSPROP
997 TM_BASE	SCALAR ARRAY	ARRAY(13), SINGLE, ALIGNED, STATIC, CONSTANT XREF: 0 0997 2 1021 2 1026 2 1029 2 1033 2 1035
700 TOTAL_TIME_STEPS	INTEGER	SINGLE, ALIGNED, STATIC XREF: 0 0700 4 0737 NOT REFERENCED
526 TS	SCALAR	*** SEE STRUCTURE TEMPLATE ATMOSPROP
609 TWO_ZETA_OMEGA	SCALAR	SINGLE, ALIGNED, STATIC XREF: 0 0609 4 0617 2 0627
762 U_PRED	3 - VECTOR	DOUBLE, TEMPORARY XREF: 0 0762 4 0775 2 0776 6 0777 2 0778
866 UNIV_GAS_CONST	SCALAR	SINGLE, ALIGNED, STATIC, CONSTANT XREF: 0 0866 2 0868
981 USATMOS62	PROCEDURE	XREF: 2 0582 2 0734 2 0785 0 0981
901 V_BAR	SCALAR	SINGLE, ALIGNED, INPUT-PARM XREF: 0 0901 0 0907 2 0956
851 V_BAR	SCALAR	SINGLE, ALIGNED, ASSIGN-PARM XREF: 0 0851 0 0855 4 0878 4 0898 NOT REFERENCED
581 V_BAR	SCALAR	SINGLE, ALIGNED, STATIC XREF: 0 0581 4 0583 2 0584
928 V_BAR_L	SCALAR	SINGLE, ALIGNED, STATIC XREF: 0 0928 4 0956 2 0959 2 0966
929 V_BAR_MAX	SCALAR	SINGLE, ALIGNED, STATIC, CONSTANT XREF: 0 0929 2 0956
930 V_BAR_MIN	SCALAR	SINGLE, ALIGNED, STATIC, CONSTANT XREF: 0 0930 2 0956
720 V_BAR_PRED	SCALAR	SINGLE, ALIGNED, STATIC XREF: 0 0720 4 0747 2 0748
931 V_BAR_TABLE	SCALAR ARRAY	ARRAY(18), SINGLE, ALIGNED, STATIC, CONSTANT XREF: 0 0931 2 0959 2 0966
513 V_FINAL_MAG	SCALAR	SINGLE, ALIGNED, INITIAL XREF: 0 0513 2 0636 2 0765
513 V_MAG_CHANGE	SCALAR	SINGLE, ALIGNED, INITIAL XREF: 0 0513 2 0636 2 0765
721 V_MAG_PRED	SCALAR	DOUBLE, ALIGNED, STATIC XREF: 0 0721 4 0730 2 0765 4 0782
93 V_NAV	3 - VECTOR	DOUBLE, ALIGNED, INITIAL XREF: 0 0093 2 0729
94 V_NAV_MAG	SCALAR	DOUBLE, ALIGNED, INITIAL XREF: 0 0094 2 0636
722 V_PRED	3 - VECTOR	DOUBLE, ALIGNED, STATIC XREF: 0 0722 4 0729 2 0730 2 0731 2 0782 2 0783 2 0788 2 0798 2 0817 2 0818 2 0820 4 0821 2 0824 2 0826 4 0827 2 0830 2 0832 4 0833 2 0836 4 0837
851 V_REL_MAG	SCALAR	SINGLE, ALIGNED, INPUT-PARM XREF: 0 0851 0 0852 2 0872 2 0876
95 V_REL_MAG	SCALAR	DOUBLE, ALIGNED, INITIAL XREF: 0 0095 2 0583 2 0586 2 0589 2 0610 2 0624 2 0625
723 V_REL_MAG_PRED	SCALAR	SINGLE, ALIGNED, STATIC XREF: 0 0723 4 0732 2 0747 2 0769 2 0771 4 0784
96 V_REL_NAV	3 - VECTOR	DOUBLE, ALIGNED, INITIAL XREF: 0 0096 2 0586
724 V_REL_PRED	3 - VECTOR	SINGLE, ALIGNED, STATIC XREF: 0 0724 4 0731 2 0732 2 0771 4 0783 2 0784
862 VISCOSITY	SCALAR	SINGLE, ALIGNED, STATIC XREF: 0 0862 4 0873 2 0874 2 0876
725 VR_E	3 - VECTOR	DOUBLE, ALIGNED, STATIC XREF: 0 0725 4 0798 2 0799
480 WE_NAV	3 - VECTOR	SINGLE, ALIGNED, INITIAL XREF: 0 0480 2 0731 2 0783 2 0798
546 X	SCALAR	SINGLE, ALIGNED, STATIC XREF: 0 0546 4 0559 2 0560 4 0561 6 0562 2 0563 2 0567
547 Y	SCALAR	SINGLE, ALIGNED, STATIC XREF: 0 0547 4 0563 2 0564 4 0565

HAL/S STD 360-24.20

INTERMETRICS, INC.

APRIL 27, 1987 14:13:28.85

DCL NAME	TYPE	ATTRIBUTES & CROSS REFERENCE
548 Z	SCALAR	6 0566 2 0567 SINGLE, ALIGNED, STATIC XREF: 0 0548 4 0558 2 0559 2 0563 2 0567
763 Z_PRED	SCALAR	DOUBLE, TEMPORARY XREF: 0 0763 4 0776 2 0777
513 ZETA_QDOT	SCALAR	SINGLE, ALIGNED, INITIAL XREF: 0 0513 2 0617

LIST OF REFERENCES

1. Freeman, D.C., Powell, R.W., Naftel, J.C., and Wurster, K.E., "Definition of an Entry Research Vehicle", AIAA Paper 85-0969, AIAA 20th Thermophysics Conference, Williamsburg, Virginia, June 1985.
2. Morth, R., *Reentry Guidance for Apollo*, MIT Document R-532, January 1966.
3. *Shuttle Level C FSSR, Part A, Entry Through Landing Guidance*, STS 83-0001A, December 15, 1982.
4. Lerner, E.J., "Supercomputer in a Six-Inch Cube", *Aerospace America*, Vol. 4, No. 11, November 1986, pp. 13-14.
5. Brand, T.J., Brown, D.W., and Higgins, J.P., *Space Shuttle G&N Equation Document No. 24 (Revision 2), Unified Powered Flight Guidance*, CSDL C-4108, June 1974.
6. Higgins, J.P., "An Aerobraking Guidance Concept for a Low L/D AOTV", CSDL Memo No. 10E-84-04, May 24, 1984.
7. Young, J.D., Underwood, J.M., et al., "The Aerodynamic Challenges of the Design and Development of the Space Shuttle Orbiter", *Space Shuttle Technical Conference*, NASA CP-2342 Part 1, held at the Lyndon B. Johnson Space Center, Houston, Texas, June 28-30, 1983.

~~PRECEDING PAGE BLANK NOT FILMED~~

8. *Terrestrial Environment (Climatic) Criteria Guidelines for Use in Aerospace Vehicle Development, 1982 Revision*, NASA TM 82473, June 1982.
9. Justus, C.G., Fletcher, G.R., Gramling, F.E., and Pace, W.B., *The NASA/MSFC Global Reference Atmosphere Model - MOD 3, (with Spherical Harmonic Wind Model)*, NASA Contractor Report 3256, March 1980.
10. Findley, J.T., Kelly, G.M., and Troutman, P.A., *Final Report - Shuttle Derived Atmospheric Density Model*, NASA Contractor Report 171824, November 1986.
11. Bryson, A.E., Mikami, K., and Battle, C.T., "Optimum Lateral Turns for a Re-Entry Glider", *Aerospace Engineering*, March, 1962, pp. 18-23.
12. Wagner, W.E., "Roll Modulation for Maximum Re-Entry Lateral Range", *Journal of Spacecraft*, Vol. 2, No. 5, September-October 1965.
13. Zondervan, K., Bauer, T., Betts, J., and Huffman, W., "Solving the Optimal Control Problem Using a Nonlinear Programming Technique Part 3: Optimal Shuttle Reentry Trajectories", AIAA Paper 84-2039, AIAA/AAS Astrodynamics Conference, Seattle, Washington, August 1984.
14. Powell, R.W., Naftel, J.C., and Cunningham, M.J., "Performance Evaluation of an Entry Research Vehicle", AIAA Paper 86-0270, AIAA 24th Aerospace Sciences Meeting, Reno, Nevada, January 1986.
15. *Program to Optimize Simulated Trajectories (POST) Volume I - Formulation Manual*, NASA CR-132689, April 1975.

16. *U.S. Standard Atmosphere, 1962*, Prepared under the sponsorship of NASA, U.S. Air Force, and U.S. Weather Bureau, Published by the US Government Printing Office, 1962.
- 17: Battin, R.H., *An Introduction to the Mathematics and Methods of Astrodynamics*, forthcoming book, 1987.
18. Scott, C.D., et al., "The Aerothermodynamics and Thermal Protection System Challenges for an Aerobraking Orbital Transfer Vehicle", Presented at the NASA Symposium on Recent Advances in TPS and Structures for Future Space Transportation Systems, held on December 13-15, 1983.
19. *Aeroassist Flight Experiment, AFESIM All-Digital Functional Simulator, Simulator Definition Documentation, Volume 1*, CSDL-R-1951, March 27, 1987.
20. Phillips, R.E., "Three Aspects of Covariance/Monte Carlo Analysis: Bias, Reducing Dimensionality and Systematically Choosing Error Vectors", CSDL Memo No. 10E-86-18, June 23, 1986.

